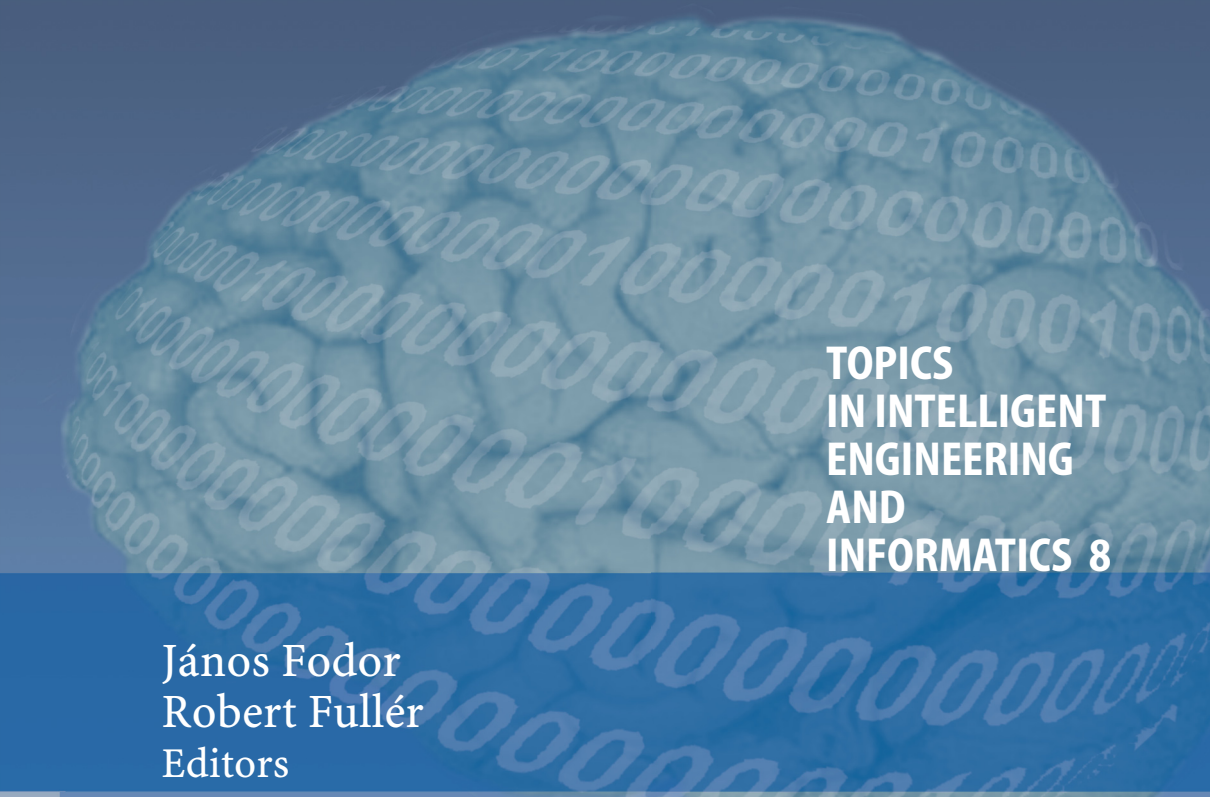

TOPICS IN INTELLIGENT ENGINEERING AND INFORMATICS 8

János Fodor
Robert Fullér
Editors

Advances in Soft Computing, Intelligent Robotics and Control

Springer

Topics in Intelligent Engineering and Informatics

Volume 8

For further volumes:
http://www.springer.com/series/10188

János Fodor · Robert Fullér
Editors

Advances in Soft Computing, Intelligent Robotics and Control

Springer

Editors
János Fodor
Institute of Applied Mathematics
Óbuda University
Budapest
Hungary

Robert Fullér
Department of Applied Mathematics
John von Neumann Faculty of Informatics
Óbuda University
Budapest
Hungary

ISSN 2193-9411 ISSN 2193-942X (electronic)
ISBN 978-3-319-05944-0 ISBN 978-3-319-05945-7 (eBook)
DOI 10.1007/978-3-319-05945-7
Springer Cham Heidelberg New York Dordrecht London

Library of Congress Control Number: 2014934569

Printed on acid-free paper

Springer is part of Springer Science+Business Media (www.springer.com)

Dedication

The volume is dedicated to Prof. Dr. Imre J. Rudas on the occasion of celebrating his 65^{th} birthday and expressing our respect to his outstanding, high level achievements of 11 years rectorship.

Foreword

I am very pleased to have an opportunity to write a foreword to "Advances in Soft Computing, Intelligent Robotics and Control", dedicated to my esteemed friend, Imre J. Rudas on the occasion of his 65th anniversary. In the course of his long and distinguished career as a researcher, educator and administrator, Imre has contributed importantly to the advancement of our understanding of how to conceive, design and construct intelligent systems. Imre's work makes a skilled use of concepts and techniques drawn from a broad range of methodologies, principally soft computing, fuzzy logic and robotics. Imre is a man of vision and initiative. He is a true leader.

As my tribute to Imre, I should like to share with the readers of this Volume, some of my thoughts and ideas which relate to an issue which underlies much of Imre's work—achievement of human-level machine intelligence. My thoughts and views reflect my long-standing interest in machine intelligence, going back to the beginning of my teaching and research career. The beginning of my teaching and research career coincided with the debut of the computer age and the birth of artificial intelligence. It was my fortune to be able to observe at close distance, and participate in, the advent of the Information Revolution—a revolution which fundamentally changed the way we live and work today.

Back in the late forties and early fifties of last century, there were many exaggerated expectations of what was around the corner. It was widely predicted that human-level machine intelligence would become a reality in a few years' time. In a short paper published in 1950, entitled "Thinking machines—a new field in electrical engineering", I included some of the headlines which appeared in the popular press at that time. One of them read, "Electric Brain Capable of Translating Foreign Languages is Being Built". Today, we have fairly good translation programs, but nothing that can approach the quality of human translation. In 1948, on the occasion of inauguration of IBM's relay computer, Howard Aiken, Director of Harvard's Computation Laboratory, said, "There is no problem in applied mathematics that this computer cannot solve". What is remarkable is that Aiken made this claim about a relay computer which had a memory of about one thousand words. His claim could not be farther from truth.

Putting exaggerated expectations aside, tremendous progress has been made in our ability to construct machines which can process huge volumes of information at high speed and with high reliability. But achievement of human-level machine intelligence remains a challenging problem. In what follows, I will briefly address a basic question: Why achievement of human-level machine intelligence proved to be a much more difficult problem than it was thought to be at the dawn of the computer age?

Humans have a remarkable capability to reason with information which is imprecise, uncertain and partially true. In large measure, today's computers employ the classical, Aristotelian, bivalent logic. Bivalent logic is intolerant of imprecision and partiality of truth. It is my conviction that to simulate human reasoning, it is necessary to employ a logic in which the objects of reasoning and computation are classes with unsharp (fuzzy) boundaries. Bivalent logic is not the right logic for reasoning and computation with objects of this type. What is needed for this purpose is fuzzy logic. Basically, fuzzy logic is a system of reasoning and computation in which the objects of reasoning and computation are classes with unsharp (fuzzy) boundaries. In my view, human-level machine intelligence cannot be achieved without the use of fuzzy logic. What should be underscored is that this view is at variance with conventional wisdom.

A Litmus test of human-level machine intelligence is natural language understanding. In large measure, existing approaches to natural language understanding are based on bivalent logic and probability theory. In a natural language, a word, w, is typically a label of a class with unsharp (fuzzy) boundaries. In this sense, almost all words in a natural language have a fuzzy meaning. Examples. Tall, fast, heavy, beautiful, likely, etc. There are two choices in representing the meaning of a fuzzy word. First, as a probability distribution; and second, as a fuzzy set or, equivalently, as a possibility distribution. A problem which arises is: If the meaning of a word, w, is represented as a probability distribution, then not w cannot be represented as a probability distribution. By contrast, if the meaning of w is represented as a possibility distribution, then the meaning of not w is a possibility distribution which is very simply related to the possibility distribution of w. A more complex problem is that of composing the meaning of a proposition from the meanings of its fuzzy constituents. Traditional approaches to semantics of natural languages do not have this capability. Fuzzy logic has this capability because it is designed to compute with classes which have unsharp (fuzzy) boundaries.

In conclusion, I believe that to achieve human-level machine intelligence it will be necessary to employ fuzzy logic. This does not mean, however, that the use of fuzzy logic will necessarily lead to achievement of human-level machine intelligence. Many other problems will have to be solved. What is my conviction is that without the use of fuzzy logic, human-level machine intelligence cannot be achieved. As was stated earlier, this view is at variance with conventional wisdom. History will judge who is right.

The editors, Professors János Fodor and Róbert Fullér and the publisher, Springer, deserve our thanks and congratulations for producing a Volume which is a significant contribution to the literature of soft computing, fuzzy logic and robotics.

January 23, 2014

Lotfi A. Zadeh
Berkeley, CA

Preface

Soft computing, intelligent robotics and control, and some applied mathematical aspects – the main subjects of this volume – are in the core of interest of an illustrious and successful scientific researcher, an exceptional leader, and an incredibly great man. He is Professor Imre J. Rudas, the Rector of Óbuda University, Budapest, Hungary. He becomes 65 this April, and this fact motivated us to edit this volume. This is a token of appreciation and friendship of his colleagues, students and friends.

Professor Rudas's achievements are long-lasting both in science and in leadership. Because of space limitations we mention just a few facts and figures from his rich oeuvre. He has published more than 700 papers in books, scientific journals, and peer reviewed international conference proceedings, delivered more than 50 plenary talks at international conferences, and received more than 2000 independent citations for his publications. He founded Acta Polytechnica Hungarica, an international peer-reviewed scientific journal, which started to own impact factor after 6 years of its existence. He is the founder of seven IEEE sponsored international conference and symposium series. He is the only rector in the Hungarian higher-education who could establish a new university (Óbuda University) by upgrading an existing institution (Budapest Tech), through the fulfillment of high standards.

For those who do not know professor Rudas personally, we would like to picture him with the help of two appraisals.

Gyula Sallai (professor, Budapest University of Technology and Economics) writes as follows:

> "Imre J. Rudas is a prominent, distinguished personality of the Hungarian higher education, whose thoughts concentrate on strengthening the reputation and professional success of the organization directed by him, who is a strategist, professor and team builder in one person, who catches with keen insight:
>
> – the strategic opportunities,
> – the prospective breakthroughs in scientific research and
> – the effective professionals that can make stronger his team;

who establishes success of his institutional plans, and realizes them by

- firm faith, focusing on the objectives,
- carrying his smaller and larger collectives with him and
- receiving with recognition of the Hungarians within and beyond the frontier, and the wider international community;

who, nevertheless remains the man at all times, with whom it is good to be together, to turn an idea over in our mind or devise a plan, and to drink a glass of good wine."

János Dusza (professor at Óbuda University, Member of the Presidium of the Slovak Academy of Sciences, External Member of the Hungarian Academy of Sciences) writes:

"I first met Professor Rudas in 2011 in Kosice, Slovakia. Kosice is not just a city I call home but also where Prof. Rudas received his first Doctor Honoris Causa degree, conferred on him by the Technical University of Kosice.

I was, prior to our first meeting, very aware of his reputation as an internationally recognized expert in the field of computational cybernetics, robotics with special emphasis on robot control, fuzzy control and fuzzy sets.

Being a scientist active in the field of advanced ceramics and coatings, I was concerned that we would find little of common scientific overlap. I was delighted to find that not only were there many conversational topics we enjoyed discussing, but the possibility of future collaborative projects also became obvious.

At first, it was the interdisciplinary research into the field of robotics with regard to advanced materials with exceptional tribological properties. Professor Rudas's overview, knowledge of the initial problems and further collaborative suggestions were particularly welcome and greatly appreciated.

Secondly it was the management of education and research. Without hesitation, I would say that Professor Rudas's understanding, foresight and experience in strengthening his University's core ethos and reputation during his leadership was unsurpassed in anyone I had met before, or since.

The third area was in international collaboration. He provided strong support to many young scientists and members of the Hungarian scientific community in the Carpathian Basin and throughout the world. I highly appreciate these activities and I am very happy to have been personally involved.

I would particularly like to emphasize Professor Rudas's ability to see unrecognized skills and talents in others and his desire to ensure that each individual's potential is fully realized.

Only our personal friendship has meant more to me than our work together and I look forward to developing both in the future."

The present volume is a collection of 20 chapters written by respectable experts of the fields. Professor Rudas's wide spectrum of interests is reflected in the variety of these contributions, dealing with three major topics.

The first part of the book addresses issues of intelligent robotics, including robust fixed point transformation design, experimental verification of the input-output feedback linearization of differentially driven mobile robot and applying kinematic synthesis to micro electro-mechanical systems design.

The second part of the book is devoted to fundamental aspects of soft computing. This includes practical aspects of fuzzy rule interpolation, subjective weights based meta learning in multi criteria decision making, swarm-based heuristics for an area exploration and knowledge driven adaptive product representations.

The last part concerns with different problems, issues and methods of applied mathematics. This includes perturbation estimates for invariant subspaces of Hessenberg matrices, uncertainty and nonlinearity modelling by probabilistic metric spaces and comparison and visualization of the DNA of six primates.

The editors are grateful to the authors for their excellent work. Thanks are also due to Dr. Péter Kárász for his editorial assistance and sincere effort in bringing out the volume nicely in time.

We do hope that readers will benefit from the content of this volume, and will find it intellectually stimulating and professionally rewarding.

January 27, 2014

János Fodor
Robert Fullér
Budapest, Hungary

Contents

Part I: Intelligent Robotics and Control

Part II: Soft Computing

Part III: Applied Mathematics

Part I
Intelligent Robotics and Control

Control Algorithms for Plants Operating Under Variable Conditions, Applications

Stefan Preitl[1], Radu-Emil Precup[1], Zsuzsa Preitl[2], Alexandra-Iulia Stînean[1], Mircea-Bogdan Rădac[1], and Claudia-Adina Dragoş[1]

[1] Politehnica University Timisoara
Department of Automation and Applied Informatics
Bd. V. Parvan 2, RO-300223 Timisoara, Romania
{stefan.preitl,radu.precup,mircea.radac,claudia.dragos}@aut.upt.ro,
kassandra3107@yahoo.com
[2] Siemens AG, Erlangen, Germany (former at Politehnica University Timisoara and at Budapest University of Technology and Economics)
zsuzsap@yahoo.com

Abstract. The chapter deals with development, analysis and applicability of several easy applicable control algorithms, dedicated to plants working under continuously variable conditions: variable plant parameters or (the worst case) variable structure, variable reference and variable load (disturbance). Two speed control applications are selected and treated from the wide range of such applications: a case specific to the metallurgical industry, and the speed control of an electric (hybrid) vehicle model. The efficiency of the algorithms is tested and illustrated on different plant models and also on laboratory equipment with variable moment of inertia. The presented algorithms are easily adaptable to similar applications.

Keywords: Control algorithms, electrical driving systems, variable conditions, mathematical models, switching logic.

1 Introduction

Many industrial and non-industrial control applications are dedicated to plants working under continuously variable conditions, e.g., variable parameters and/or structure, variable reference and variable load disturbance, conditions which depends on the plant evolution. Representative applications are the domains of drives, i.e., electrical, hydraulic, pneumatic driving systems and thermal systems according to the examples given in [1–7].

Many theoretical and practical aspects may be solved in order to improve the control system performance expressed as performance specifications such as zero control error, robustness, good transients and disturbance rejection. For example:

1. The continuous variability of the inputs and parameters and the presence of the nonlinearities;

J. Fodor and R. Fullér (eds.), *Advances in Soft Computing, Intelligent Robotics and Control,* Topics in Intelligent Engineering and Informatics 8,
DOI: 10.1007/978-3-319-05945-7_1,

2. The presence of elasticity in power transfer (mechanical, for example) and derived, working in resonant regimes and suppress the oscillations, a notch filter may be inserted in the controller's structure [3, 5];
3. Complex optimization aspects in energy management [8, 9];
4. The presence of system noise and of actuating limits which reduce the control effect and the effect of the AWR measure, where the use of trajectory reference compensator and the mixing the effect of different modern control algorithms can ensure better robustness and control performances [2].
5. Nonlinearities in basic physical laws, for example, of the thermoelectric effects reflected, e.g., in Stefan-Boltzmann's law [10], etc.

Using the fact that in many applications relatively good models of the plant can be available, many theoretical, technical and practical control solutions can be developed and implemented as model-based control (MBC) solutions [2, 11–18] offering good control system performance.

Regarding the main idea, the control of plants working under continuously variable conditions, the chapter treats some easy applicable control algorithms. These algorithms are based on an output control strategy and tested on two class of application, on a laboratory equipments and/or simulation on detailed mathe-matical models of the plant.

The controlled plants are presented using relatively detailed Mathematical Models (MMs): the electrical driving system for an electric (hybrid) vehicle (EHV), for which the moment of inertia is relatively constant for a drive cycle, and a drive system with continuously Variable Moment of Inertia (VMI). Both plants have continuously variable inputs (reference and disturbance). Both applications are connected to drives with BLDC motors (BLDC-ms) or, particularly, with DC motors (DC-ms), using Cascade Control Structures (CCSs).

2 Practical Control Structures and Algorithms, Development Aspects for Plants Working Under Continuously Variable Conditions

A set of control algorithms (c.a.s) will be presented as follows as output control strategies. A part of the c.a.s is based on a single control loop and another one is based on the CCs. The analysed structures make use of an optimised inner (current) control loop. Therefore, the main control task, namely the speed control, is fulfilled by the main loop, by the speed controller which must be well designed.

2.1 The Classical Control Loop with PI(D) Controller

Due to the fact that the application is characterized mainly by continuously variable parameters in a relatively large domain, the control solution with bump-less switching of the c.a. can be a good, practical and relatively easily to implement option. The structure of this control solution is given in Fig. 1.

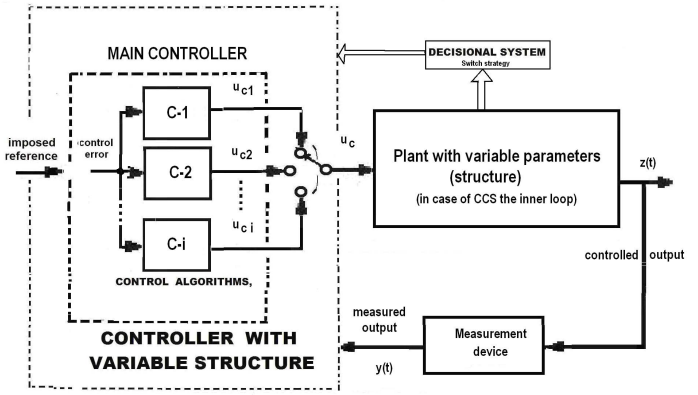

Fig. 1. The CCS with a switching logic for a speed controller

If the parameters of the plant are continuously variable and, as a consequence, the model can be easily linearised, the main aim of the designer is to bring the model in a benchmark type form [11]. Therefore, the design using classical or derived PI(D) control structures, becomes very convenient, and switching c.a.s are usable.

For example the switching structure for the classical PI controller with the transfer function (t.f.).

$$H_C(s) = \frac{k_c}{s}\left(1 + sT_c\right) = \frac{k_C}{sT_i}\left(1 + sT_i\right), \tag{1}$$

is presented in Fig. 2, and the corresponding digital c.a. has the form

$$\begin{aligned} u_{jk} &= -\frac{p_{1pi}^{(j)}}{p_{0pi}^{(j)}} \cdot u_{j,k-1} + \frac{q_{1pi}^{(j)}}{p_{0pi}^{(j)}} \cdot e_{j,k-1} + \frac{q_{0pi}^{(j)}}{p_{0pi}^{(j)}} \cdot e_{jk}, \\ j &= 1, 2, 3 \text{ c.a.}(j), \qquad e_{jk} = e_k \end{aligned} \tag{2}$$

with the parameters given by

$$\begin{aligned} q_{0pi} &= k_C + \frac{k_C T_e}{2T_i}, \quad & q_{1pi} &= -\left(k_C - \frac{k_C T_e}{2T_i}\right), \\ p_{0pi} &= 1, & p_{1pi} &= -1. \end{aligned} \tag{3}$$

In the cases of the considered applications, both of them as electrical driving systems, the design methods due to Kessler (the Modulus-Optimum method, MO-m and the Symmetrical Optimum method, SO-m synthesized in [11]) and various extensions derived from them are strongly recommended. Some remarkable extensions have been proposed by different authors: the Extended

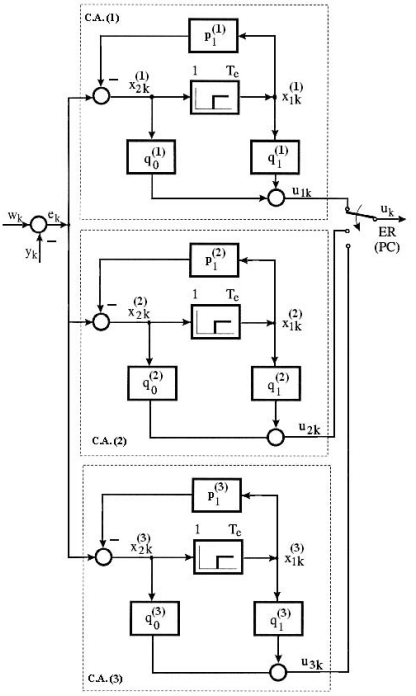

Fig. 2. Detailed block diagram of controller switching

Symmetrical Optimum method, ESO-m [17], the double parameterization based Symmetrical Optimum method, 2-p-SO-m given in [9] and also synthesized in [59], and [18–23, 27], etc. Moreover, the use of controllers with non-homogenous structure allows the construction of different forms of 2-DOF PI(D) structures [25–27] (Fig. 3).

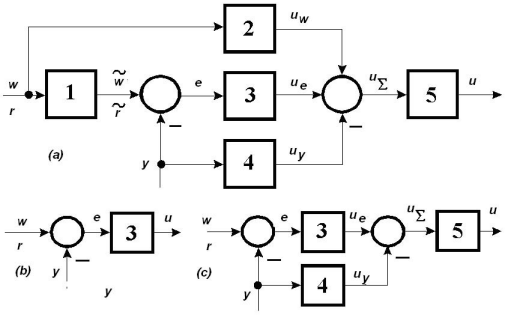

Fig. 3. Typical classical controller structures with extensions (basis for 2-DOF PI(D) controllers)

Due to the modifications of plant parameters, modifications in the c.a. must be included in different forms. Therefore, the controllers with switching can be considered as adaptive. They should have the benefit of taking into account such variations and retune its parameters. The switching structure is presented for the classical discrete PI c.a., but it can represent also other derived structures. Illustrative examples can be the Takagi-Sugeno PI type fuzzy controllers, the classical 2-DOF controllers, etc.

Beside the classical PI controller, the next section will consider the main controller in extended forms of 2-DOF and 2-DOF-PI(D) controllers, a PI Takagi-Sugeno Fuzzy Controller, a PI Quasi-Relay Sliding Mode controller and a Neuro-Fuzzy controller. The theoretical support for the controller design has been reported by the authors in terms of different forms. All solutions are based on the locally linearised MMs.

2.2 The Classical 2-DOF Control Loop and Extensions to 2-DOF PI(D) Controllers

The Basic structure. Polynomial design technique. The Control Structure (CS) with a 2-DOF controller uses two distinct controllers, Fig. 4, where (1) the reference filter with discrete t.f. $T(z)$ and (2) the feedback controller with discrete t.f. $S(z)$. The common part is represented by the discrete t.f. $R(z)$, which include the integral components of the controller.

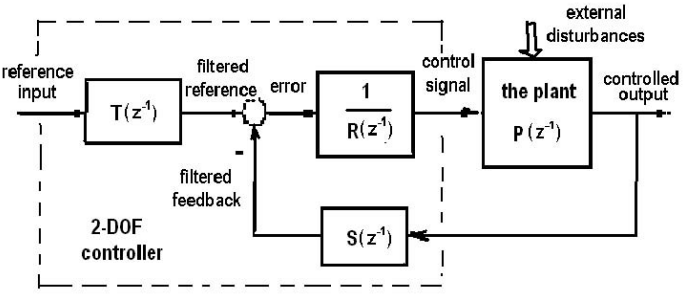

Fig. 4. Structure of the classical 2-DOF controller and control structure

In opposite with an one Degree of Freedom controller (1-DOF), in case of the 2-DOF controller structure, the enlisted requirements (Section 2.1) can be separately adjusted without influencing one another. The pragmatic design technique seat of the solution of a polynomial Diophantine equation, with different

particularities in treating constrains [9, 29, 32]. Supposing the plant characterised with the pulse transfer function (t.f.) calculated from the continuous model:

$$\begin{aligned} P(z) &= \left(1 - z^{-1}\right) Z\left\{\frac{P(s)}{s}\right\} \quad \text{and} \\ \frac{B(z)T(z)}{A(z)R(z) + B(z)S(z)} &= \frac{B_m(z)}{A_m(z)} \frac{A_0(z)}{A_0(z)}, \end{aligned} \tag{4}$$

where the servo performance specifications are imposed by a reference model in the form $B_m(z)/A_m(z)$, $T(z)$, $R(z)$, $S(z)$ are unknown polynomials; $A_m(z)$ determine the poles of the closed loop and $A_0(z)$ is the observer polynomial. Different causality conditions and degree conditions for the polynomials must be imposed in the development of the classical 2-DOF controller.

After accomplishing all operations, the final form of the Diophantine equation over the ring of polynomials is

$$A(z)R'(z) + B^-(z)S(z) = A_m(z)A_0(z) \tag{5}$$

having as solutions the coefficients of the $T(Z)$, $R(z)$, $S(z)$ polynomials. The polynomials $B^-(z)$ and $R'(z)$ in (5) are components of the factorized forms of $B(z)$ and $R(z)$ as follows:

$$B(z) = B^+(z)B^-(z) \quad \text{and} \quad B_m(z) = B^-(z)B'_m(z) \tag{6}$$

$$R(z) = B^+(z)R'(z) \quad \text{and} \quad R'(z) = (z-1)^1 R_1(z) \tag{7}$$

The $T(z)$, $R(z)$, $S(z)$ polynomials are finally obtained. Other development strategies are given in [31] and [36].

2-DOF PI(D) structures. Fig. 5 gives some particular structures derived from Fig. 3 [18, 25–27]. If the controllers presented in Fig. 5 are characterized by continuous t.f. with the tuning parameters $\{k_R, T_i, T_d, T_f\}$ [11], the expressions of $C(s)$ and $C_F(s)$ are [29]:

$$\begin{aligned} C(s) &= \frac{u(s)}{e(s)} = k_R \left(1 + \frac{1}{sT_i} + \frac{sT_d}{1 + sT_f}\right), \\ C_F(s) &= \frac{u_f(s)}{r(s)} = k_R \left(\alpha_1 + \alpha_2 \frac{sT_d}{1 + sT_f}\right). \end{aligned} \tag{8}$$

For the structure given in Fig. 5(b) (with the notation) the t.f.s are

$$\begin{aligned} C^*(s) &= \frac{u(s)}{e(s)} = k_R \left[(1 - \alpha_1) + \frac{1}{sT_i} + (1 - \alpha_2) \frac{sT_d}{1 + sT_f}\right], \\ C_P(s) &= \frac{u_f(s)}{r(s)} = k_R \left(\alpha_1 + \alpha_2 \frac{sT_d}{1 + sT_f}\right). \end{aligned} \tag{9}$$

Depending on the values of α_1 and α_2 (parameters), for the presented blocks the behaviours from in Table 1 are obtained. The choice of a certain representation of the controller depends on:

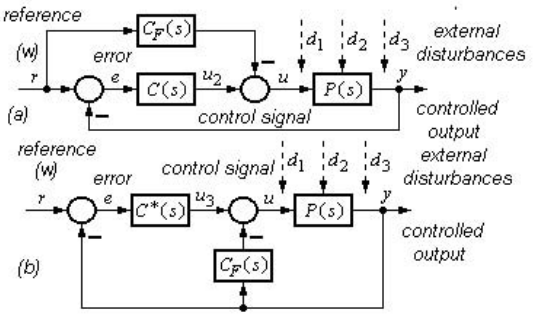

Fig. 5. Structures of 2-DOF PI(D) controllers as extension of an 1-DOF controller

1. The structure of the available controller;
2. The adopted algorithmic design method; and
3. The result of this design.

The table contains information regarding a possible extension with a reference filter $F(s)$.Other connections between 2-DOF and extended with input filters of 1-DOF controller structures are synthesized in [26, 29–31, 33], etc.

Table 1. Connections between 2-DOF controller and extended 1-DOF controller structure (P – proportional, D – derivative, I – integral, L1(2) – first (second) order filter with lag)

		$F(s)$	–	$F(s)C(s)$	$C(s)$	Remarks
Fig. 4(a)		–	C_F	$C(s) - C_F(s)$	$C(s)$	–
Fig. 4(b)		–	C_P	$C^*(s)$	$C^*(s) + C_P(s)$	–
α_1	α_2	–	–	(ref. channel)	(feedback)	
0	0	1	0	PID	PID	1-DOF controller
0	1	PDL2	DL1	PI	PID	1-DOF with non-
1	0	PD2L2	P	PID-L1	PID	homogenous behaviour
1	1	PL2	PDL2	I	PID	
α_1	α_2	PID controller with pre-filtering (2-DOF controller)				

2.3 Extensions to Fuzzy Controller Solutions. 2-DOF Takagi-Sugeno PI(D) Fuzzy Controllers

The Takagi-Sugeno PI quasi-continuous fuzzy controller structure (TS-PI-FC) with output integration (OI), Fig. 6, was adopted based on the continuous-time PI controller solution. The algorithm is modelled by the recurrent equations

with variable parameters; finally this leads to the PI quasi-continuous digital controller with output integration (OI) [30, 31, 36]:

$$\begin{aligned} \Delta u_k &= K_P \Delta e_k + K_i e_k = K_P \left(\Delta e_k + \alpha e_k\right), \\ K_P &= k_C \left(1 - \frac{T_e}{2T_i}\right), \quad K_i = \frac{k_C T_e}{T_i} \quad \alpha = \frac{K_i}{K_P} = \frac{2T_e}{2T_i - T_e}, \\ B_{\Delta e} &= \frac{K_i}{K_P} B_e, \quad B_{\Delta e} = \alpha B_e, \quad B_{\Delta u} = K_i B_e \end{aligned} \tag{10}$$

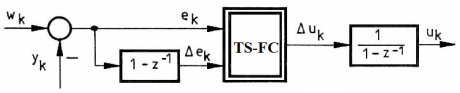

Fig. 6. TS-PI-FC (OI) structure with output integration

The TS-PI-FC is characterized by the following features:

(i) The fuzzification is performed by means of three membership functions $\{N, ZE, P\}$ pointing out the TS-PI-FC tuning parameters $\{B_e, B_{\Delta e}, B_{\Delta u}\}$;
(ii) The inference engine uses the SUM and PROD operators assisted by the rule base presented in Table 2 [3]; and
(iii) It employs the weighted average method for defuzzification.

Table 2. Rule base of TS-PI-Fuzzy Controller with Output Integration (also for Input Integration)

$\Delta e_k / e_k$	N	ZE	P
P	$K_{p1}[\Delta e_k + \alpha_1 e_k]$	$K_{p2}[\Delta e_k + \alpha_2 e_k]$	$K_{p3}[\Delta e_k + \alpha_3 e_k]$
ZE	$K_{p4}[\Delta e_k + \alpha_4 e_k]$	$K_{p5}[\Delta e_k + \alpha_5 e_k]$	$K_{p6}[\Delta e_k + \alpha_6 e_k]$
N	$K_{p7}[\Delta e_k + \alpha_7 e_k]$	$K_{p8}[\Delta e_k + \alpha_8 e_k]$	$K_{p9}[\Delta e_k + \alpha_9 e_k]$

The expressions of the c.a.s are

$$\begin{aligned} u_{jk} &= u_{j,k-1} + K_{Pi}^{(j)} \left[\left(1 - \alpha_i^{(j)}\right) e_{jk} - e_{j,k-1}\right], \quad i = 1, \ldots, 9 \\ e_{jk} &= w_k - y_k = e_k, \qquad\qquad\qquad\qquad j = 1, 2, 3 \text{ for the c.a.}(j) \end{aligned} \tag{11}$$

Extended 2-DOF PI(D) Fuzzy Control structures can be defined on the basis of the structures illustrated in Fig. 5 and 6. 2-DOF FCs are proposed in [30] and [31], and they are defined on the basis Takagi-Sugeno fuzzy blocks FB-Tc as illustrated in Figs. 7 to 10.

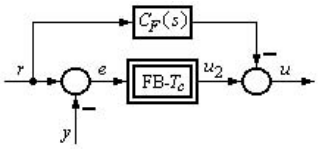

Fig. 7. Structure of feed-forward 2-DOF PI-fuzzy controller

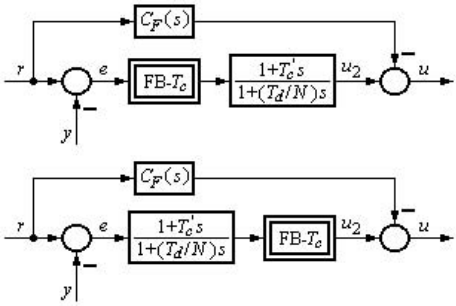

Fig. 8. Structures of feed-forward 2-DOF PID-fuzzy controllers

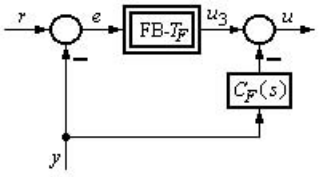

Fig. 9. Structure of feedback 2-DOF PI-fuzzy controller

To develop the PI(D)-FC, the continuous-time PI controllers must be expressed in one of its incremental PI quasi-continuous digital version (10), that leads to

$$\Delta u_{i,k} = K_{Pi}\Delta e_{i,k} = K_{Ii}\left(\Delta e_{i,k} + \delta_i e_{i,k}\right), \qquad i = \overline{1,2}, \tag{12}$$

where $\{K_{Pi}, K_{Ii}, \delta_i\}$ can be easily calculated from the continuous t.f. The rule bases of the two blocks FC_i can be expressed in terms of the decision table shown in Table 3, representing the consequent part of the inference rules.

The strictly positive parameters of the PI-FCs are $\{B_{ei}, B_{\Delta ei}, B_{\Delta ui}, m_i, n_i, p_i\}$ which are in correlation with the shapes of the input membership functions, Fig. 11, and the parameters m_i, n_i and p_i (Table 3), $m_i < n_i < p_i$, have been added to the standard version of PI-FCs to improve the CS performance by modifying the input-output static map of the blocks FC_i.

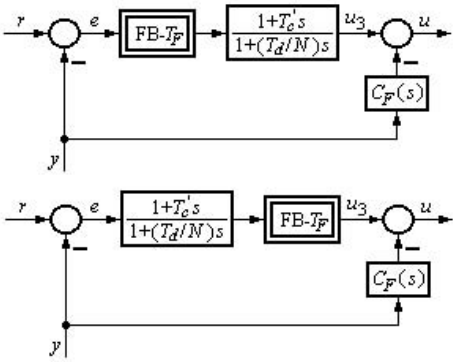

Fig. 10. Structures of feedback 2-DOF PID-fuzzy controller

Table 3. Decision Table of FCi, $i = \overline{1,2}$

$\Delta e_{i,k} \setminus e_{i,k}$	NB	NS	ZE	PS	PB
PB	$\Delta u_{i,k}$	$m_i\Delta u_{i,k}$	$n_i\Delta u_{i,k}$	$p_i\Delta u_{i,k}$	$p_i\Delta u_{i,k}$
PS	$m_i\Delta u_{i,k}$	$\Delta u_{i,k}$	$m_i\Delta u_{i,k}$	$n_i\Delta u_{i,k}$	$p_i\Delta u_{i,k}$
ZE	$n_i\Delta u_{i,k}$	$m_i\Delta u_{i,k}$	$\Delta u_{i,k}$	$m_i\Delta u_{i,k}$	$n_i\Delta u_{i,k}$
NS	$p_i\Delta u_{i,k}$	$n_i\Delta u_{i,k}$	$m_i\Delta u_{i,k}$	$\Delta u_{i,k}$	$m_i\Delta u_{i,k}$
NB	$p_i\Delta u_{i,k}$	$p_i\Delta u_{i,k}$	$n_i\Delta u_{i,k}$	$m_i\Delta u_{i,k}$	$\Delta u_{i,k}$

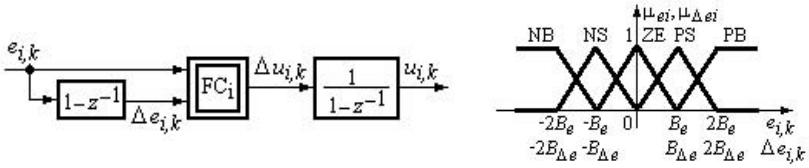

Fig. 11. The PI-FC structure and initial input membership functions of FC_i, $i = \overline{1,2}$

The development method dedicated to the two TS-PI-FCs consists of five steps detailed in [25, 33, 35].

Other TS-FC-based control solution for plants with time variable parameters – e.g. with VMI – are presented in [28, 34] where a Two Input-Single Output Takagi-Sugeno (TISO) Linear Time Variant (LTV) is used to model the controlled plant. Other applications are presented also in [37, 38].

2.4 The PI Quasi-Relay Sliding Mode Controller

The structure of a classical PI quasi relay sliding-mode controller with parameter adaptation is presented in Fig. 12. The design steps of the controller are presented as follows on the basis of mainly [12] and [17]:

(a) For the classical PI part. (i) The variable parameter T_i can be determined in terms of the pole-zero cancellation regarding the t.f. of the plant.
(b) For the sliding mode part. (ii) The positive parameter c is chosen taking into account the imposed performance: $c < a_2$, where a_2, a_1 and b are the parameters in Ackerman's form of the state-space representation of the plant model; (iii) The parameter α is calculated by taking into account the desired existence domain for the sliding mode control.

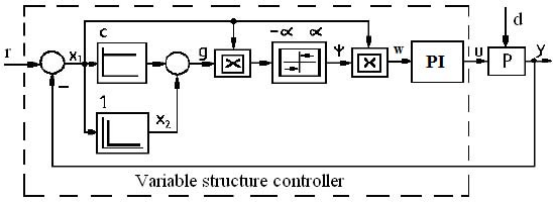

Fig. 12. The PI quasi relay sliding mode controller (the classical structure)

The control law is presented in its parallel form

$$\begin{aligned} u(t) &= \Psi(t)x_1(t) + \frac{1}{T_i}\int_0^t \Psi(\tau)x_1(\tau)\mathrm{d}\tau, \qquad x_1 = e, \\ \Psi(t) &= \alpha \,\mathrm{sgn}\left\{g(t)x_1(t)\right\}, \end{aligned} \tag{13}$$

where the parameter α is tuned in terms of

$$\alpha < \frac{-\left|\left(c^2 - a_2 c + a_1\right)x_1(t) - f(t)\right|}{|x_1(t)| + \frac{1}{T_i}\int_0^t x_1(\tau)\mathrm{d}\tau}. \tag{14}$$

The expressions and parameters of the digital c.a.s are similar to (10) and (11), having different values and with the expressions of the control algorithm also given in [24, 31, 40–43].

2.5 The Hybrid Neuro-Fuzzy TS PI Controller and the Design Approach

The presented structure of the extended fuzzy control system contains a hybrid Takagi-Sugeno PI-neuro-fuzzy controller (T-S PI-N-FC) [4] Fig. 13, where: AB is the adaptation block, RM is the reference model, r is the reference input, e_k

is the control error, k is the index of the current sampling interval, $k \in \mathbb{Z}$, and q^{-1} is the backward shift operator.

The parameter $B_{e,k}$ replaces the parameter B_e specific to the T-S PI-FC with Input Integration (-II) [3, 12, 17] given in Fig. 14. T-S FB is the nonlinear Takagi-Sugeno fuzzy block without dynamics; $e_{I,k}$ is the integral of control error e_k:

$$e_{Ik} = e_{I,k-1} + T_s e_k, \qquad T_k \text{ – the sampling period.} \tag{15}$$

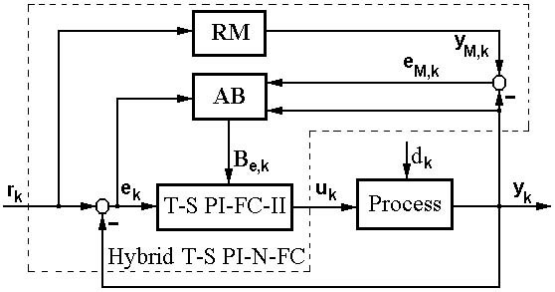

Fig. 13. Fuzzy control system structure with hybrid T-S PI-NF-C

T-S FB has the following features: (i) The fuzzification is carried out by means of the input membership functions presented in Fig. 14(b), which points out two tuning parameters, B_e and B_{eI}; (ii) It uses the SUM and PROD operators in the in-ference engine, and the weighted average method for defuzzification.

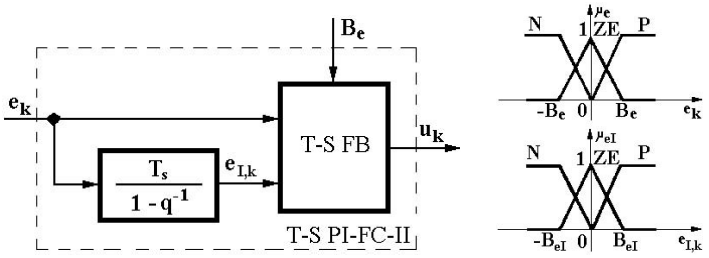

Fig. 14. Structure of T-S PI-FC-II and the input membership functions

The complete rule base of T-S PI-FC-II is formulated such that to ensure the combination of nine separately designed PI controllers with t.f.s given in (1) rewritten with superscripts:

$$H_C^m(s) = \frac{k_C^m}{sT_i^m}\left(1 + T_i^m s\right), \qquad m = 1, \ldots, 9. \tag{16}$$

Discretising (16), the quasi-continuous digital PI control algorithm results as

$$u_k^m = k_C^m e_k + \frac{k_C^m}{T_i^m} e_{I,k}, \qquad m = 1, \ldots, 9, \tag{17}$$

u_k^m is the control signal produced by the m^{th} PI algorithm, $m = 1, \ldots, 9$. The algorithms are introduced in the consequents of the rules of T-S PI-FC-II, expressed as

$$\begin{aligned} \text{Rule } m\text{:} \quad & \text{IF } e_k \text{ IS } LT_{m1} \text{ AND } e_{I,k} \text{ IS } LT_{m2} \\ & \text{THEN } u_k^m = k_C^m e_k + \frac{k_C^m}{T_i^m} e_{I,k}, \qquad m = 1, \ldots, 9, \end{aligned} \tag{18}$$

where $LT_{ml} \in \{N, ZE, P\}$, $m = 1, \ldots, 9$, $l \in \{1, 2\}$ are the input linguistic terms with the membership functions defined in Fig. 14(b). The modal equivalence principle [18] is applied and modified to obtain the covering of all input linguistic terms:

$$B_{eI} = \left(\min_{m=1\ldots9} T_i^m \right) B_e. \tag{19}$$

The parameter B_e is online adapted by the Model Reference Adaptive Control (MRAC) structure presented in Fig. 14 and is discussed in details in [56, 57]. Based on the (continuous) t.f., the RM block sets the CS performance specifications. The AB consists of a single unbiased neuron with a linear activation function, characterized by a recurrent equation that ensures the training in the framework of back propagation with momentum factor [56]:

$$\begin{aligned} w_k &= -\eta e_{M,k} \frac{\Delta y_k}{\Delta B_{e,k}} e_k + \lambda \Delta w_{k-1}, \\ w_k &= w_{k-1} + \Delta w_k, \\ B_{e,k} &= q_k e_k, \end{aligned} \tag{20}$$

where w_k is the input weight of the neuron, $0 \leq \eta \leq 1$ is the learning rate, and $0 \leq \lambda \leq 1$ is the momentum factor. More details regarding the design are presented in [56–58].

The design approach guarantees the stability of the fuzzy control system. The fuzzy control system dedicated to a class of servo systems with variable parameters ensures the behaviour of control systems with bump-less combinations of separately tuned linear PI controllers as shown in [23, 25, 30].

3 Examples of Electrical Driving Systems. Mathematical Models

In the symmetrical operating mode the Mathematical Models (MMs) of BLDC-ms and of classical DC-ms are very close [6, 7, 44–47]. That leads to similarities in the derived benchmark-type models used in development of control solutions.

Since the control of the main characteristic variables (speed and position) of servo drives with DC-m and BLDC-m is well-known and product on a large scale by industry such control solutions are characterized as LCA solutions. The inner loop (the current loop) can differ but it can be relatively easy optimized.

3.1 The Mathematical Model of a BLDC-m (Servo Drive)

The matrix form of the main equations of the MM of a BLDC-m is given in [6, 7, 44–47, 50]:

$$\begin{bmatrix} V_{AS} \\ V_{BS} \\ V_{CS} \end{bmatrix} = \begin{bmatrix} R_a & 0 & 0 \\ 0 & R_b & 0 \\ 0 & 0 & R_c \end{bmatrix} \begin{bmatrix} i_{as} \\ i_{bs} \\ i_{cs} \end{bmatrix} + \frac{\mathrm{d}}{\mathrm{d}t} \begin{bmatrix} L_a & L_{ab} & L_{ac} \\ L_{ba} & L_b & L_{bc} \\ L_{ca} & L_{cb} & L_c \end{bmatrix} \begin{bmatrix} i_{as} \\ i_{bs} \\ i_{cs} \end{bmatrix} + \begin{bmatrix} e_a \\ e_b \\ e_c \end{bmatrix}, \quad (21)$$

where: R_a, R_b, R_c and L_a, L_b, L_c – the resistance and the phase inductance, L_{ab}, L_{bc}, L_{ca} – the mutual (between phases) inductance, e_a, e_b, e_c – the electromotive voltage, V_{AS}, V_{BS}, V_{CS} and i_{as}, i_{bs}, i_{cs} – the phase voltages and currents. Based on it, the electromagnetic torque me of BLDC-m results as

$$m_e = \frac{e_a i_{as} + e_b i_{bs} + e_c i_{cs}}{\omega_r}. \quad (22)$$

The model for the mechanical part – the movement equation is well-known:

$$m_e = J_e \frac{\mathrm{d}}{\mathrm{d}t} \omega_r + k_f \omega_r + m_{\mathrm{Load}}, \quad (23)$$

where m_{Load} is the load torque (i.e., a time variable load-type disturbance) and the moment of inertia (constant or more generally, time variable) can be expressed as

$$J_e(t) = J_{\mathrm{BLDC}+J_{\mathrm{mech}}(t)}. \quad (24)$$

Based on functionality of the BLDC-m, the informational block diagram of a BLDC-m with permanent magnets is appropriate to the informational block diagram of the DC-m. A block diagram of a BLDC-m drive developed for the control purpose is represented in Fig. 14 [33]. This diagram is related to the detailed online switching scheme for the PWM converter illustrated in Fig. 15. Extensive control strategies for BLDC-m applications described in literature.

3.2 The Mathematical Model of an Electric HEV with DC-m (BLDC-m)

The traction and the optimization of fuel consumption for an electric vehicle (EV) (more generally, HEV) [9] consists in the electric driving system but can include extensions relative the primary energy sources [8, 9, 51]. The primary energy sources of these vehicles can be different:

1. Pure electrical sources, based on batteries;
2. Hybrid primary energy sources with different structures and components.

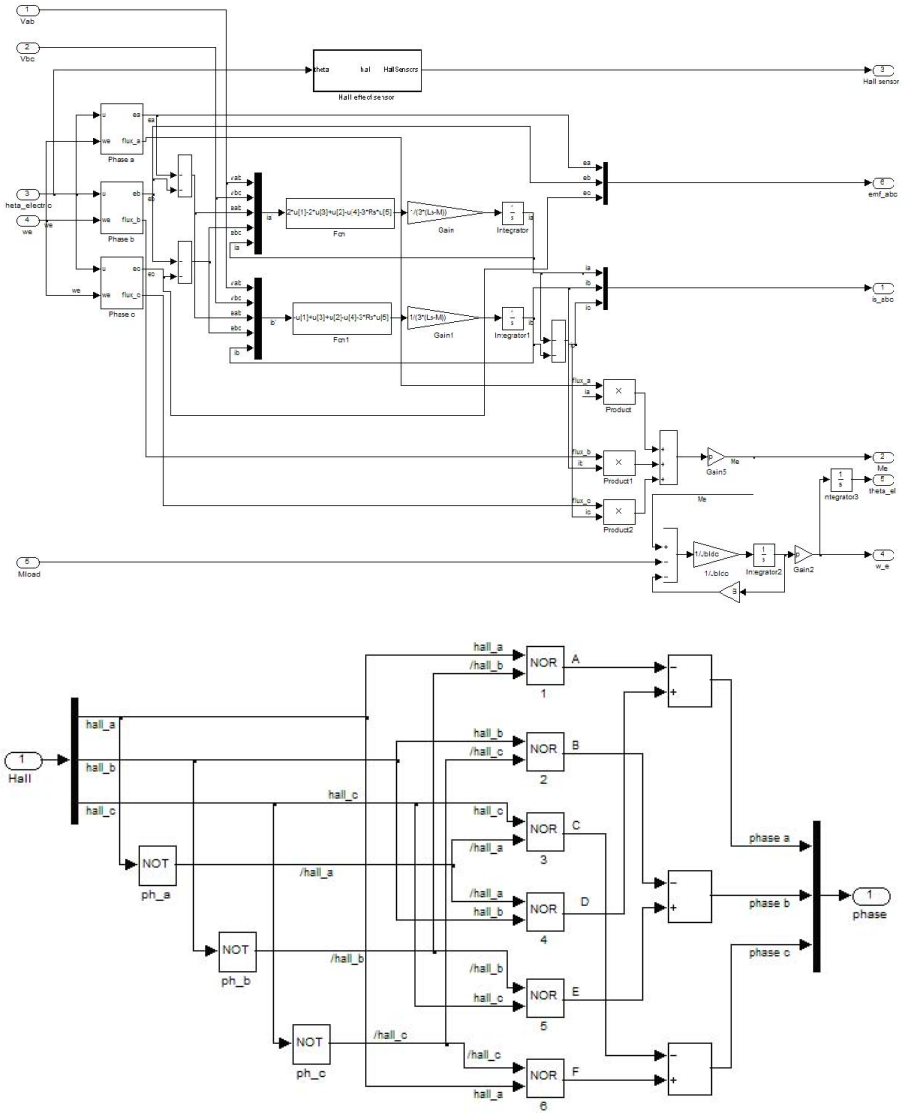

Fig. 15. The equivalent circuit of a BLDC-m control solution

In case of HEVs, the electrical machine, e.g., the DC-m or the BLDC-m, can work as a motor (traction regime) or as a generator (in regenerative braking regime). Considering the case of DC-m the functional block diagram of an electrical driving system as part of an HEV (EV) is presented in Fig. 16, and it offers support for detailed mathematical modelling [6, 7, 9, 48, 49].

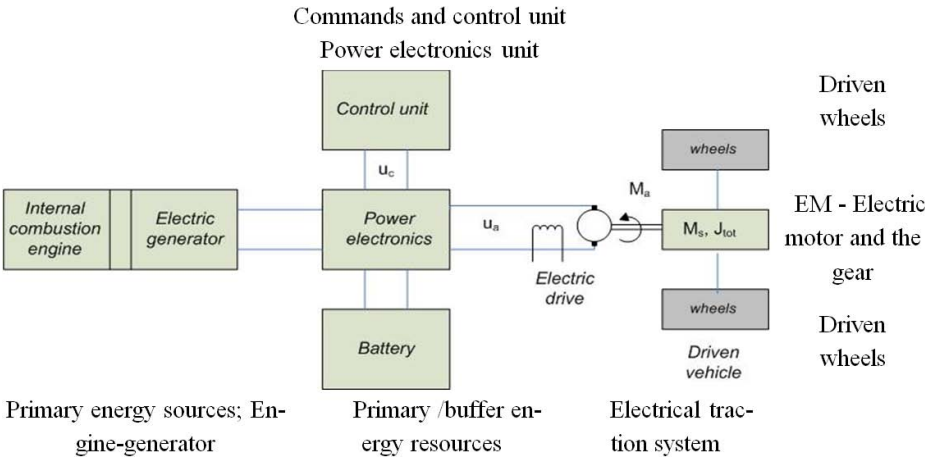

Fig. 16. Basic diagram of a hybrid electric vehicle

Vehicle Movement. The vehicle dynamics can be modelled using the basic dynamical relations for vehicle motion, considering also the rolling resistance, hill climbing and aerodynamic drag. The basic relations that describe the driven sys-tem consist of the simple longitudinal dynamics of the vehicle are

$$\omega(t) = \frac{f_r}{w_r} v(t), \qquad M_d(t) = \frac{w_r}{f_r} F_d(t), \tag{25}$$

$$F_d(t) = m\dot{v}(t) + \frac{1}{2}\rho v^2(t) A_d C_d + mg\big(\cos(\gamma(t))C_r + \sin(\gamma(t))\big). \tag{26}$$

where F_d is the drive force, m is the mass of vehicle, v is its velocity, ρ is the air density, A_d is the frontal area of the vehicle, C_d is the air drag coefficient, C_r is the rolling resistance coefficient, γ is the road rise angle, $M_d = M_s$ is the torque required from the EM, f_r is the final drive ratio, and w_r is the wheel radius.

Driving System with DC-m. The basic equations that characterize the functionality of the system are

$$\begin{aligned} L_a di_a + R_a i_a = u_a - e \quad \text{with} \quad u_a \approx k_A u_c, \qquad T_a = \frac{L_a}{R_a}, \\ e = k_e \omega, \qquad M_a = k_m i_a, \qquad M_d(t) = \frac{w_r}{f_r} F_d(t), \\ J_{\text{tot}0}\dot{\omega} = M_a - M_s - M_f, \qquad J_{\text{tot}} = J_m + J_{\text{veh}} + J_w, \end{aligned} \tag{27}$$

where the classical notations were used (in SI units). The inertia of the system can change with maximum +50% (in some cases much more) regarded to the basic value $J_{\text{tot}0}$, which corresponds to the vehicle without passengers, is

$$J_{\text{tot}} = J_{\text{tot}0} + \Delta J_t \quad \text{with} \quad \Delta J_t \le 0.50 J_{t0}. \tag{28}$$

Using equations (25)–(27), the block diagram of system can be built and based on it, the t.f. with respect to the control signal $H_{\omega,uc}(s)$ can be derived

$$H_{\omega,uc}(s) \approx k_A \frac{1/k_e}{(1+sT_a)(1+sT_m)} \quad \text{with} \quad T_m = \frac{J_{\text{tot}} R_a}{k_m k_e}, \tag{29}$$

where T_m is the mechanical time constant, and this form corresponds to a second order with lag benchmark type model.

Numerical data related to the application (as part of an HEV) are defined in [52] and used in [9] and presented in Table 4. Other electrical data (from the car builder): $R_a \approx 0.1\ \Omega$; $k_A = 30$ V/V, gain and time constant of actuator; $k_{Mi} = 0.0238$ V/A; $k_{M\omega} = 0.0178$ V/(rad/sec) gains for current and speed sensors.

Table 4. Numerical values for the DC-m

Torque [Nm]	Rotation [rot/min]	Usef.power [kw]	Voltage [V]	Current [A]	Nom.Power [kw]	Efficiency [%]	El.time const [sec]
50.16	1605	8.43	77.6	126	10.00	86.18	0.1

Numerical values regarded to the vehicle (from the car builder) [9]: total mass of vehicle, including an 80 kg heavy driver: $m_{\text{tot}} = 1860$ kg; frontal area of vehicle: $A_d = 2.4\ \text{m}^2$; air drag coefficient: $C_d = 0.4$; air density: $\rho = 1.225\ \text{kg/m}^3$; rolling resistance coefficient: $C_r = 0.015$; wheel radius: $w_r = 0.3$ m; final drive ratio: $f_r = 4.875$ Nm/(rad/sec). Using the energy conservation principle, the numerical value is

$$J_{\text{veh}} = 1860 \cdot \frac{0.3^2}{4.875^2} = 7.04\ \text{kg m}^2. \tag{30}$$

Let us consider the moment of inertia of the wheels and electric motor, J_W, then result the value of the total inertia J_{tot}:

$$J_W = 1.56\ \text{kg m}^2, \qquad J_{\text{tot}} = J_{\text{veh}} + J_W = 8.6\ \text{kg m}^2 \tag{31}$$

which is reflected in the mechanical time constant of the plant. For the two time constants are $T_m = 5.43$ sec and $T_a = 0.1$ sec resulting in a value of $m \approx 0.2$. This value can be used in controller design based on 2p-SO-m [9, 27].

3.3 Application with Variable Inputs and Variable Moment of Inertia

Some driving systems are characterized by variable inputs, VMI and coupled oscillating mechanisms. For such applications, the developer of a proper c.a. must solve three main problems:

1. The adequate modification of the reference input (ω_0);
2. The choice of a proper CS and tuning method for the controller for the plant working under the VMI conditions;
3. Attenuate the oscillations (this problem, solved in [3], is not treated in this chapter).

The treated example concerns the speed control of a winding system, Fig. 17, having a rigid connection in the driving part. In case of a winding process [33], the main conditions to be fulfilled by the control solutions are

$$\begin{aligned} v_t(t) = \text{const} \quad &\Rightarrow \quad \omega_0(t) = \frac{k}{r_t(t)}, \\ f_t(t) = \text{const}, \quad &\text{and} \quad J_e(t) = \frac{1}{2}\rho\pi l r^4(t). \end{aligned} \tag{32}$$

The continuous change of the reference $\omega_0(t)$ can be ensured on the basis of the radius $r(t)$. The speed control can be solved in various ways, for example:

1. Using a cascade CS with two loops - the current loop - and the speed loop (With, conventional or advance controller, see paragraph 4);
2. Using a state feedback CS and superpose and a Zero-Steady-state Error Controller.

The changing in a large domain of the equivalent moment of inertia $J_e(t)$, illustrated in Fig. 18, requires much attention in the controller design.

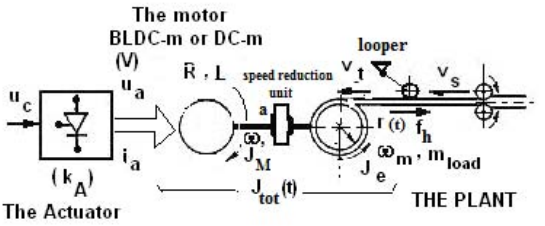

Fig. 17. Functional diagram of VIWP and reference input correction system

Neglecting the frictions, simplified but highly acceptable state-space MMs of the plant can be derived. Indifferent from the motor type (BLDC-m or DC-m), linearising the model at some representative operating points, the following simply input-output benchmark-type t.f.s can be obtained (see also (29)):

– in the speed control applications:

$$\begin{aligned} H_P(s) &= \frac{k_P}{(1+sT_\Sigma)(1+sT_1)} \quad \text{or} \\ H_P(s) &= \frac{k_P}{(1+sT_\Sigma)(1+sT_1)(1+sT_2)}, \end{aligned} \tag{33}$$

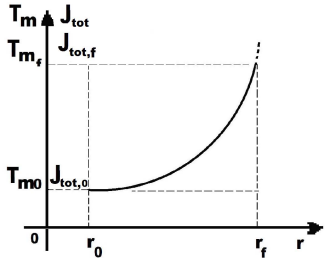

Fig. 18. The inertia and mechanical time constant variation as function of drum radius

– in the position control applications:

$$H_P(s) = \frac{k_P}{s\,(1 + sT_\Sigma)} \quad \text{or}$$
$$H_P(s) = \frac{k_P}{s\,(1 + sT_\Sigma)\,(1 + sT)}, \tag{34}$$

with $T_1 > T_2 \gg T_\Sigma$, but $T_1 = f(J_e(t))$ is/can be time-variable, Fig. 18.

If the variation range of $J_e(t)$ is relatively small the controller structure can be relatively simply; if the variation range of $J_e(t)$ is large, adaptive or variable structure controllers must be used [33]. However, the evaluation of the VMI ($J_e(t)$) can be a difficult task for the control designer. If the parameters changing $\{l, r(t), \rho\}$ are measurable, the problem has relatively easy solutions. If not, the changes in inertia can be evaluated using different estimation schemes; for example in [3], a relatively simple stable observer for a single-mass mechanical model of the plant is presented; more complex fuzzy model observers were developed and presented in literature.

The developed bump-less switching strategy in the controller structure (algorithm) (Figs. 1 and 2) is applicable without difficulties to both mentioned c.a.s, the classical PI(D) controller and the TS-FCs. The developed CSs are discussed considering two case studies (plants):

The simulated case that involves DC-m drive with VMI, characterized by the following parameters: rated voltage $u_{an} = 24\,\mathrm{V}$, rated current $i_{an} = 3.1\,\mathrm{A}$, rated speed $\omega = 3000\,\mathrm{rpm}$, rated torque $M_{e,n} = 0.15\,\mathrm{Nm}$, rotor inertia $J_m = 0.18 \cdot 10^{-4}\,\mathrm{kg\,m^2}$, terminal resistance $R_s = 2\,\Omega$, mechanical time constant $T_m = 0.013\,\mathrm{s}$, electrical time constant $T_a = 0.001\,\mathrm{s}$, torque constant $k_m = 0.056\,\mathrm{Nm/A}$. The increasing radius $r(t)$ determines an increase of the value of the total moment of inertia from $J_{\mathrm{tot},0} = 0.18 \cdot 10^{-4}\,\mathrm{kg\,m^2}$ to $J_{\mathrm{tot},f} = 1.372 \cdot 10^{-4}\,\mathrm{kg\,m^2}$, and corresponding, the increasing of the mechanical time constant T_m.

Laboratory application, with $J_e(t)$ variable "in steps"; the equipment Model 220 Industrial plant is presented in Fig. 19 [53]. The equipment allows for the realization of three different mechanical structures. The experiments have been conducted for different control structures and controllers, see Section 4.3. For this application, the numerical values of the parameters are synthesized in Table 5.

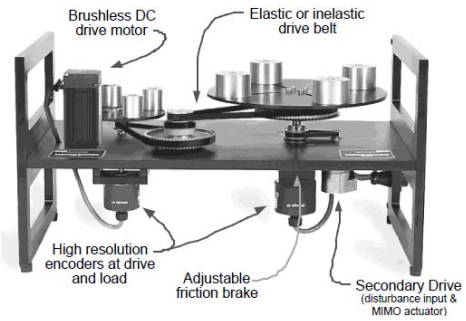

Fig. 19. Model 220 Industrial Plant Emulator (M 220 IPE)

Table 5. Numerical values for M 220 IPE

Parameters	Values of the parameters
J_{dd}	$0.00040\,\mathrm{kg\,m^2}$
J_{dl}	$0.0065\,\mathrm{kg\,m^2}$
J_{p_backlash}	$0.000031\,\mathrm{kg\,m^2}$
$J_{wd}(4 \times 0.2\,\mathrm{kg}$ at $r_{wd} = 0.05\,\mathrm{m})$	$0.0021\,\mathrm{kg\,m^2}$
$J_{wd}(4 \times 0.5\,\mathrm{kg}$ at $r_{wd} = 0.05\,\mathrm{m})$	$0.00561\,\mathrm{kg\,m^2}$
$J_{wl}(4 \times 0.2\,\mathrm{kg}$ at $r_{wd} = 0.1\,\mathrm{m})$	$0.00824\,\mathrm{kg\,m^2}$
$J_{wl}(4 \times 0.5\,\mathrm{kg}$ at $r_{wd} = 0.1\,\mathrm{m})$	$0.0206\,\mathrm{kg\,m^2}$
$J_{pd}(n_{pd} = 24)$ or $J_{pl}(n_{pl} = 24)$	$0.000008\,\mathrm{kg\,m^2}$
$J_{pd}(n_{pd} = 36)$ or $J_{pl}(n_{pl} = 36)$	$0.000039\,\mathrm{kg\,m^2}$
c_1	$0.004\,\mathrm{Nm/rad/s}$
c_2	$0.05\,\mathrm{Nm/rad/s}$
k	$8.45\,\mathrm{Nm/rad}$

4 Control Solutions for Driving Systems with BLDC-m and DC-m

4.1 Cascade Control of the Electric Drive (Servo-Drive) for a HEV

Controller Design. Two control solutions are presented for the HEV application presented in Section 3.2, Both solutions have two control loops in a CCS [9, 52] which differs in external control loop (vehicle speed ω):

1. CCS with a classical PI controller, Fig. 20, and
2. CCS with a 2-DOF PI controller, Fig. 21, which includes a forcing block to correct the current reference for the inner loop; the effect of this is that the settling time of the system will decrease.

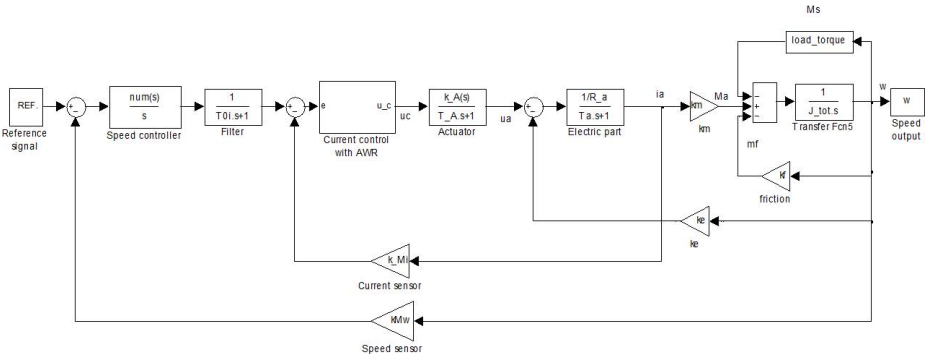

Fig. 20. Cascade control structure for the DC-m with PI controller

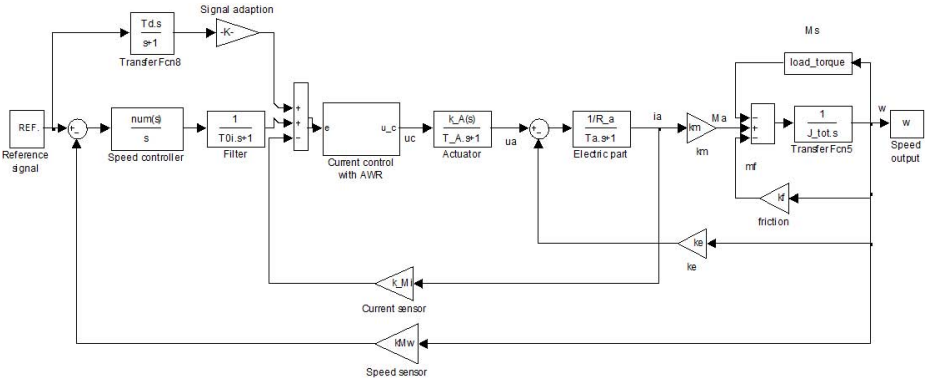

Fig. 21. Cascade control structure for the DC-m: speed control with reference forcing block

The inner control loop consists of a PI controller with AWR measure; the con-troller parameters were calculated based on the MO-m having the design relation (33) [11]:

$$H_{Cc}(s) = \frac{k_{ci}}{s}\left(1 + sT_{ci}\right), \quad K_{ci} = \frac{1}{2k_{pi}T_{\Sigma i}}, \quad T_{ci} = T_a. \tag{35}$$

The controller parameters results as $k_{ci} \approx 7$ and $T_{ci} = 0.1\,\mathrm{s}$. The AWR measure was introduced to attenuate the effects of going into limitation of the controller; other methods for handling the constraints in the control signal can also be used.

Neglecting the friction coefficient in the plant, k_f, for a simplified design of the speed controller for the plant a simplified t.f. can be considered:

$$H_p(s) = \frac{k_p}{s\,(1 + sT_{\Sigma\omega})}, \tag{36}$$

where $T_{\Sigma\omega} \approx 2T_{\Sigma\omega} + T_{i0}$ stands for the current loop and parasitic time constants ($T_{i0} \approx 0.05\,\mathrm{s}$), k_p characterizes the dynamics of the mechanical part of the driving system (J_{tot}), the inverse of the current sensor k_{Mi} and the speed sensor $k_{M\omega}$. So, the speed controller is of PI type having the parameters $k_{c\omega} \approx 35.0$ and $T_{c\omega} = 1.75\,\mathrm{s}$.

For the second case the controller is the same and the feed forward correction term is a Derivative with first order Lag type filter (DL1) with the t.f.

$$H_{ff}(s) = \frac{56s}{1 + s}. \tag{37}$$

Simulation Results and Interpretation. The considered simulation scenario is part from the urban part of the NEDC (New European Drive Cycle) used in testing vehicle's HEV (more generally, EV) consumption [9], consisting in an acceleration part, a part with constant velocity and a part of deceleration until a stop is reached. The load of the system is taken into account by means of (25)–(27) [49, 52]. Both CS behaviours are simulated and the comparison of the currents and dynamics is performed. Sensitivity aspects for a change in the mass of the plant are also treated in [9]. The registered variables are: the velocity (speed), the current and the electromagnetic torque M_a vs. disturbance torque M_s.

- *The case of simple CCS with PI controller.* The simulation results are depicted in Figs. 22, 23 and 24.
- *The case of CCS with correction in the current reference, the 2-DOF-PI solu-tion.* The differences in the speed are insignificant. So the differences in the current behaviour between the solutions are depicted, together with the active power (dashed line – simple cascade structure, solid line – structure with current correction), Figs. 25 and 26. It can be remarked that the active differences in the consumed energy (power) are proportional with the current.

- *The simple cascade structure with modified load.* The presented simulation refers the case when the mass of the vehicle is changed with +25% of it

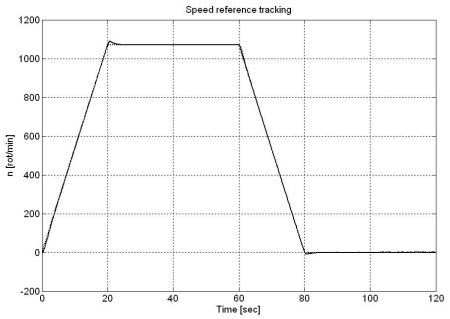

Fig. 22. Speed reference tracking

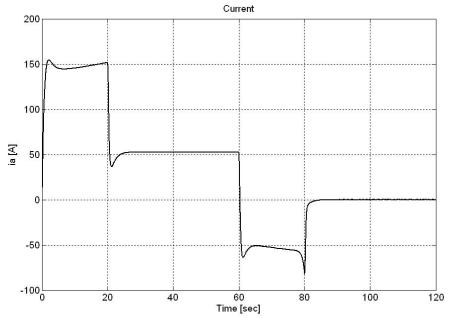

Fig. 23. Current response

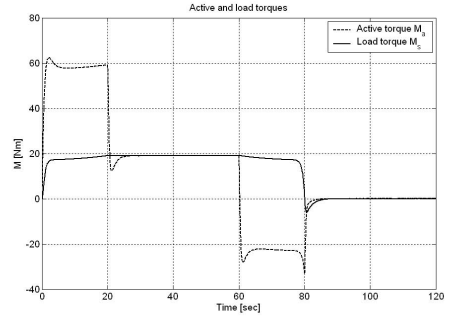

Fig. 24. Active torque M_a versus disturbance torque M_s

(solid line – original load, dashed line – increased load): $m_{\text{veh}} = m_{\text{veh0}} + \Delta m$, resulting $m_{\text{veh}} = 2332\,\text{kg}$. The simulations are presented in Figs. 27 and 28 (for the first cascade structure). Other cases are presented and discussed in detail in [9].

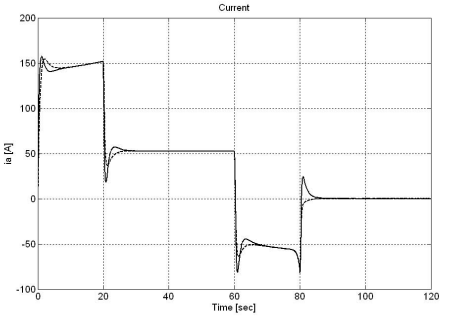

Fig. 25. Comparison of the currents

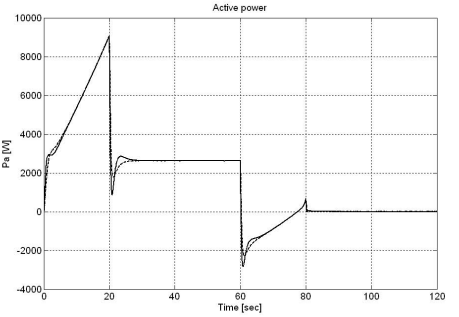

Fig. 26. Comparison of the active powers

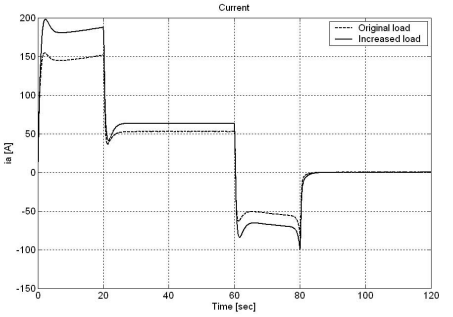

Fig. 27. Behaviour of the current

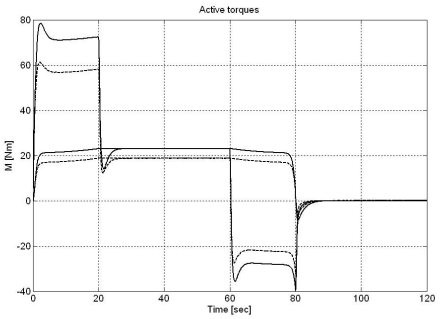

Fig. 28. Active torque M_a vs. disturbance torque M_s

The simulated cases reflect a very good behaviour of the CSs regarding reference tracking, disturbance rejection and also low sensitivity to parameter changes. More then, test simulation extended for the NEDC confirm the summarised results. Alternative solutions can be the GPC and different adaptive and variable structure controller solutions presented in Section 2 and in [9, 50, 54, 55].

4.2 Control Solution for the Electric Drive with BLDC-m and DC-m with VMI (the Winding System)

The DC-m drive with VMI in the simulated case. The cascade control structure (CCS) with PI(D) Speed Controller with Bump-less Switching for the speed controller is presented in Fig. 1. Due to the fact that the application has continuously variable parameters in a large domain, the control solution with bump-less switching of the c.a. is a good and practical option.

The development of the speed controller was considered in the context of Section 2 as follows:

1. in its classical PI controller (as the basic case);
2. an extension for a fuzzy PI Takagi-Sugeno Fuzzy controller;
3. a PI Quasi-Relay Sliding Mode Controller and
4. a Neuro-Fuzzy Controller.

All solutions are based on the locally linearised MMs. The "best controller-plant combinations" are summarized (dashed) in Table 6 after testing on laboratory equipment [53]. The most favourable case analysis is conducted in [60].

The basic CCS with discrete-time PI control algorithm. For the winding system the controller switching between PI c.a. (Figs. 1 and 2). Depending on the

Table 6. Combination between plant parameters and controller parameters

	r_0/J_0	$r_{\text{med}}/J_{\text{med}}$	$r_{\max}/J_{\max}$
C-1-ω Optimal for r_0	Case study 1.1 $r_0, Cr_0 - \omega$	Case study 1.2 $r_{\text{med}}, Cr_0 - \omega$	Case study 1.3 $r_{\max}, Cr_0 - \omega$
C-2-ω Optimal for r_{med}	Case study 2.1 $r_0, Cr_{\text{med}} - \omega$	Case study 2.2 $r_{\text{med}}, Cr_{\text{med}} - \omega$	Case study 2.3 $r_{\max}, Cr_{\text{med}} - \omega$
C-3-ω Optimal for $r_{\max}$	Case study 3.1 $r_0, Cr_{\max} - \omega$	Case study 3.2 $r_{\text{med}}, Cr_{\max} - \omega$	Case study 3.3 $r_{\max}, Cr_{\max} - \omega$

imposed performances the c.a.s can be designed using the MO-m, the ESO-m or the 2p-SO-m; the switching structure presented in Figs. 1 and 2 was applied without difficulties. The calculated values for the controller parameters (for the speed controller, the dashed cases) are synthesized in Table 7.

Table 7. Controller parameters (for the PI c.a.)

Controller type	The values for the parameters					
	k_C	T_i	q_{0pi}	q_{1pi}	p_{0pi}	p_{1pi}
0	1	2	3	4	5	6
C-i_a	0.5	0.0333	0.5019	−0.4981	1	−1
C-1-ω_{11}	0.1	0.125	0.1001	−0.0999	1	−1
C-2-ω_{22}	0.055	0.0688	0.0551	−0.0549	1	−1
C-3-ω_{33}	0.0025	0.0031	0.0026	−0.0024	1	−1

The Takagi-Sugeno PI Fuzzy Controllers. The Takagi-Sugeno PI (TS-PI-FC) quasi-continuous fuzzy controller structure (TS-PI-FC) with OI was adopted based on the continuous-time PI controller solution. The algorithm is modelled by the recurrent equations with variable parameters. Finally this leads to the PI quasi-continuous digital controller with OI (11), [58] (based on [34] other alternative solution can be done). The bump-less transfer of the command is structural ensured by the TS-FC. The expressions of the control algorithms are given by relation (11).

The PI Quasi-Relay Sliding Mode Controller. The block diagram of the PI quasi relay sliding mode controller – in its classical structure – is presented in Fig. 12. The fuzzy-block of the controller is defined using the principles synthesized in [61]: for the inputs in the nonlinear FC block three linguistic terms are used (with triangular and trapezoidal form, TL_{ek} and $TL_{\Delta ek} \in \{N, ZE, P\}$, $B_e = 13$

and $h = 0.00025\,\mathrm{s}$; the inference engine use the SUM and PROD operators and the rule base is a complete one defined by 9 rules

$$\begin{aligned}
&\text{IF } e_k \text{ IS } N \text{ AND } \Delta e_k \text{ IS } P \text{ THEN } \Delta u_k = K_{p1}\left[\Delta e_k + \alpha_1 e_k\right],\\
&\text{IF } e_k \text{ IS } Z \text{ AND } \Delta e_k \text{ IS } P \text{ THEN } \Delta u_k = K_{p2}\left[\Delta e_k + \alpha_2 e_k\right],\\
&\text{IF } e_k \text{ IS } P \text{ AND } \Delta e_k \text{ IS } P \text{ THEN } \Delta u_k = K_{p3}\left[\Delta e_k + \alpha_3 e_k\right],\\
&\text{IF } e_k \text{ IS } N \text{ AND } \Delta e_k \text{ IS } Z \text{ THEN } \Delta u_k = K_{p4}\left[\Delta e_k + \alpha_4 e_k\right],\\
&\text{IF } e_k \text{ IS } Z \text{ AND } \Delta e_k \text{ IS } Z \text{ THEN } \Delta u_k = K_{p5}\left[\Delta e_k + \alpha_5 e_k\right],\\
&\text{IF } e_k \text{ IS } P \text{ AND } \Delta e_k \text{ IS } Z \text{ THEN } \Delta u_k = K_{p6}\left[\Delta e_k + \alpha_6 e_k\right],\\
&\text{IF } e_k \text{ IS } N \text{ AND } \Delta e_k \text{ IS } N \text{ THEN } \Delta u_k = K_{p7}\left[\Delta e_k + \alpha_7 e_k\right],\\
&\text{IF } e_k \text{ IS } Z \text{ AND } \Delta e_k \text{ IS } N \text{ THEN } \Delta u_k = K_{p8}\left[\Delta e_k + \alpha_8 e_k\right],\\
&\text{IF } e_k \text{ IS } P \text{ AND } \Delta e_k \text{ IS } N \text{ THEN } \Delta u_k = K_{p9}\left[\Delta e_k + \alpha_9 e_k\right].
\end{aligned} \tag{38}$$

The parameters of the digital control algorithms are

$$\begin{aligned}
&u_{jk} = u_{j,k-1} - K_{Pi}^{(j)}\left[\left(1-\alpha_i^{(j)}\right)e_{jk} - e_{j,k-1}\right], \qquad j = 1,\ldots,9,\\
&e_{jk} = w_k - y_k = e_k, \qquad j = 1,2,3 \text{ for the c.a.}(j).
\end{aligned} \tag{39}$$

The Hybrid Neuro-Fuzzy Takagi-Sugeno quasi PI Controller (T-S PI-N-FC). The CS structure is presented in Fig. 29. The reference model (MR) is a PL2 block ($b_2 = b_1 = 0$, $b_0 = 1$; $a_2 = T_{\mathrm{imp}}^2$, $a_1 = 2\zeta_{\mathrm{imp}}T_{\mathrm{imp}}$, $a_0 = 1$ with $\zeta_{\mathrm{imp}} = 1$, $T_{\mathrm{imp}} = 1$), having the discrete equivalent in form

$$\begin{aligned}
&y_{m,k} = -d_1 y_{m,k-1} - d_2 y_{m,k-2} - c_0 r_k + c_1 r_{k-1} + c_2 r_{k-2},\\
&c_0 = -\frac{h^2}{\left(h+2T_{\mathrm{imp}}\right)^2}, \quad c_1 = \frac{2h^2}{\left(h+2T_{\mathrm{imp}}\right)^2}, \quad c_2 = \frac{h^2}{\left(h+2T_{\mathrm{imp}}\right)^2},\\
&d_1 = \frac{2\left(h^2 - 4T_{\mathrm{imp}}^2\right)}{\left(h+2T_{\mathrm{imp}}\right)^2}, \quad d_2 = \frac{\left(h-4T_{\mathrm{imp}}\right)^2}{\left(h+2T_{\mathrm{imp}}\right)^2}.
\end{aligned} \tag{40}$$

The adaptation block BA modifies the rule base of the FC. The parameters of the speed controllers are the same as those given in Table 7, the differences are provided by the tuning parameters $\{B_e, B_{\Delta e}, B_{\Delta u}\}$ for the TS-PI-FC and by the parameters $\{B_e, B_{eI}, B_u\}$ for the hybrid T-S PI-N-FC [33, 63].

Simulation results. From the simulation results synthesized in [33] and in Figs. 30(a)–(c), 31(a)–(c) and 32(a)–(c) illustrate suggestively that the CS-s ensure good behaviours as good tracking, small overshoots and settling times. The two fuzzy control systems – the TS-PI-FC with output integration and the T-S PI-N-FC – ensure improved performance compared to the linear control system. The implementation of the hybrid T-S PI-N-FC on a BLDC-m based servo system with a similar benchmark MM leads to good experimental results [33].

Figs. 31(a)–(c) and Figs. 32(a)–(c) illustrate that the best performances are provided by case study 1.1, case study 2.2 and case study 3.3.

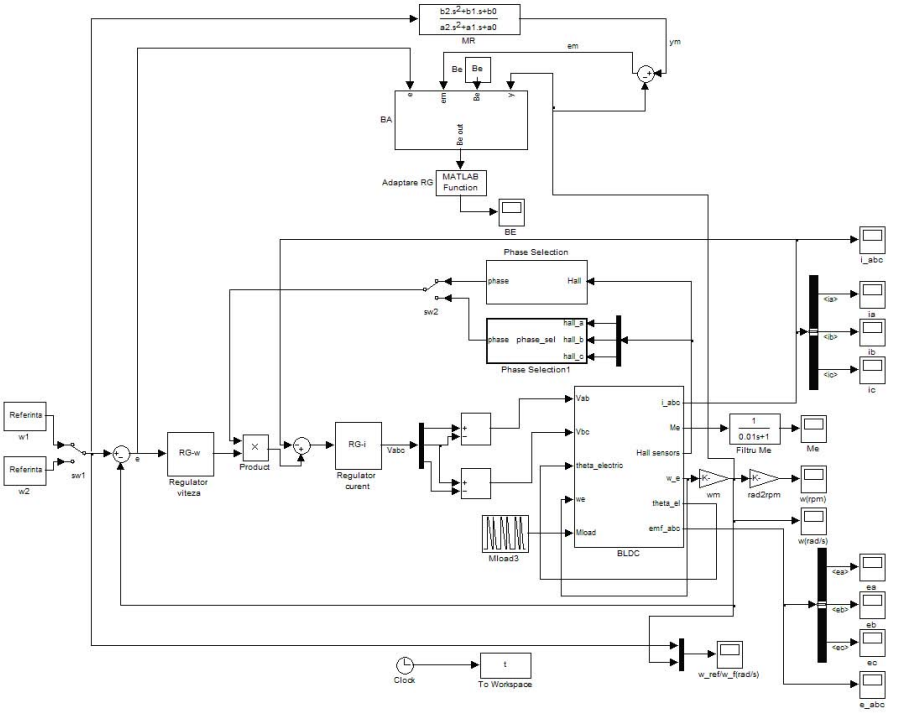

Fig. 29. Block diagram of the Hybrid Neuro-Fuzzy Takagi-Sugeno quasi PI Controller

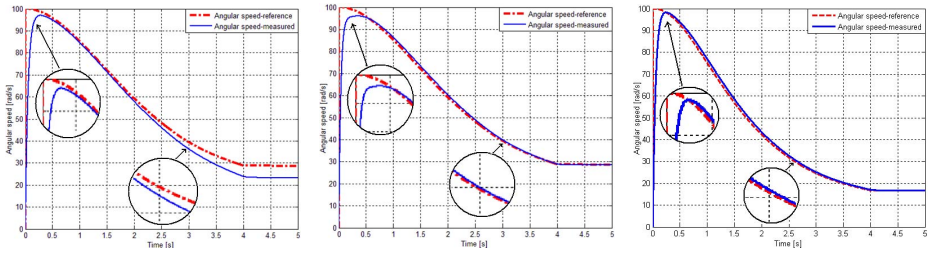

Fig. 30. Simulation results for (a) linear, (b) fuzzy and (c) neuro-fuzzy CS for DC-m based servo system with VMI: angular speed (reference input and measured angular speed) versus time

The Model 220 Industrial Plant Emulator (M 220 IPE) (electric drive with BLDC-m). Experiments and simulations have been conducted for the M 220 IPE application [33] using the details described in Sections 3.1 and 3.3.d, for different equipment facilities, different CSs, different inputs and different operating scenarios. Only the case of rigid transmission is treated to assess the main control performance.

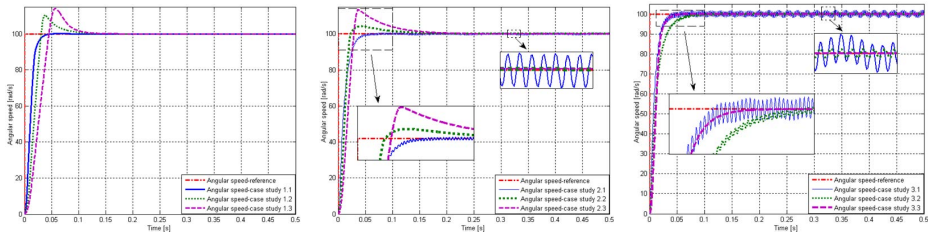

Fig. 31. Simulation results for fuzzy control system (TS-PI-FC with OI) of DC m based servo: (a) angular speed versus time (b) angular speed versus time (cases 2.1–2.3),(c) angular speed versus time (cases 3.1–3.3)

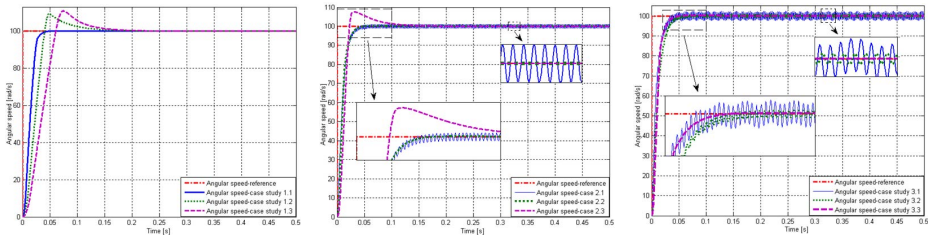

Fig. 32. Simulation results for neuro-fuzzy control system (T-S PI-N-FC) of DC-motor based servo (cases 3.1-3.3): (a) angular speed versus time (b) angular speed versus time (c) angular speed versus time

The developed CCS. Figs. 33, 34 and 35 illustrate the main four control structures. Due to a particularity in the equipment (software) the implementation of the natural PI controller must be extended with a serial PDL1 filter. Therefore, each case results in real PID controllers.

– The CCS with external PI(D) controller, the basic solution, presented in Fig. 33. The controller's t.f. and the values for the parameters calculated with the ESO-m for $\beta = 9$ are

$$H_{\text{PID-C}} = \frac{k_r}{s}\left(1 + sT_r\right)\left(1 + sT_r'\right), \qquad k_r = 0.001, \qquad T_r = 0.05\,\text{s}, \qquad T_r' = 1.95\,\text{s}. \tag{41}$$

– The CCS with classical 2-DOF control solution, presented in Fig. 34. The values of the parameters of the controller's t.f. are given in Table 8.
– The CCS with sliding-mode PI-D controller solution, presented in Fig. 35. The parameters of the controllers have been calculated, and they are synthesized in Table 9.
– The CCS with Takagi-Sugeno FC solution with PD+I controller, Fig. 36. The parameters of the controllers have been calculated, and they are synthesized in Table 10.

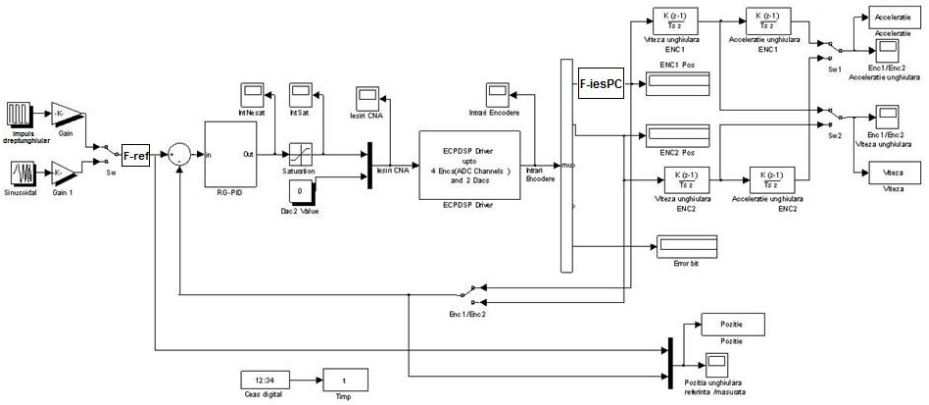

Fig. 33. The CCS with external PI(D) as the basic control solution

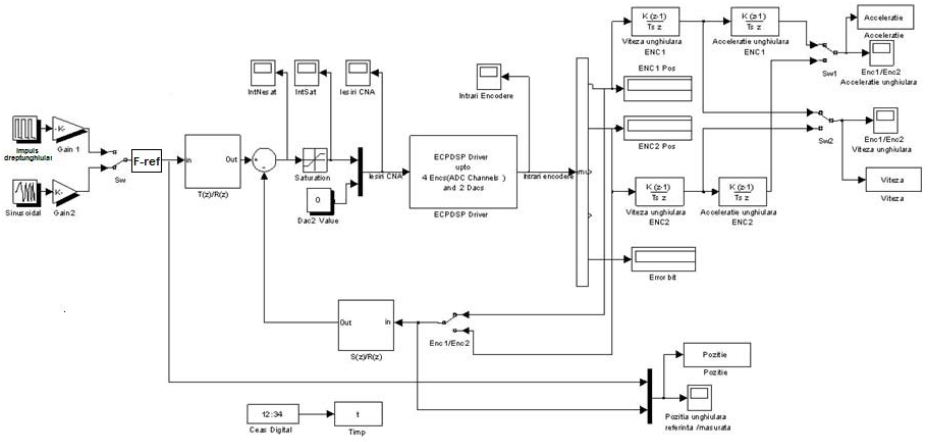

Fig. 34. The CCS with external classical 2-DOF control solution

Table 8. The values of the polynomials $R\left(z^{-1}\right)$, $S\left(z^{-1}\right)$ and $T\left(z^{-1}\right)$

$R\left(z^{-1}\right)$			$S\left(z^{-1}\right)$			$T\left(z^{-1}\right)$		
r_0	r_1	r_2	s_0	s_1	s_2	t_0	t_1	t_2
0.028	−0.040	0.012	0.049	−0.094	0.045	0.042	−0.08	0.038

– The CCS with 2-DOF Takagi-Sugeno FC solution with PD+I as main controller and filters blocks on the reference and feedback channel, Fig. 37. The values of the controller's parameters are synthesized in Table 11.

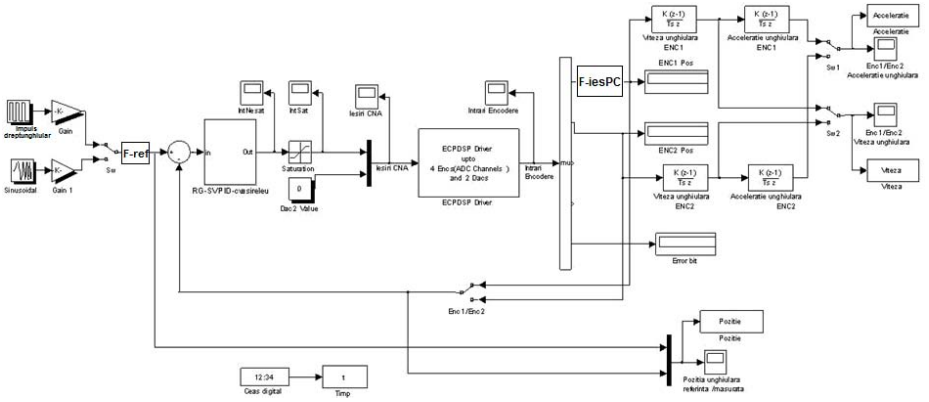

Fig. 35. The CCS with sliding-mode PI-D controller

Table 9. The values of the controller's parameters

Sliding mode parameters		PID controller, $H_{\text{RG-PID}}$					
c	α	K_p	K_i	K_d	k_r	T_r	T_r'
1	2	3	4	5	6	7	8
10000	1.75	0.2	0.1	0.01	0.1	0.05	1.95

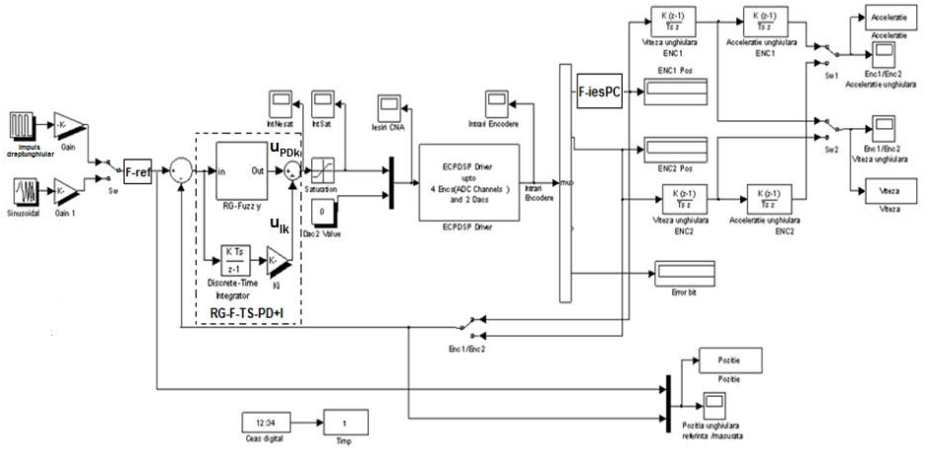

Fig. 36. The CCS with Takagi-Sugeno FC solution with PD+I controller

Simulation results. The solutions were tested as positioning CS so the input reference was an angular position [33]. All solutions gives good control performances; the best results are given by the 2-DOF Takagi-Sugeno FC solution with PD+I as main controller and filters blocks on the reference and feedback channel.

Table 10. The values of the controller's parameters

Ccontroller parameters					
K_p	K_i	K_d	k_1	k_2	α
0.2	0.1	0.01	2.5	0.2	0.08

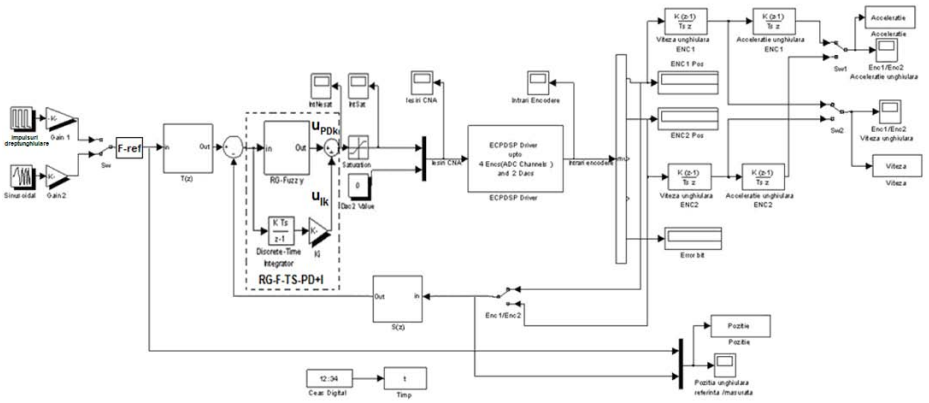

Fig. 37. The CCS with 2-DOF Takagi-Sugeno FC solution with PD+I controller

Table 11. The values of the controller's parameters

2-DOf controller						TS-FC with PD+I controller			
$T\left(z^{-1}\right)$			$S\left(z^{-1}\right)$			RG-F-TS-PD			I
t_0	t_1	t_2	s_0	s_1	s_2	k_1	k_2	α	K_i
0.042	−0.08	0.038	0.049	−0.094	0.045	2.5	0.2	0.08	0.1

5 Conclusions

Using some practical development methods which can be implemented as LCA solutions, this chapter has synthesized some pragmatic control solution, dedicated to plants working under continuously variable conditions: variable plant parameters or (the worst case) variable structure, variable reference and variable load (disturbance). From a large case of such applications, two speed control applications, namely with DC-m and with BLDC-m, have been treated: a case specific to the metallurgical industry and the speed control of an electric (hybrid) vehicle model. The efficiency of the algorithms has been tested and illustrated on different plant models and also on laboratory equipment with variable moment of inertia. The presented algorithms are easily adaptable to similar applications. Several fuzzy and nonlinear elements can be incorporated [64–70, 70, 72–74].

Acknowledgments. This work was supported by a grant of the Romanian National Authority for Scientific Research, CNCS – UEFISCDI, project number PN-II-ID-PCE-2011-3-0109. Also, the work was partially supported by the strategic grants POSDRU 6/1.5/S/13 (2008) and POSDRU ID 77265 (2010) of the Ministry of Labour, Family and Social Protection, Romania, co-financed by the European Social Fund – Investing in People.

Main abbreviations

AWR	Anti-Windup Reset	1-DOF	one Degree of Freedom
MBC	Model-Based Control	2-DOF	two Degree of Freedom
MM	Mathematical Model	FC	Fuzzy Controller
EV	Electric Vehicle	TS-FC	Takagi-Sugeno Fuzzy Controller
HEV	(Hybrid) Electric Vehicle	TS-PI(D)-FC	Takagi-Sugeno PI(D) Fuzzy Controller
VMI	Variable Moment of Inertia	OI	(with) output integration
BLDC-m	Brush-Less DC motor	II	(with) input integration
CS	Control Structure	P, I, D	the Proportional, Integral, Derivative components
CCS	Cascade Control Structure	L1, L2	first /second order filter with lag
c.a.	control algorithm	DP-CS	Dynamic Programming (based) Control Strategy
t.f.	transfer function	MPC	Model Predictive Control
MO-m	Modulus-Optimum method	GPC	Generalized Predictive Control
SO-m	Symmetrical Optimum method	ESO-m	Extended Symmetrical Optimum method
2-p-SO-m	double parameterization based Symmetrical Optimum method		

References

1. Christian, J.A., Turbe, M.A., Kabo, E.M., Manno, L.C., Johnson, E.N.: Development of a variable inertia reaction wheel system for spacecraft attitude control. In: Proceedings of AIAA Guidance, Navigation, and Control Conference and Exhibit, Providence, RI, USA, 13 p. (2004)
2. Akpolat, Z.H., Asher, G.M., Clare, J.C.: A practical approach to the design of robust speed controllers for machine drives. IEEE Trans. Ind. Electron. 47, 315–324 (2000)
3. Mink, F., Bahr, A.: Adaptive speed control for drives with variable moments of inertia and natural drequencies. LTi DRIVES GmbH Entwicklung Software, Lahnau, Germany (2011)
4. Lamar, K.: Digital control of permanent magnet synchronous motors. In: Proc. Budapest-Tech Jubilee Conference, Budapest, Hungary, pp. 213–228 (2004)

5. Modi, V.J., Karray, F., Mah, H.A.: Composite Control Scheme for Joint Tracking and Active Vibration Suppression of Mobile Flexible Manipulator Systems. Acta Astronautica 36, 261–275 (1995)
6. Crowder, R.M.: Electric Drives and their Controls. Oxford University Press Inc., New York (1998)
7. Rizzoni, G.: Priciples and Applications of Electrical Engineering. McGraw-Hill (2000)
8. Preitl, Z., Bauer, P., Bokor, J.: Fuel Consumption Optimization for Hybrid Solar Vehicle. In: Proc. Workshop on Hybrid Solar Vehicles, Salerno, Italy (2006)
9. Preitl, Z.: Control design methods for optimal energy consumption systems, PhD Thesis, Supervisors: Prof. Dr. József Bokor, member of The Hungarian Academy of Science, Budapest University of Technology and Economics (2009)
10. Ťapák, P., Huba, M., Žáková: Constrained Control for Systems with Relative Degree One. In: Proc. 17th IFAC World Congress, Seoul, South Korea, vol. 17, pp. 5814–5819 (2008)
11. Åström, K.J., Hägglund, T.: PID controller theory: Design and tuning. Instrument Society of America, Research Triangle Park, NC (1995)
12. Ozawa, S., Furuya, H.: Feedback Liniearization Technique in Variable Inertia Systems. Trans. Japan Soc. Aero Space Sci. 45(147), 1–9 (2002)
13. Möhler, R.R.: Applications to Bilinear Control. Prentice Hall, Englewood Cliffs (1991)
14. Sherer, C.: Mixed H_2/H_∞ Control. In: Trends in Control: An European Perspective, Volume of the Special Contributions to the ECC, pp. 173–216 (1995)
15. Chiali, M., Gahinet, P.: H_∞ Design with Pole Placement Constraints: an LMI Approach. IEEE Trans. Automat. Control 41, 358–367 (1996)
16. Åström, K.J., Panagopoulos, H., Hägglund, T.: Design of PI controllers based nonconvex optimization. Automatica 34, 585–601 (1998)
17. Preitl, S., Precup, R.-E.: Extension of tuning relations after symmetrical optimum method for PI and PID controllers. Automatica 35(10), 1731–1736 (1999)
18. Preitl, S., Precup, R.-E.: Linear and Fuzzy Control Extensions of the Symmetrical Optimum Method. In: Proc. International Conference on Complex Systems: Synergy of Control, Computing & Communications (COSY 2011), Ohrid, Republic of Machedonia, pp. 59–68 (2011)
19. Vrancic, D., Peng, Y., Strmcnik, S.: A new PID controller tuning method based on multiple integrations. Control Engineering Practice 7(5), 623–633 (1999)
20. Vrancic, D., Strmcnik, S., Juricic, D.: A magnitude optimum multiple integration tuning method for filtered PID controller. Automatica 37(9), 1473–1479 (2001)
21. Papadopoulos, K.G., Mermikli, K., Margaris, N.I.: Optimal tuning of PID controllers for integrating processes via the symmetrical optimum criterion. In: Proc. 19th Mediterranean Conference on Control and Automation (MED 2012), Corfu, Greece, pp. 1289–1294 (2011)
22. Papadopoulos, K.G., Mermikli, K., Margaris, N.I.: On the automatic tuning of PID type controllers via the magnitude optimum criterion. In: Proc. 2012 IEEE International Conference on Industrial Technology (ICIT 2012), Athens, Greece, pp. 869–874 (2012)
23. Papadopoulos, K.G., Margaris, N.I.: Extending the symmetrical optimum criterion to the design of PID type-p control loops. Journal of Process Control 22(1), 11–25 (2012)
24. Loron, L.: Tuning of PID controllers by the non-symmetrical optimum method. Automatica 33(1), 103–107 (1997)

25. Precup, R.-E., Preitl, S.: Development of some fuzzy controllers with non-homogenous dynamics with respect to the input channels meant for a class of systems. In: Proc. European Control Conference (ECC 1999), Karlsruhe, Germany, paper index F56, 6 p. (1999)
26. Araki, M., Taguchi, H.: Two-degree-of-freedom PID controllers. Int. J. Control Automat. Syst. 1, 401–411 (2003)
27. Preitl, Z.: Model Based Design Methods for Speed Control, Applications. PhD Thesis, "Politehnica" University of Timisoara, Editura Politehnica, Timisoara, Romania (2008)
28. Preitl, S., Precup, R.-E., Preitl, Z.: Aspects concerning the tuning of 2-DOF fuzzy controllers. In: Proc. Xth Triennial International SAUM Conference on Systems, Automatic Control and Measurements (SAUM 2010), Nis, Serbia, pp. 210–219 (2010)
29. Miklosovic, R., Gao, Z.: A robust two-Degree of Freedom control design Technique and its practical application. In: Proc. 39th IAS Annual Meeting Conference Record of the 2004 IEEE Industry Application Conference, vol. 3, pp. 1495–1502 (2004)
30. Preitl, S., Precup, R.-E., Dragos, C.-A., Radac, M.-B.: Tuning of 2-DOF fuzzy PI(D) controllers, laboratory applications. In: Proc. 11th International Conference on Computational Intelligence and Informatics (CINTI 2010), Budapest, Hungary, pp. 237–242 (2010)
31. Bagheri, P., Nemati, H.: Novel tuning strategy for two-degree-of-freedom PI controllers. In: Proc. 18th IFAC World Congress, Milano, Italy, pp. 6757–6762 (2011)
32. Preitl, Z., Levendovszky, T.: Computer Aided Design of Two-Degree-of-Freedom (2DOF) Controllers. Buletinul Stiintific al Universitatii "Politehnica" din Timisoara, Romania, Seria Automatica si Calculatoare 48(62), 70–75 (2003)
33. Stinean, A.-I.: Contribuţii la Dezvoltarea unor Soluţii de Reglare Dedicate Sistemelor de Actionare Electrică cu Parametri Variabili si cu Intrări Variabile in Timp. Ph.D. thesis, Politehnica University of Timisoara, Timisoara, Romania (2014) (in Romanian)
34. Precup, R.-E., Preitl, S.: Fuzzy Controllers. Editura Orizonturi Universitare, Timisoara (1999)
35. Stinean, A.-I., Preitl, S., Precup, R.-E., Dragos, C.-A., Radac, M.-B.: Classical and Fuzzy Approaches to 2-DOF Control Solutions for BLDC-m Drives. In: Pap, E. (ed.) Intelligent Systems: Models and Applications. TIEI, vol. 3, pp. 175–193. Springer, Heidelberg (2013)
36. Proceedings of 18th IFAC World Congress, Milan, Italy (2011)
37. Bay, O.F., Bal, G., Demirbas, S.: Fuzzy Logic Based Control of a Brushless DC Servo Motor Drive. In: Proc. 7th International Power Electronics & Motion Control Conference Exhibition (1996), Budapest, Hungary, vol. 3, pp. 448–452 (1996)
38. Lomonova, E.A., Miziurin, S.R., Klaassens, J.B.: Brushless Machines as Electromechanical Actuators for Flight Control Systems. In: Proc. 7th International Power Electronics & Motion Control Conference Exhibition, Budapest, Hungary, vol. 2, pp. 627–631 (1996)
39. Vaščák, J., Madarász, L.: Adaptation of fuzzy cognitive maps - a comparison study. Acta Polytechnica Hungarica 7, 109–122 (2010)
40. Preitl, S., Precup, R.-E., Preitl, Z.: Control structures and algorithms, vol. 1, 2. Editura Orizonturi Universitare, Timisoara (2009) (in Romanian)
41. Cao, W., Yeng, C.S., Chakravarthy, V.K.: An integrated nonlinear observer with sliding mode estimation for a class of nonlinear uncertain systems. In: Proc. 42nd IEEE Conference on Decision and Control, pp. 5741–5746 (2003)

42. Zhang, J., Shi, P., Xia, Y.: Robust adaptive sliding-mode control for fuzzy systems with mismatched uncertainties. IEEE Trans. Fuzzy Syst. 18, 700–711 (2010)
43. Utkin, V., Guldner, J., Shi, J.: Sliding Mode Control in Electro-mechanical Systems. CRC Press, Boca Raton (2009)
44. Baldursson, S.: BLDC motor modelling and control - A Matlab/Simulink implementation. M.Sc. Thesis, Institutionen för Energi och Miljö, Göteborg, Sweden (2005)
45. Nasar, S.A., Boldea, I.: Electric Drives, 2nd edn. CRC Press (2005)
46. Dixon, J.W., Real, I.: Current control strategy for brushless dc motors based on a common DC signal. IEEE Trans. Power Electron. 17, 232–240 (2002)
47. Yasuhiko, D.: Servo Motor and Motion control Using Digital Signal Processors, Texas Instruments. Prentice Hall, Englewood Cliffs (1990)
48. Bauer, P., Preitl, Z., Gaspar, P., Szabo, Z., Bokor, J.: Modelling of a Series Hybrid Electric Vehicle. In: Workshop on Hybrid Electric Vehicle Modelling and Control, Istanbul, Turkey (2007)
49. Preitl, Z., Kulcsár, B., Bokor, J.: Mathematical Models of a Hybrid Electric Vehicles. In: Proc. 8th International Conference on Technical Informatics (CONTI 2008), Timisoara, Romania, 6 p. (2008)
50. Tsai, T.-C., Tsai, M.-C.: Power Control of a Brushless Permanent Magnet Electric Machine for Exercise Bikes. In: Proc. 15th IFAC Triennial World Congress, Barcelona, Spain, 6 p. (2002)
51. Workshop Papers, Workshop on Hybrid Solar Vehicles, Salerno, Italy (2006)
52. Preitl, Z., Bauer, P., Bokor, J.: Cascade control solution for traction motor for hybrid electric vehicles. Acta Polytechnica Hungarica 4(3), 75–88 (2007)
53. ECP M 220, Industrial emulator/servo trainer model 220 system, testbed for practical control training, Bell Canyon, CA, USA. Educational Control Products (2010)
54. Musardo, C., Rizzoni, C., Guezennec, Y., Staccia, B.: A-ECMS: An Adaptive Algorithm for Hybrid Electric Vehicle Energy Management. European Journal of Control 11, 509–524 (2005)
55. Tsai, T.-C., Tsai, M.-C.: Power Control of a Brushless Permanent Magnet Electric Machine for Exercise Bikes. In: Proc. 15th IFACT Triennial World Congress, Barcelona, Spain (2002)
56. Precup, R.-E., Preitl, S.: On a hybrid PI-neuro-fuzzy controller meant for a class of non-minimum phase systems. In: Proc. 7th European Congress on Intelligent Technologies and Soft Computing (EUFIT 1999), Aachen, Germany, 6 p. (1999)
57. Precup, R.-E., David, R.-C., Petriu, E.-M., Rădac, M.-B., Preitl, S., Fodor, J.: Evolutionary optimization-based tuning of low-cost fuzzy controllers for servo systems. Knowledge-Based Systems 38, 74–84 (2013)
58. Stînean, A.-I., Preitl, S., Precup, R.-E., Dragoş, C.-A., Rădac, M.-B., Crainic, M.: Adaptable fuzzy control solutions for driving systems working under continuously variable conditions. In: Proc. 14th IEEE International Symposium on Computational Intelligence and Informatics (CINTI 2013), Budapest, Hungary, pp. 231–237 (2013)
59. Preitl, S., Stinean, A.-I., Precup, R.-E., Preitl, Z., Petriu, E.-M., Drago, C.-A., Rădac, M.-B.: Controller design methods for driving systems based on extensions of symmetrical optimum method with DC and BLDC Motor Applications. In: Proc. IFAC Conference on Advances in PID Control (PID 2012), Brescia, Italy, pp. 264–269 (2012)

60. Stinean, A.-I., Preitl, S., Precup, R.-E., Dragos, C.-A., Petriu, E.M., Radac, M.-B.: Choosing a Proper Control structure for a mechatronic system with variable parameters. In: Proc. 2nd IFAC Workshop on Convergence of Information Technologies and Control Methods with Power Systems (ICPS 2013), Cluj-Napoca, Romania, pp. 29–34 (2013)
61. Precup, R.-E., Preitl, S.: On some low cost hybrid PI-neuro-fuzzy controllers for the second-order "right half plane zero" system. In: Proc. 13th CSCS Conference, pp. 170–175. Editura Politehnica Press, Bucharest (2001)
62. Stînean, A.-I., Preitl, S., Precup, R.-E., Petriu, E.-M., Dragoş, A.-C., Rădac, B.-M.: Solutions for avoiding the worst case scenario in driving system working under continuously variable conditions. In: Proc. IEEE 9th International Conference on Computational Cybernetics (ICCC 2013), Tihany, Hungary, pp. 339–344 (2013)
63. Stînean, A.-I., Preitl, S., Precup, R.-E., Dragoş, A.-C., Petriu, E.-M., Rădac, B.-M.: Low-Cost Neuro-Fuzzy Control Solution for Servo Systems with Variable Parameters. In: Proc. 2013 IEEE International Conference on Computational Intelligence and Virtual Environements for Measurement Systems and Applications (CIVEMSA 2013), Milano, Italy, pp. 156–161 (2013)
64. Precup, R.-E., Preitl, S.: Popov-type stability analysis method for fuzzy control systems. In: Proc. Fifth EUFIT 1997 European Congress, Aachen, Germany, pp. 1306–1310 (1997)
65. Carlsson, C., Fullér, R.: Optimization under fuzzy if-then rules. Fuzzy Sets and Systems 119(1), 111–120 (2001)
66. Baranyi, P., Tikk, D., Yam, Y., Patton, R.J.: From differential equations to PDC controller design via numerical transformation. Computers in Industry 51(3), 281–297 (2003)
67. Tar, J.K., Rudas, I.J., Bitó, J.F., Horváth, L., Kozlowski, K.: Analysis of the effect of backlash and joint acceleration measurement noise in the adaptive control of electro-mechanical systems. In: Proc. 2003 IEEE International Symposium on Industrial Electronics (ISIE 2003), Rio de Janeiro, Brazil, vol. 1, pp. 286–291 (2003)
68. Tanelli, M., Sartori, R., Savaresi, S.M.: Combining slip and deceleration control for brake-by-wire control systems: A sliding-mode approach. Eur. J. Control 13(6), 593–611 (2007)
69. Rudas, I.J., Fodor, J.: Intelligent systems. International Journal of Computers, Communications & Control 3, 132–138 (2008)
70. Blažič, S.: A novel trajectory-tracking control law for wheeled mobile robots. Robotics and Autonomous Systems 59(11), 1001–1007 (2011)
71. Tikk, D., Johanyák, Z.C., Kovács, S., Wong, K.W.: Fuzzy rule interpolation and extrapolation techniques: criteria and evaluation guidelines. Journal of Advanced Computational Intelligence and Intelligent Informatics 15(3), 254–263 (2011)
72. Angelov, P., Yager, R.: A new type of simplified fuzzy rule-based systems. International Journal of General Systems 41(2), 163–185 (2012)
73. Melin, P., Castillo, O.: A review on the applications of type-2 fuzzy logic in classification and pattern recognition. Expert Syst. Appl. 40(13), 5413–5423 (2013)
74. Petra, M.I., De Silva, L.C.: Implementation of folding architecture neural networks into an FPGA for an optimized inverse kinematics solution of a six-legged robot. International Journal of Artificial Intelligence 10(S13), 123–138 (2013)

Feedback Linearization of the Differentially Driven Mobile Robot: An Experimental Verification

Wojciech Kowalczyk and Krzysztof Kozłowski

Poznań University of Technology,
Poznań, Poland
{wojciech.kowalczyk,krzysztof.kozlowski}@put.poznan.pl

Abstract. In this paper experimental verification of the input-output feedback linearization of differentially driven mobile robot is presented. This technique is especially useful in multi-level formation control because it allows to separate platform motion control from the formation control. It also allows high level controller not to be aware of the type of the robot. The disadvantage of this method is that the orientation cannot be directly controled. In the paper experiments aimed at selecting the appropriate value of so-called hand position that is design parameter for the feedback linearization are presented.

1 Introduction

One of basic problems of wheeled mobile robot control is the existence of nonholonomic constraints in the most commonly used structures. Algorithms for the control in the complex environment (complex and/or dynamic obstacle presence, multiple robots [3]) and teleoperation [2] often assume that the mobile platform has no constrains. There are of course omnidirectional robots, for example KUKA youBot mobile platform with four mecanum wheels, however, the platform with two differentially driven wheels is most frequently used because of the strength, simplicity and the ability to use in difficult terrain comparing to omnidirectional robots. To simplify the control for such robots nonlinear feedback can be used to transform the system into the multidimensional integrator. This technique requires to select the value of the so-called hand position [4] is a design parameter.

In this paper experiments aimed at selecting the appropriate value of this parameter are presented. Hand position is a new output for the control system. The natural choice for the hand position is a point on the line perpendicular to the robot wheels. The proper selection of the distance between the wheel axis and the hand position play an important role for the behavior of the control system. In this paper series of experiments using MTracker mobile robot are presented. They were aimed at selecting the appropriate hand position for set-point control. In the external loop simple proportional controller was applied.

From the theoretical point of view the only restriction on the distance between the wheel axis and the hand position L is $L \neq 0$ due to inability to calculate (7)

J. Fodor and R. Fullér (eds.), *Advances in Soft Computing, Intelligent Robotics and Control,* Topics in Intelligent Engineering and Informatics 8,
DOI: 10.1007/978-3-319-05945-7_2,

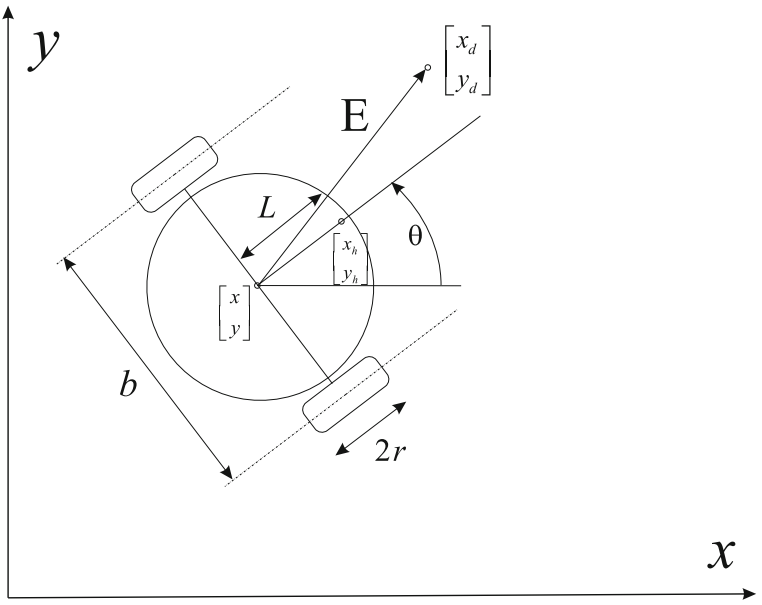

Fig. 1. Differentially driven mobile robot

for $L = 0$. In practise, however, other parameters associated with some technical solutions applied in the robot play an important role.

In some application e.g. when the mass of the effector is large compared to the mass of the robot it is logical to place it in the center of the robot. Unfortunately the geometrical center of the robot is usually near the axis of the wheels. This leads to the small value of L and as this parameter is in the denominator of the Eq. (7) its reciprocal scales the desired angular velocity of the platform to the large values. Use of the small value of L leads to achievement of velocity constraints of the actuators. These phenomenon can be seen in the experimental results presented in the following sections. The achievement of the velocity constrains depends also on the input values $[u_x \quad u_y]^T$ and this way on the setting(s) of the external (in presented case proportional) controller and the task to perform (large value of E may also leads to the actuator limit achievement).

There are also negative consequences for the large values of the L. In this case the quantization rotary encoders may affect the accuracy of the positioning of the hand position. The accuracy of wheel positioning is limited i.e. by the resolution of the rotary encoders. Inaccuracy of the encoders affects both accuracy of the position coordinates x, y and orientation θ of the platform. The new output is given by (6) in which L is a multiplier of trigonometric function of θ. In result inaccuracies of the encoders are amplified disturb the hand position.

Input-output feedback linearization and decoupling can be also applied to the dynamic model of the differentially driven mobile robot [4], [5], [6] and [7].

The article is organized as follows. In the section 2 control algorithm is presented. In the section 3 experiments and comments are included. In the final section 4 concluding remarks are given.

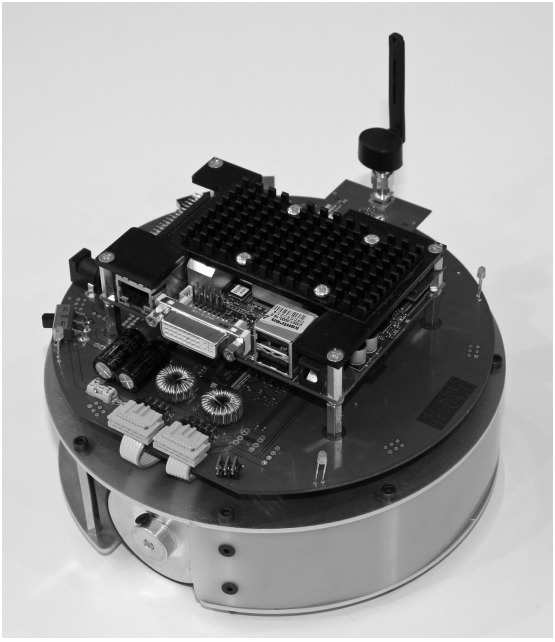

Fig. 2. MTracker robot

Kinematic model of the differentially driven mobile robot (Fig. 1) is given by the following equation:

$$\begin{bmatrix} \dot{x} \\ \dot{y} \\ \dot{\theta} \end{bmatrix} = \begin{bmatrix} \cos\theta & 0 \\ \sin\theta & 0 \\ 0 & 1 \end{bmatrix} \begin{bmatrix} v \\ \omega \end{bmatrix}, \tag{1}$$

where x, y and θ are position and orientation coordinates of the robot, respectively, $\boldsymbol{u} = \begin{bmatrix} v\ \omega \end{bmatrix}^T$ is the control vector that includes v - linear velocity and ω - angular velocity of the platform.

Control values for the platform are transformed to the wheel velocities:

$$\omega_R = \frac{v + \frac{1}{2}b\omega}{r}, \quad \omega_L = \frac{v - \frac{1}{2}b\omega}{r}. \tag{2}$$

where r is the radius of the wheel of the robot and b is the distance between wheels.

To take into account velocity limit $\omega_{wmax} > 0$ of the robot actuators the control scaling procedure is used. Denoting by $\boldsymbol{\omega} = [\omega_R \ \omega_L]^T$ the computed and non-limited control input vector from (2), the limited input $\boldsymbol{\omega}_d = [\omega_{R_d} \ \omega_{L_d}]^T$ can be obtained as follows:

$$\boldsymbol{\omega}_d(\tau) = \frac{\boldsymbol{\omega}(\tau)}{s(\tau)}, \tag{3}$$

where

$$s(\tau) = \max\left\{1, \frac{|\,\omega_R(\tau)\,|}{\omega_{wmax}}, \ \frac{|\,\omega_L(\tau)\,|}{\omega_{wmax}}\right\} \geq 1. \tag{4}$$

Scaling procedure keeps the direction of the limited control vector $\boldsymbol{\omega}_d$ equal to the previously computed control vector $\boldsymbol{\omega}$.

2 Feedback Linearization

Model of the robot is feedback linearized [1] to simplify robot motion control.

Hand position point $\boldsymbol{h} = [x_h \ \ y_h]^T$ located at some distance form the axis of the robot wheels is the new output coordinate for the robot. It is computed by the following equation:

$$\boldsymbol{h} = \begin{bmatrix} x + L\cos(\theta) \\ y + L\sin(\theta) \end{bmatrix}. \tag{5}$$

Differentiating above equation with respect to time and substituting (1) into the result one obtains:

$$\dot{\mathbf{h}} = \begin{bmatrix} v\cos(\theta) - L\omega\sin(\theta) \\ v\sin(\theta) + L\omega\cos(\theta) \end{bmatrix}. \tag{6}$$

Replacing hand position time derivative $\dot{\mathbf{h}}$ with the new input $[u_x \ \ u_y]^T$ and transforming result to obtain velocities for the platform on the left hand side one obtains feedback linearizing control law:

$$\begin{bmatrix} v \\ \omega \end{bmatrix} = \begin{bmatrix} 1 & 0 \\ 0 & \frac{1}{L} \end{bmatrix} \begin{bmatrix} \cos(\theta) & \sin(\theta) \\ -\sin(\theta) & \cos(\theta) \end{bmatrix} \begin{bmatrix} u_x \\ u_y \end{bmatrix}. \tag{7}$$

Substituting (7) into (6) and simplifying the feedback linearized model of the system is obtained:

$$\dot{\mathbf{h}} = \begin{bmatrix} u_x \\ u_y \end{bmatrix}. \tag{8}$$

For the transformed system given by (8) simple proportional controller is applied:

$$\begin{bmatrix} u_x \\ u_y \end{bmatrix} = K_p \left(\begin{bmatrix} x_t \\ y_t \end{bmatrix} - \begin{bmatrix} x \\ y \end{bmatrix} \right), \tag{9}$$

where K_p is constant control gain and $[x_t \ \ y_t]$ is the desired position.

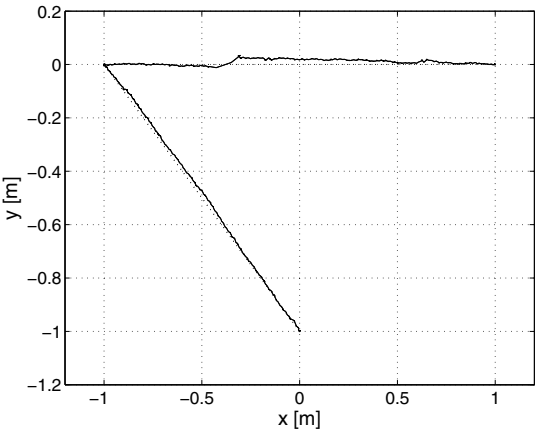

Fig. 3. Experiment 1: Position on the (x, y) plane

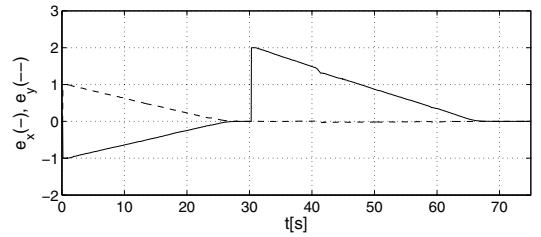

Fig. 4. Experiment 1: Errors as a function of time

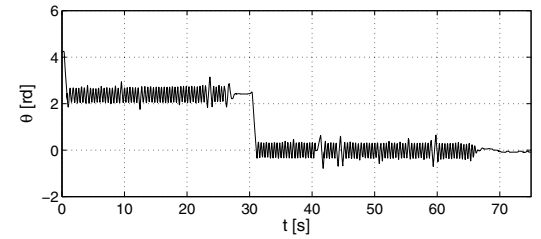

Fig. 5. Experiment 1: Orientation as a function of time

3 Experiments

Experimental verification were preformed with MTracker robot (Fig. 2). Physical dimensions of the robot relevant for the analysis are as follows: the radius of the robot $R_r = 170$mm, the radius of the wheels $r = 24.5mm$, the distance between wheels $b = 148mm$ (Fig. 1). The resolution of the optical encoders mounted on the rotor of motors is $32ticks/rev$ and the gear ratio is 14.

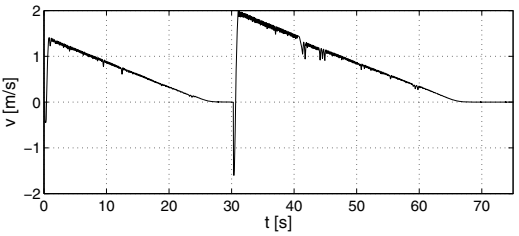

Fig. 6. Experiment 1: Control of linear velocity

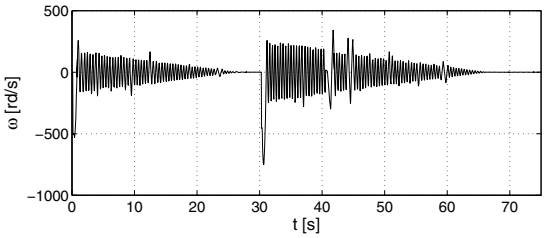

Fig. 7. Experiment 1: Control of angular velocity

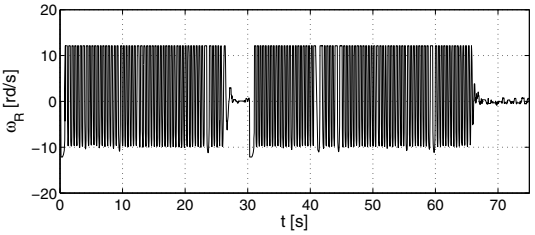

Fig. 8. Experiment 1: Control of the right wheel

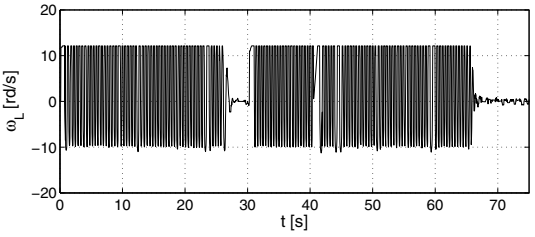

Fig. 9. Experiment 1: Control of the left wheel

Optical encoder quantization transformed to the axis of the robots wheel is $77.7 ticks/rd$. The uncertainty of the wheel position is doubled quantization transformed to the path travelled by the wheel and is $0.63mm$. This is also the maximum uncertainty of the platform position along the line perpendicular

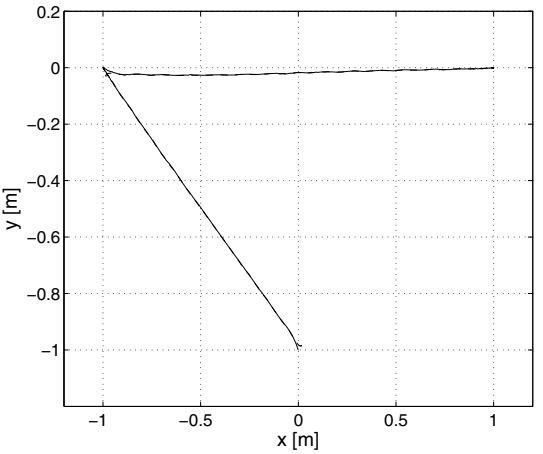

Fig. 10. Experiment 2: Position on the (x, y) plane

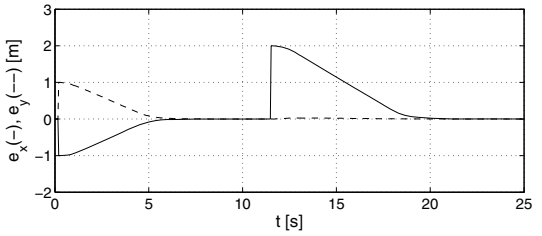

Fig. 11. Experiment 2: Errors as a function of time

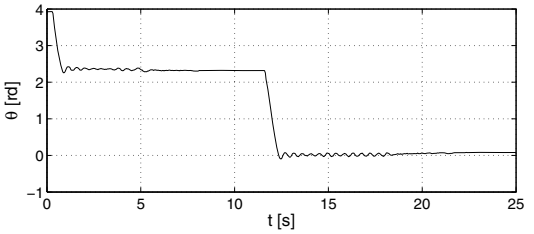

Fig. 12. Experiment 2: Orientation as a function of time

to the wheel axis. Assuming that there are no multiple changes of the motion direction between sensor ticks the uncertainty of the platform position along the wheel axis is much less.

As previously mentioned, selection of L parameter is often the compromise between task/application requirements and constraints of the feedback linearization

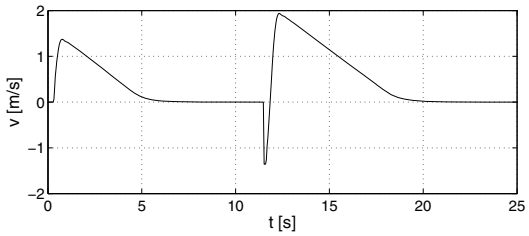

Fig. 13. Experiment 2: Control of linear velocity

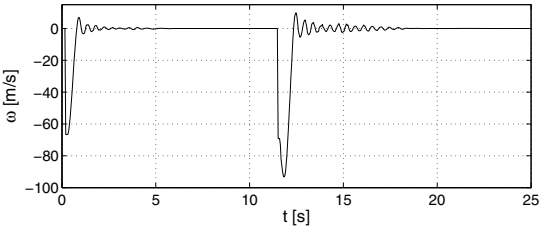

Fig. 14. Experiment 2: Control of angular velocity

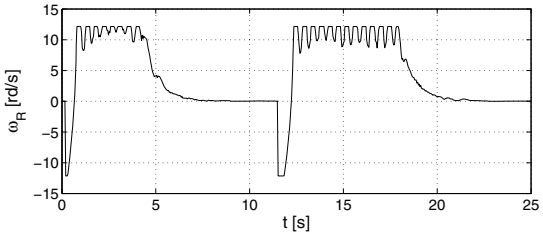

Fig. 15. Experiment 2: Control of the right wheel

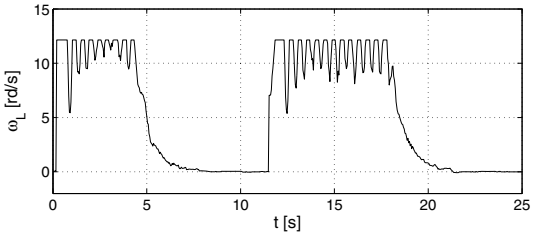

Fig. 16. Experiment 2: Control of the left wheel

method in connection with the time delay in the system, gear backlash, optical encoder quantization errors, localization system accuracy, maximum velocity produced by the actuators and others. Proper choice of L is also coupled with the other units of the control system. In all presented experiments control gain in (9)

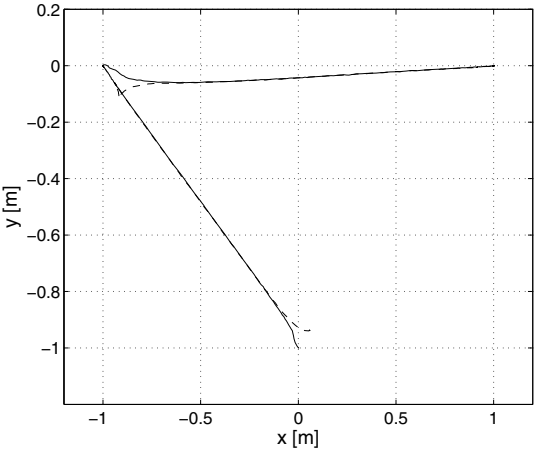

Fig. 17. Experiment 3: Position on the (x, y) plane

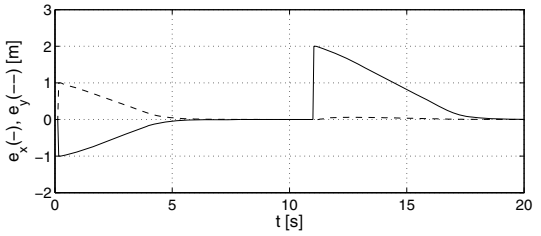

Fig. 18. Experiment 3: Errors as a function of time

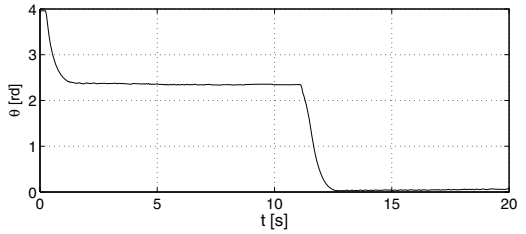

Fig. 19. Experiment 3: Orientation as a function of time

was $K_p = 1$. If K_p parameter is changed (e.g. increased, to reduce convergence time) the best choice of L may also change.

In the experiment 1 distance between hand position and the wheel axis was $L = 3.125mm$ that is very small (in comparison to the robots dimensions). This may be the good choice for hand position due to mass balance, especially if the mass of the effector is large. In Fig. 3 the path of the robot in (x, y) plane is shown. The initial position of robot is $(0, -1m)$. The desired position

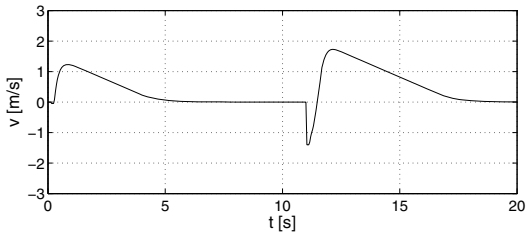

Fig. 20. Experiment 3: Control of linear velocity

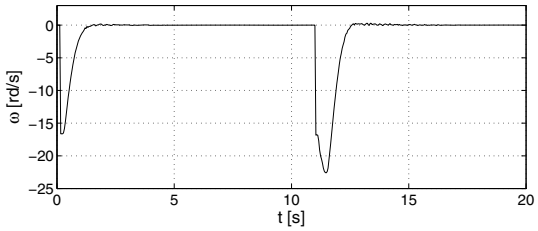

Fig. 21. Experiment 3: Control of angular velocity

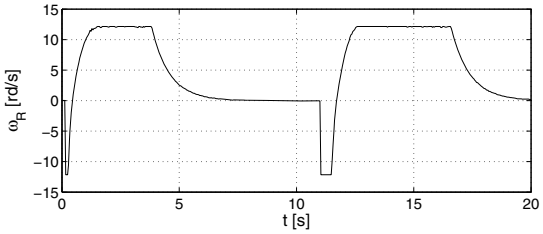

Fig. 22. Experiment 3: Control of the right wheel

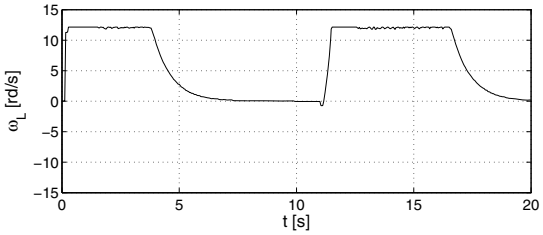

Fig. 23. Experiment 3: Control of the left wheel

is $(-1m, 0)$ (phase 1 of the experiment) and after the hand positon reaches this coordinates next desired position is $(1m, 0)$ (phase 2 of the experiment). Both the geometrical center of the robot $[x \;\; y]^T$ and hand position $[x_h \;\; y_h]^T$ are represented by the single line due to the small distance between these points (L). As can be observed in Fig. 4 position error components converge to near zero

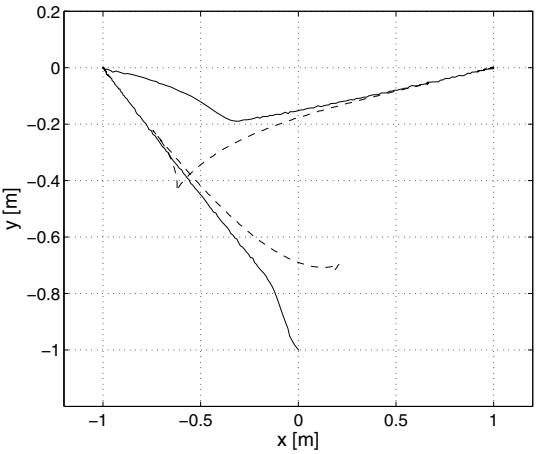

Fig. 24. Experiment 4: Position on the (x, y) plane

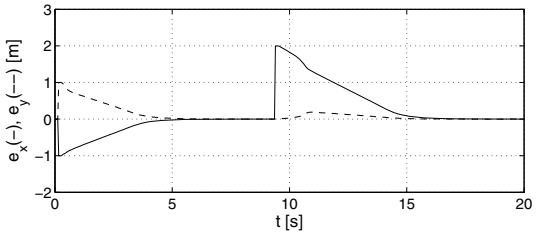

Fig. 25. Experiment 4: Errors as a function of time

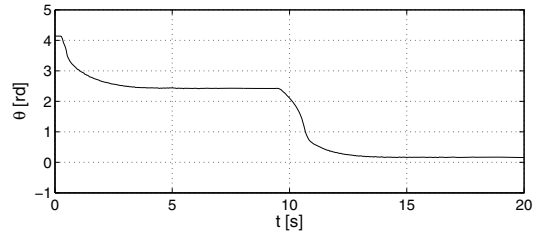

Fig. 26. Experiment 4: Orientation as a function of time

value in $26s$ and $36s$ in subsequent phases. The final position error components (e_x, e_y) in the second stage of the experiment were $(-0.16mm, 1.396mm)$. The orientation of the platform θ oscillates in relatively wide range $(\pm 0.4rd)$ with high frequency about the line towards the desired position during the transient state. The amplitude of the oscillation make this setting of L useless for most applications. The oscillation vanishes near the desired position. Linear control v and angular control ω for the platform are shown in Figs. 6 and 7. Angular control

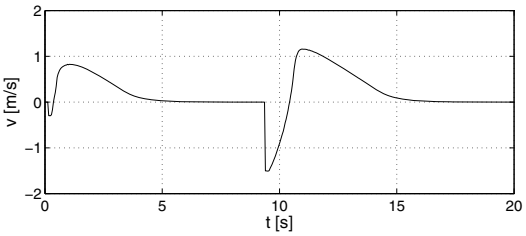

Fig. 27. Experiment 4: Control of linear velocity

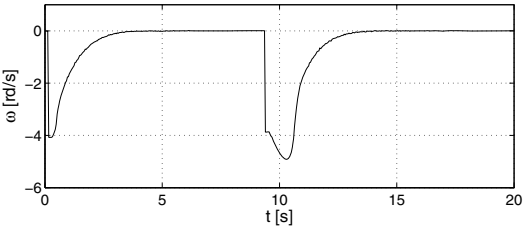

Fig. 28. Experiment 4: Control of angular velocity

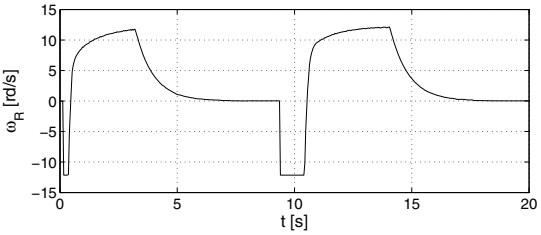

Fig. 29. Experiment 4: Control of the right wheel

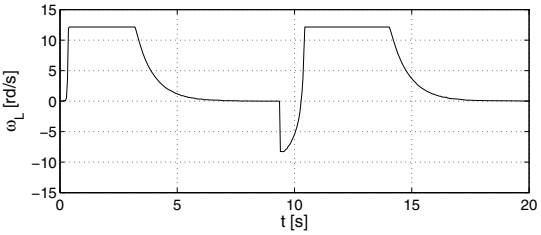

Fig. 30. Experiment 4: Control of the left wheel

oscillates with huge amplitude. After transformation to the wheel velocities and scaling signals (3) shown in Figs. 8 and 9 are obtained. The wheel velocities oscillate between the upper limit and near the lower limit value during the transient state.

In the experiment 2 $L = 21.25mm$ was set. Fig. 10 presents the paths of the hand position (solid line) and center of the robot (dashed line). Position error components (Figs. 11) reduces faster comparing with the previous experiment: $6s$ (stage 1) and $7s$ (stage 2). The final position error components e_x, e_y were $(-0.46mm, 0.72mm)$. In Fig. 12 orientation of the platform is presented. The amplitude of the oscillation is $\pm 0.1rd$ and fades during the transient state. The linear control for the platform is shown in Fig. 13. It is smoother in comparison with the experiment 1. Also angular velocity of the platform is smoother and its amplitude is reduced remaining, however, large. Wheel velocities ω_R and ω_L oscillate during initial parts of the experiment stages reaching velocity limit.

In the experiment 3 $L = 85.0mm$ was set that is the radius of the robot (hand position placed at the boundary of the robot). Fig. 17 presents the paths of the hand position (solid line) and center of the robot (dashed line). Position error components (Fig. 18) decreases to near zero value similarily as in the previous experiment. The final position error components e_x, e_y were $(-0.48mm, 0.25mm)$. In Fig. 19 orientation of the platform is presented. Oscillations are not observed. The linear control Fig. 20 and angular control Fig. 21 are smoother in comparison to these in previous experiments. Wheel velocities ω_R and ω_L reach the limit for large E (initial parts of stage 1 and stage 2 of the experiment).

In the experiment 4 $L = 340.0mm$ was set that is useless in most application, however, to get the full review how the L parameter influence the control this case was also tested. Fig. 24 presents the paths of the hand position (solid line) and center of the robot (dashed line). Position error components (Figs. 25) decreases to a near zero value one second earlier in comparison to experiment 3 (in both stages of the experiment). The final values of the error components e_x, e_y were $(-0.05mm, 1.78mm)$. In θ signal oscillation was not observed Fig. 26. The linear control (Fig. 27) and angular control (Fig. 28) are smooth and reduced comparing to the previous cases. Wheel velocities ω_R and ω_L also reach the limit but only for a short period of time during both stages of the experiment).

4 Conclusions

In this paper experiments aimed at selecting the appropriate value of the hand position were presented. Depending on the particular robot properties this selection may be easy or not. It depends on the application requirements as they may determine the position of the effector placing, on the properties of the actuators including quantization of the encoders, velocity limits on wheels, tendency to slip, backlash in gears and may other.

In the tested MTracker robot small distance between the wheel axis and the hand position caused oscillation in the orientation signal. This did not affected the position of robot significantly due to high frequency of the oscillation, however, increased task execution time and leads to the wear of mechanisms quickly. For a relatively large values of the distance between the wheel axis and the hand position no negative effect were observed. This is due to the high quality of the component used: gear, high resolution of the encoders, small inertias in the

system etc. It is worth to mention that in all cases the final position error was very small and there were no oscillations.

References

1. Isidori, A.: Nonlinear control systems. Springer (1995)
2. Kowalczyk, W., Kozłowski, K.R.: The Israeli Conference on Robotics Teleoperation of the group of mobile robots, Tel Aviv, Israel (November 2013)
3. Kowalczyk, W., Kozłowski, K.: Artificial potential based control for a large scale formation of mobile robots, pp. 285–291 (June 17, 2004)
4. Lawton, J.R.T., Beard, R.W., Young, B.J.: A Decentralized Approach to Formation Maneuvers. IEEE Transaction on Robotics and Atomation 19(6), 933–941 (2003)
5. Khoukhi, A., Shahab, M.: Stabilized Feedback Control of Unicycle Mobile Robots. International Journal of Advanced Robotic Systems 10, 187 (2013)
6. Carona, R., Aguiar, A.P., Gaspar, J.: Control of Unicycle Type Robots. Tracking, Path Following and Point Stabilization. In: Proc. of IV Jornadas de Engenharia Electronica e Telecomunicacoes e de Computadores, Lisbon, Portugal, pp. 180–185 (November 2008)
7. DeVon, D., Bretl, T.: Kinematic and Dynamic Control of a Wheeled Mobile Robot. In: Proceedings of the 2007 IEEE/RSJ International Conference on Intelligent Robots and Systems, San Diego, CA, USA, October 29-November 2, pp. 4065–4070 (2007)

Model-Based Disease Treatment: A Control Engineering Approach

Levente Kovács

Óbuda University,
John von Neumann Faculty of Informatics,
Budapest, Hungary
kovacs.levente@nik.uni-obuda.hu

Abstract. Computer engineering opens new ways in healthcare including a more exact treatment possibility of different diseases. By modeling the disease and using control engineering methods it is possible to refine the treatment, but also to seek for optimal solutions/therapies. The current work summarizes the results of model-based disease treatment researches in the field of physiological modeling and control carried out at the Physiological Controls Group of the Obuda University. The developed and presented optimal algorithms and strategies focus on three diseases with high public health impact: diabetes (the artificial pancreas problem), obesity (predicting obesity-related risks) and cancer (antiangiogenic therapy). The studies are done in strong collaboration with different Hungarian hospitals, from where measurement data were obtained.

1 Introduction

Development of computer science, control engineering and measurement theory gives the possibilities of the biomedical engineering interdisciplinary research field to spread. The aim of physiological control–a subdiscipline of biomedical engineering [1]–is to study, model and apply identification and control strategies in order to understand and help automated treatment of various diseases or injuries of the human body.

In many biomedical systems, external controllers provide biosignal input / inject given specific dosage substituting the internal, physiological procedure because patient's body cannot ensure it / produce it. The outer control might be partially or fully automated. The regulation has several strict requirements, but once it has been designed, it permits not only to facilitate the patient's life, but also to optimize (if necessary) the amount of the used dosage. The newly formed Physiological Controls Group of the Óbuda University together with the Control Engineering and Information Technology of the Budapest University of Technology and Economics and the Semmelweis University from Budapest are investigating the mentioned problem.

The current work summarizes three of our research tasks connected to modeling and control of diseases with high public health impact: diabetes, obesity and cancer [2].

J. Fodor and R. Fullér (eds.), *Advances in Soft Computing, Intelligent Robotics and Control,* Topics in Intelligent Engineering and Informatics 8,
DOI: 10.1007/978-3-319-05945-7_3,

Diabetes is named by the World Health Organization (WHO) as the "disease of the future" [3]. Statistics of the International Diabetes Federation (IDF) show that the European Region has the highest number and the highest incidence rate of type 1 diabetes (T1DM) in children from any other region worldwide [4]. Diabetes is diagnosed if for some reasons the human body is unable to control the normal glucose-insulin interaction (e.g. glucose concentration level is constantly out of the 70-110 mg/dL range). The consequences of diabetes are mostly long-term: cardiovascular diseases, neuropathy, retinopathy [5]. Hence, diabetes is a serious metabolic disease, which should be artificially controlled, and from engineering point of view its treatment can be represented by an outer control loop, to replace the partially or totally deficient blood glucose control system of the human body. Our approach was to design robust optimal control algorithms to maintain the normoglycaemic blood glucose range and in this way to extend the applicability of individualized therapies formulated in the literature [6].

Obesity is named by the WHO the "disease of today" as it is considered an endemic in the most part of the developed world [7]. In Hungary, according to [8], 1.5 million Hungarian are definitely obese, whilst an additional 2.7 million can be considered overweight. Together, this is almost the half of the Hungarian population. In the last few decades, increased occurrence of several morbidities were casually linked to obesity, such as non-insulin dependent diabetes mellitus (T2DM), stroke, ischemic heart disease (IHD), immunological and reproductive dysfunctions and certain neoplasms [9]. From these, stroke and IHD is amongst the first three in the list of mortality rates in Hungary [10]. These all confirm that obesity poses a significant risk. Hence, early intervention is needed to prevent the onset of obesity and obesity-associated comorbidities. Early, focused intervention presumes however an efficient screening method which can select those people who are prone to obesity even when they are healthy otherwise. Hence, our approach focused on the investigation of new ways in which obesity-related risks can be assessed.

Regarding the third mentioned disease, *cancer* is one of the most destructive illness nowadays, which is lethal in most cases. According to recent statistics, 1.3 million people of the European Union is estimated to die from cancer in 2013 [11]. Unfortunately, Hungary is the leading country of the European Union (and also in top ten in the world) in mortality data of all types of cancer [12,13]. There are classical therapies, such as chemotherapy and radiation therapy, but chemical agents and ionizing radiation have effects on certain healthy cells of the patient as well. Treatments which are based on specific molecules that target a signalling pathway in the growth and development of a tumor cell are called targeted molecular therapies (TMTs). Antiangiogenic therapy [14] is a type of TMTs, which inhibits angiogenesis (forming new blood vessels). Preventing tumor cells from grow and develop, the tumor can be kept in a dormant state, where the cellular proliferation rate balanced by the apoptotic rate, thus the tumor will be unable to grow in size beyond a few milimeters [14]. Consequently, our aim was to combine the advantages of control theory with the antiangiogenic therapy in order to optimize the treatment.

2 Modern Robust Control Algorithms for Type 1 Diabetes

The quest for artificial pancreas can be structured in three different tasks [6]: continuous glucose sensor for measurements, insulin pump for infusion and control algorithm problem.

To design an appropriate control, an adequate model is necessary. From the many models appeared in the literature [15] and the wide palette of control strategies [6], it become evident that modeling of the glucose-insulin system and controlling its behavior are two tightly connected questions that cannot be separated. Model predicted control proved to be an efficient solution for individualized treatment of type 1 diabetes [6], but due to insulin sensitivity and patient variability hard constraints are also beneficial [16,18].

Hence, we have focused on one of the most complex model (the Sorensen-model) [17] and developed a nonlinear model based robust control algorithm [18]. The nonlinear model-based approach was realized using LPV (Linear Parameter Varying) methodology capturing the validity of the Sorensen-model inside a polytopic region and building up the LPV model as a linear combination of the linearized models derived in each polytopic point [18,19].

The LPV based robust controller was developed to minimize the meal disturbance level over the performance output for all possible variation of the parameter within the determined polytope:

$$\min_{K} \|G\| = \min_{K} \sup_{\varrho \in F_p} \sup_{\|d\| \neq 0} \frac{\|z_{y1}\|}{\|d\|}, \tag{1}$$

where d denotes the meal disturbance input and z describes the glucose variation. G represents the transfer function of the system and K the H_∞ controller in question. A priori information is injected to the controller throughout the augmentation of the nominal plant (Fig. 1) with extra dynamics, called weighting functions and Δ unstructured uncertainty blocks [18,19]:

- W_p the performance weighting function;
- W_m the disturbance (glucose) input weighting function;
- W_i, W_{im} the input multiplicative uncertainty weighting functions;
- W_u the control input weighting function;
- W_o the output multiplicative uncertainty weighting function;
- W_{n1}, W_{n2} the sensor noise weighting functions.

During the H_∞ control design and using γ-iteration algorithm, based on the weighing functions presented in [18], $\gamma = 1.0096$ solution was obtained (the tolerance for the algorithm was set to 0.01).

During the controller design sensor noise and input and output multiplicative uncertainty were taken into account. The obtained γ value represents the upper limit of the robust performance criterion, which means that the formulated system requirements are quite severe. However, this could be an advantage in the

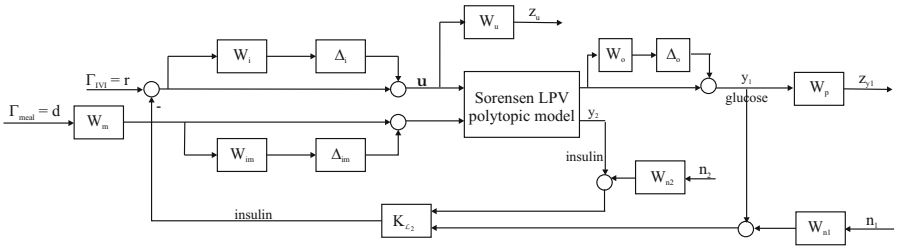

Fig. 1. The augmented nonlinear model based robust control system

validation process. Simulations were tested on the reference value taken from the literature, and proven that hyperglycaemia is avoided [18,19].

Consequently, in the next validation step the obtained controller was tested on real patient data, by using glucose absorption of the well-known and largely approved model of [20].

Minimum 1 week's real data of 83 type 1 diabetic patients (aged between 6–52 years) obtained from different insulin pump centers of Hungary were taken under investigation [21] using real data obtained from Medtronic's insulin pumps. In all of the cases hypoglycemia is avoided and less hyperglycemic episodes can be observed (77.16% less then in case of clinically measured (real) data). It also turned out that blood glucose values were kept 94.6% in the 3.9-7.8 mmol/L normoglycaemic interval [21].

From the investigated cases, results of one case are presented in the following.

Fig. 2 compares results of three days of the developed controller with real data of a 43 year old woman (she is on insulin pump for three years being noted with moderate compliance). It can be seen that the output of the controller kept the blood glucose level almost all the time in the normal 3.9-7.8 mmol/L range, avoiding hypoglycemic episodes.

3 Laboratory Results Based Automatic Classification of Obesity in Adolescents

Measuring and predicting obesity and overweight is a complex task, hindered significantly by the varying definitions. However, it is accepted that both states are characterized by elevated quantities of fat tissue, but we are still lacking exact, strict, widely used diagnostic criteria.

While indirect indicators, such as body mass index (BMI) or waist circumference (WC) are widely used [22], their predictive power is limited and they are especially unfit to predict obesity-related risk. Direct indicators, such as dual-emission X-ray absorptiometry (DXA) or bioelectric impedance analysis can precisely characterize fat distribution on the other hand, giving a sound estimation of obesity-related risk. However, they are simply unfit for screening in wider populations, mostly due to radiation exposure they cause and their expensiveness [23].

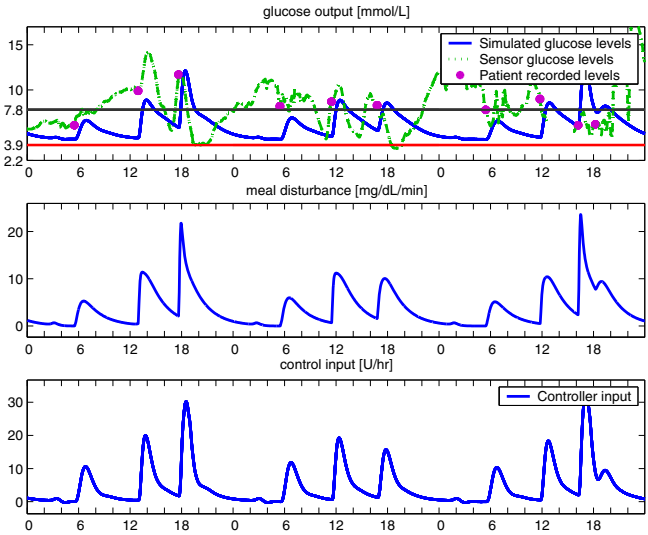

Fig. 2. Comparison of simulated robust controller output (solid line) and sensor real data (dashed line) using absorption scenario of [7]. Blood glucose levels measured from fingertips (dots) are also shown.

Hence, our aim was to resolve this problem by investigating new ways in which obesity-related risks can be assessed. The combination of usual clinical techniques (anthropometric measurements, laboratory parameters) and bioelectric impedance analysis were taken into account. The research is focused on adolescent population (aged 14-18 years) being the optimal target population on which early intervention could and should be performed to best prevent the adverse health consequences. The project included a multicenter clinical study of healthy and obese population. Such study has not yet been performed on Hungarian adolescent population from this aspect.

The study included the recording of routine blood test parameters of both obese and healthy subjects. The question rose whether these parameters could be used to discriminate the two groups. We have collected data from $n = 393$ adolescents, including both healthy and obese ones during our study [24].

The healthy control group consisted of volunteers from several Hungarian secondary schools. Every involved child participated with full written informed consent and the study was pre-authorized by the Hungarian Regional Bioethical Commission. Participants were required to show up for fasting examination early in the morning.

Examinations of the healthy volunteers included anthropometrical measurements, body composition analysis (with InBody 3.0 multi-frequency bioelectric impedance analyzer), blood sample drawing for standard laboratory parameters and recording of anamnesis. Measurements were carried out by doctors and nurses of the Heim Pál Children's Hospital, Budapest, Hungary [25].

The obese group consisted of children treated in the Heim Pál Children's Hospital, with their main diagnosis being E66.9 (according to ICD-10) "Obesity, unspecified", with no comorbidity or significant other illness.

We have performed a complex statistical analysis on the recorded parameters with special focus on the 27 laboratory variables. Statistical analysis was performed with R statistical program package (version 2.9.0), including custom scripts. Additional calculation was done with PASW/SPSS (version 18.0) and gretl (version 1.8.7) statistical program packages. Univariate and multivariate analysis was performed. We have investigated the distributions of the different laboratory results and we have examined the effect of obesity on them. It was shown that many laboratory parameter significantly differ according to state; we have interpreted these differences from the medical point of view [25].

Cluster Analysis and Principal Component Analysis (PCA) / Factor was also performed [25,26]. They allowed us to group the laboratory values into well-separated groups: RBC (Red Blood Cells) count, hemoglobin and hemotocrit formed the "macroscopic RBC descriptors" cluster; MCV (Mean Cell Volume) and MCH (Mean Cell Hemoglobin) the "microscopic RBC descriptors" cluster; liver enzymes GOT, GGT and GPT can also be grouped in separate cluster, while absolute neutrophil granulocyte count, absolute monocyte count and CRP formed the "inflammation" cluster; finally serum sodium and serum chloride grouped the "inorganic serum components" cluster, while serum total protein and serum albumin formed the "organic serum components" one. Many interesting observation can be made by comparing such correlational connections between healthy and obese subjects, for example total cholesterol and triglyceride levels are associated with the "macroscopic RBC descriptors" group in healthy children, but are moving largely independently from that in obese subjects [25].

Finally, logistic regression was applied in order to model our investigations about the discriminatory power of laboratory results, now in a multivariate sense. In case of males, the final model used only 6 variables and had an overall classification rate of 89.6%. (Negative predictive value: 89.0%, positive predictive value: 90.3%.) In case of females, the logistic regression classification model even topped the male ones: it used only 5 variables, and still had an overall classification rate of 87.7%. (Negative predictive value: 87.9%, positive predictive value: 87.5%.) This model is given in Table 1 as an example [25,26].

Table 1. Logistic regression model to classify females into obese/healthy groups

	β	S.E.	Wald	df	Sig.	exp(β)
RBCCount	2.367	1.099	4.641	1	0.031	10.669
MCV	0.188	0.123	2.348	1	0.125	1.207
MCH	−0.975	0.311	9.834	1	0.002	0.377
CRP	0.281	0.105	7.171	1	0.007	1.324
Triglycerides	2.593	0.748	12.026	1	0.001	13.364
Constant	−3.020	9.720	0.097	1	0.756	0.049

4 Optimal Control of Tumor Growth Using Antiangiogenic Chemotherapy

Clinical aspects of angiogenic inhibition are discussed more detailed in [27] and [28]. A model for tumor growth under angiogenic inhibition was presented in [29], and validated using experiments on mice with lungs cancer. This model represented the starting point of the model-based antiangiogenic investigations giving direct connection to control theory. Optimal bang-bang control was designed on a simplified model in [30]. Anti-angiogenic therapy combined with radiotherapy was discussed in [31].

The model of [29] meant the starting point of our research. In antiangiogenic therapy the most efficient drug is endostatin [32]. The disadvantage of the therapy is the high cost of the drug; hence, its utilization should be optimized. As a result, we have started to design optimal model-based cancer algorithms in terms of drug usage.

Optimal control has a wide literature in control theory and date back to the revolutionary work of Pontryagin [33]. It has implications in classical control theory [34], modern control theory [19], soft computing applications [35] or even biomedical applications [36].

The simplified model of [29] and presented in [30] assumed that the tumor volume and the endothelial volume move together. Hence, we went further, and our theoretical investigations on the model proved that we can assume the administered inhibitor concentration by the simple differential equation [37,38]:

$$\dot{g} = -\lambda_3 g + u \tag{2}$$

where g is the administered inhibitor concentration, λ_3 is the drug's clearance, and u is the inhibitor administration rate. In this way the Dirac delta type rates, which means that the drug was given to the patient in the form of injections was changed by step function input types corresponding to infusion treatment. These assumptions were demonstrated by symbolic computations made on steady state and dynamic analysis [39].

Tumor growth can be examined on Fig. 3 where the simulation starts from $x_1 = 200$ mm^3 tumor volume, $x_2 = 200$ mm^3 endothelial volume and the control input $u = 0$ for the whole time during the simulation [38].

The tumor grows rapidly in the first two months then reaches its steady-state in about four months. The endothelial cell volume grows faster, as the difference between the endothelial cell volume and tumor cell volume is the motor of the tumor growth. Other dominant parameter in tumor growth speed is the tumor growth rate parameter, which is the feature of the tumor, so we can only affect the total tumor cell volume by decreasing the total endothelial cell volume.

After examining the working point linearization of the nonlinear model together with linear control characteristics (observability and controllability), a Linear Quadratic (LQ) controller and an observer based on pole-placement was designed on the considered model [39,40].

A saturation block was also placed in the control structure with zero lower bound as negative input has no physiological meaning [40].

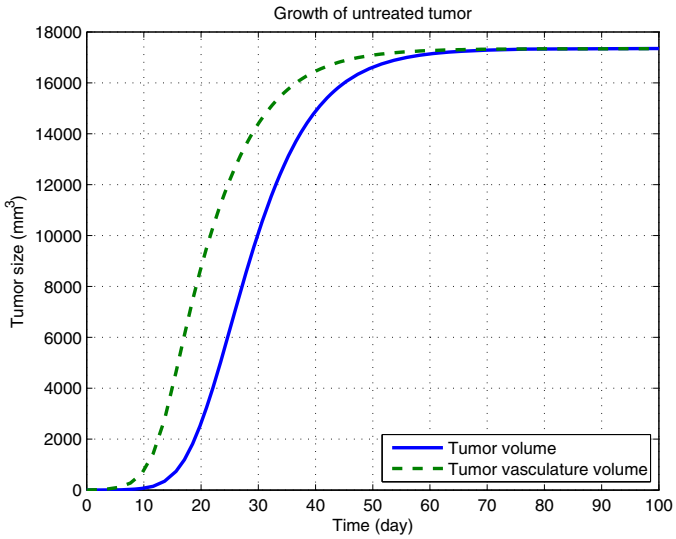

Fig. 3. Tumor and endothelial cell growth with no control input

In case of LQ design, the weighting matrix R was chosen to have a great value ($R = 10^5$), since the administered inhibitor (as the material used for the control) is quite expensive, while Q was chosen to select the energy of the tumor volume (x_1) and the administered inhibitor (x_3) [40]:

$$Q = \begin{bmatrix} 1 & 0 & 0 \\ 0 & 0 & 0 \\ 0 & 0 & 1 \end{bmatrix}. \tag{3}$$

In case of upper limit of the saturation block, we have made an iterative search to obtain its optimal value. We have started with 200 mg/kg/day, and decreased the upper limit with 1 unit step size until the control became inefficient. The simulations were run with 120 days treatment period. For each simulation result we calculated the total concentration of endostatin used in the treatment period, and treat this quantity as a cost function to be minimized. It has resulted that the cost function has a minimum at 79 units of saturation [38].

Fig. 4 depicts the simulation results for the optimal treatment. The tumor volume decreases rapidly and reaches 69 mm^3 in about 40 days. It can be seen that the input has two main periods. At the first period, the saturated input is at the maximum 79 units, and at the second period it is at 14.73 units [40].

The characteristics of the input are the same for the other simulation setups as well. They start with the maximum value and then they drop to a constant input at 14.7 units. The main role of the designed controller is to determine the switching time, when the maximal input is switched to the steady-state value [40].

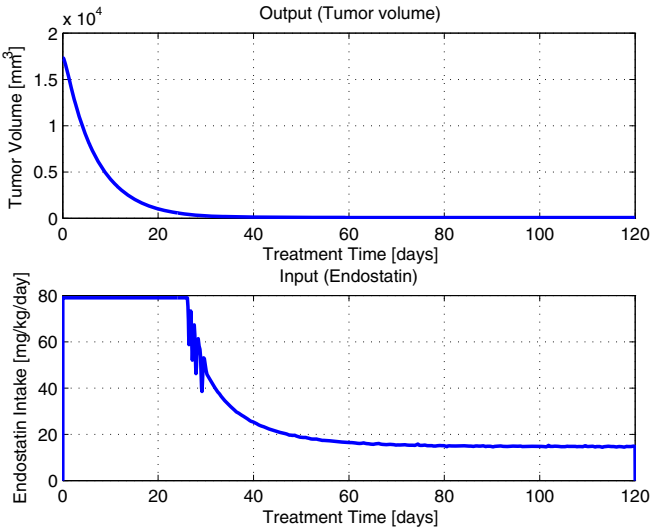

Fig. 4. Simulation results with the upper limit of 79 units on the input saturation

5 Conclusions

The current work summarized the results of model-based disease treatment researches in the field of physiological modeling and control carried out at the Physiological Controls Group of the Óbuda University.

Regarding diabetes, the Hungarian artificial pancreas research topic was briefly summarized. The developed nonlinear model-based LPV robust controller was created on the most complex Sorensen-model and our quasi in-silico results were tested and compared on real data of 83 type 1 diabetes patient. The developed framework kept the blood glucose level more than 90% of the time inside the 70-120 mg/dL interval (without any recalibration of the algorithm) proving its robustness. Hypoglycemia (not caused from physical activity) is efficiently avoided. The research proved that there is a real hope in developing a general (robust) framework, which could keep by hard constraints blood glucose level inside a defined interval; moreover, it is not sensitive to different meal intake profiles. Hence, it could efficiently support individualized control (ex. model predictive control (MPC)) protocols appeared in the literature [6].

It is planned to extend the robust framework with hard constraints regarding different life-style situations (physical activity, stress) as well as increasing number of simulated test cases on real data provided by pump centers members of the newly created Hungarian Artificial Pancreas working group associated to the Hungarian Diabetes Association.

Regarding obesity, we performed a clinical study to investigate the connections of obesity and laboratory results, and its implications in screening on Hungarian adolescent population, which was never before examined from this aspect. We

could confirm that obesity causes systematical changes in the laboratory parameters. Differences between the means of these parameters of obese and healthy children also support the view of obesity as a chronic inflammation state. These differences also make the idea plausible to use the laboratory results for the classification of individuals. The true classification rate of 85-90% in both sexes of the logistic regression-based model could be in fact used to classify adolescents and also to be used in our risk prediction investigation.

Finally, regarding our investigations in the field of model-based cancer treatment, simulation results showed that even a simple optimal therapy can be beneficial. Our first obtained results show that an optimal therapy could start with an intense period, where the tumor volume is compressed, followed by a maintaining period, where the minimal value of inhibitor is given to the patient. This maintaining period can be continued till the remaining tumor cells are destroyed by another type of antitumor therapy. The main significance of the controller is in the allocation of the switching time, when the intense period should be terminated, and the maintaining period should be started.

Further investigations will be focused on other the application of other optimal control strategies (nonlinear control, modern robust control) as well as on model identification, model verification and biostatistic evaluation based on mice experiments in cooperation with clinical experts.

Acknowledgment. Levente Kovács was supported by the János Bolyai Research Scholarship of the Hungarian Academy of Sciences. This work was partially supported by the National Development Agency's GOP-1.1.1-11-2012-0055 project titled "DIALOGIC – Mathematical model-based decision support system to improve diabetes health management". The research work was also supported by the European Union and co-funded by the European Social Fund, project title: "Telemedicine-focused research activities in the field of Mathematics, Informatics and Medical Sciences", project number: TÁMOP-4.2.2.A-11/1/KONV-2012-0073.

The author thanks the members of the Physiological Controls Group, PhD students Péter Szalay, György Eigner, István Péter Sas for their work in the artificial pancreas problem, Dr. Tamás Ferenci for his work in the biostatistical investigation regarding obesity, PhD student Johanna Sápi for her work in the antiangiogenic tumor treatment. Special thanks are given to Dániel András Drexler and Dr. István Harmati from the Budapest University of Technology and Economics for their support in the model-based cancer treatment investigations.

The author say special thanks to the Hungarian Artificial Pancreas working group's insulin pump centers for the real data provided to validate the nonlinear model-based type 1 diabetes robust control algorithm as well as for Prof. Dr. László Barkai, president of the Hungarian Diabetes Association for his continuous support.

The author thank the secondary schools involved in obesity classification project: Fazekas Mihály (Budapest), Leövey Klára (Budapest), Puskás Tivadar (Budapest) and Esze Tamás (Mátészalka) Primary and Secondary Grammar

Schools. We say special thanks to Bétéri Csabáné for her cooperation in organizing the study at Mátészalka.

Finally, regarding the antiangiogenic research task, the authors say special thanks to Dr. Zoltán Sápi, deputy head of the 1st Department of Pathology and Experimental Cancer Research Institute from Semmelweis University Budapest, for his precious medical comments regarding the interpretation of the obtained results.

References

1. Bonzino, J.: The Biomedical Engineering Handbook. CRC in cooperation with IEEE Press (1995)
2. Kovács, L., Sápi, J., Ferenci, T., Szalay, P., Drexler, D., Eigner, G., Sas, P.I., Harmati, I., Kozlovszky, M., Sápi, Z.: Model-based optimal therapy for high-impact diseases. In: Proc. INES 2013 – 17th International Conference on Intelligent Engineering Systems, Costa Rica, pp. 209–214 (2013)
3. Wild, S., Roglic, G., Green, A., Sicree, R., King, H.: Global prevalence of diabetes – Estimates for the year 2000 and projections for 2030. Diab. Care 27(5), 1047–1053 (2004)
4. (April 8, 2013), `http://www.idf.org/diabetesatlas/diabetes-young-global-perspective`
5. Fonyó, A., Ligeti, E.: Physiology, Medicina, 3rd edn., Budapest (2008)
6. Cobelli, C., Dalla Man, C., Sparacino, G., Magni, L., de Nicolao, G., Kovatchev, B.: Diabetes: Models, Signals, and Control (Methodological Review). IEEE Rev. Biomed. Eng. 2, 54–96 (2009)
7. Andersen, R.E.: Obesity: etiology, assessment, treatment, and prevention. Human Kinetics Publishers, Champaign (2003)
8. SRI for Health, "Hungary's healthcare and social system", Budapest: Strategic Research Institute for Health (2004)
9. Avram, M.M., Avram, A.S., James, W.D.: Subcutaneous fat in normal and diseased states: 1. Introduction. J. Am. Acad. Dermat. 53, 663–670 (2005)
10. Hungarian Central Statistical Institute, Mortality by common death causes (1990), `http://portal.ksh.hu/pls/ksh/docs/hun/xstadat/xstadateves/iwnh001.html`
11. Malvezzi, M., Bertuccio, P., Levi, F., La Vecchia, C., Negri, E.: European cancer mortality predictions for the year 2013. Ann. Oncol. 24(3), 792–800 (2013)
12. WHO, International Agency of Research on Cancer, `http://www-dep.iarc.fr/`
13. WHO, Global Health Observatory, `http://www.who.int/gho/en/`
14. Wu, H.C., Huang, C.T., Chang, D.K.: Anti-angiogenic therapeutic drugs for treatment of human cancer. J. Cancer 4(2), 37–45 (2008)
15. Chee, F., Tyrone, F.: Closed-loop control of blood glucose. LNCIS, vol. 368. Springer, Heidelberg (2007)
16. Femat, R., Ruiz-Velazquez, E., Quiroz, G.: Weighting Restriction for Intravenous Insulin Delivery on T1DM Patient via H_∞ Control. IEEE T. Autom. Sci. Eng. 6(2), 239–247 (2009)
17. Sorensen, J.T.: A physiologic model of glucose metabolism in man and its use to design and assess improved insulin therapies for diabetes. PhD Thesis, Dept. of Chemical Eng. Massachusetts Institute of Technology, Cambridge (1985)
18. Kovács, L., Benyó, B., Bokor, J., Benyó, Z.: Induced L2-norm Minimization of Glucose-Insulin System for Type I Diabetic Patients. Comp. Meth. Prog. Biomed. 102(2), 105–118 (2011)

19. Kovács, L., Szalay, P., Almássy, Z., Barkai, L.: Applicability Results of a Nonlinear Model-Based Robust Blood Glucose Control Algorithm. J. Diab. Sci. Tech. 7(3), 708–716 (2013)
20. Dalla Man, C., Rizza, R., Cobelli, C.: Meal simulation model of the glucose-insulin system. IEEE T. Biomed. Eng. 54(10), 1740–1749 (2007)
21. Kovács, L., Szalay, P., Almássy, Z., Benyó, Z., Barkai, L.: Quasi In-Silico Validations of a Nonlinear LPV Model-based Robust Glucose Control Algorithm for Type I Diabetes. In: Proc. of IFAC WC 2011 – 18th World Congress of the International Federation of Automatic Control, Milano, Italy, pp. 7114–7119 (2011)
22. Mamtani, M., Kulkarni, H.: Predictive Performance of Anthropometric Indexes of Central Obesity for the Risk of Type 2 Diabetes. Arch. Med. Research 36, 581–589 (2005)
23. Jebb, S.A., Elia, M.: Techniques for the measurement of body composition: A practical guide. Int. J. Obes. Relat. Metab. Disorders 17, 611–621 (1993)
24. Ferenci, T.: Biostatistical analysis of obesity related parameters in Hungarian children. MSc Thesis, Budapest University of Technology and Economics (2009) (in Hungarian)
25. Ferenci, T.: Two Applications of Biostatistics in the Analysis of Pathophysiological Processes. PhD Thesis, Óbuda Univeristy, Budapest (2013)
26. Ferenci, T., Almássy, Z., Kovács, A., Kovács, L.: Effects of obesity: a multivariate analysis of laboratory parameters. In: Proc. of 6th Int. Symp. on Appl. Comput. Intell. Inf., Timisoara, Romania, pp. 629–634 (2011)
27. Kerbel, R.S.: A cancer therapy resistant to resistance. Nature 390, 335–336 (1997)
28. Kerbel, R., Folkman, J.: Clinical translation of angiogenesis inhibitors. Nature Rev. Cancer 2, 727–739 (2002)
29. Hahnfeldt, P., Panigrahy, D., Folkman, J., Hlatky, L.: Tumor development under angiogenic signaling: A dynamical theory of tumor growth, treatment response, and postvascular dormancy. Cancer Resarch 59, 4770–4775 (1999)
30. Ledzewitz, U., Schatler, H.: A synthesis of optimal controls for a model of tumor growth under angiogenic inhibitors. In: Proc. 44th IEEE Conference on Decision and Control, and the European Control Conference, pp. 934–939 (2005)
31. Ergun, A., Camphausen, K., Wein, L.M.: Optimal Scheduling of radiotherapy an angiogenic inhibitors. Bullet. Math. Biol. 65, 407–424 (2003)
32. O'Reilly, M.S., Boehm, T., Shing, Y., Fukai, N., Vasios, G., Lane, W.S., Flynn, E., Birkhead, J.R., Olsen, B.R., Folkman, J.: Endostatin: An endogenous inhibitor of angiogenesis and tumor growth. Cell 88, 277–285 (1997)
33. Pontryagin, L.S.: Mathematical Theory of Optimal Processes. Interscience Publishers (1962)
34. Lantos, B.: Theory and Design of Control Systems I-II. Akadémia Kiadó, Budapest (2005) (in Hungarian)
35. Precup, R.E., Preitl, S.: Optimisation criteria in development of fuzzy controllers with dynamics. Eng. Applic. Artif. Intellig. 17(6), 661–674 (2004)
36. Kovács, L., Paláncz, B.: Glucose-insulin control of Type1 diabetic patients in H_2/H_∞ space via computer algebra. In: Anai, H., Horimoto, K., Kutsia, T. (eds.) Ab 2007. LNCS, vol. 4545, pp. 95–109. Springer, Heidelberg (2007)
37. Drexler, D.: Optimal control of tumor-based deseases' chemotherapy. MSc thesis, Budapest University of Technology and Economics (2011) (in Hungarian)

38. Drexler, D.A., Harmati, I., Kovács, L.: Optimal control of tumor growth using antiangiogenic chemotherapy. In: Proc. of 3rd Int. Conf. on Recent Achievements in Mechatronics, Automation, Computer Sciences and Robotics, Targu-Mures, Romania, pp. 273–284 (2011)
39. Drexler, D.A., Kovács, L., Sápi, J., Harmati, I., Benyó, Z.: Model-based analysis and synthesis of tumor growth under angiogenic inhibition: a case study. In: Proc. of IFAC WC 2011 – 18th World Congress of the International Federation of Automatic Control, Milano, Italy, pp. 5012–5017 (2011)
40. Kovács, L., Szalay, P., Ferenci, T., Drexler, D.A., Sápi, J., Harmati, I., Benyó, Z.: Modeling and Control Strategies of Diseases with High Public Health Impact. In: Proc. INES 2011 – 15th International Conference on Intelligent Engineering Systems, Poprad, Slovakia, pp. 23–28 (2011)

Application of Artificial Intelligence Techniques in Monitoring Drilling Processes

Gyula Hermann

Institute of Applied Mathematics
John von Neumann Faculty of Informatics
Óbuda University
Bécsi út 96/b, 1034 Budapest, Hungary

1 Introduction

Tool wear and tool breakage are two important aspects of the metal cutting process that are not well understood. Tool wear has a strong effect on both the dimensional accuracy and the surface finish of the workpiece. Wear can reach values that lead to catastrophic failure of the tool, resulting in high forces which in turn may damage the workpiece or even the machine tool. This fact stresses the importance of tool monitoring.

Various methods for tool wear sensing have been proposed and evaluated in the past but none of them proved to be universally successful due to the complex nature of the cutting processes. There are two methods for online tool condition monitoring in machining processes. These methods have been classified into direct (optical, radioactive and electrical resistance, etc.) and indirect (acoustic emission, motor current, cutting force, vibration, etc.) sensing methods according to the sensors used. Recent investigations focus on the development of the methods which monitor the cutting process indirectly by measuring parameters such as tool vibration, force cutting, acoustic emission, motor current, etc.

The applied indirect methods suffer from the fact that not only the wear but other process parameters also influence the measurement results. These are the workpiece and tool materials, the geometry of the cutting tool and the technological parameters: cutting speed, feed and depth of cutting.

In order to improve the decision about the tools condition the majority of applications rely on various signal sources at the same time and merge them after filtering out unavoidable noises inherent to cutting and extracting the features carrying information about the . Obvious solutions for fusion of the sensory signals are the artificial neural networks and fuzzy rule-based systems.

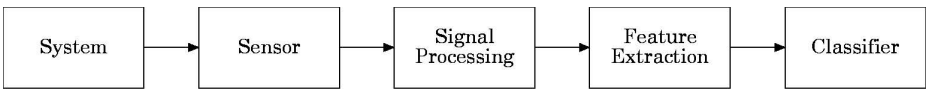

Fig. 1. The signal processing chain of a tool monitoring system

J. Fodor and R. Fullér (eds.), *Advances in Soft Computing, Intelligent Robotics and Control,* Topics in Intelligent Engineering and Informatics 8,
DOI: 10.1007/978-3-319-05945-7_4,

An artificial neural network consists of a number of identical processing units usually structured in two to four layers. The fundamental processing element is the perceptron, which calculates the weighted sum of its input, and passes the result through a non-linear threshold function: a simple signum function, a hyperbolic tangent or the sigmoid. The non-linear behaviour of the threshold function allows a neural network to extend the reach of pattern classification capabilities into the domain of generalised non-linear functions.

Fuzzy logic is a convenient way to map an input space to an output space. The mapping provides a basis from which decisions can be made. The process of fuzzy inference involves membership functions, fuzzy logic operators, and if-then rules. A membership function is a curve that defines how each point in the input space is mapped to a membership value (or degree of membership) between 0 and 1. There are two types of fuzzy inference systems Mamdani-type and Sugeno-type.

2 Overview of the Various Signals Generated by Machining

Forces and Torque in Cutting Processes. Torque, drift and feed force with the strain measurement are all measures of cutting forces and are strongly depend on the tool wear. These dynamic parameters generally increase as the tool gradually wears due to the increasing friction between tool and workpiece.

Monitoring the torque and thrust force is the most common method to collect information about the amount of tool wear in drilling. Cutting forces are affected by experimental conditions such as cutting speed and feed, workpiece material and type of the tool.

AE Signal Associated with a Cutting Process. Machine tool operators have for a long time used their ears as a means of monitoring the cutting process. Skilled machine tool operators are able to judge the change of the tool condition especially the variation of tool wear and an emerging tool failure. They are also able to predict surface the finish simply by listening to the cutting process. The term acoustic emission refers to the release of strain energy in the form of elastic waves associated with the deformation in the frequency range of $20 - 2000$ kHz [1].

The various sources of acoustic emission in machining are listed below:

- plastic deformation and shear of work material
- deformation and sliding friction at the chip-tool surface
- sliding friction at the tool flank
- chip breaking and their impact on the cutting tool or workpiece
- normal and abnormal wear of the tool
- mechanical and thermal crack of the tool

In conventional machining, acoustic emission is largely due to rubbing and friction at shear zone. In the precision machining, however, it is believed that the

majority of AE signal generation is generated through the interaction of the tool tip with microstructural features of the workpiece, such as voids, inclusions, grain boundaries, and bulk dislocation interactions in the shear zone [2,3,8].

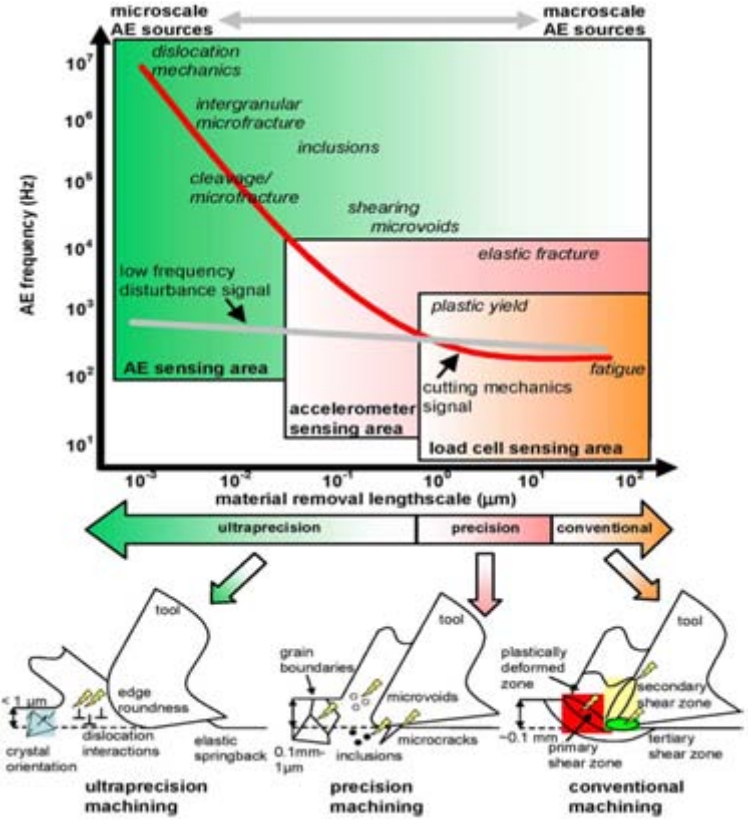

Fig. 2. AE sources at various stages of material removal

There are two types of acoustic emissions: the high amplitude, somewhat erretic, low frequency type called the burst emission which is generally associated with surface events, such as slip line formation and surface microcracks and the lower amplitude, steady and high frequency type called continuous emission that is generally associated with internal mechanism activity.

In recent years many researchers have investigated AE signals from metal cutting processes and their feasibility for in-process monitoring of tool conditions. The majority of the publications deal with the monitoring and supervision of turning and milling. One important goal of studying the AE from metal-cutting processes has been understanding the toolwear related AE variations and evaluating their capability for in-process monitoring of the tool condition. Two possibilities have been identified. One is the increase of the level AE energy (the RMS value of the signal) with increase of the flank wear. The other one is the

increase of the density and event counts (the number of events) exceeding a certain threshold.

Iwata and Morikawi [10] observed that the RMS voltage of the AE signal increased significantly as the carbide tool wore during the machining of carbon steel workpiece. They reported that flank wear has a more significant effect on the average RMS value than the change of cutting speed. Later it was found that cutting speed has a major influence in increasing the average RMS level and that the magnitude of the average AE signal increases abruptly as the tool wear penetrates through the coating of coated tools.

The relationship between the mean value of the AE signal and the flank was also studied by Kannetey-Asibu and Dornfeld [7]. They observed that the AE level change decreases or stops when the flank wear reaches some intermediate value. This phenomenon was attributed to the rapidly developing crater wear. Therefore they suggested the skew of the statistical distribution of the RMS value as a better indicator of the tool wear. Another interesting observation of this group was that the frequency spectrum contains dominant frequencies at 80 and 150 kHz and that the power spectrum amplitude at these frequencies increases with the tool wear.

Inasaki and Yonetsu [5] have found that the AE amplitude is independent of the depth of cut and the feed per revolution but increases continuously with the increasing cutting speed. For constant cutting speed, AE increases approximately linearly with the flank wear over the whole range of the cutting speed. The authors reported that the flank wear estimated using the AE signal and the optically measured values showed very good agreement, with less than 15% deviation.

Tool wear has also a significant effect on the density of pulse events in the AE signal. Iwata and Moriwaki [10] observed that the pulse count per cut increases with increasing flank wear up to about 120 μm and remained constant above that, but the data showed a significant degree of scatter. Inasaki and Yonetsu [5] found sudden increase in the even count rate after a tool developed extensive flank wear and at the same time an increase in the standard deviation of the count rate at this point. This phenomenon was attributed to the development of microcracks in the tool. Although the pulse event count seems to be well correlated to flank wear, many problems inhibit the usage of this relationship in process monitoring. The major problem is that a system based on this principle has to be calibrated for each specific machining condition and the selection of the threshold level for the pulse event count is somewhat arbitrary.

Tool fracture results in a sudden increase of the AE amplitude as it was already observed by Inasaki and Yonetsu [9]. Analysis of the data from cutting experiments using various speeds, feeds and depth of cuts also showed that the ratio of the AE amplitude before and after the breakage exceeds 1.8. Using this ratio they were able to detect edge chipping with fracture are of about 0.1 mm^2. In case of significantly worn tool this shift decreases. However, by filtering out the frequencies below 300 kHz the effect of wear can be reduced and even the detection of microcracks was reported.

In a recent paper R. Teti, K. Jemielniak, G. O'Donnell, D. Dornfeld [11] give an overview of the different approaches to tool condition monitoring. They also compare them from various points of view. Beside force base detection special attention is given to acoustic emission based systems and signal fusion techniques applied in current experimental setups.

Hase [4] describes the application acoustic emission monitoring of the tool condition in a high precision turning environment they have found that Sensing contact of cutting tool and workpiece would be possible with high precision of 0.1 μm using the AE technique, the amplitude of the AE signal increases as the spindle rotating speed and the cutting depth increase, adhesion of the workpiece material to the rake face of the cutting tool (the formation of built-up edge) can be identified by detecting a high frequency AE signals of more than 1 MHz. The same results were achived by S. Min, J. Lidde, N. Raue, D. Dornfeld [9].

Vibration Generated by Machining Processes. Vibrations in machining can be divided into two groups: dependant and independent of the manufacturing process itself. Independent vibration include forced vibration caused by machine components, e.g. unbalance of rotating parts, inertia forces of reciprocating parts and kinematic inaccuracies of drives. Vibration dependant on metal cutting can demonstrate a number of characteristics as a function of the process, e.g. interrupted cutting. The varying cutting forces that occur during metal cutting may result from non-homogeneity and properties variations in the work material. Tool engagement conditions during machining play a notable role in the vibration produced. The self excited vibration characteristic known as chatter is the most renowned type of vibration in machining and it leads to surface finish deterioration and decrease of tool life. Chatter occurs due to the waviness regeneration caused by material surface and tool interaction at particular spindle rotational frequencies, and by mode coupling where relative vibration between workpiece and tool.

3 Drill Condition Monitoring

3.1 Description of the Solution

Drill wear was classified into seven types: the outher corner wear, the flank wear, land wear, crater wear, two types of chisel edge wear and chipping on the cutting edges. Out of the various wear patterns the outer corner wear is considered as the most appropriate performance index of drill life.

Drilling operation represents approximately 40% of all machining operation. Therefore the role of monitoring tool condition became important, especially in case of small twisted drills with diameter in the $0.5 - 5$ mm range. Drill wear can be classified in outer corner wear, flank wear, land wear, crater wear, two types of chisel edge wear and chipping on the cutting edges. Corner wear is the best performance index of drill life. As wear cannot be measured directly in the process, indirect measuring methods have to be applied. For this purpose process

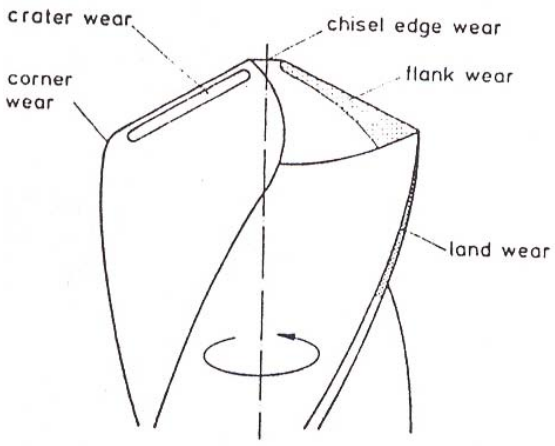

Fig. 3. Various types of wear on a twist drill

signatures like cutting and trust force, torsional vibration, acoustic emission, etc. can be used.

Increasing wear at the outher corner or margins excite torsional vibration in the worn drill, causing a periodic change in the length of the tool due to its spiral form, resulting in chip thickness variation. The cutting speed at the outher corners of the vibrating drill is several times higher than in a stable process. The wear-induced vibration can be detected using acoustic emission sensors.

For the fusion of sensory signals neural networks is the obvious solution. The neural network structure used in our investigations was a multilayer feed-forward neural network that uses the backpropagation learning algorithm. The input layer has one node for each feature extracted from the raw signature. In the output layer, the number of perceptrons is determined by the number of possible classes and their coding.

In our case for monitoring the drill condition the following features have been used:

- rms value of the power in the band $0 - 300$ Hz
- rms value of the power in the band $300 - 600$ Hz
- rms value of the power in the band $600 - 1000$ Hz
- rms of the power in the band $1000 - 1500$ Hz
- rms of the power in the band $1000 - 1500$ Hz
- rms of the power in the band $1500 - 2000$ Hz

3.2 Experimental Setup

The experimental drill monitoring system was set up on a manually operated conventional milling machine.

For capturing the acoustic emission and the vibration signals an AKL 85 and a KD 91 broadband sensor were attached to the workpiece close (50 mm) to the

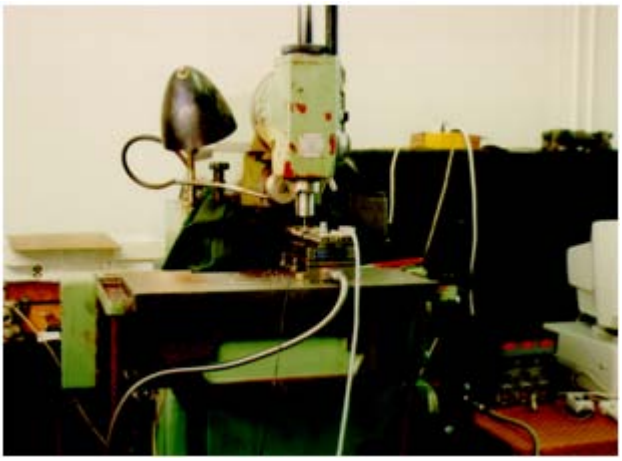

Fig. 4. Experimental setup of the drilling process

actual cutting zone. The feed force was measured by a Kistler dynamometer. The signals were amplified by charge amplifiers.

The acoustic emission signal was directly processed by a Krenz broadband spectrum analyzer with 2 MHz bandwidth and at the same time the RMS value was sampled by a data acquisition board on a personal computer. The force and vibration signals were processed using the same data acquisition board, but with a much lower sampling rate.

3.3 Experimental Results

The aim of experiments was finding suitable features for tool wear and failure detection. As the experiments proved, the torsional vibration resulted in dominant frequencies in both the AE and the low frequency vibration spectrum. The power spectrum of the AE signal has a dominant frequency around 80 kHz and shows dramatic increase at the end of the tool life. One can also notice the appearance of a new peak at 100 kHz in the spectrum of the worn tool.

The experiments showed no significant influence of the cutting parameters and the workpiece material on the place of the dominant frequencies in the AE spectrum, only their amplitude was effected.

The behaviour of the low frequency vibration signal as function of the tool wear was also investigated. A rather similar pattern signalling excessive tool wear and tool failure was found. As it can be seen in Fig.7 there is a dominant frequency in the spectrum in the neighbourhood of 6.5 kHz. The amplitude of this peak shows close correlation with the condition of the tool. Moreover, it was found that the frequency of this peak is independent of the machining parameters (revolution, feed) and the material of the workpiece.

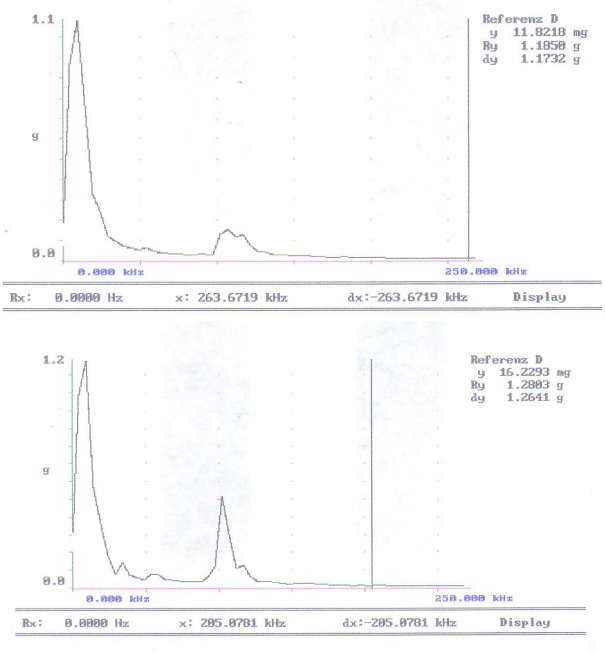

Fig. 5. AE spectrum of sharp and worn 1.5 mm diameter twist drill (material KO36 feed 25 mm/min, 2500 rev/min)

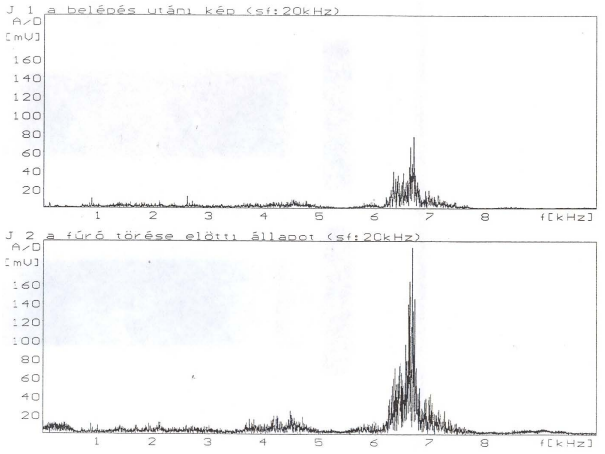

Fig. 6. Vibration spectrum of 1.5 mm diameter twist drill (material KO36 feed 25 mm/min, 2500 rev/min)

The third signal measured during the machining experiments was the feed force. In the subsequent figure the AE average value shown together with the value of the feed-force. One can notice the increase of the AE activity as the tool wears. This trend in the AE activity can be observed even after the toolbreak when the force falls back to a low value.

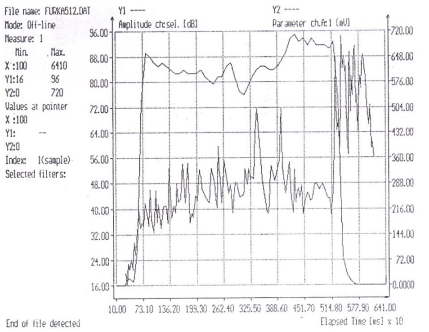

Fig. 7. AE activity and feedforce during tool failure

However, at the end of a cut similar signature can be observed even under normal cutting conditions. This can lead to incorrect recognition of the tool conditions. To avoid recognition mistakes, information about the signal trend is incorporated in the decision process.

In our experiment for sensor fusion two types of networks has been used: multilayer feedforward network and the single category based classifier which is actually a weighted majority based decision-maker. The tables below summarise the correct recognition rates, that was achieved, by the two networks in the various sensor fusion experiments.

Table 1. Correct recognition rate of the multilayer feedforward network

Sensor Combination	Correct Recognition Rate
RMS AE + Force	94%
RMS AE + Vibration	72%
Vibration + Force	85%

Table 2. Correct recognition rate of the single category based classifier

Sensor Combination	Correct Recognition Rate
RMS AE + Force	96%
RMS AE + Vibration	75%
Vibration + Force	89%

Table 3. The influence of the number of input features on the correct recognition rate is given in case of a single category based classifier

Number of Input Features	Correct Recognition Rate
2	94%
4	96%
6	96%
8	82%

Table 4. Recognition rate using fuzzy reasoning

Tool condition	Recognition Rate
Initial	61%
Normal	89%
Acceptable	81%
Severe	76%
Tool failure	100%

4 Conclusion

An on-line drill wear/failure monitoring system was developed and evaluated in this study. On the basis of these investigations the following conclusions can drawn:

- By applying a neural network in combination with an AR time series model a considerable improvement in the correct tool condition recognition rate can be achieved.
- The AE RMS + Force signal based tool wear detection system is insensitive to the changes of the cutting conditions and can operated over a wide range of cutting parameters.
- It was recognised that for tool wear detection a relatively small neural network works well.
- The single category based classifier has the advantage over the multilayer feedforward network the in can learn unsupervised which is advantageous in an industrial environment.

References

1. Brinksmeier, E.: Prediction of Tool Fracture in Drilling. Annals of the CIRP 39(1) (1990)
2. Chae, J., Park, S.S., Freiheit, T.: Investigation of micro-cutting operations. International Journal of Machine Tools & Manufacture 46, 313–332 (2006)
3. Dornfeld, D.A., Min, S., Takeuchi, Y.: Recent Advances in Mechanical Micromachining. Annals of the CIRP 55(2), 745–768 (2006)
4. Hase, A.: Acoustic Emission Signal during Cutting Process on Super-Precision Micro-Machine Tool. In: Proceedings of Global Engineering, Science and Technology Conference, Singapore, October 3-4 (2013)

5. Inasaki, I., Yonetsu, S.: In-Process Detection of Cutting Tool Damage by Acoustic Emission Measurement. In: Proceedings of the 22nd International Machine Tool Design and Research Conference, Manchester University, UK, pp. 261–268 (1981)
6. Iwata, K., Morikawi, T.: An Application of Acoustic Emission Measurement to In-Process Sensing of Tool Wear. Annals of the CIRP 25(1), 21–26 (1977)
7. Kannatey-Asibu, E., Dornfeld, D.A.: A Study of Tool Wear Using Statistical Analysis of Metal-Cutting. Acoustic Emission Wear 76, 247–261 (1983)
8. Lee, D.E., Hwang, I., Valente, C.M.O., Oliveira, J.F.G., Dornfeld, D.A.: Precision manufacturing process monitoring with acoustic emission. International Journal of Machine Tools & Manufacture 46, 176–188 (2006)
9. Min, S., Lidde, J., Raue, N., Dornfeld, D.: Acoustic emission based tool contact detection for ultra-precision machining. CIRP Annals – Manufacturing Technology 60, 141–144 (2011)
10. Moriwaki, T.: Application of Acoustic Emission Measurement to Sensing of Wear and Breakage of Cutting Tool. Bull. Japan Soc. of Prec. Eng. 17(3) (1983)
11. Teti, R., Jemielniak, K., O'Donnell, G., Dornfeld, D.: Advanced monitoring of machining operations. CIRP Annals – Manufacturing Technology 59, 717–739 (2010)

Functional Synthesis of a New Class of Micro Electro-Mechanical Systems

Nicola Pio Belfiore

Sapienza University of Rome,
Department of Mechanical and Aerospace Engineering,
via Eudossiana, 18, 00184 Rome, Italy
nicolapio.belfiore@uniroma1.it
http://dima.uniroma1.it/belfiore/

Abstract. This paper discloses a new method of functional synthesis of a new class of MEMS (Micro Electro-Mechanical Systems) that could be conceived thanks to: (a) a new concept flexural hinge (that has been recently patented by the Author) and (b) the accurate detection of a MEMS device pseudo-rigid-body equivalent mechanism, which allows the application of several classic algorithms well known in kinematic synthesis. The adopted approach is explained and two examples are presented. Finally, basic information is provided for the MEMs technology based construction process that has been used for prototyping.

Keywords: MEMS, kinematic synthesis, functional design, micro robotics.

1 Introduction

During the last decades MEMS devices have been increasingly employed for many purposes, such as, for example, accelerometers, gyroscopes, inkjet printers, pressure sensors, microphones, switching, energy harvesting, drug delivery systems, and many other types of sensors and actuators [1–11]. More recently, a new flexural hinge has been proposed for the design of MEMS [12–17], which discloses how to build a new class of multi Degrees of Freedom (DOF) MEMS devices. However, there are still many issues to be investigated such as, for example, the construction methods, the geometric optimization, the overall compliance characterization and control [18, 19] and, mainly, the design method, which the present paper is dedicated to. MEMS and compliant mechanisms are similar in many aspects since they can move because they are both composed of flexible (thinner) and pseudo-rigid (thicker) subparts. Therefore, all the methods developed for the study of the compliant mechanisms can be adopted for the study of MEMS devices. Thanks to some important papers presented in literature, such as, for example, Howell's and Midha's [20–23], the pseudo-rigid-body model has been introduced and refined to simulate a compliant mechanism for many types of geometry and loadings. The main advantage of using the pseudo-rigid-body equivalent mechanism consists in the fact that it can be analyzed as an ordinary

J. Fodor and R. Fullér (eds.), *Advances in Soft Computing, Intelligent Robotics and Control,* Topics in Intelligent Engineering and Informatics 8,
DOI: 10.1007/978-3-319-05945-7_5,

mechanism with revolute joints and there-fore many different approaches can be used for topological [24–26] and kinematic higher order [27, 28] synthesis.

2 Theoretical Basis

The overall motion of MEMS devices can be understood only if the relative motion between any pair of adjacent *pseudo-rigid* links is identified. Unfortunately, this relative motion is not easy to figure out because it depends not only on geometry, but also on the intensity of the load which inflects the compliant parts. There are some basic strategies developed in order to set up the *most reliable* pseudo-rigid body model of a given compliant mechanism: the simplest one consists in substituting a flexible sub-part, connecting pseudo-rigid bodies i and j, by a revolute joint R whose center is positioned in correspondence of the center C_R of the finite relative rotation between pseudo-rigid links i and j. However, flexible parts have been simulated also by using two RR or even three RRR revolute joints. In the present investigation one single R, revolute joint, substitution is considered, because RR and RRR substitutions make the equivalent mechanism very impractical for the application of the kinematic synthesis methods and they introduce a great number of idle DOF.

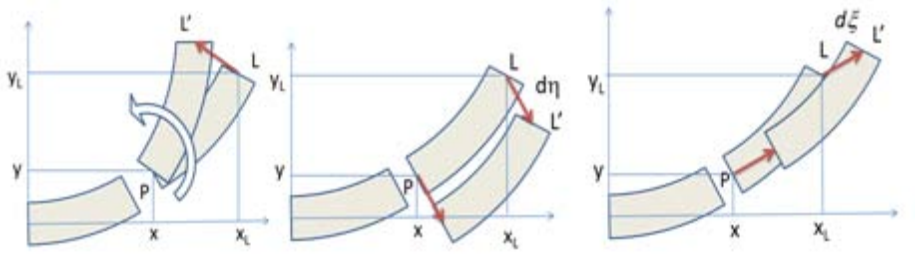

Fig. 1. Displacement of the end section center L due to the moment (a), shear (b) and normal tension (c) in the elementary section P

Considering that the flexible sub-parts often consist of linear or curved beams, a pre-liminary analysis has been performed in order to ascertain where center CR could be positioned to.

2.1 Approximate Calculation of the Center C_R of the Relative Rotation

A curved beam has been analyzed herein by assuming that: (a) the Hooke's Law holds for the material, (b) the external forces act in the plane which contains the curved beam axis; (c) the inflection axis is always normal to this plane;

(d) the material is isotropic and homogeneous. According to the Euler-Bernoulli static beam equation, given a torque M_k applied to the end section of a curved beam, the end section overall rotation $\Delta\vartheta$ form the initial A_0B_0 to the final A_kB_k position, is obtained by summing the infinitesimal rotations due to the deformations of all the elements along the curved axis s, from $s = 0$ (framed section) to $s = L$ (end section):

$$\Delta\vartheta = -\int_0^L \frac{M\mathrm{d}s}{EI}, \tag{1}$$

where M is the bending moment in the beam, E is the elastic modulus and I is the second moment of area of the beam cross-section. With reference to Fig. 1, the end section displacement LL' from its initial position A_0B_0 to its final position A_kB_k can be represented by the displacements Δx and Δy of the end section midpoint L. The latter are obtained by summing up the contributions due to tensile/compressive force N, Fig. 1(c), shear force T, Fig. 1(b), and to the bending moment M, Fig. 1(a), in all the cross-section elements in the beam, from $s = 0$ to $s = L$, namely,

$$\Delta x = \int_0^L \frac{M\mathrm{d}s}{EI}(y_L - y) + \int_0^L \frac{N\mathrm{d}x}{EA} + \int_0^L \chi\frac{T\mathrm{d}y}{GA}, \tag{2}$$

$$\Delta y = -\int_0^L \frac{M\mathrm{d}s}{EI}(x_L - x) + \int_0^L \frac{N\mathrm{d}y}{EA} - \int_0^L \chi\frac{T\mathrm{d}x}{GA}, \tag{3}$$

where G is the shear modulus, A is the beam cross-section area, and $\chi > 1$ is a shear correction factor introduced in order to allow the non-uniform shear strain to be ex-pressed as a constant. Eqns. (1)–(3) can be used to obtain the positions A_kB_k of the beam end section for increasing values of the external torque $M_{k+1} > M_k$, as reported in Fig. 2. By using the theory of displacement matrices, as for example in [17], the coordinates x_{0k} and y_{0k} of the center of the finite rotation of the end-section from the initial position to the k-th one can be expressed as the functions

$$x_{0k} = x_L + \frac{\Delta x}{2} - \Delta y\frac{\sin(\Delta\vartheta)}{2\,(1-\cos(\Delta\vartheta))} \tag{4}$$

$$y_{0k} = y_L + \frac{\Delta y}{2} + \Delta x\frac{\sin(\Delta\vartheta)}{2\,(1-\cos(\Delta\vartheta))} \tag{5}$$

of $\Delta\vartheta$, Δx and Δy. Fig. 2 shows the positions of 4 finite rotation centers. By iterating the procedure 20 times, it could be ascertained that the less the module of the exter-nally applied moment M_k, the more the corresponding center C_{0k} gets close to the center C of the elastic weights of the beam. Such result suggests the idea of creating the pseudo-rigid body model by substituting, in the compliant mechanism, any elastic beam by a revolute joint R positioned in correspondence of the center of the elastic weights of the beam.

2.2 Kinematic Synthesis of the PRB Equivalent Mechanism

By using the results obtained in the previous paragraph, the development of new MEMS devices can be based on the adoption of a pseudo-rigid-body (PRB for short) mechanism which is obtained by introducing, for each elastic joint (flexible curved beam), one revolute joint R whose center is placed in correspondence of the center of the elastic weights of the flexible beam. This method is simpler and also more accu-rate than those which use, for each elastic joint, two RR or even three RRR revolute joints [29, 30].

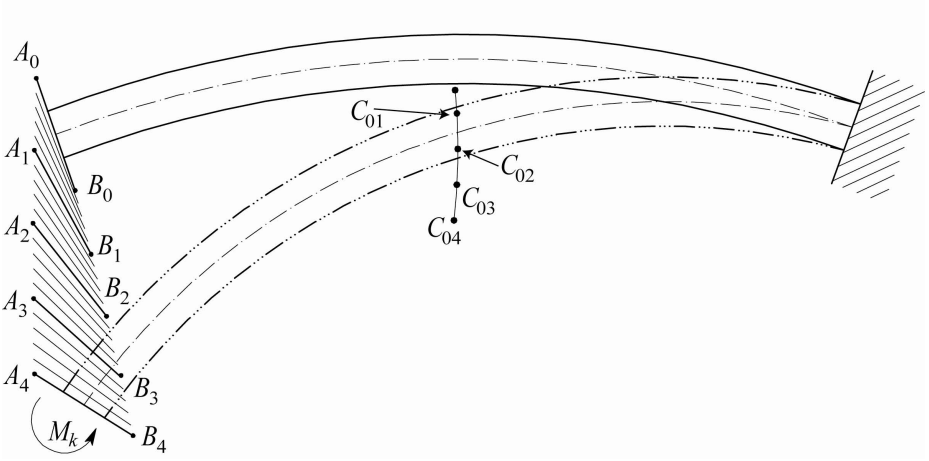

Fig. 2. Displacements A_kB_k of the end section A_0B_0 of a curved beam subject to incremental torques M_k and their correspondent centers of the relative motions C_{0k}, with $k = 1, 2, 3, 4$

The correspondence between *compliant mechanisms* and *PRB models* is not a bijective function because obtaining a PRB mechanism starting from a compliant mechanism is, intrinsically, an approximate procedure. In fact, since the centers of the relative motions between adjacent links depend on the applied loads, generally it doesn't exist a unique *PRB model* which is able to substitute the original *compliant mechanism* without errors in motion reproduction. Hence, for a given compliant mechanism there are many PRB models which simulate the motion, but they all will do that *approximately.* Analogously, the *inverse* process of building a compliant mechanism (MEMS device) starting from a *PRB mechanism* will not admit a unique solution and there will be, generally, several solutions which can be generated. By using this inverse approach, it is possible to use type [31] and kinematic synthesis.

Three main classic problems of kinematic synthesis have been investigated in the past century, namely, rigid body guidance, function generator and path generator. Except for the first, they can be studied both for finite and infinitesimal

motion, and, so, a large variety of applications has been developed for many purposes. As far as MEMS devices are concerned, the limited mobility around the neutral configuration suggests the idea that infinitesimal motion could be the preferred theoretical back-ground. However, as shown in previous works [12–16], silicon allows an unexpectedly large inflection and so the new silicon flexural hinges, embedded in the new class of MEMS, offer a range of relative rotations approximately equal to $[-20°, +20°]$. Therefore, it is not convenient to exclude the class of algorithms explicitly conceived for the finite displacements. The Author has attempted to give an estimation of the attitude of the main classes of algorithms used in kinematic synthesis to yield promis-ing results in MEMS design and such assessment is resumed in Table 1.

Table 1. A rough estimation (2014) of all the possible applications of the methods developed in Kinematic Synthesis to MEMS design and optimization

MEMS Synthesis	Function generator	Path generator	Rigid Body Guidance
Finite motion	*very promising*	*very promising*	*Promising*
Infinitesimal motion	*rare applications*	*very promising*	*Unpractical*

In the following paragraphs it will be shown how the synthesis of a PRB mechanism can be done by using classic approaches in kinematic synthesis, such as Burmester's and Generalized Burmester's Theory [32], Freudenstein's equation, and Suh's and Radcliffe's Displacement Matrices Synthesis [33] for finite motions.

3 Design Method

Once a method to establish a reliable, although approximate, compliant-to-PRB mechanism correspondence is chosen, the whole design approach can be based on classic design steps. Hence, provided that the procedure based on single R substitution of the compliant beams, as described in paragraphs 2.1 and 2.2, is accepted, the following steps can be adopted.

1. Number and Type synthesis of the PRB mechanism
2. Kinematic Synthesis of the PRB mechanism
3. Construction of the real *compliant mechanism (MEMS device)* from the PRB mechanism
4. Kinetostatic Validation via FEA and/or theoretical modeling
5. Prototyping and experimental validation

In the following paragraph, Steps 2, 3 and 5 will be exemplified.

4 Examples of Application

In this paragraph two examples of applications are considered. As a first case study, the kinematic synthesis of a 3 DOF parallel plane [34] platform for finite displacements is considered, for three assigned orientations of the mobile platform. The second case study consists in the synthesis of a mechanism which generates a circular arc with the fourth order of approximation in the neighborhood of a coupler point. For this problem the class of algorithms dedicated to infinitesimal motion is considered [35].

4.1 Function Generator for Finite Displacements

With reference to Fig. 3, the design goal is supposed to be the synthesis of a parallel micro-robot with three prescribed platform angular positions ψ_1, ψ_2, and ψ_3 for three corresponding prescribed angular positions of an input link φ_1, φ_2, and φ_3, assuming that the platform tip M had null displacements. Assuming also that the parallel plat-form is supported by two symmetric binary legs, symbols a and b will stand for the lengths of the leg links, while c will represent the half length of the upper platform link.

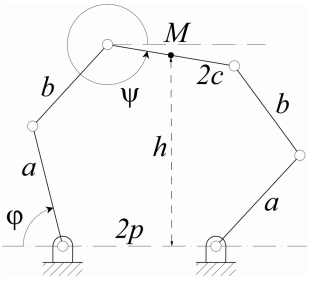

Fig. 3. Nomenclature

While the frame link length $2p$ and the platform tip M height h (with respect to the frame link) are supposed to be known parameters, the lengths a, b, and c are unknown. Hence, the synthesis of a function generator mechanism consists in finding the unknown lengths in such a way that the three pairs of angles (φ_1, ψ_1), (φ_2, ψ_2), and (φ_3, ψ_3) hold for three configurations.

Application of the Freudenstein's Equation. According to the Nomenclature defined in Fig. 3 and to the assumed requirements, it is possible to consider the tip point M as a fixed point in the plane, since only the rotations are inquired, and, so, the distance between the first revolute joint and point M remains positioned as in the undeformed neutral configuration. As shown in Fig. 4(a) this

distance will be referred to as $d = \sqrt{h^2 + p^2}$, where h is the point M height with respect to the frame link and p is the frame link half-length. According to the Figure, angle χ can be easily obtained from the system geometry, being $\frac{h}{p} = \tan\chi$.

Since three pairs of angles φ and ψ are given, the following system of equations can be written

$$\begin{cases} R_1 \cos\varphi_i - R_2 \cos\psi_i + R_3 = \cos(\varphi_i - \psi_i) \\ i = 1, 2, 3 \end{cases} \tag{6}$$

and solved with respect to R_1, R_2 and R_3. Since d is known, the unknown variables of the problem can be obtained:

$$\begin{cases} c = \dfrac{d}{R_1} \\ a = \dfrac{d}{R_2} \\ b^2 = a^2 + c^2 + d^2 - 2acR_3 \end{cases} \tag{7}$$

Table 2. Dimensions a, b and c of the links, as obtained by applying the Freudenstein's equation for the prescribed set of input and output angles

Input angles			**Output angles**			**Link dimensions (μm)**		
φ_1	φ_2	φ_3	ψ_1	ψ_2	ψ_3	a	b	c
105°	115°	135°	37°	59°	81°	27	36	22

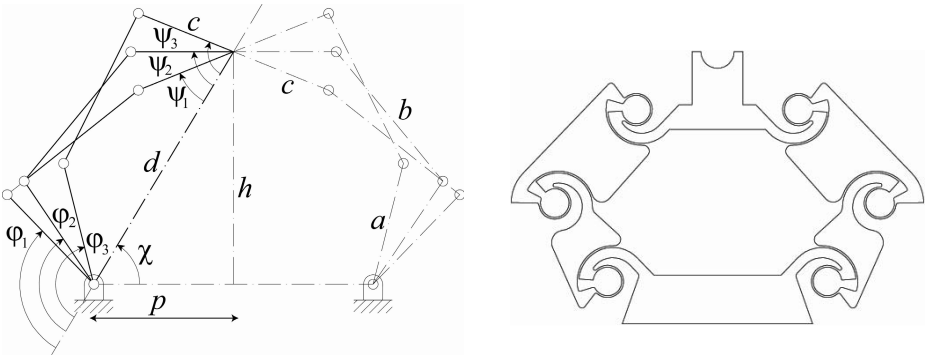

Fig. 4. Application of the Freudenstein's equation to the synthesis of a four-bar linkage function generator (a) embedded in a planar MEMS technology based 3 DOF platform (b)

Numerical Results. A representative example of application of the general method based on the Freudenstein's equation for the generation of a function generation four-bar linkage is reported herein. Given the frame link half-length $p = 30\,\mu$m and the undeformed platform height $h = 50\,\mu$m, Freudenstein's equation could be applied to a *virtual* four-bar linkage a, b, c and d which works as a function generator (for three prescribed pairs of φ and ψ angles) embedded *inside* the kinematic structure of the parallel platform. Fig. 4(a) displays pictorially the idea of embedding a four-bar linkage in the parallel mechanism and it reports the adopted nomenclature and symbols. The numerical values are summarized in Table 2.

Deduction of the Real MEMS Device and Prototyping. Starting from the PRB mechanism that has been obtained by using Freudenstein's equation, a *real* compliant mechanism (or MEMS) can be built, for example, as the one depicted in Fig. 4(b). Fig. 5 shows a detail of a sample from the family of the silicon micro-robots prototypes that have been manufactured via Reactive-Ion Etching RIE process and that are based on the new flexural hinge [36, 37].

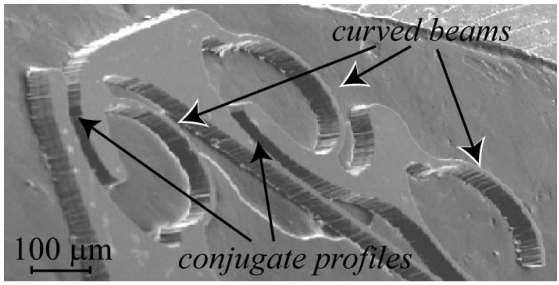

Fig. 5. A SEM (Scanning Electron Microscope) detailed view of three flexural hinge of a silicon microrobot

In Fig. 5 three silicon flexural hinges, each one being composed of a flexible curved beam and a pair of conjugate profiles, are represented by means of a SEM image. This MEMS device has been obtained by means of a $50\,\mu$m depth RIE Etching.

4.2 Kinematic Synthesis of Path Generator Mechanism for Infinitesimal Motion

As a second case study the kinematic synthesis of a path generator mechanism for infinitesimal motion is considered. A circular arc is considered as the prescribed path and a fourth order accuracy is required for the approximating coupler curve.

Application of the Classic Burmester's Theory. Among the variety of methods for the kinematic synthesis of mechanisms, those based on the geometric invariants have been used in many applications. The geometric invariants $a(\varphi)$ and $b(\varphi)$ are introduced as the coordinates of the origin of the Canonic Reference System attached to the mobile plane with respect to the fixed (absolute) reference frame. Both coordinates are regarded as a function of the angular position of the mobile reference frame and their first a_1, b_1 and higher order derivatives a_2, b_2, ..., a_n, b_n, with respect to φ are introduced as *geometric invariants*. The first, second, third and fourth order derivatives have the meaning of the *geometric velocity*, *acceleration*, *jerk* and *jounce* of the origin of the mobile reference system. By introducing the Canonic Reference System (C, ξ, η), which has the origin positioned in correspondence of the instantaneous center of rotations C, and the axes ξ and η tangent and orthogonal, respectively, to the *centrodes* in C, the expression of the *cubic of stationary curvature* can be expressed in a simplified form

$$\left(\xi^2 + \eta^2\right)(\xi a_3 + \eta b_3) + 3\xi b_2\left(\xi^2 + \eta^2 - b_2\eta\right) = 0. \tag{8}$$

Eqn. (8) represents the locus of points (of the mobile plane) for which the trajectory has a stationary curvature radius. The Burmester's points can be found by solving the system of equations composed of Eqn. (8) and of the stationary condition for the second order derivative

$$\frac{\mathrm{d}^2\kappa}{\mathrm{d}\varphi^2} = 0 \tag{9}$$

of the curvature $\kappa = \frac{\mathrm{d}\varphi}{\mathrm{d}s}$, where s is the scalar abscissae along the trajectory. Although the locus defined by Eqn. (9) has no interesting meaning, this condition, if taken together with condition (8), defines a discrete number of points whose trajecto-ry describes an arc of circle with fourth order approximation.

Table 3. Numerical values for the crank, coupler, rocker and frame link lengths, crank angle and coordinates of one Burmester's point

Independent design variables					Output variables		
Crank length	Coupler length	Rocker length	Frame link length	Crank angle	B_x	B_y	curvature radius
45 μm	140 μm	200 μm	260 μm	70°	−277 μm	282 μm	1.7 mm

For the set of data given in Table 3, which includes the lengths of the crank DL, coupler LE, rocker EM, frame DM and the given crank angle with respect to the frame, one feasible Burmester's point could be found by solving the system of equations (8) and (9). The path of B, attached to the coupler, does approximate a circular arc with a fourth order approximation. Point B coordinates and the trajectory curvature radius are given also in Table 3.

Construction of the Real Device. Starting from the given four-bar linkage and using the position of point B, a path generator MEMS device could be built by means of single R substitution. Each revolute joint R of the resultant four-bar linkage has been substituted by a new concept flexural hinge. As shown in Fig. 7, point B must be attached to the pseudo-rigid coupler link.

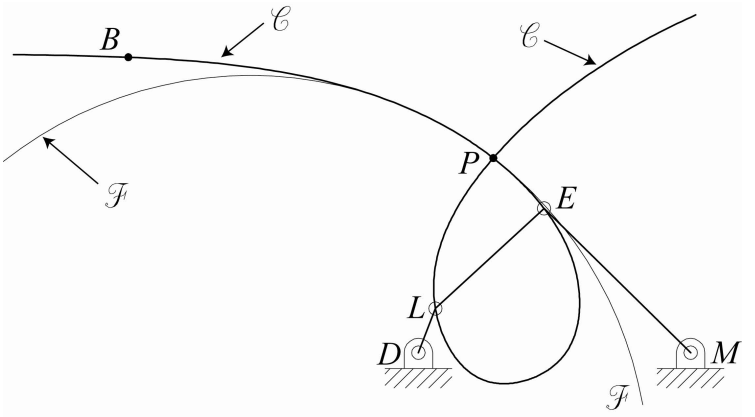

Fig. 6. Detection of the inflection circle $\mathscr{F}$, the cubic of stationary curvature curve $\mathscr{C}$ and of point B, which is one of the Burmester's point

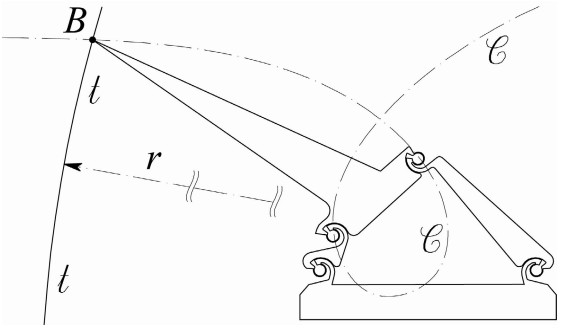

Fig. 7. The MEMS technology based silicon micro four bar linkage generating the circular arc t (r being the radius) in the neighborhood of point B, which is one of the Burmester's point

5 Conclusions

In this paper, firstly the inflexion of a generic curved beam has been analyzed by means of Euler Bernoulli element model: the study of the relative displacements among the beam extreme sections showed how to build a method, based on single revolute joint R substitution, for detecting a feasible *pseudo rigid body mechanism* which could be considered as the equivalent of a given *compliant*

mechanism. Then, the idea of applying kinematic synthesis to MEMS design, via R substitution, has been explained and two examples have been presented: function generation for finite displacements by means of Freudenstein's equation and path generation for infinitesimal motion by means of the classic Burmester's theory. For each problem, one possible MEMS device has been presented. Prototypes could be obtained by using Reactive Ion Etching (RIE) process. The whole method relies on the use of a new concept flexural hinge that has been recently patented by the Author.

References

1. Nguyen, N.-T., Huang, X., Chuan, T.K.: MEMS-micropumps: A review. Journal of Fluids Engineering, Transactions of the ASME 124(2), 384–392 (2002)
2. Cook-Chennault, K.A., Thambi, N., Sastry, A.M.: Powering MEMS portable devices - A review of non-regenerative and regenerative power supply systems with special emphasis on piezoelectric energy harvesting systems. Smart Materials and Structures 17(4), art. no. 043001 (2008)
3. Grayson, A.C.R., Shawgo, R.S., Johnson, A.M., Flynn, N.T., Li, Y., Cima, M.J., Langer, R.: A BioMEMS review: MEMS technology for physiologically integrated devices. Proceedings of the IEEE 92(1), 6–21 (2004)
4. Ho, C.-M., Tai, Y.-C.: Review: MEMS and its applications for flow control. Journal of Fluids Engineering, Transactions of the ASME 118(3), 437–447 (1996)
5. Tsai, N.-C., Sue, C.-Y.: Review of MEMS-based drug delivery and dosing systems. Sensors and Actuators, A: Physical 134(2), 555–564 (2007)
6. Tanaka, M.: An industrial and applied review of new MEMS devices features. Micro-electronic Engineering 84(5-8), 1341–1344 (2007)
7. Chuang, W.-C., Lee, H.-L., Chang, P.-Z., Hu, Y.-C.: Review on the modeling of electrostatic MEMS. Sensors 10(6), 6149–6171 (2010)
8. Tekin, T.: Review of packaging of optoelectronic, photonic, and MEMS components. IEEE Journal on Selected Topics in Quantum Electronics 17(3), art. no. 5740939, 704–719 (2011)
9. Jones, B.E., Yan, T.: MEMS force and torque sensors/a review. Measurement and Control 37(8), 236–241 (2004)
10. Bogue, R.: Recent developments in MEMS sensors: A review of applications, markets and technologies. Sensor Review 33(4), art. no. 17094935, 300–304 (2013)
11. Nenzi, P., Crescenzi, R., Dolgyi, A., Klyshko, A., Bondarenko, V., Belfiore, N.P., Balucani, M.: High density compliant contacting technology for integrated high power modules in automotive applications. In: Proceedings - Electronic Components and Technology Conference, art. no. 6249111, pp. 1976–1983 (2012)
12. Belfiore, N.P., Verotti, M., Crescenzi, R., Balucani, M.: Design, optimization and construction of MEMS-based micro grippers for cell manipulation. In: Proceedings of the ICSSE 2013 - IEEE International Conference on System Science and Engineering, art. no. 6614642, pp. 105–110 (2013)
13. Belfiore, N.P., Emamimeibodi, M., Verotti, M., Crescenzi, R., Balucani, M., Nenzi, P.: Kinetostatic optimization of a MEMS-based compliant 3 DOF plane parallel platform. In: Proceedings of the ICCC 2013 - IEEE 9th International Conference on Computational Cybernetics, art. no. 6617600, pp. 261–266 (2013)

14. Belfiore, N.P., Balucani, M., Crescenzi, R., Verotti, M.: Performance analysis of compliant MEMS parallel robots through pseudo-rigid-body model synthesis. In: ASME 2012 11th Biennial Conference on Engineering Systems Design and Analysis, ESDA 2012, vol. 3, pp. 329–334 (2012)
15. Balucani, M., Belfiore, N.P., Crescenzi, R., Genua, M., Verotti, M.: Developing and modeling a plane 3 DOF compliant micromanipulator by means of a dedicated MBS code. In: Technical Proceedings of the 2011 NSTI Nanotechnology Conference and Expo, NSTI-Nanotech 2011, vol. 2, pp. 659–662 (2011)
16. Balucani, M., Belfiore, N.P., Crescenzi, R., Verotti, M.: The development of a MEMS/NEMS-based 3 D.O.F. compliant micro robot. In: Proceedings of the 19th International Workshop on Robotics in Alpe-Adria-Danube Region, RAAD 2010, art. no. 5524590, pp. 173–179 (2010)
17. Belfiore, N.P., Simeone, P.: Inverse kinetostatic analysis of compliant four-bar linkages. Mechanism and Machine Theory 69, 350–372 (2013)
18. Belfiore, N.P., Verotti, M., Di Giamberardino, P., Rudas, I.J.: Active Joint Stiffness Regula-tion to Achieve Isotropic Compliance in the Euclidean Space. Journal of Mechanisms and Robotics 4(4), art. no. 041010 (2012)
19. Belfiore, N.P., Di Giamberardino, P., Rudas, I.J., Verotti, M.: Isotropy in any RR planar dyad under active joint stiffness regulation. In: Proceedings of the 19th International Workshop on Robotics in Alpe-Adria-Danube Region, RAAD 2010, art. no. 5524581, pp. 219–224 (2010)
20. Howell, L.L., Midha, A., Norton, T.W.: Evaluation of equivalent spring stiffness for use in a pseudo-rigid-body model of large-deflection compliant mechanisms. Journal of Mechanical Design, Transactions of the ASME 118(1), 126–131 (1996)
21. Yu, Y.-Q., Howell, L.L., Lusk, C., Yue, Y., He, M.-G.: Dynamic modeling of compliant mechanisms based on the pseudo-rigid-body model. Journal of Mechanical Design, Transactions of the ASME 127(4), 760–765 (2005)
22. Midha, A., Howell, L.L., Norton, T.W.: Limit positions of compliant mechanisms using the pseudo-rigid-body model concept. Mechanism and Machine Theory 35(1), 99–115 (2000)
23. Edwards, B.T., Jensen, B.D., Howell, L.L.: A pseudo-rigid-body model for initially-curved pinned-pinned segments used in compliant mechanisms. Journal of Mechanical Design, Transactions of the ASME 123(3), 464–468 (2001)
24. Belfiore, N.P.: Distributed Databases for the development of Mechanisms Topology. Mechanism and Machine Theory 35(12), 1727–1744 (2000)
25. Belfiore, N.P.: Atlas of remote actuated bevel gear wrist mechanisms of up to nine links. International Journal of Robotics Research 12(5), 448–459 (1993)
26. Belfiore, N.P., Pennestr, E.: An atlas of linkage-type robotic grippers. Mechanism and Machine Theory 32(7), 811–833 (1997)
27. Pennestri, E., Belfiore, N.P.: On the numerical computation of Generalized Burmester Points. Meccanica 30(2), 147–153 (1995)
28. Pennestri, E., Belfiore, N.P.: Modular third-order analysis of planar linkages with applications. American Society of Mechanical Engineers, Design Engineering Division (Publication) DE 70(pt. 1), 99–103 (1994)
29. Yu, Y.-Q., Feng, Z.-L., Xu, Q.-P.: A pseudo-rigid-body 2R model of flexural beam in compliant mechanisms. Mechanism and Machine Theory 55, 18–33 (2012)
30. Chen, G., Xiong, B., Huang, X.: Finding the optimal characteristic parameters for 3R pseudo-rigid-body model using an improved particle swarm optimizer. Precision Engineering 35(3), 505–511 (2011)

31. Her, I., Midha, A.: Compliance Number Concept for compliant mechanisms and Type Synthesis. Journal of Mechanisms, Transmissions, and Automation in Design 109(3), 348–355 (1987)
32. Freudenstein, F., Bottema, O., Koetsier, M.T.: Finite conic-section Burmester Theory. Journal of Mechanisms 4(4), 359–373 (1969)
33. Suh, C.H., Radcliffe, C.W.: Synthesis of Plane Linkages With Use of the Displacement Matrix. J. Eng. Ind. 89(2), 206–214 (1967)
34. Belfiore, N.P.: Brief note on the concept of planarity for kinematic chains. Mechanism and Machine Theory 35(12), 1745–1750 (2000)
35. Di Benedetto, A., Pennestr?, E.: Introduction to mechanism kinematics, vol. 1, 2 & 3. Casa Editrice Ambrosiana, Milano (1993-1999) (in Italian)
36. Belfiore, N.P., Scaccia, M., Ianniello, F., Presta, M.: Selective compliance hinge. US Patent 8,191,204, WO2009034551A1 (2012)
37. Belfiore, N.P., Ianniello, F., Perfetti, L., Presta, M., Scaccia, M.: Selective compliance wire actuated mobile platform, particularly for endoscopic surgical devices. US Patent US 20110028988 A1, WO 2009034552 A3 (2009)

Symbiosis of RFPT-Based Adaptivity and the Modified Adaptive Inverse Dynamics Controller*

József K. Tar[1], János F. Bitó[1],
Annamária R. Várkonyi-Kóczy[2], and Adrienn Dineva[3]

[1] Óbuda University, H-1034 Budapest, Bécsi út 96/B, Hungary,
Antal Bejczy Center of Intelligent Robotics
tar.jozsef@nik.uni-obuda.hu, bito@uni-obuda.hu
http://irob.uni-obuda.hu/?q=en
[2] Óbuda University, H-1034 Budapest, Bécsi út 96/B, Hungary,
Donát Bánki Faculty of Mechanical and Safety Engineering
koczy.annamaria@bgk.uni-obuda.hu
http://www.bgk.uni-obuda.hu/indexeng.php
[3] Óbuda University, H-1034 Budapest, Bécsi út 96/B, Hungary,
Doctoral School of Applied Informatics
dineva.adrienn@phd.uni-obuda.hu
http://phd.uni-obuda.hu/

Abstract. The use of Lyapunov's "direct" method for designing globally asymptotically stable controllers generates numerous, practically disadvantageous restrictions. The "Adaptive Inverse Dynamic Controller for Robots (AIDCR)" therefore suffers from various difficulties. As alternative design approach the "Robust Fixed Point Transformations (RFPT)" were introduced that instead of parameter tuning adaptively deforms the control signals computed by the use of a fixed approximate system model by observing the behaviour of the controlled system. It cannot guarantee global asymptotic stability but it is robust to the simultaneous presence of the unknown external disturbances and modelling imprecisions. In the paper it is shown that the RFPT-based design can co-operate with a modified version of the AIDCR controller in the control of "Multiple Input-Multiple Output (MIMO)" Systems. On the basis of certain function approximation theorems it is expected that this symbiosis works well in a wider class of physical systems than robots.

Keywords: adaptive control, Lyapunov function, adaptive inverse dynamics controller, robust fixed point transformations.

1 Introduction: Lyapunov's "Direct" Method and Its Potential Alternatives

In designing the control for strongly non-linear systems whenever the range of the nominal motion cannot be located in the close vicinity of some "working

* The authors thankfully acknowledge the grant provided by the Project *TÁMOP-4.2.2.A-11/1/KONV-2012-0012: Basic research for the development of hybrid and electric vehicles* – The Project is supported by the Hungarian Government and co-financed by the European Social Fund.

J. Fodor and R. Fullér (eds.), *Advances in Soft Computing, Intelligent Robotics and Control*, Topics in Intelligent Engineering and Informatics 8,
DOI: 10.1007/978-3-319-05945-7_6,

point" the only efficient method seems to be Lyapunov's "*direct*" one that is based on his doctoral thesis on the stability of motion of non-linear systems [1]. This ingenious problem tackling became well known in the Western World due to translations in the sixties (e.g. [2]) mainly for its exceptional efficiency. It is well known that that the most of the coupled non-linear systems of differential equations cannot be integrated in closed analytical form, therefore the properties of the solutions cannot be concluded by studying the solution itself. This fact means significant difficulty even in our days when efficient numerical tricks and huge, cheap computing power is available since the numerical solutions generally cannot be extrapolated outside the domain of actual computations. *By the application of relatively simple estimations Lyapunov was able to determine various stability properties (e.g. stability, uniform stability, global stability, asymptotic stability, exponential stability) of the solution without knowing or revealing any other significant and interesting details of the motion.*

In the practice of control engineers normally quadratic Lyapunov functions are used. Certain *adaptive techniques* as the AIDCR, or the *"Adaptive Slotine–Li Controller"* [3] assume the existence *formally exactly known* analytical system models in which the parameters are only approximately known. They achieve *globally asymptotically stable* solutions by parameter tuning that corresponds to some machine learning.

Other adaptive techniques as e.g. the *"Model Reference Adaptive Controllers (MRAC)*" (e.g. [4,5,6]) tune *rather control than model parameters* and normally also are designed by the use of Lyapunov functions.

The global stability achieved by these methods seem to be attractive for engineering applications, however, it can be noted that in the great majority of practical applications stability criteria are set only for bounded error regions (e.g. [7]), i.e. it seems to be "too rigorous" for practical use. Since the *primary design intent* in most cases may consists in the precise prescription of the trajectory tracking error relaxation that is not revealed by Lyapunov's technique sometimes the application of *evolutionary methods* is needed for properly setting the control parameters that normally are free ones in the Lyapunov function (e.g. [8,9]). Regarding other disadvantages of the Lyapunov function-based technique the observations as follows can be done: (a) it corresponds to a *satisfactory condition*, i.e. the failure of finding a Lyapunov function for a given problem is not conclusive for the stability of that problem; (b) finding an appropriate Lyapunov function is not an easy task, it cannot be solved by the use of some algorithm.

To evade the difficulties related to the Lyapunov function technique alternative solutions were searched for (well summarized in [11]). The main idea behind them was the use of an *approximate dynamic system model* to calculate the necessary torque or force to realize the second time-derivative that is needed for the *kinematically prescribed trajectory tracking error relaxation.* Instead of tuning the *model parameters* it *adaptively deforms these second derivatives* to compensate the effects of modelling errors and unknown external disturbances. The most efficient deformation was found by a convergent iterative sequence generated by the RFPT transformations (e.g. [10]). The mathematical foundation of

this approach was Stefan Bancah's "Fixed Point Theorem" [12] that states that *in a linear, complete, normed metric space the contractive maps generate Cauchy sequences that necessarily are convergent and converge to the fixed point of this map*. Since the necessary conditions of contractivity are valid only in a bounded region this approach generally cannot guarantee global stability. Furthermore, since it is not in the possession of *a priori exact information on the model structure* no asymptotic convergence can be guaranteed: the method permanently utilizes the freshest information on the motion of the controlled system, and according to the principle of causality it utilizes the *past information* in the *future*. In contrast to the abundant number of the free parameters of a quadratic Lyapunov function the RFPT-based method has only three adaptive parameters that can be set easily and can be kept fixed in the case of various control tasks. If needed, i.e. when the basin of convergence may be left various tuning methods were constructed for tuning only one of the adaptive control parameters (e.g. [13,14]). In this manner the RFPT-based method was made competitive with the Lyapunov function based technique regarding global stability. Furthermore, it was found that in this manner a novel design methodology can be built up to create MRAC controllers, too (e.g. [15]).

Till now the coexistence and possible co-operation of the RFPT-based approach and the methods applying adaptive model tuning was not studied. In the present paper it is shown that *a modification of the AIDRC controller* can well co-operate with the RFPT-based adaptivity in the following manner. Whenever no unknown external disturbances are present the two methods complete each other: efficient parameter tuning is going on while the tracking error is kept at low level due to the RFPT-base control; as the tuned model is improved the burdens of the RFPT-based controller step by step decrease and finally no adaptive deformation is needed since *the system finally uses the exact model*. If unknown external perturbations are present the parameter tuning happens on the basis of false information, however, the RFPT-based design keeps the tracking error at low level and efficiently compensates the simultaneous effects of the disturbances and the improper tuning. *The theoretical basis of the convergence always remains Banach's Fixed Point Theorem* [12].

2 The AIDCR with Modified Tuning Rule

This method assumes the validity of a special condition: in the equations of motion the dynamic parameters of the system must be separable into an array the is multiplied by a kinematically known matrix. This condition also is valid for the here used 2 Dof system obtained by coupling two generalized 1 DoF van der Pol oscillator the original version of which was developed to describe non-linear oscillations in a triode in 1927 [16]. For the sake of simplicity the properties of the original and the modified version of the AIDCR controller are explained by the use of this paradigm.

2.1 The Coupled van der Pol Oscillators

$$\begin{aligned} m_1\ddot{q}_1 + \mu_1\left(q_1^2 + q_2^2 - c\right)\dot{q}_1 + k_1 q_1 + \beta_1 q_1^3 + \lambda_1 q_1^5 = F_1, \\ m_2\ddot{q}_2 + \mu_2\left(q_1^2 + q_2^2 - c\right)\dot{q}_2 + k_2 q_2 + \beta_2 q_2^3 + \lambda_2 q_2^5 = F_2 \end{aligned} \tag{1}$$

in which $m_1 = 10$ kg denotes the *inertia* of oscillator 1, $\mu_1 = 1$ N/(ms) corresponds to some viscous damping if $q_1^2 + q_2^2 - c > 0$ and to some *external excitation* if $q_1^2 + q_2^2 - c < 0$, $c = 3$ m^2 describes the coupling of the two subsystems, $k_1 = 100$ N/m is a spring stiffness, $\beta_1 = 1$ N/m^3 and $\lambda_1 = 2$ N/m^5 are coefficients of non-linear corrections for the distance-dependent spring stiffness, F_1 and F_2 denote the active control forces, and q_1, q_2 stand for the *observable* generalized coordinates. The second sub-system has the parameters as $m_2 = 15$ kg, $\mu_2 = 2$ N/(ms), $k_2 = 120$ N/m, $\beta_2 = 2$ N/m^3, and $\lambda_2 = 3$ N/m^5.

The *initial approximate model* has the following parameters: $\hat{m}_1 = 5$ kg, $\hat{\mu}_1 = 2$ N/(ms), $\hat{c} = 3.5$ m^2, $\hat{k}_1 = 110$ N/m, $\hat{\beta}_1 = 0.9$ N/m^3, $\hat{\lambda}_1 = 1.5$ N/m^5, $\hat{m}_2 = 5$ kg, $\hat{\mu}_2 = 2$ N/(ms), $\hat{k}_2 = 110$ N/m, $\hat{\beta}_2 = 3$ N/m^3, and $\hat{\lambda}_2 = 4$ N/m^5.

The model parameters can be arranged into an array as

$$\Theta \stackrel{def}{=} [m_1, \mu_1, \mu_1 c, k_1, \beta_1, \lambda_1, m_2, \mu_2, \mu_2 c, k_2, \beta_2, \lambda_2]^T \tag{2}$$

while the coefficients of this array are the non-zero elements of a matrix of size 2×12 as $Y_{1,1} \stackrel{def}{=} \ddot{q}_1$, $Y_{1,2} \stackrel{def}{=} \dot{q}_1\left(q_1^2 + q_2^2\right)$, $Y_{1,3} \stackrel{def}{=} -\dot{q}_1$, $Y_{1,4} \stackrel{def}{=} q_1$, $Y_{1,5} \stackrel{def}{=} q_1^3$, $Y_{1,6} \stackrel{def}{=} q_1^5$, $Y_{2,7} \stackrel{def}{=} \ddot{q}_2$, $Y_{2,8} \stackrel{def}{=} \dot{q}_2\left(q_1^2 + q_2^2\right)$, $Y_{2,9} \stackrel{def}{=} -\dot{q}_2$, $Y_{2,10} \stackrel{def}{=} q_2$, $Y_{2,11} \stackrel{def}{=} q_2^3$, and $Y_{2,12} \stackrel{def}{=} q_2^5$ by the use of which (1) takes the form as

$$\begin{bmatrix} F_1 \\ F_2 \end{bmatrix} = Y\left(q, \dot{q}, \ddot{q}\right)\Theta. \tag{3}$$

By the use of this paradigm the AIDCR controller can be built up as follows:

2.2 The Modified Tuning Rule

Assume that for the *nominal trajectory* the following kinematic data are *a priori* known: $q^N(t)$, $\dot{q}^N(t)$, and $\ddot{q}^N(t)$. By the use of two positive feedback gains K_1 and K_2 the *approximate version* of (1) can be used for the calculation of the forces in a manner in which PD-type corrections are applied by the tracking errors $e(t) \stackrel{def}{=} q^N(t) - q(t)$ as

$$\begin{aligned} \hat{m}_1\left(\ddot{q}_1^N + K_1 e_1 + K_2 \dot{e}_1\right) + \hat{\mu}_1\left(q_1^2 + q_2^2 - \hat{c}\right)\dot{q}_1 + \hat{k}_1 q_1 + \hat{\beta}_1 q_1^3 + \hat{\lambda}_1 q_1^5 = F_1, \\ \hat{m}_2\left(\ddot{q}_2^N + K_1 e_2 + K_2 \dot{e}_2\right) + \hat{\mu}_2\left(q_1^2 + q_2^2 - \hat{c}\right)\dot{q}_2 + \hat{k}_2 q_2 + \hat{\beta}_2 q_2^3 + \hat{\lambda}_2 q_2^5 = F_2. \end{aligned} \tag{4}$$

In the lack of external disturbances the forces in (4) are the same as in (1). Via eliminating the force terms and subtracting from both sides $[\hat{m}_1\ddot{q}_1, \hat{m}_2\ddot{q}_2]^T$ the remaining terms can be so rearranged that at one side of the equations the array

of the modelling errors multiplied by Y appears, while on the other side the *known quantity* $[\hat{m}_1(\ddot{e}_1 + K_1 e_1 + K_2 \dot{e}_1), \hat{m}_2(\ddot{e}_2 + K_1 e_2 + K_2 \dot{e}_2)]^T$ remains:

$$\begin{bmatrix} \hat{m}_1(\ddot{e}_1 + K_1 e_1 + K_2 \dot{e}_1) \\ \hat{m}_2(\ddot{e}_2 + K_1 e_2 + K_2 \dot{e}_2) \end{bmatrix} = Y\left(q, \dot{q}, \ddot{q}\right) \left(\Theta - \hat{\Theta}\right). \tag{5}$$

Equation (5) has a *very simple geometric interpretation*: at a given time instant the projections of the 12 dimensional error array $(\Theta - \hat{\Theta})$ are known in the directions of two vectors defined by the two rows of matrix Y. The original AIDCR does not directly utilize this information. Instead of that, in order to construct a Lyapunov function, it multiplies both sides of (5) with the *inverse of the approximate inertia matrix* (hence originates the expression "inverse dynamics" in the name of the method), and deduces the parameter tuning rule from the prescription that the Lyapunov function must have negative time-derivative.

The geometrically interpreted information in (5) can directly be utilized as follows. If *exponential decay rate* could be realized for the parameter estimation error the *array equation* $\frac{d}{dt}\left(\Theta - \hat{\Theta}\right) = -\alpha\left(\Theta - \hat{\Theta}\right)$ $(\alpha > 0)$ should be valid. If we multiply both sides of this equation with a *projector* determined by *a few pairwisely orthogonal unit vectors* as $\sum_i e^{(i)} e^{(i)^T}$ the equation $\sum_i e^{(i)}\left(\dot{\Theta}_i - \dot{\hat{\Theta}}_i\right) = -\alpha \sum_i e^{(i)}\left(\Theta_i - \hat{\Theta}_i\right)$ is obtained. This situation can well be approximated if we use the Gram-Schmidt algorithm (e.g. [17,18]) for finding the *orthogonal components* of the rows of matrix Y in (5). We can apply the tuning rule *only for the known components* in the form: $\frac{d}{dt}(\Theta - \hat{\Theta}) = -\alpha \sum_i \frac{\tilde{y}^{(i)} \tilde{y}^{(i)^T}}{\|\tilde{y}^{(i)}\|^2 + \varepsilon}(\Theta - \hat{\Theta})$ in which $\tilde{y}^{(i)}$ denotes the transpose of the orthogonalized rows of matrix Y, and a small $\varepsilon > 0$ evades division by zero whenever the norm of the appropriate row is too small. Since the scalar product is a *linear operation* during the orthogonalization process the appropriate linear combinations of the scalar products in the LHS of (5) can be computed.

3 Combination with the RFPT

It is evident that all the above considerations remain valid if in the LHS of (4) instead of $\left(\ddot{q}^N + K_1 e + K_2 \dot{e}\right)$ different feedback terms are used. Therefore this term can be replaced by its iterative variant obtained from the RFPT-base design as follows:

$$\begin{gathered} h(t_n) \stackrel{def}{=} f\left(r(t_n)\right) - r^d\left(t_{n+1}\right), \quad e(t_n) \stackrel{def}{=} h(t_n)/\|h(t_n)\|, \\ \tilde{B}(t_n) \stackrel{def}{=} B_c \sigma(A_c \|h(t_n)\|) \\ r(t_{n+1}) \stackrel{def}{=} \left(1 + \tilde{B}(t_n)\right) r(t_n) + \tilde{B}(t_n) K_c e(t_n) \end{gathered} \tag{6}$$

in which $\sigma(x) \stackrel{def}{=} \frac{x}{1+|x|}$, $r^d_{n+1} \stackrel{def}{=} \ddot{q}^N + K_1 e + K_2 \dot{e}$, r_n denotes the adaptively deformed control signal used in control cycle n, and $f\left(r(t_n)\right) \stackrel{def}{=} \ddot{q}(t_n)$, i.e.

the *observed system response* in cycle n. It is evident that if $f\left(r(t_n)\right) = r^d(t_{n+1})$ then $r(t_{n+1}) = r(t_n)$, that is the solution of the control task (i.e. the appropriate adaptive deformation) is the fixed point of the mapping defined in (6). Therefore the same tuning rule can used in (7) as previously but the known information at the LHS is different. It is evident that if the parameter estimation error is great, the difference between the *adaptively deformed control signal* $r_i(t)$ and the *realized 2nd time-derivative* $\ddot{q}_i(t)$ is significant, therefore at the LHS of (7) considerable quantity is available for parameter tuning.

$$\begin{bmatrix} \hat{m}_1(r_1 - \ddot{q}_1) \\ \hat{m}_2(r_2 - \ddot{q}_2) \end{bmatrix} = Y\left(q, \dot{q}, \ddot{q}\right)\left(\Theta - \hat{\Theta}\right). \tag{7}$$

Since the details of the convergence were discussed in ample literature references in the sequel only simulation results will be presented to reveal the co-operation of the RFPT-based adaptivity and model parameter tuning.

4 Simulation Results

The simulations were made by a sequential program written in SCILAB with simple Euler integration with fixed time-steps of 0.1 ms. This time-resolution also corresponded to the cycle time of the assumed controller. The *kinematically prescribed trajectory tracking rule* corresponded to the feedback gains $K_1 = \Lambda^2$, $K_2 = 2\Lambda$ with $\Lambda = 10/\mathrm{s}$, the *adaptive control parameters* were $K_c = -10^6$, $B_c = 1$, and $A_c = 10^{-8}$. The learning rate was determined by $\alpha = 5/\mathrm{s}$.

4.1 Simulations without Unknown External Disturbances

At first the RFPT-based was studied in the case free of any external disturbances. Figure 1 describes the details of the trajectory tracking and trajectory tracking errors. The precise tracking is evident in spite of the considerable parameter estimation errors. Figure 2 reveals considerable learning activity. *These figures well illustrate the theoretical expectation that the RFPT-based adaptivity and the parameter learning activity can well co-operate.*

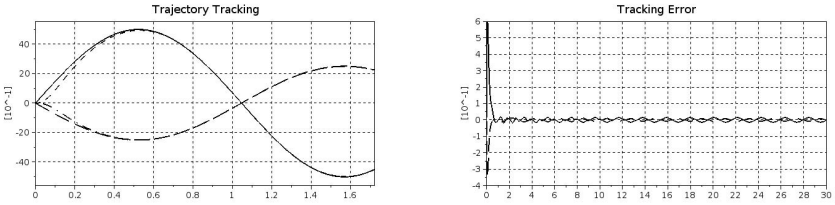

Fig. 1. Trajectory tracking [q_1^N: solid, q_2^N: dashed, q_1: dense dash, q_2: dash-dot lines LHS], and trajectory tracking error [for q_1: solid, for q_2: dashed lines RHS] for the RFPT-based design without unknown external disturbances, time is described in the horizontal axes in s units

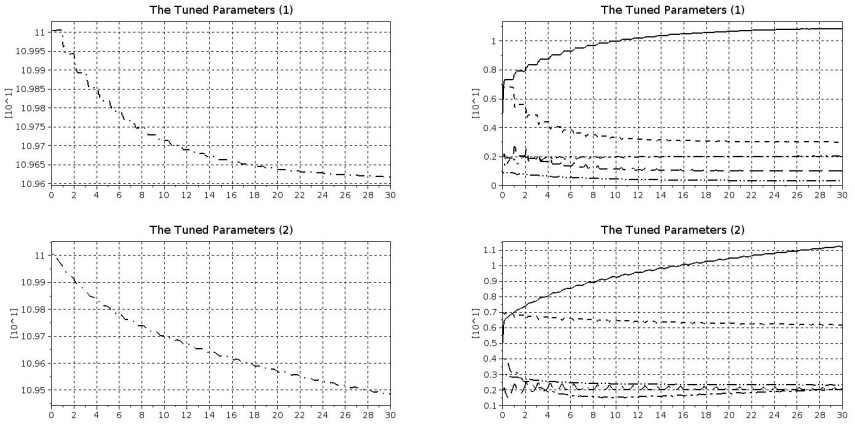

Fig. 2. The tuned dynamic system parameters for subsystem 1 (at the top) and for subsystem 2 (at the bottom) for the RFPT-based design without unknown external disturbances, time is described in the horizontal axes in s units [$\hat{\Theta}_1$: solid, $\hat{\Theta}_2$: dashed, $\hat{\Theta}_3$: dense dash, $\hat{\Theta}_4$: dash-dot, $\hat{\Theta}_5$: dash-dot-dot, and $\hat{\Theta}_6$: longdash-dash lines]

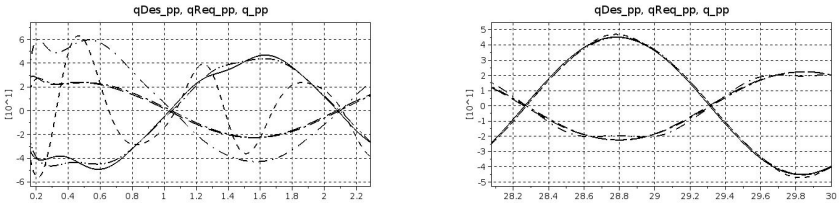

Fig. 3. Operation of the RFPT-based adaptivity: [the *kinematically prescribed "Desired" values*: $\ddot{q}_1^{Des}$: solid, $\ddot{q}_2^{Des}$: dashed, the *adaptively deformed "Required" values*: $\ddot{q}_1^{Req}$: dense dash, $\ddot{q}_2^{Req}$: dash-dot, and the *simulated values*: $\ddot{q}_1$: dash-dot-dot, $\ddot{q}_2$: longdash-dash lines] at the early (LHS) and the late (RHS) phases of parameter tuning, time is described in the horizontal axes in s units

The efficiency of parameter learning is well exemplified by Fig. 3 revealing the initial and the late phases of the control session: *at the beginning the dynamic model was very imprecise, therefore considerable adaptive deformation was done* by the RFPT-based design. In the later phase, *when the model already became precise, only minimal extent of adaptive deformation was necessary.*

Figure 4 displays the significance of the RFPT-based design in an alternative manner: it describes the tracking error and tracking of the phase trajectories without external disturbances when the RFPT-based deformation was switched off: the initial tracking error was great and it only slowly decreased as the parameter tuning process proceeded. The details of parameter tuning (Fig. 5) were similar to the case in which the RFPT-based adaptivity was switched on.

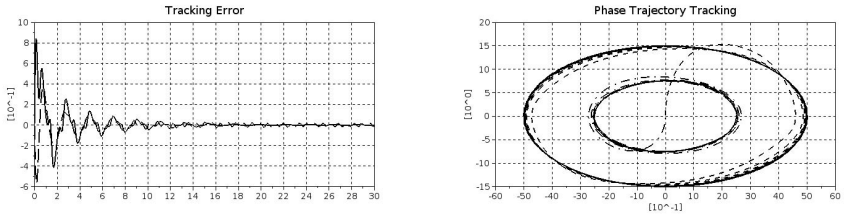

Fig. 4. Trajectory tracking error [for q_1: solid, for q_2: dashed lines, time is described in the horizontal axis in s units (LHS)] and the phase trajectory tracking (i.e. the $\dot{q}_i$ vs. q_i charts) [for q_1^N: solid, for q_2^N: dashed, for q_1: dense dash, for q_2: dash-dot lines (RHS)] without unknown external disturbances and without RFPT-based adaptivity

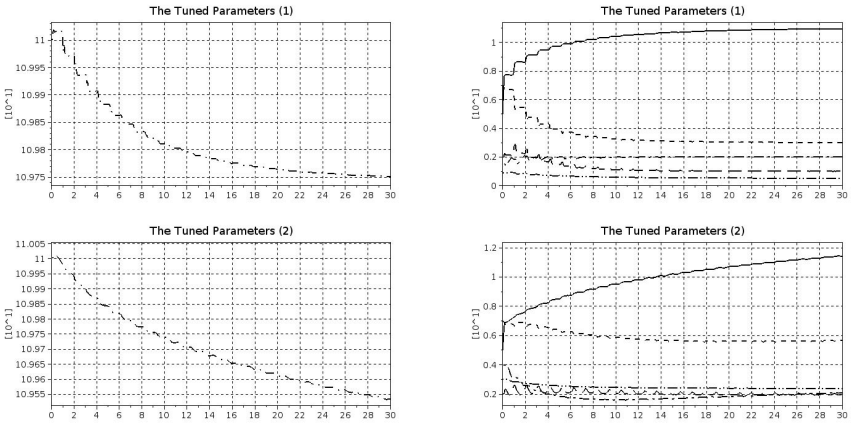

Fig. 5. The tuned dynamic system parameters for subsystem 1 (at the top) and for subsystem 2 (at the bottom) without unknown external disturbances and RFPT-based adaptivity, time is described in the horizontal axes in s units [$\hat{\Theta}_1$: solid, $\hat{\Theta}_2$: dashed, $\hat{\Theta}_3$: dense dash, $\hat{\Theta}_4$: dash-dot, $\hat{\Theta}_5$: dash-dot-dot, and $\hat{\Theta}_6$: longdash-dash lines]

4.2 Simulations with Temporal Unknown External Disturbances

In this subsection the effects of *temporal unknown external disturbances* are studied via simulations.

At first the the lack of RFPT-based adaptivity is investigated. Figures 6, 7, and 8 reveal that the parameter tuning process was corrupted by the unknown external disturbances and the trajectory tracking errors became quite considerable.

When the RFPT-based adaptivity was switched on the trajectory tracking became precise (Figs. 9, 10), however, since the parameter tuning happened on the basis of false information it was corrupted again (Fig. 8).

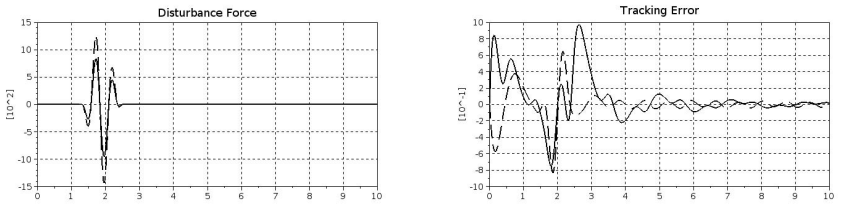

Fig. 6. Disturbance forces [for F_1^{Dist}: solid, for F_2^{Dist}: dashed lines (LHS)], and trajectory tracking error [for q_1: solid, for q_2: dashed lines (RHS)], and trajectory tracking error [for q_1: solid, for q_2: dashed lines RHS] with unknown external disturbances and without RFPT-based adaptation, time is described in the horizontal axes in s units

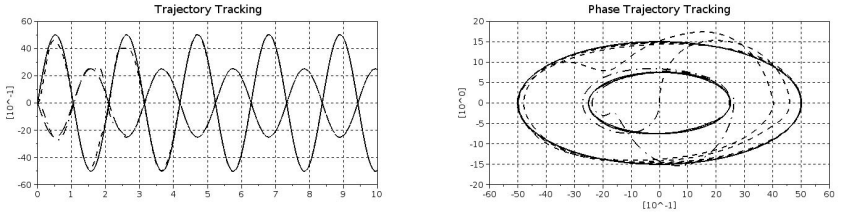

Fig. 7. Trajectory (LHS) and phase trajectory (RHS) tracking [for q_1^N: solid, for q_2^N: dashed, for q_1: dense dash, for q_2: dash-dot lines] with temporal unknown external disturbances and without RFPT-based adaptation, time is described in the horizontal axes in s units

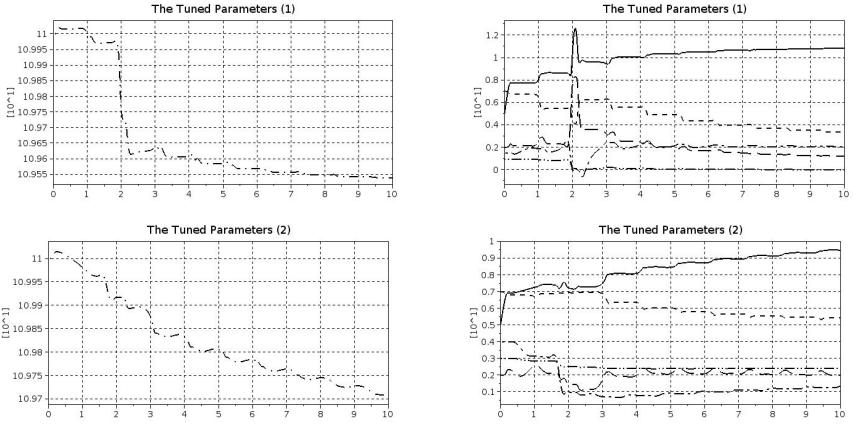

Fig. 8. The tuned dynamic system parameters for subsystem 1 (at the top) and for subsystem 2 (at the bottom) with unknown external disturbances and without RFPT-based adaptivity, time is described in the horizontal axes in s units [$\hat{\Theta}_1$: solid, $\hat{\Theta}_2$: dashed, $\hat{\Theta}_3$: dense dash, $\hat{\Theta}_4$: dash-dot, $\hat{\Theta}_5$: dash-dot-dot, and $\hat{\Theta}_6$: longdash-dash lines]

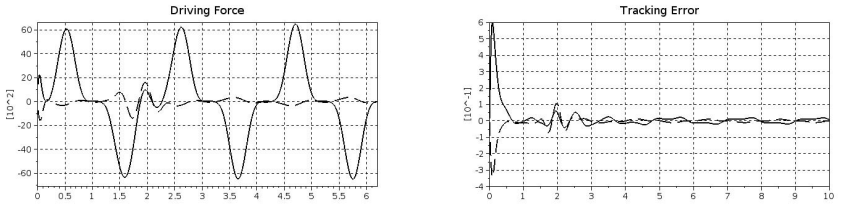

Fig. 9. The driving forces [for F_1: solid, for F_2: dashed lines (LHS)], and trajectory tracking error [for q_1: solid, for q_2: dashed lines (RHS)], and trajectory tracking error [for q_1: solid, for q_2: dashed lines RHS] with unknown external disturbances and RFPT-based adaptation, time is described in the horizontal axes in s units

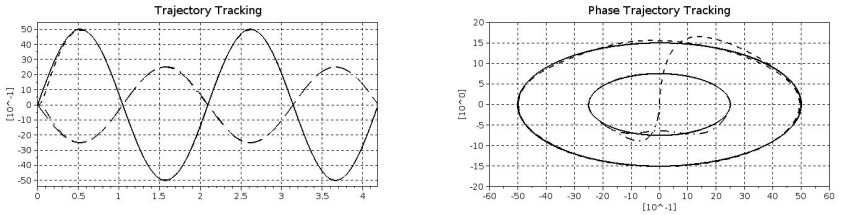

Fig. 10. Trajectory (LHS) and phase trajectory (RHS) tracking [for q_1^N: solid, for q_2^N: dashed, for q_1: dense dash, for q_2: dash-dot lines] with temporal unknown external disturbances and RFPT-based adaptation, time is described in the horizontal axes in s units

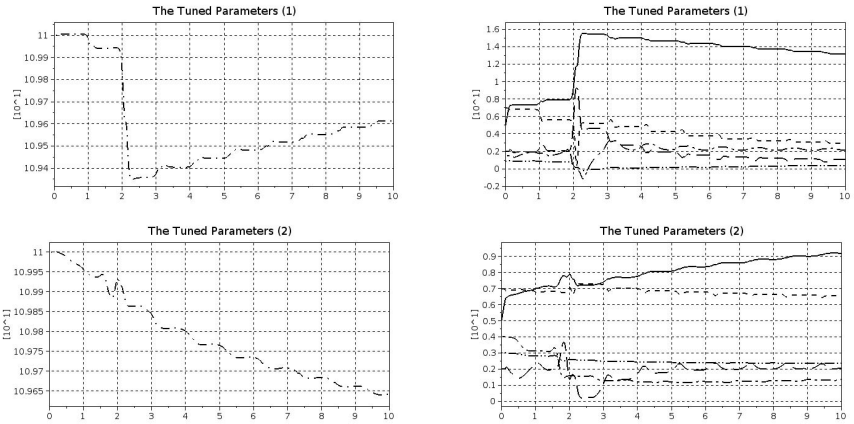

Fig. 11. The tuned dynamic system parameters for subsystem 1 (at the top) and for subsystem 2 (at the bottom) with unknown external disturbances and RFPT-based adaptivity, time is described in the horizontal axes in s units [$\hat{\Theta}_1$: solid, $\hat{\Theta}_2$: dashed, $\hat{\Theta}_3$: dense dash, $\hat{\Theta}_4$: dash-dot, $\hat{\Theta}_5$: dash-dot-dot, and $\hat{\Theta}_6$: longdash-dash lines]

5 Conclusions

In this paper the symbiosis of RFPT-based adaptivity and the *"Modified Adaptive Inverse Dynamics Controller"* was theoretically proved and illustrated via simulation results for two coupled, strongly non-linear, generalized van der Pol oscillators.

The main idea on the basis of which analytical model learning and the RFPT-based design needing only a rough approximate model can co-exist and co-operate consists in evading the use of the Lyapunov function based stability proof since it demands too rigorous formal limitations. It was shown that tuning of the parameters of the *formally exact analytical model* was possible without the use of any Lyapunov function by direct utilization of the available information on the modelling errors on the basis of simple and lucid geometric interpretation. The stability of the new controllers is guaranteed by *"Banach's Fixed Point Theorem"*.

It is worthy of note that the novel method (as well as its original version) yields correct parameter tuning only in the lack of unknown external disturbances. However, while the trajectory tracking of the original, Lyapunov function based *"Adaptive Inverse Dynamics Controller"* is considerably corrupted by such disturbances, the novel method guarantees precise trajectory and phase trajectory tracking even in this case at least if these disturbances are of temporal nature.

It is also worthy of note that the dynamic model under consideration had the special property that the array of the dynamic model parameters was separable and it was multiplied by a matrix of kinematically known quantities. On the basis of the modern function approximation theorems ([19,20]) it is expected that this approach can be extended for more general cases as Bernard and Slotine already mentioned a possible extension of the Lyapunov function based method for wavelets in [21].

In the future similar investigations are planned for completing the appropriate modification of the *"Slotine-Li Adaptive Robot Controller"* with the RFPT-based adaptive design.

References

1. Lyapunov, A.M.: A general task about the stability of motion. PhD Thesis, University of Kazan (1892) (in Russian)
2. Lyapunov, A.M.: Stability of motion. Academic Press, New York (1966)
3. Slotine, J.-J.E., Li, W.: Applied Nonlinear Control. Prentice Hall International, Inc., Englewood Cliffs (1991)
4. Nguyen, C.C., Antrazi, S.S., Zhou, Z.-L., Campbell Jr., C.E.: Adaptive control of a Stewart platform-based manipulator. Journal of Robotic Systems 10(5), 657–687 (1993)
5. Somló, J., Lantos, B., Cát, P.T.: Advanced Robot Control. Akadémiai Kiadó, Budapest (2002)

6. Hosseini-Suny, K., Momeni, H., Janabi-Sharifi, F.: Model reference adaptive control design for a teleoperation system with output prediction. J. Intell. Robot. Syst. 1–21 (2010), doi:10.1007/s10846-010-9400-4
7. Kovács, L.: Modern robust control in patophysiology from theory to application. In: IEEE 11th International Symposium on Applied Machine Intelligence and Informatics (SAMI 2013), p. 13 (2013)
8. Sekaj, I., Veselý, V.: Robust output feedback controller design: Genetic algorithm approach. IMA J. Math. Control Info. 22(3), 257–265 (2005)
9. Chen, J.L.: Chang, Wei-Der: Feedback linearization control of a two-link robot using a multi-crossover genetic algorithm. Expert Systems with Applications 2(pt. 2), 4154–4159 (2009)
10. Tar, J.K., Bitó, J.F., Nádai, L., Tenreiro Machado, J.A.: Robust Fixed Point Transformations in adaptive control using local basin of attraction. Acta Polytechnica Hungarica 6(1), 21–37 (2009)
11. Tar, J.K.: Adaptive Control of Smooth Nonlinear Systems Based on Lucid Geometric Interpretation (DSc Dissertation). Hungarian Academy of Sciences, Budapest, Hungary (2012)
12. Banach, S.: Sur les opérations dans les ensembles abstraits et leur application aux équations intégrales (About the Operations in the Abstract Sets and Their Application to Integral Equations). Fund. Math. 3, 133–181 (1922)
13. Tar, J.K., Nádai, L., Rudas, I.J., Várkonyi, T.A.: RFPT-based adaptive control stabilized by fuzzy parameter tuning. In: 9th European Workshop on Advanced Control and Diagnosis (ACD 2011), Budapest, Hungary, pp. 1–8 (2011)
14. Kósi, K., Tar, J.K., Rudas, I.J.: Improvement of the stability of RFPT-based adaptive controllers by observing "precursor oscillations". In: Proc. of the 9th IEEE International Conference on Computational Cybernetics, Tihany, Hungary, July 8-10, pp. 267–272 (2013)
15. Tar, J.K., Bitó, J.F., Rudas, I.J.: Replacement of Lyapunov's direct method in model reference adaptive control with robust fixed point transformations. In: Proc. of the 14th IEEE International Conference on Intelligent Engineering Systems 2010, Las Palmas of Gran Canaria, Spain, pp. 231–235 (2010)
16. Van der Pol, B.: Forced oscillations in a circuit with non-linear resistance (reception with reactive triode). The London, Edinburgh, and Dublin Philosophical Magazine and Journal of Science 7(3), 65–80 (1927)
17. Gram, J.P.: Über die Entwickelung reeler Funktionen in Reihen mittelst der Methode der kleinsten Quadrate. Journal für die Reine und Angewandte Mathematik 94, 71–73 (1883)
18. Schmidt, E.: Zur Theorie der linearen und nichtlinearen Integralgleichungen I. Teil: Entwicklung willkürlicher Funktionen nach Systemen vorgeschriebener. Matematische Annalen 63, 442 (1907)
19. Weierstraß, K.: Über die analytische Darstellbarkeit sogenannter willkürlicher Functionen einer reellen Veränderlichen. Sitzungsberichte der Akademie zu Berlin (1885)
20. Stone, M.H.: A generalized Weierstrass approximation theorem. Math. Magazine 21, 167–184, 237–254 (1948)
21. Bernard, C.P., Slotine, J.-J.E.: Adaptive control with multiresolution bases. In: Proceedings of the 36th IEEE Conference on Decision and Control, San Diego, CA, December 10-12, vol. 4, pp. 3884–3889 (1997)

Part II
Soft Computing

Subjective Weights Based Meta-Learning in Multi-criteria Decision Making

Hamido Fujita[1] and Yu-Chien Ko[2]

[1] Software and Information Science, Iwate Prefectural University, Takizawa, Japan
issam@iwate-pu.ac.jp
[2] Department of Information Management, Chung Hua University,
707, Sec.2 Wufu Road, Hsinchu 30012, Taiwan
eugene@chu.edu.tw

Abstract. In decision making most approaches are taking into account objective criteria, however, the subjective correlation among decision makers provided as preference utility is necessary to be presented to provide confidence preference additive among decision makers reducing ambiguity and produce better utility preferences measurement for subjective criteria among decision makers. We can look to subjective decision making using DRSA by providing subjective utility function based on knowledge we get from document or data (login files or else) using Meta learning concept to provide support for decision makers to revise their criteria based on meta learning concept as ensemble learning mechanism to have subjective weights. The support is subjective to experts' knowledge on the criteria and also additive weighting of criteria in relation to users (subjective manner).

Keywords: subjective weights, preference utility, Meta learning (ML), Dominance-based rough set approach (DRSA).

1 Introduction

Decision Support Systems (DSS) technologies in major is based on objective analysis of criteria. The analysis outcome is ranking of alternatives based on criteria that are weighted due to expert's opinions in relation to their experiences and also according to grounded situations. The approaches that are used in ranking these criteria are based on statistical analysis or experiences of experts. It is majorly based on analyzing experts' preferences in relation to alternatives that need to be ranked. Decision makers may have imprecise knowledge on how to weight these alternatives or criteria. In most cases, DMs use ordinal and linguistics values to express preferences as independent. This means that preferences definition and its values have no correlation or linkage among each other. Also, assuming that the aggregation operators are linear based on additive properties of independence. This is in fact not realistic in actual situation and subjective to DMs' nature. The fundamental idea is mainly back to Savage [1] on having experts providing utility function on the degree on their trust in the preference

J. Fodor and R. Fullér (eds.), *Advances in Soft Computing, Intelligent Robotics and Control*, Topics in Intelligent Engineering and Informatics 8,
DOI: 10.1007/978-3-319-05945-7_7,

setting. Savage [1] called this as subjective utility theory which provides a basis on quantifying the DMs trust value in their preferences scoring [2], using preference utility relation.

The idea basically provides subjectivity criteria based on preference trust value set by a DM. This value can be either increasing or decreasing based on the final decision. In some cases decision makers need to have negotiations to achieve best consensus [3]. Different aggregation functions and operators were developed [4], as an extension to the additive aggregation operators [5]; order weighted geometric operator [6], induced Ordered weight Average [7], linguistic aggregation operator [8], and others. These operators do not provide subjective relation to criteria nor to decision makers who define the weight of these criteria. This is because criteria relationships are assumed to be independent for analysis and computation purpose. Consensuses [3] among decision makers have been studied by many researchers. However these approaches are not taken into account the subjective information in regard to the situation in which criteria values could be changed (adjusted). Also some researchers provide theoretical solution more than looking directly to the novel context of these criteria. There are aspects that can be called as mental models reflect the setting of each criterion in separate fashion in relation to a set of subjective models that are providing collective reflection to those criteria. Such reflection would be used to have multiplicative weight on the objective criteria to a situated decision making to achieve better selection and ranking for alternatives. Power average based aggregations functions define by many authors with their extensions are based on multiplicative preference relations among decision makers [7]. In practice this is not realistic as the achieved aggregated preferences is not reflecting the subjective issues of possible change that decision makers may have in regard to the criteria dynamics. This is similar in situation if moderator is involved. The moderator is objective in their scenarios to moderate the decision makers' preferences. Providing support function based on arithmetic mean [5] providing means to assist on regulating consensus using power average, however this support not taking into account subjective relations of these preferences when contents of criteria have some relation to the decision of other decision makers during the aggregation methods. These methods are ranging from scoring and outranking, distance-based, utility functions like in this article.

This research intends to propose an approach of solving subjective weights by Meta learning based on dominance-based rough set approach (MLDRSA) which defines subjective weights by logical implications then solves the significant feature of all subjective preferences. The significant feature is presented as a convergent type of subjective weights (CSW). The subjective influence between criteria will be presented as an individual type of subjective weights (ISW). These two types are both defined in terms of logical implications constructed in a hierarchical structure. By referring to AHP [9,10], CSW and ISW can be integrated into a linear formula to find out the most significant feature, described in Section 3. The conceptual process of MLDRSA is presented in Fig. 2.

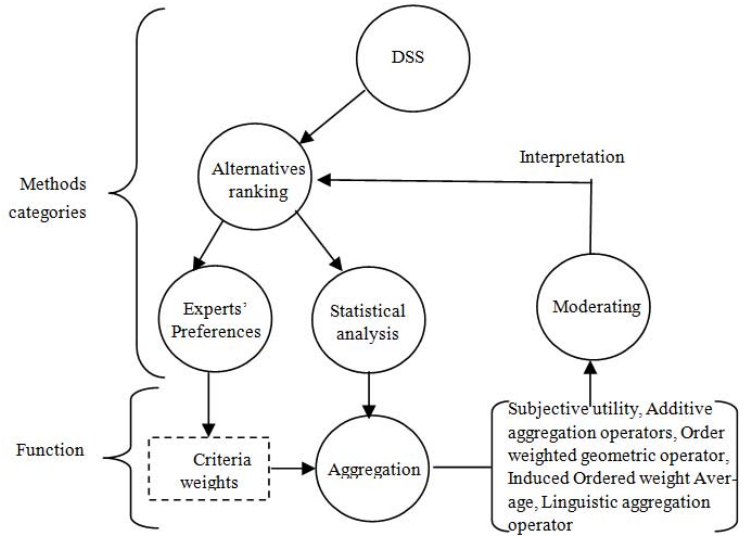

Fig. 1. The past subjective weighting of DSS

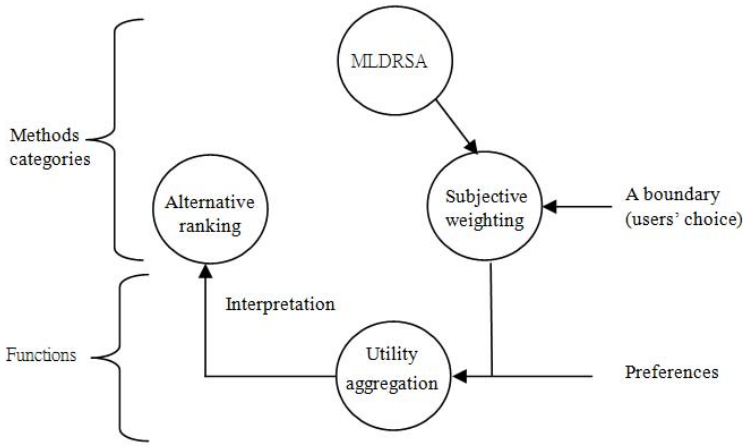

Fig. 2. The process of MLDRSA

The remainder of this paper is organized as follows: Section 2 reviews decision support systems, meta learning, and dominance-based rough set approach. Section 3 presents the design and implementation of MLDRSA. Section 4 addresses application results of MLSW, and Section 5 presents discussions on the subjective weights and the case study about the criteria relationship. Finally, concluding remarks are stated to close the paper.

2 Literature Review

The literatures of the related theories are presented following DSS, ML, and DRSA. The aggregation techniques of DSS, the knowledge extraction of ML, and the tech-nique of applying logics to the criteria relationship are given in details.

2.1 Decision Support Systems (DSS)

Decision support system (DSS) are essential research area that play a major role in utilizing experts knowledge for providing advises in different kind of domain and applications, like stock market, medical advisors and etc. There are many techniques that are modeling to handle uncertain criteria like fuzzy analytic network process [11], and fuzzy TOPSIS [12]. These techniques based on assumptions that the criteria are independent using additive type aggregation model. These techniques are practically not feasible to handle uncertain situation. Other models are introduced to handle uncertain situation, for example in case when conflict among experts [13] or case when there criteria are represented using intuitionistic fuzzy [14] in DSS, or using rough set [15].

DSS is kernel of rules that organized to provide intelligent service based on input of criteria with an attributes assigned from databases, or a question given by user, or a query given by a system. It is a sort of Intelligent DSS (IDSS) that improve quality of DMs [16]. For more coverage on DS please refer to [17]. In this paper we look to IDSS based DM expertise in providing attributes on a set of criteria. These attributes are linguistics variables. In our context DSS is related to multi criteria decision support based aggregation model which is called preference model [18]. These systems are to provide DMs a knowledge recommendation to a set of objects related to solutions candidates. It is based on attributes and criteria evaluations that can be applicable to applications like medical diagnosis and economic predictions as in this paper.

2.2 Meta Learning (ML)

We have selected Meta Learning as it can learn from past experience by collecting knowledge from other resources like expert profile or experience in specific preferences. Meta-learning helps solve problems in classification and regression. ML is combination of machine learning and data-mining [19]. In our context, ML is based on feature of given criteria in relation to a DM profile. In machine learning community this matter is considered as a learning task, and named as ML or learning about learning [20]. From samples data or cases studies we extract methods for evaluation [19]. We have selected DRSA for such purpose where attributes are defined as preference-ordered scales, condition attributes (related to criteria) and the decision attribute (assignment). This would provide explicit relationship and knowledge between criteria and attributes. The method evaluation would produce prediction analysis or base level methods. On the meanwhile from the sample data we extract characteristics of these criteria

that are given by the DMs [21]. The extraction facilitates meta-level attributes. The meta-level attributes and prediction analyses are combined to produce meta-learning based criteria reflecting the characteristics of DMs like rule generation based on attribute classification [22] to deduct machine learning rules. These characteristics provide subjective ranking utility (grouping) for providing DMs with support on increasing their trust in providing attribute in similar fashion as in cross-validation.

2.3 Dominance-Based Rough Set Approach (DRSA)

DRSA is a powerful mathematical technique of relational structure and can induce conditional preferences for classification, sorting, choice, and ranking for preference order criteria values and predefined classes —[23]. The induced preferences for the ranking can imply the evidences to achieve the dominance class. There are four parts to illustrate this concept. First is the ranking unions: $Cl_t^{\geq}$ (the upward union of classes which includes objects ranked at least t^{th}) and $Cl_t^{\leq}$ (the downward union of classes which includes objects ranked less than t^{th}), where Cl is a cluster set containing preference-ordered classes Cl_t, $t \in T$ and $T = \{1, 2, \ldots, n\}$. The formulations for the above statement can be expressed as $Cl = \{Cl_1, \ldots, Cl_t, \ldots, Cl_n\}$, $Cl_1 = \{y \in U : y \text{ is ranked in the top position}\}$, $Cl_2 = \{y \in U : y \text{ is ranked in the second position}\}$, ..., and $Cl_n = \{y \in U : y \text{ is ranked in the bottom position}\}$ where U is a set with decision-makers' preference orders and n is the number of preference-ordered classes. For all $s, t \in T$ and $s \geq t$ (rank of $s \geq$ rank of t), every object in Cl_s is preferred to be at least as good as any of object in Cl_t. The upward union is constructed as $Cl_t^{\geq} = \bigcup_{s \geq t} Cl_s$ for $s \geq t$; inversely, the downward union as $Cl_t^{\leq} = \bigcup_{s < t} Cl_s$ for $s < t$. A representation of the upward union, called the dominating set, can rely on a set of criteria, P. It follows the dominance principle of requiring each chosen object at least as good as object x in all considered criteria of P. The granules of a dominating set based on P can be viewed as the granular cones in the criteria value space. Vice versa, the dominated set for the downward union follows the dominance principle and has the granules in the opposite direction. These cones are named as P-dominating and P-dominated sets [24], respectively.

Second is about the dominance sets. For instance, object y dominates object x with respect to a criteria set P (denotation yD_Px). A dominance set means an important set. Given $x, y \in U$ and P, the dominance sets are formulated as:

$$\begin{aligned} P\text{-dominating set:} \quad & D_P^+(x) = \{y \in U : yD_Px\}, \\ P\text{-dominated set:} \quad & D_P^-(x) = \{y \in U : xD_Py\}, \end{aligned}$$

where $x, y \in Cl$, $y \succsim_q x$ for $D_P^+(x)$, $x \succsim_q y$ for $D_P^-(x)$, and all $q \in P$.

Third is about the use of relevant evidences to explain the ranking unions with conditional preferences. For instance of assigning objects into P-dominating set, evidences have two types. One is called consistent evidence, i.e., objects can be properly assigned into $D_P^+(x)$ and $Cl_t^{\geq}$. The other is inconsistent evidence, i.e., objects assigned in $Cl_t^{\geq}$ possibly violate the dominance principle of $D_P^+(x)$. In

other words, this inconsistent evidence is not a member of a dominating set but assigned to the upward union. Therefore, inconsistent evidence is the major part making induction degenerate. According to the dominance consistency, there are three approximations defined for relevant evidences.

$$\underline{P}(Cl_t^{\geq}) = \{x \in U : D_P^+(x) \subseteq Cl_t^{\geq}\}, \qquad \overline{P}(Cl_t^{\geq}) = \bigcup_{x \in Cl_t^{\geq}} D_P^+(x),$$

$$\underline{P}(Cl_t^{<}) = \{x \in U : D_P^-(x) \subseteq Cl_t^{<}\}, \qquad \overline{P}(Cl_t^{<}) = \bigcup_{x \in Cl_t^{<}} D_P^-(x),$$

and

$$Bnp(Cl_t^{\geq}) = \overline{P}(Cl_t^{\geq}) - \underline{P}(Cl_t^{\geq}),$$
$$Bnp(Cl_t^{<}) = \overline{P}(Cl_t^{<}) - \underline{P}(Cl_t^{<}),$$

where $t = 1, 2, \ldots, n$, $Bnp(Cl_t^{\geq})$ and $Bnp(Cl_t^{<})$ are P-doubtful regions. Objects in P-doubtful regions are inconsistent. In a simple word, $\underline{P}(Cl_t^{\geq})$ requires the largest union of P-dominating sets to be properly included in $Cl_t^{\geq}$. $\overline{P}(Cl_t^{\geq})$ requires the smallest union of P-dominating sets to contain all elements of $Cl_t^{\geq}$ while allowing some inconsistent objects.

Finally, the following is about the three measures related to the evidential weight.

- Accuracy rate (AR) [25,17]
  The accuracy rate presents the ratio of the proper assignment to the possible assignment. Two typical accuracy rates (α) are listed as:

$$\alpha(Cl_t^{\geq}) = \frac{\left|\underline{P}(Cl_t^{\geq})\right|}{\left|\overline{P}(Cl_t^{\geq})\right|} = \frac{\left|\underline{P}(Cl_t^{\geq})\right|}{\left|U\right| - \left|\underline{P}(Cl_t^{<})\right|},$$
$$\alpha(Cl_t^{<}) = \frac{\left|\underline{P}(Cl_t^{<})\right|}{\left|\overline{P}(Cl_t^{<})\right|} = \frac{\left|\underline{P}(Cl_t^{<})\right|}{\left|U\right| - \left|\underline{P}(Cl_t^{\geq})\right|}.$$

  The symbol α is used to present 'a ratio of the cardinalities of P-lower approximation to those of P-upper approximation, i.e., the degree of the properly classifying approximation relative to the possibly classified approximation'.
- Coverage rates (CR) [26,17]
  The coverage rate expresses 'the probability of objects in the P-lower approximation relatively belonging to the corresponding union of decision classes', defined by Pawlak and Greco [26,17]. There are two typical coverage rates (CR) for the upward unions $Cl_t^{\geq}$ and the downward union $Cl_t^{<}$, which are formulated as follows:

$$CR(Cl_t^{\geq}) = \frac{\left|\underline{P}(Cl_t^{\geq})\right|}{\left|Cl_t^{\geq}\right|}, \qquad CR(Cl_t^{<}) = \frac{\left|\underline{P}(Cl_t^{<})\right|}{\left|Cl_t^{<}\right|}.$$

– Certainty rate (Cer) [26]
  A certainty rate of RST is formulated as:

$$\mathrm{Cer}(\phi, \psi) = \frac{\mathrm{Card}\,\|\phi \cap \psi\|}{\mathrm{Card}\,\|\phi\|} \quad \text{for} \quad \phi \to \psi,$$

  where ϕ and ψ are sets for condition and conclusion. Card $|\cdot|$ means the number of elements in a set. In a reverse way to explain the certainty rate, the ratio can be used to express the degree of the noise within the condition for implication.

Saaty (2001) proposed that pair-wise comparisons and inductions can be formulated as ratios, and then transformed the comparisons into the priority of criteria, or the criteria weights [12]. He also mentioned that the ratios represent how much more or less a criterion is as compared to another, and that its application can determine how close the criteria are. Furthermore, he emphasized that ratio operations are independent from irrelevant alternatives. Thus the ratio scales derived from different scales (criteria) can be implemented mathematically to generate a characteristic ratio with invariance. Based on these theories, a multiplication of ratios can express the quality of induction. These ratio operations can be further used to solve the evidential uncertainty, as mentioned in next section.

3 Subjective Weighting Model

MLDRSA conjunctively and disjunctively links the logical relationships among criteria then transforms the relationships into multiplicative and additive operations of AHP. The integration of logics and arithmetic through DRSA and linear functions provides the convergent utilities for subjective analysis. The information system of MLDRSA is defined in 3.2, the transformation is specified in 3.3, and the dataset of this research is presented in 3.1.

3.1 Dataset

International Institute for Management Development (IMD) annually publishes WCY, a well-known report which ranks and analyzes how a nation's environment can create and develop sustainable enterprises [27,28]. WCY is a product cooperating with fifty-four partner institutes worldwide. Its ranking considers broad perspectives by gathering the latest and most relevant data on the subject and by analyzing the policy consequence. The dataset include 59 nations, 4 consolidated factors, and 20 criteria in Table 1 [29].

The dataset of this research is collected from WCY 2012, which adopts all criteria and nations, i.e., 20 criteria and 59 nations (objects shown by x or z). The top ten nations are Canada, Germany, Hong Kong, Norway, Qatar, Singapore, Sweden, Switzerland, Taiwan, and USA, which will be used to validate our proposed method. 29 upper half nations will be validated, too.

Table 1. Four factors and twenty criteria of WCY-IMD 2012

	Economic Performance		Business Efficiency
q_1	Domestic Economy	q_{11}	Productivity and Efficiency
q_2	International Trade	q_{12}	Labor Market
q_3	International Investment	q_{13}	Finance
q_4	Employment	q_{14}	Management Practices
q_5	Prices	q_{15}	Attitudes and Values
	Government Efficiency		Infrastructure
q_6	Public Finance	q_{16}	Basic Infrastructure
q_7	Fiscal Policy	q_{17}	Technological Infrastructure
q_8	Institutional Framework	q_{18}	Scientific Infrastructure
q_9	Business Legislation	q_{19}	Health and Environment
q_{10}	Societal Framework	q_{20}	Education

3.2 Definitions of the Subjective Weighting

All preferences of subjective criteria categorized by a selected rank could be linearly transformed into a product of an eigenvalue, λ, and an eigenvevector, $[q_i'']$, which follows the linear transformation [30]. $[q_i'']$ can represent the objective characteristic of PEW by considering all preferences. Technically, $[q_i'']$ is required parallel to $[q_i''] \times$ PEW. The eigenvalue has two meanings. The first means the direction of eigenvevector, i.e., $\lambda > 0$, toward the same direction of PEW, and $\lambda < 0$, toward the reverse direction of PEW. The second means the quantitative significance of the eigenvevector by approximating the maximum λ. In this research the maximum λ associates Subjective weights which comprise $[q_i'']$. Followings illustrate the defini-tions and implementation models.

Definition 1. *The information system of subjective weights*

This system only contains objects, subjective criteria, ranking functions, and ranks obtained from the ranking functions. The ranking function transforms the preferences within the same criterion into ranks. One point to note: this system does not contain information of alternatives selection.
$IS\_MLSW = (U, Q, f, R)$, *where* $U = \{y \mid y = 1, 2, \ldots, n\}$, $Q = \{q_1, q_2, \ldots, q_n\}$, $f : U \times Q \to R$, *R is a ranking set,* $R \in \{1^{st}, 2^{nd}, \ldots, n^{th}\}$.

Definition 2. *An induction rule between subjective criteria*

$q^{\geq}_{j,t'} \to q^{\geq}_{i,t}$ *represents how a criterion* q_j *supports nations to achieve the top t positions in* q_i *where* $q^{\geq}_{j,t'}$, $(q^{\geq}_{j,t'} = \bigcup_{s \geq t'} q_{j,s})$, *is also a ranking union containing the top t positions with respect to* q_j, $q^{\geq}_{i,t}$, $(q^{\geq}_{i,t} = \bigcup_{s \geq t} q_{i,s})$ *is also a ranking union containing the top t positions with respect to* q_i. *This rule associates the ranking evidences of criterion* q_j *to a ranking union of* q_i, *which is independent to addition or removal of other criteria. Our design can be conceptualized as in Fig. 3.*

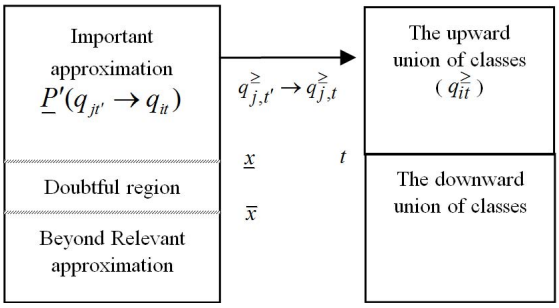

Fig. 3. Approximations based on the induction evidences

Definition 3. *The induction evidences*

Under the induction rule $q^{\geq}_{j,t'} \to q^{\geq}_{i,t}$, *there are two approximations defined with boundaries* $\underline{x}$ *and* $\overline{x}$ *where* $\underline{x} \in q^{\geq}_{i,t}$, $\overline{x} \in q^{\geq}_{i,t}$, *and the rank of* $\underline{x}$ *is always higher than or equal to that of* $\overline{x}$. $\underline{x}$ *is assumed as the boundary of the important evidences and* $\overline{x}$ *as the boundary of the relevant evidences. These two types of evidences are defined as:*

Important evidences: $D^+_P(\underline{x})$, *relevant evidences:* $D^+_P(\overline{x})$.

The important evidences belong to the upper part of the relevant evidences in Fig. 4. The approximations based on the induction evidences are defined as:

Important approximation: $\underline{P}'(q^{\geq}_{j,t'} \to q^{\geq}_{i,t}) = D^+_P(\underline{x}) \cap q^{\geq}_{i,t}$,

Relevant approximation: $\overline{P}'(q^{\geq}_{j,t'} \to q^{\geq}_{i,t}) = D^+_P(\overline{x})$,

Doubtful region: $D^+_P(\overline{x}) - D^+_P(\underline{x})$.

Important approximation, same as the lower approximation of DRSA, contains the important evidences belonging to the ranking union. Relevant approximation, same as the upper approximation of DRSA, contains the evidences above the boundary $\overline{x}$ *and requires that* $\overline{x}$ *belongs to the ranking union. Doubtful region contains the evidences that are relevant but not important. The noise in this area is dissimilar to the important evidence, and is called distinguished noise. Therefore, the noise within the approximations is defined as:*

Undistinguished noises: $D^+_P(\underline{x}) - \underline{P}'(q^{\geq}_{j,t'} \to q^{\geq}_{i,t})$,

Distinguished noises: $D^+_P(\overline{x}) - D^+_P(\underline{x}) - \overline{P}(q^{\geq}_{j,t'} \to q^{\geq}_{i,t})$.

The distinguished noises are objects away from the important evidences, and normally located in the doubtful region. The undistinguished noises are together with the important evidences and cannot be separated by objective methods. Obviously, the more evidences in $\underline{P}'(q^{\geq}_{j,t'} \to q^{\geq}_{i,t})$ *the more important* P *is; the more noise in* $\overline{P}'(q^{\geq}_{j,t'} \to q^{\geq}_{i,t})$ *the less relevant* P *is. Due to the impact of noises,* $\underline{x}$ *and* $\overline{x}$ *are non-deterministic priori. Therefore,* $\underline{x}$ *and* $\overline{x}$ *are presented as slash lines in Fig. 4. They can be specified by approximating the optimal classification with the minimum distinguished noises.*

Definition 4. *Measures of the induction evidences*
Three measures related to the evidential weight of Fig. 4 are defined below.

- *Evidence-accuracy rate (α') [25,17]*
  An accuracy rate presents the ratio of 'Important approximation' to 'Relevant approximation', i.e., the degree of the properly classified evidence relative to the possibly relevant evidences, and is defined as:

$$\alpha' = \frac{\left|\underline{P}'(q^{\geq}_{j,t'} \rightarrow q^{\geq}_{i,t})\right|}{\left|\overline{P}'(q^{\geq}_{j,t'} \rightarrow q^{\geq}_{i,t})\right|}.$$

  α' for a logical implication represents the degree of necessary condition of 'Important approximation' in the relevant evidences.
- *Evidence-coverage rates (CR') [26,17]*
  A coverage rate expresses the ratio of 'Important approximation' relatively belonging to the ranking union, and is defined as:

$$CR' = \frac{\left|\underline{P}'(q^{\geq}_{j,t'} \rightarrow q^{\geq}_{i,t})\right|}{\left|q^{\geq}_{i,t}\right|}.$$

  CR' for a logical implication represents the degree of sufficient condition that 'Important approximation' influences the ranking union.
- *Evidence-certainty rate (Cer') [26]*
  A certainty rate expresses the ratio of objects in 'Important approximation' relatively belonging to the important evidences:

$$\mathrm{Cer}' = \frac{\left|\underline{P}'(q^{\geq}_{j,t'} \rightarrow q^{\geq}_{i,t})\right|}{\left|D^{+}_{P}(\underline{x})\right|},$$

  where $|\cdot|$ means the number of evidences in a set. Cer' represents the degree of reliability of $\underline{P}'(Cl^{\geq}_{t})$.

Definition 5. *The quality classification rate*
The classification rate for $q^{\geq}_{j,t'} \rightarrow q^{\geq}_{i,t}$ needs to consider both sufficient and necessary conditions. The product of CR' and α' will be a unique value on an indifference curve, which originates from the product of sufficient and necessary ratios for the indifferent induction rules. The induction measures are independent to addition or removal of other criteria. The product values thus can be used for preference orders. Further, the quality of classification needs have the reliability concern. According to the logical implication, a quality classification can be formulated as:
Quality classification $\Longleftrightarrow$ Minimum uncertainty

'Quality classification if and only if minimum uncertainty' can be processed by mathematics to get a unique value on an indifference curve. Therefore, the quality classification rate based on evidential weight can be formulated below.

Model I: Solving g'_{ji}.

$$\begin{aligned} \text{Max} \quad & g'_{ji} = \text{Cer}' \times CR' \times \alpha' \\ \text{s.t.} \quad & \text{Cer}' = \frac{\left|\underline{P}'(q^{\geq}_{j,t'} \to q^{\geq}_{i,t})\right|}{\left|D^{+}_{P}(\underline{x})\right|} \\ & CR' = \frac{\left|\underline{P}'(q^{\geq}_{j,t'} \to q^{\geq}_{i,t})\right|}{\left|q^{\geq}_{i,t}\right|} \\ & \alpha' = \frac{\left|\underline{P}'(q^{\geq}_{j,t'} \to q^{\geq}_{i,t})\right|}{\left|\overline{P}'(q^{\geq}_{j,t'} \to q^{\geq}_{i,t})\right|} \end{aligned}$$

Model I will approximate a unique value, g'_{ji}, to consistently enlighten the relevance and importance of criterion q_j supporting nations to achieve the benchmarking positions on q_i. g'_{ji} can be used as an evidential weight like a slope in Fig. 4 also illustrates how noise in the doubtful region is reduced by Model I. This process cuts nations into yes or no supporting evidences when approximating the quality classification. The vagueness in the doubtful region will diminish due to the optimal solution. The noise in 'Important evidences' will be counted as imprecision to the classification. The ranking position of $\overline{x}$ will become as high as possible to reduce the noise of 'Important evidences.' The ranking position of $\overline{x}$ also becomes highest to reduce distinguished noises. When approximating the optimal solution, $\underline{x}$ and $\overline{x}$ will be adjusted to the same position, and g'_{ji} is solved as the slope of Fig. 4.

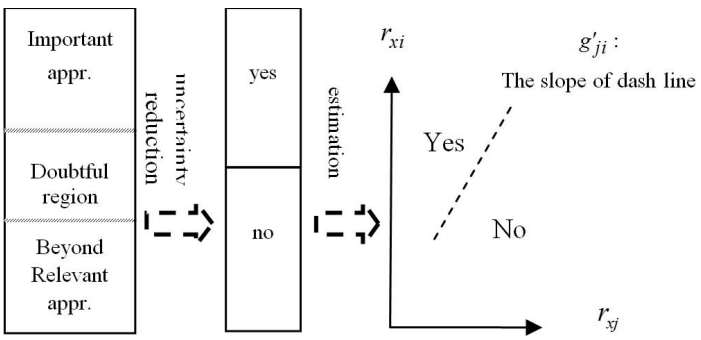

Fig. 4. The process of uncertainty reduction on criterion q_i

3.3 Implementation of the Subjective Weighting

Definition 6. ISW *matrix and* **CSW** *vector*

The subjective weight for all $q^{\geq}_{j,t'} \rightarrow q^{\geq}_{i,t}$ *is formulated as* sw_{ji}*. The logical associations between any two attributes are formulated as* $\left[g'_{ji}\right]_{m\times m}$ *which is abbreviated as* **ISW***, i.e.,* $\mathbf{ISW} = \left[g'_{ji}\right]_{m\times m}$.

$$\mathbf{ISW} = \begin{bmatrix} g'_{11} & \cdots & g'_{1i} & \cdots & g'_{1m} \\ \vdots & & \vdots & & \vdots \\ g'_{j1} & \cdots & g'_{ji} & \cdots & g'_{jm} \\ \vdots & & \vdots & & \vdots \\ g'_{m1} & \cdots & g'_{mi} & \cdots & g'_{mm} \end{bmatrix}, \tag{1}$$

where g'_{ji} *is within a range* $0 \sim 1$ *and* $g'_{ji} = 0$ *when* $j = i$*. Each* g'_{ji} *means a quantitative value of the relevance and importance of* q_j *to* q_i*. Furthermore,* **CSW** *is defined as* $[q''_i]_{m\times 1}$*:*

$$\mathbf{CSW} = [q''_i]_{m\times 1} \tag{2}$$

Definition 7. *Linear transformation*

The linear transformation between $\left[g'_{ji}\right]_{m\times m} \times [q''_i]_{m\times 1}$ *and* $[q''_i]_{m\times 1}$ *is defined as Eq.* (3)*.*

$$\left[g'_{ji}\right]_{m\times m} \times [q''_i]_{m\times 1} = \lambda\,[q''_i]_{m\times 1} \tag{3}$$

where λ *is the eigenvalue and* $[q''_i]_{m\times 1}$ *is the eigenvector of* **ISW***, i.e,* **CSW***. In details,* **CSW** *is the priori of Eq.* (2)*.* $[q''_i]$ *represents the posteriori, i.e., the quality classification rate for* $q^{\geq}_{it'} \rightarrow O^{\geq}_{t}$ *where* O *plays as the objective distinguishing the dominating and dominated unions. Therefore,* $[q''_i]$ *can be treated as the vector of subjective weights. The solving of the linear transformation is designed in Model II in terms of Lingo 12.*

Model II: Solving $[q''_i]_{m\times 1}$

$$\begin{aligned} &\text{Max} \quad \lambda \\ &\text{s.t.} \quad \left[g'_{ji}\right] \times [q''_i] = \lambda\,[q''_i]\,, \end{aligned}$$

where g''_i represents the optimal evidential weight of q_i to the objective of all other criteria. The details of Eq. (3) can be presented as Eq. (4).

$$\begin{bmatrix} 0_{11} & \cdots & & \cdots & g'_{1m} \\ \vdots & & \vdots & & \vdots \\ & \cdots & 0_{jj} & \cdots & \\ \vdots & & \vdots & & \vdots \\ g'_{m1} & \cdots & & \cdots & 0_{mm} \end{bmatrix} \times \begin{bmatrix} g''_1 \\ \vdots \\ \\ \vdots \\ g''_m \end{bmatrix} = \lambda \begin{bmatrix} g''_1 \\ \vdots \\ \\ \vdots \\ g''_m \end{bmatrix} \tag{4}$$

Eq. (4) can be further simplified as Eq. (5).

$$\sum_{i=1}^{m} g'_{ji} \times g''_i = \lambda g''_i \quad \text{for all } j \tag{5}$$

Technically, g'_{ji} and g''_i are the probability measures in two successive states. g''_i is a convergent probability of criterion q_i toward the objective of all subjective preferences and can be treated as a weight of q_i by requiring $\sum_{i=1}^{m} q_i = 1$. In logical implications, **ISW** plays the premise. The products, $g'_{ji} \times g''_i$, presents conjunctive implications as Eq. (6) shown in Fig. 5.

$$\left(q^{\geq}_{j,t'} \rightarrow q^{\geq}_{i,t}\right) \wedge \left(q^{\geq}_{it'} \rightarrow O^{\geq}_{t}\right) \tag{6}$$

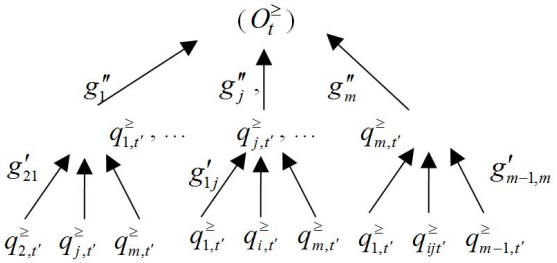

Fig. 5. The hierarchical implications of Eq. (6)

In our design, **CSW** can be derived from **ISW**. The closest characteristic of all subjective criteria, i.e., the whole preferences, is quantitatively expressed by **CSW**.

4 Application Results

Meta learning about WCY has two parts, i.e., (1) the subjective weights which give the importance and relevance of criteria toward the top and upper half of competitive-ness (2) the subjective rules which give the ranks of alternatives for decision makers.

4.1 The Resulted Subjective Weights

The Eigen weights for the top ten and the upper half levels in 2012 are solved and presented in Table 2. The values of Institutional Framework (q_8) are bold which means the highest weights. The top 10 nations not only have good institutional framework but also pursue health and environment (q_{19}) for citizens, which is grounded with grey color.

Table 2. Subjective weights of WCY 2012

The top 10 level				The upper half level			
g''_1	0.038	g''_{11}	0.041	g''_1	0.049	g''_{11}	0.058
g''_2	0.041	g''_{12}	0.027	g''_2	0.038	g''_{12}	0.045
g''_3	0.046	g''_{13}	0.063	g''_3	0.049	g''_{13}	0.054
g''_4	0.026	g''_{14}	0.071	g''_4	0.043	g''_{14}	0.059
g''_5	0.013	g''_{15}	0.056	g''_5	0.031	g''_{15}	0.051
g''_6	0.053	g''_{16}	0.055	g''_6	0.037	g''_{16}	0.056
g''_7	0.024	g''_{17}	0.063	g''_7	0.032	g''_{17}	0.059
g''_8	0.076	g''_{18}	0.036	g''_8	0.061	g''_{18}	0.057
g''_9	0.063	g''_{19}	0.073	g''_9	0.055	g''_{19}	0.055
g''_{10}	0.068	g''_{20}	0.063	g''_{10}	0.059	g''_{20}	0.054

4.2 The Subjective Rules

The subjective rules based on a simple utility function, $SUF(x) = \sum_j^m g''_j r_{jx}$, for the top ten and the upper half nations are deduced as:

R1: if $SUF(x) \geq 67.98$ then $x \in$ the top ten nations
$\text{Cer}' = 1, \quad CR' = 0.9, \quad \alpha' = 1$
$SUF(x) = 0.038 \times r_{x,1} + \cdots + 0.063 \times r_{x,20}$;

R2: if $SUF(x) \geq 60.69$ then $x \in$ the upper half nations
$\text{Cer}' = 1, \quad CR' = 1, \quad \alpha' = 1$
$SUF(x) = 0.049 \times r_{x,1} + \cdots + 0.054 \times r_{x,20}$.

Obviously, R1 and R2 successfully classify the benchmarking nations and prove that Eigen weights really exist for all preferences at high accuracy. The proposed PEW is thus verified true with high accuracy by deduction rules.

4.3 Achievements of MLDRSA

The subjective rules show MLDRSA's alterative selections have high consistency with the objective ranks of WCY 2012. This encourages that (1) MLDRSA can provide the important and relevant information among criteria, (2) MLDRSA can enhance DSS in alternatives selection. These two achievements are further discussed next.

5 Discussions on MLDRSA and the Case Study

This section has two parts. One is about the technique discussion. The other is a case study about Meta learning on the subjective weights for policy making.

5.1 Technique Discussion

The technique discussion has four stages, the goal, methodology, applications, and comparison. This research aims to create an approach of Meta learning to find out the subjective weights which contain the importance and relevance evidences toward the closest feature of WCY 2012. MLDRSA methodology defines the logical implications for the relationships among criteria, transforms the implications into linear operations, and deduces subjective weights and rules. Based on the rigid and solid logics and mathematical operations, the empirical results are reliable than DRSA and the regular utility functions. Their comparisons are presented in Table 3.

Table 3. Comparison among the related techniques

Weakness	DRSA	Regular utility functions	MLRDSA
Subjective weights w/o experts	0	0	1
Utilities aggregation	0	1	1
Logical implications	1	0	1
Total advantages	1	1	3

The comparisons show the regular utility function considers aggregation but does not consider the logical implications. In the case of logical implications, DRSA is good at interpreting the relationship of criteria toward the objective ranks but do not consider the aggregation. Only MLDRSA has all these three merits.

5.2 The Case Study about MLDRSA

The subjective weights between the top and upper nations reveal two learning points. The first learning point is that both of them have the highest weights in the institutional framework (q_8) of government performance. Obviously, the government is the core of competitiveness. The resulted ICW shows that the productivity and efficiency (q_{10}) has the biggest influence on the institutional framework (q_8), the management practices (q_{14}) is the second, and the public finance (q_6) is the third. This is more significant for the top nations because the difference among criteria is bigger than the upper nations. The second learning point shows the upper nations need to consider wider scope because the subjective weights are closer than the top nations. This means that nations should build competitiveness from the fundamentals instead of a few criteria only. The resulted ICW shows that the influence from criteria on the institutional framework (q_8) is stronger than the top nations. The biggest two criteria are the management practices (q_{14}) and the scientific infrastructure (q_{18}).

5.3 The Future Work

Even some criteria relationships are learned from MLDRSA there are more knowledge can be learned. We here provide some points that deserve deeper study in the future. First, deduced knowledge might be available. Second, more types of subjective weights could be derived from Meta learning techniques. Third, the aggregation of subjective weights could be explored for interpretation this would solve of the uncertain information during rule induction to construct a certain rule set for evaluation.

6 Concluding Remarks

This research proposes a type of subjective weights which do not require experts involved but are derived from DRSA and RS. The results show that the subjective rules have the objective selections of the benchmarking and upper half nations from WCY 2012. The objective evidences verify the correctness of the subjective weights. The deduction process of the subjective weights is built from logics and mathematics which provide a solid and complete theoretical fundamental. Therefore, the weight is reliable with minimum uncertainty. The subjective weights disclosed here is just a beginning. In forthcoming work we are applying the subjective weights in medical diagnosis and possibly other applications in the near future.

References

1. Savage, J.L.: The Foundations of Statistics. John Wiley, New York (1954)
2. Savage, J.L.: Elicitation of personal probabilities and expectations. Journal of American Statistical Association 66, 783–801 (1971)
3. Herrera-Viedma, E., Cabrerizo, F.J., Kacprzyk, J., Pedrycz, W.: A review of soft consensus models in a fuzzy environment. Information Fusion 17(1), 4–13 (2014)
4. Fujita, H., Herrera-Viedma, E.: Special issue: Intelligent Decision Making Support Tools. Knowledge-Based Systems (2013) (article in press)
5. Yager, R.R., Alajlan, N.: A generalized framework for mean aggregation: Toward the mod-eling of cognitive aspects. Information Fusion 17(1), 65–73 (2014)
6. Chiclana, F., Herrera, F., Herrera-Viedma, E.: Integrating multiplicative preference relations in a multipurpose decision-making model based on fuzzy preference relations. Fuzzy Sets Syst. 122, 277–291 (2001)
7. Yager, R.R., Filev, D.P.: Induced ordered weighted averaging operators. IEEE Trans. System, Man, Cybernetics 29, 141–150 (1999)
8. Herrera, F., Herrera-Viedma, E.: Linguistic decision analysis: steps for solving decision problems under linguistic information. Fuzzy Sets Syst. 115, 67–82 (2000)
9. Saaty, T.L.: A scaling method for priorities in hierarchical structures. Journal of Mathematical Psychology 15(3), 234–281 (1977)
10. Saaty, T.L.: Decision making hierarchies. The Analytic Network Process, 2nd edn. RWS Publications (2001)
11. Onut, S., Kara, S.S., Isik, E.: Long term supplier selection using a combined fuzzy MCDM approach: A case study for a telecommunication company. Expert Systems with Applications 36, 3887–3895 (2009)

12. Wang, J., Cheng, C., Huang, K.: Fuzzy hierarchical TOPSIS for supplier selection. Applied Soft Computing Journal 9, 377–386 (2009)
13. Noor-E-Alam, M., Lipi, T.F., Hasin, M.A.A., Ullah, A.M.M.S.: Algorithms for fuzzy multi expert multi criteria decision making (ME-MCDM). Knowledge-Based Systems 24(3), 367–377 (2011)
14. Qian, G., Wang, H., Feng, X.: Generalized hesitant fuzzy sets and their application in decision support system. Knowledge-Based Systems 37, 357–365 (2013)
15. Greco, S., Matarazzo, B., Slowinski, R.: Rough set theory for multicriteria decision analysis. European Journal of Operational Research 129(1), 1–47 (2001)
16. Holsapple, C.W.: Decisions and knowledge. In: Burstein, F., Holsapple, C.W. (eds.) Handbook on Decision Support Systems, pp. 21–53. Springer, Berlin (2008)
17. Arnott, D., Pervan, G.: Eight key issues for the decision support systems discipline. Decision Support Systems 44(3), 657–672 (2008)
18. Figueira, J., Greco, S., Ehrgott, M.: Multiple Criteria Decision Analysis: State of the Art Surveys. Springer, New York (2005)
19. Vilalta, R., Giraud-Carrier, C., Brazdil, P., Soares, C.: Using Meta-Learning to Support Data Mining. International Journal of Computer Science & Applications I(1), 31–45 (2004)
20. Matijaš, M., Suykens, J.A.K., Krajcar, S.: Load forecasting using a multivariate meta-learning system. Expert Systems with Applications 40(11), 4427–4437 (2013)
21. Cheng, J.-W., Chiu, W.-L., Tzeng, G.-H.: Do impression management tactics and/or super-visor-subordinate guanxi matter? Knowledge-Based Systems 40, 123–133 (2013)
22. Ma, T., Leong, J., Cui, M., Tian, W.: Inducing positive and negative rules based on rough set. Information Technology Journal 8, 1039–1043 (2009)
23. Greco, S., Matarazzo, B., Slowinski, R.: Extension of the rough set approach to multicriteria decision support. INFOR 38(3), 161–193 (2000)
24. Slowinski, R., Greco, S., Matarazzo, B.: Rough Sets in Decision Making. Encyclopedia of Complexity and Systems Science. Springer, New York (2009)
25. Pawlak, Z.: Rough set approach to knowledge-based decision support. European Journal of Operational Research 99(1), 48–57 (1997)
26. Pawlak, Z.: Rough sets, decision algorithms and Bayes' theorem. European Journal of Operational Research 136(1), 181–189 (2002)
27. U.S. President's Commission on Industrial Competitiveness, Global competition: The new reality. U.S. Government Printing Office, Washington, D.C. (1985)
28. Porter, M.E.: The competitive advantage of nations. The Free Press, MacMillan (1990)
29. IMD, World Competitiveness Yearbook. Institute Management Development, Lausanne, Switzerland (2012), `http://worldcompetitiveness.com/OnLine/App/Index.htm`
30. Kolman, B.: Introductory linear algebra with application, 5th edn. Maxwell Macmillan International, Singapore (1993)

Modeling of Complex Multidimensional Nonlinear Systems Using Neural System with Deep Architectures

Bogdan M. Wilamowski[1] and Janusz Korniak[2]

[1] Electrical and Computer Engineering Dept.,
Auburn University, AL, USA
wilam@ieee.org
[2] University of IT and Management in Rzeszow, Poland
jkorniak@wsiz.rzeszow.pl

Abstract. Reviews of several methods for modeling of complex multidimensional nonlinear systems were presented. It turns out that power of neural networks grows linearly with its width and exponentially with its depth. Unfortunately training of traditional MLP Multi-Layer Perceptron deep architectures is very difficult. The paper presents couple solution to this problem. One solution is to use neural network with connections across layers such as FCC Fully Connected Cascade or BMLP - Bridged Multi-Layer Perceptron. Another alternative is to use DNN - Dual Neural Networks which is described with more details.

Keywords: Neural networks, deep learning, neural architectures, learning algorithms.

1 Introduction

In order to analyze and control complex systems in most cases, researchers follow the advice: "be wise and linearize", and then traditional well-developed techniques in linear control theory and statistics can be used. Unfortunately many systems, including most engineering systems, have nonlinear characters, and the linearization approach may significantly change their behavior. What is even worse is that many phenomena in natural systems, and even in engineering systems, cannot be described by mathematical formulas. For example, the relation of car traffic intensity as a function of time of day, day of week, or day of year are nonlinear and cannot be described by mathematical equations. The problem becomes even more complicated if we would like, for example, to predict the traffic based on past information in different locations. Many problems in environmental, chemical, mechanical, or manufacturing engineering have a similar nature. In some cases only static nonlinear relations are important, but often everything may also have a dynamic nature. Fortunately any dynamic nonlinear system can be described by the set of state equations (Fig. 1(a)). If mathematical descriptions are not possible then a dynamic nonlinear system can be

J. Fodor and R. Fullér (eds.), *Advances in Soft Computing, Intelligent Robotics and Control,* Topics in Intelligent Engineering and Informatics 8,
DOI: 10.1007/978-3-319-05945-7_8,

$$y_1 = \int f_1(x_1, x_2, \cdots x_n, y_1, y_2, \cdots y_n)\ dt$$
$$y_2 = \int f_2(x_1, x_2, \cdots x_n, y_1, y_2, \cdots y_n)\ dt$$
$$\cdots$$
$$y_n = \int f_n(x_1, x_2, \cdots x_n, y_1, y_2, \cdots y_n)\ dt$$

(a)

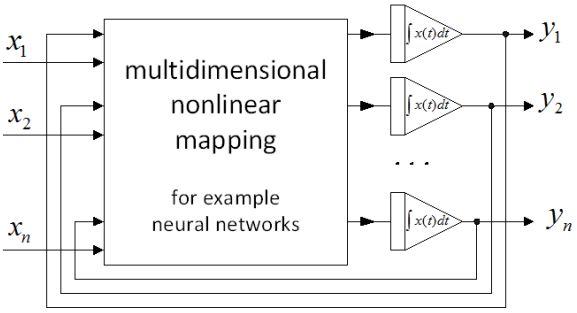

Fig. 1. Modeling of arbitrarily dynamic system by state equations or by neural networks if mathematical formulas are not known (a) state equations, (b) block diagram.

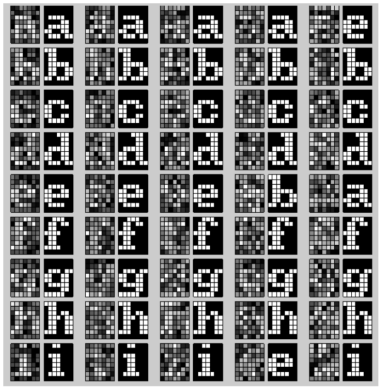

Fig. 2. Result of pattern retrieval for neural network recognizing letters with left columns with noisy images and right columns with recognized characters.

modeled by an adaptive multidimensional nonlinear system (Fig. 1(b)), where nonlinear elements are mutually connected by weights with different strengths. Such system can be trained by various optimization processes. When nonlinear elements (cells) have sigmoidal type of nonlinearity then such systems are commonly known as artificial neural networks.

Artificial intelligence and computational intelligence are two competing technologies for a solution for very complex problems. The goal of artificial intelligence is to build a system that the user will not be able to recognize if he/she

interacts with a human or machine. This approach imposes a very deep understanding of the problem by the programmer, so every small detail has to be solved by the designer. In other words in artificial intelligence, the human must be smarter than the machine. In the case of computational intelligence, the goal is to build a system which can outperform humans. One may notice that humans have difficulties with processing a large amount of data. This is especially true if data has a multidimensional character. For example, humans may have difficulty correctly recognizing noisy letters shown in Fig. 2, while even very simple neural networks can solve problems relatively easily. Similarly humans may face difficulties recognizing that sixty 4-dimensional patterns, shown in Fig. 3, have 3 well-defined clusters.

2 Background

2.1 ANN – Artificial Neural Networks

Significant success stories of the application of neural networks for solving many nonlinear problems have been reported over the past 20 years. Neural networks were successfully used for classification purposes and also as universal nonlinear approximators. In contrast to many other techniques, neural networks were not systematically developed, but they were just trained with patterns. The success of neural networks depends on proper network architecture and an adequate learning algorithm. Accomplishments of neural are not questionable despite the fact that most researchers were using far from optimal neural network architectures and rather inefficient learning algorithms [1].

The most popular neural network architecture is the Multi-Layer Perceptron (MLP) [2], which is relatively difficult to train if many hidden layers are there. Therefore, many researchers are using the MLP with a single hidden layer known also as a Single-Layer Perceptron (SLP). It was shown that the popular SLP

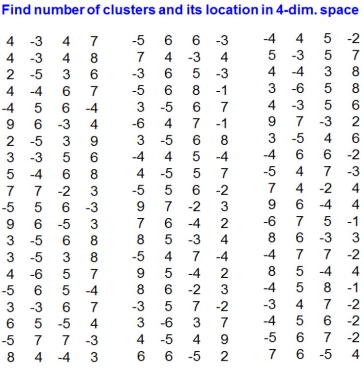

Fig. 3. Sixty 4-dimensional patterns which are difficult to be recognized by humans

architecture is very weak. For example, it was reported that in order to solve the benchmark of a 2-spiral problem the SLP architecture required 34 neurons in the hidden layer [3]. When the FCC (Fully Connected Cascade) architecture is used, the same problem can be solved with only 7 neurons [1,4]. A comparison of the efficiency of SLP and FCC architectures using other popular parity-N benchmarks are shown in Fig. 4. One may notice that with 13 neurons the SLP architecture can solve only the parity-12 problem, while the FCC architecture with 13 neurons can solve a large architecture like the parity-8911 [5,6]. One may question why most researchers still use SLP architectures, and why they are still happy with the results? There are couple answers to these questions:

– People may not be aware of the powerful abilities of other architectures.
– Most learning software was written for MLP or SLP architectures (a good example is MATLAB NN toolbox Software for training other architectures is not that easily accessible.

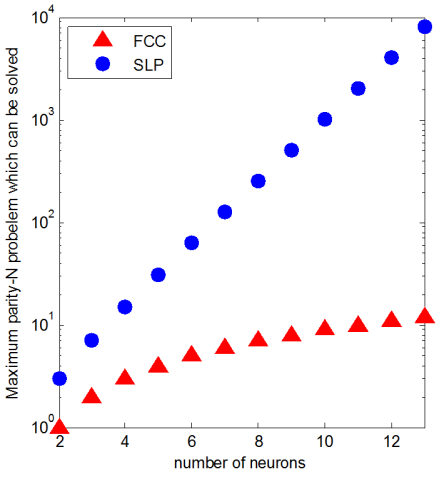

Fig. 4. Comparison go capabilities of MLP and FCC networks using parity-N problems

The most popular learning algorithm is the EBP (Error Back Propagation) [2,7], and there are many modifications of this algorithm. This is a first order algorithm with an asymptotic convergence rate. As a consequence this group of first order algorithms often requires hundreds or thousands of iterations before an acceptable error is reached. What is worse is that the EBP very seldom can train close to optimum neural networks. It is usually much easier and faster to train larger than required networks, but as a consequence such networks are losing their generalization abilities. In other words a network is responding very poorly to new patterns not used for training. Traditionally at first researchers are training small neural networks with limited success; smaller networks are difficult to train. Eventually they are increasing the size of the network, and

indeed the network can be now trained faster to smaller errors. Then once they are happy with their success, they are applying new test patterns (not used in the training), then the results are disastrous because with the increase of size the neural network has lost its generalization abilities. This is probably a prime reason for frustration with neural networks.

The best well-known algorithm for training neural networks is the second order LM (Levenberg-Marquardt) algorithm [8], [9]. The LM algorithm can solve problems up to 1000 times faster than the EBP algorithm. Also, the LM algorithm can find solutions for networks with fewer neurons, where in most cases the EBP algorithm fails. Unfortunately the LM algorithm has a couple drawbacks:

- It was developed only for MLP architectures, so other more efficient NN architectures cannot be used.
- Only relatively small problems can be solved with the LM algorithm because the size of the Jacobian is proportional to the number of training patterns, and with larger problems modern computers are not able to manipulate such huge matrixes.

The above mentioned problems encouraged researchers to look for different ways to model highly nonlinear input/output mapping, such as: FS – Fuzzy Systems [10,11,12], RBF networks [13,14,15], LVQ – Learning Vector Quantization [16] and CN – Counterpropagation Networks [17], FLN – Functional Link Networks [18], Support Vector Machines [19,20], and Deep neural network architectures [21,12]. We will briefly comment on these technologies.

2.2 FS – Fuzzy Systems

Popular Mamdani [11] and TSK [12] fuzzy architectures are very useful, but problems are practically limited to 2 or 3 dimensions; for larger dimensions the size of the rule table became prohibitively large. Various tricks for artificial increase of dimensionality have limited success. Also, the nonlinear surfaces created by fuzzy systems are relatively raw with large output errors. Fuzzy systems are often used because of their simplicity and easy hardware implementations. However, if traditional tanh activations function in NN are replaced with an Elliot function and FCC architectures are used, neural networks implemented in a microcontroller can have a shorter assembly code, faster operation, and a 100 to 1000 times smaller error than fuzzy systems [23,24].

Traditional neuro-fuzzy systems NFS [25] have a similar topology to neural network, but its operation is very different. For example, NFS uses both signal by signal multiplications and divisions, while these operations are not present in neither biological nor artificial neural networks. Therefore NFS technology actually is not making FS and NN more compatible. Fuzzy systems traditionally used triangular, trapezoidal, or Gaussian membership function. However, it is also possible to use sigmoidal activation functions to obtain almost identical results [26]. With such an approach fuzzy systems become very similar to neural networks. Therefore, using theories and concepts of fuzzy systems (more

specifically TSK architectures) [12], we may try to design neural networks using techniques typical for fuzzy systems. Also, we may move in an opposite direction, and we can use neural network learning algorithms for better tuning of fuzzy systems.

2.3 RBF – Radial Basis Function Networks

Radial Basis Function Networks are an attractive alternative for fuzzy systems. Each RBF unit can represent one rule, and resulting nonlinear surfaces are much smoother. Similar to fuzzy systems, the RBF network can be designed without necessity of training. However, recently a significant effort was devoted to improve the performance of RBF networks by adding the training procedure. It has been proven by Cover's theorem [27] that, patterns with nonlinear relationship are more likely to be linearly separable if the dimension of patterns is increased. The number of nonlinear RBF units is usually significantly larger than the number of network inputs, so input space is transformed into higher dimensional space, where patterns become linearly separable [28]. Recently, RBF networks became attractive for practical applications because of the simpler design process and improved generalization ability compared to neural networks [29]. RBF networks are also not very suitable for multiple dimensional problems because the number of RBF units may become prohibitively large.

Facing difficulties of training traditional neural networks, many researchers redirected their interest toward RBF networks. These networks are much easier to understand, and they also have traditionally better generalization ability than common neural networks. In other words they better respond to patterns, which were not used in training or in the design process. Similar to fuzzy systems, RBF networks can be designed, and they need not be trained. The problem is that RBF architectures are very wide and shallow, and their computing power is limited. Therefore we may explore RBF networks with multiple hidden layers in order to increase network depth.

2.4 LVQ – Learning Vector Quantization and Counterpropagation Networks

Learning Vector Quantization [16] and Counterpropagation Networks [17] use traditional neurons with sigmoidal activation functions. The LVQ has the same concept as the counterpropagation networks, but instead of using all training patterns, only fewer patterns representing clusters of patterns are stored in the network. In contrast to RBF networks, the stored patterns in counterpropagation networks must be normalized, and the normalization process distorts information. For example, some clusters may become indistinguishable after normalization. This problem can be solved by transformation of input patterns to higher dimensions [28]. The main disadvantage of counterpropagation networks is that for a large number of training patterns the network can become prohibitively large, even if only patterns representing clusters are stored.

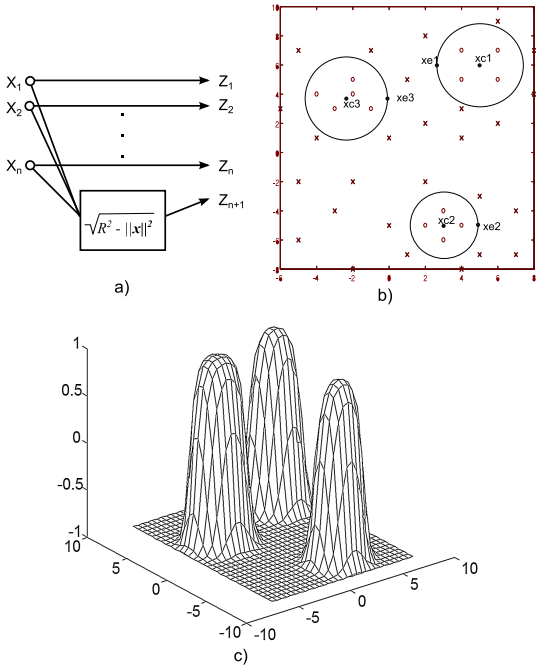

Fig. 5. Replacing normalization process with transformation to a hypersphere; (a) transformation by adding one more dimension (b) input 2-dim space (c) output of the system

These networks are very simple, but for proper operation input patterns must be normalized in a similar way like in Kohonen networks. Unfortunately such a normalization process significantly distorts input patterns, and, for example, after normalization initially easily separable clusters can be fused into one cluster. To avoid this drawback it is possible to replace the normalization process with projection patterns on a sphere in higher dimensions. This way patterns which were not linearly separable can now be separate with a single neuron. Our early results with transformation to a hypersphere of N+1 dimensions shows very encouraging results (see Fig. 5). Notice that this way the RBF networks can be replaced with traditional feed forward networks with sigmoidal activation function.

2.5 SVM – Support Vector Machines

Support Vector Machines [19,20] is a very powerful tool for finding a successful solution of many classification problems. In this technology in order to separate clusters, the number of patterns in the analysis can be significantly reduced. Instead of using all patterns, only patterns closest to the separation surface are used. These patterns are known as support vectors. Various nonlinear functions (kernels) can be used to create the separation surface. The most popular kernels

are polynomials, or Gaussian functions, similar to the one used in RBF networks. SVM is a very powerful and efficient technique, but it cannot be directly applied for multiple dimensional nonlinear mapping. For example, if the surface should be defined by a training pattern, it is not a trivial task to select support vectors and ignore other patterns. In other words most of the training patterns have to be used in the surface definition, and the main advantage of SVM can be lost.

Support Vector Machines [19,20] are capable of creating very complex nonlinear surfaces for separation patterns of two categories. It would be interesting to use SVM technology to create arbitrarily nonlinear mapping, but the solution is not obvious. The main strength of SVM is that for creation of separation surfaces only selected patterns (close to the surface) are used (Support Vectors). This significantly reduces the difficulties of the problem. A similar approach can be used but:

1. Instead of neglecting the majority of patterns, some type of pattern clustering technique can be used in order to create Support Vectors.
2. Instead of creating a separation surface between two groups of patterns, one may try to pass the surface through training patterns. However, in this case, a different importance (weight) has to be assigned to every pattern, so a reasonable compromise can be reached.
3. Initially all patterns are used in training and then in subsequent iterations patterns with large distance to the surface may need smaller weights of they can be eliminated.

2.6 Deep Neural Network Architectures

Recently, there is an emerging interest in deep neural networks [21,22], which consist of multiple hidden layers connected in the MLP architecture. These deep architectures are attractive because they provide a significantly larger computing power than shallow neural networks. It seems that deep neural networks are good candidates for modeling of complex multidimentional nonlinear systems, but the training process of these networks is very difficult [30]. This is because with an increase of the network depth the network became less transparent for training.

Because of their deepness and multiple hidden layers, these types of neural networks are very powerful [21,22], but for the same reason it is very difficult to train them [30]. Therefore, it is difficult to take advantage of their power. As one can see in Fig. 6 (dashed lines), when the number of hidden layers in the MLP architecture increases, initially the success rate increases. Then with a farther increase of the number of hidden layers, the success rate decreases, and for more than 6 hidden layers, the success rate is close to zero. When additional connections across the layers were introduced, the bridged BMLP (Bridged MLP) network becomes even more powerful, and it was much easier to train it (solid lines). Actually the success rate continuously increased with the network depth. This is a very exciting result because it gives us abilities to use and to train very powerful deep architectures of neural networks. Of course we can take advantage of these BMLP architectures only when proper learning software is used, which is capable of training arbitrarily connected feed-forward neural networks.

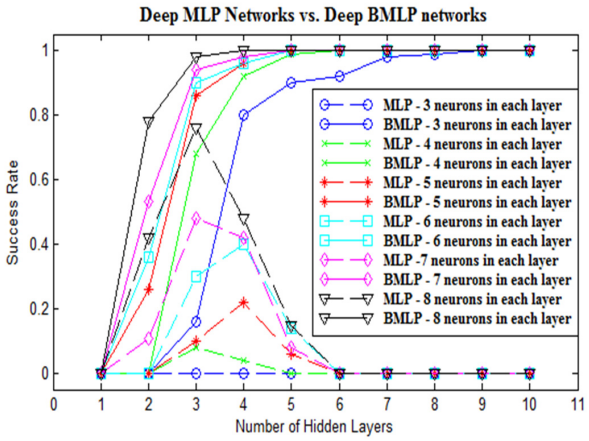

Fig. 6. Success rates comparison for training the two-spiral patterns, using different number of hidden layers (from 1 to 10). For each network, all the hidden layers consist of the same number of neurons (from 3 to 8).

3 Limitations of Neural Networks and Training Algorithms

The two-spiral problem is considered to be a good benchmark of training algorithms [31]. To solve this problem the MLP architecture with one hidden layer needs 34 neurons [3], while with the FCC architecture, only 6 neurons can be required (Fig. 7). Table 1 presents the training results of the two-spiral problem using a different number of neurons in the FCC networks. Results presented in Table 1 were obtained with the following parameters. For the EBP algorithm the learning constant is 0.005 (largest to avoiding oscillation), and the momentum is 0.5; maximum iteration is 1,000,000 for the EBP algorithm and 1,000 for the NBN algorithm; desired error= 0.01; all neurons are in the FCC networks; there are 100 trials for each case. The NBN algorithm can solve the two-spiral problem using 6 neurons (33 weights) in nearly 315 iterations. The EBP algorithm can solve the two-spiral problem only when larger networks are used. When the number of neurons is increased to 12 (102 weights), the EBP algorithm can solve it in about 400,000 iterations. One can conclude that the EBP algorithm is only successful if an excessive number of neurons are used.

Recently it was found that there are significantly more powerful neural networks than popular MLP architecture. Also, it was concluded that the most powerful known LM algorithm [9] for neural network training is not able to train no other than MLP architectures. Therefore, using the NSF support, a new very efficient NBN (neuron-by-neuron) algorithm for training arbitrarily connected neural

Table 1. Training results of two-spiral problem

Neurons	Success Rate		Average Iteration		Average Time (s)	
	EBP	NBN	EBP	NBN	EBP	NBN
6	0%	0.4%	failed	314.8	failed	1.11
7	0%	2%	failed	372.5	failed	2.12
8	0%	13%	failed	287.7	failed	0.88
9	0%	24%	failed	261.4	failed	0.98
10	0%	40%	failed	243.9	failed	1.57
11	0%	69%	failed	231.8	failed	1.62
12	63%	80%	410,254	175.1	633.91	1.70
13	85%	89%	335,531	159.7	620.30	2.09
14	92%	92%	266,237	137.3	605.32	2.40
15	96%	96%	216,064	127.7	601.08	2.89
16	98%	99%	194,041	112.0	585.74	3.82

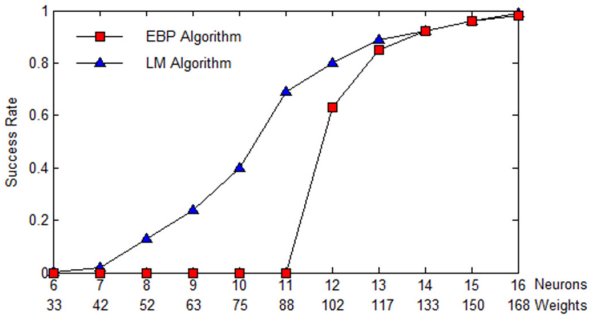

Fig. 7. Best results of two-spiral problem in 100 trails: (a) 8 neurons in FCC network (52 weights), using NBN algorithm and training time=0.82 s; (b) 12 neurons in FCC network (102 weights), using EBP algorithm and training time=694.32 s.

networks was developed [4,32]. This is a second order algorithm. The NBN algorithm is not only very fast, but it can handle arbitrarily connected neural networks. More recently this NBN algorithm was improved. Notice that the LM algorithm and the first version of the NBN algorithm were able to handle relatively small problems. The size of the problem was limited because of the size of Jacobian matrix, which is proportional to the number of patterns, and would be prohibitively large to be handled by modern computers. Following the NSF sponsored research, we have developed a modified version of NBN algorithm which can handle practically unlimited number of patterns [4]. Further improvement of the algorithm was done by elimination of the backpropagation process [33], so computation is done in a single forward pass. In many cases (multiple outputs) the algorithm is even faster than the LM algorithm. It can train feed-forward networks, which are impossible to train with other popular algorithms.

Neural networks exhibit superior performance in comparison to other methods of computational intelligence, but there are several reasons for the frustration of researchers trying to adapt neural networks for their research:

- Because it is easier to train neural networks if a larger than required number of neurons is used, researchers have a tendency to use an excessive number of neurons.
- If an excessive number of neurons are used, neural networks can be easily overtrained. This way the network is losing its ability for generalization, and it is not able to correctly process new patterns which were not used for training. This is especially visible if the number of training patterns is limited.
- In most cases the relatively inefficient MLP architecture is used instead of the more powerful topologies with connections across layers. As a result, the full power of neural networks is not utilized.
- In order to find solutions for close to optimal architectures, second order algorithms such as the NBN or the LM should be used. Unfortunately, the LM algorithm adopted in the popular MATLAB NN Toolbox [34] can handle only the MLP topology without connections across layers, and these topologies are far from optimal.
- Another drawback of the LM algorithm is that it cannot handle a large number of training patterns because the size of the Jacobian matrix may become too excessive.
- The newly developed NBN algorithm is very fast; it can train any neural network architecture, and it has no limitations for the number of patterns used in training. An additional feature of this algorithm is that individual patterns can be added or subtracted from the training set without the necessity of training the network with an entire set of patterns.

The only current limitation of the NBN algorithm [4,33] is that neural networks should not be too big, and it practically can train networks with up to 500 weights (size of Hessian matrix). If powerful neural network architectures are used, such as FCC, then with these 500 weights very complex nonlinear problems can be solved. In the case of RBF networks [35] newly developed ErrCor algorithm [36] based on the concept of NBN algorithm [4] also shows a significant advantages to other algorithms (Fig. 8). The ErrCor algorithm allows for an automatic finding of best locations of centers of hidden units, while an improved second order (ISO) algorithm [37] significantly improves the training process of RBF networks [36]. One should keep in mind that also RBF networks need to be designed as compact as possible to secure its generalization abilities.

4 DNN – Dual Neural Networks

We have completed extensive experimental studies of training various neural network architectures with different problems [30]. For example, we have trained various neural network architectures for the parity-11 problem, and we have

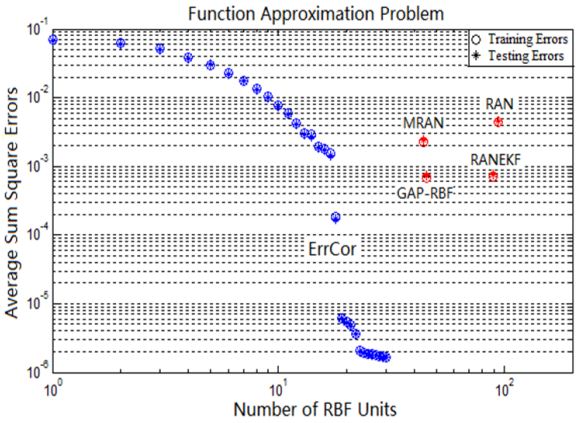

Fig. 8. Training results of ErrCor algorithm (blue points), comparing with other four algorithms (red points)

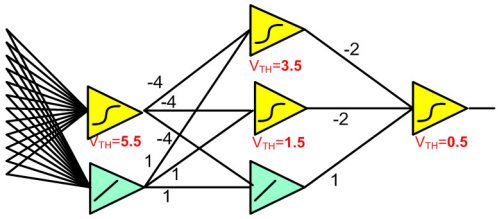

Fig. 9. Smallest MLP dual architecture (with one linear neuron in each layer), which was possible to train with the parity-11 problem

concluded that the smallest possible MLP architecture with traditional sigmoidal neurons, which we were able to successfully train, was an 11–5–5–1 architecture with 11 neurons total, shown in Fig. 9. However, if in each hidden layer we replaced the traditional sigmoidal activation function with a linear one, then we were able to train to the parity-11 problem as a small network as is shown in Fig. 10. This was a very surprising result for us. Further analysis of the trained network allowed us to find an analytical solution for this network. Values of all weights and neuron thresholds for this analytical solution are shown in Fig. 10. There is no reason to add more than one neuron to each hidden layer because two linear neurons connected in parallel can always be combined into one neuron. One may notice that such dual networks combining both neurons with linear and nonlinear activation functions are not only very powerful, but they are also easy to train.

It is possible to significantly enhance the power of neural networks by using better architectures [1,32]. It was shown that the power of neural networks is

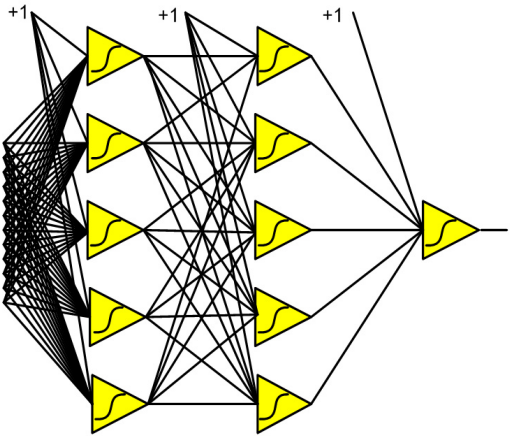

Fig. 10. Smallest MLP architecture with sigmoidal activation functions only, which was possible to train with the parity-11 problem

increasing almost exponentially with an increase of its depth (increase of the number of hidden layers). The strength of a neural network also grows with the increase of the network width (more neurons in each of hidden layer). However, the network capabilities in this case are increasing only proportionally to the network width. A good illustration of this is shown in Fig. 4 where the SLP has only one layer and the network grows wide, while the FCC network has only one neuron in each layer, and the depth of the network increases with an increase of the number on the hidden layer. Notice that with $n = 13$ neurons (12 neurons in the hidden layer and one output neuron) the SLP is capable to solve the parity-12 problem ($N = n-1$). In the case of the FCC with 13 neurons there are 12 hidden neurons/layers, and the largest parity problem is parity-8191 ($N = 2n - 1$) , where n is the number of neurons in the network.

There is no surprise that there is now a significant interest in deep neural network architectures. The problem is that the popular MLP architecture with many hidden layers is very difficult to train. One can see in Fig. 6 that if there are more than 6 hidden layers the success rate of training MLP networks becomes close to zero. This is not the case if hidden layers are bridged with connections across layers. Such bridged networks (BMLP) are much easier to train. As one can see in Fig. 6 an increase of the network depth has no negative effect on the success rate.

In order to better understand the success in training BMLP architectures let us consider a couple of transformations of BMLP into another networks. Fig. 11(a) shows FCC architecture for the parity-15 problems. The FCC network can be seen as the most advanced BMLP architecture where there are mutual connections between all neurons. Fig. 11(b) shows architecture where connections across layers were replaced with interlaced linear layers. With the

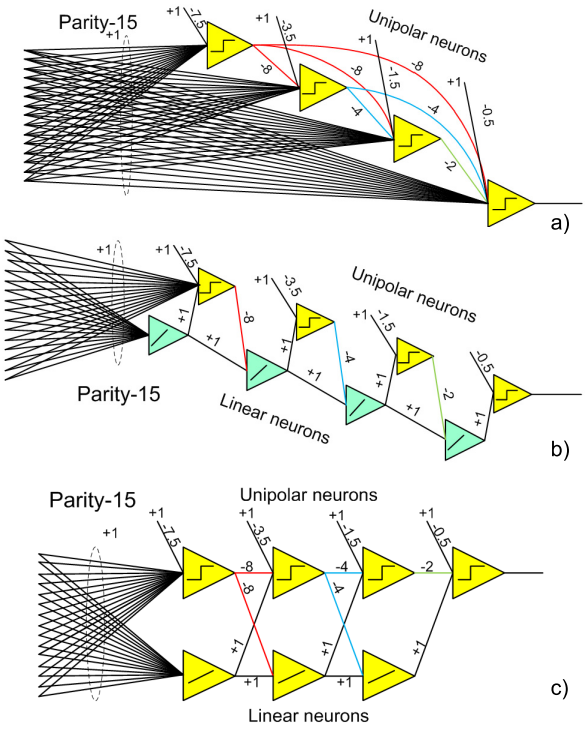

Fig. 11. Three different topologies capable of solving the parity-15 problem: (a) FCC Fully Connected Cascade, (b) with interlaced layers, and (c) DNN dual neural network.

next transformation step (Fig. 11(c)), the network can be converted into dual network architectures, where additional linear elements (neurons or summators) were added to each layer.

We already know that the NBN training algorithm can handle relatively efficiently dual networks, but it seems that further improvements are possible:

1. Because part of the network has a linear character, it should be possible to take advantage of this fact. Notice that linear networks can be trained in a single step. It would be nice if we would be able to at least partially decouple linear and nonlinear portions of the networks and use separate algorithms to train them. Another approach would be to focus solely on the nonlinear part of the network and search only for weight of the nonlinear network while weights in the linear network can be automatically adjusted in a single step using, for example, multidimensional linear regression.
2. Another possible improvement would be to take advantage of a specific feature of the NBN algorithm where training patterns are directly being added to Hessian. This should allow us to form at first a Hessian with patterns which produce small errors. Let us call it a reference Hessian, and then we

can add only patterns with errors to the reference Hessian. In order to force the system to fully recognize patterns with errors, we may add to the Hessian multiple times poorly matched patterns forcing the system to recognize these difficult to train patterns.

5 Conclusion

The traditional approach of solving complex problems and processes usually follows the following steps: at first we are trying to understand the problem under investigation and then describe it by mathematical equations. The issue is that in the computer age we are already being overwhelmed with a huge amount of data, which are very difficult to understand and process by humans. Also there are environmental and often engineering problems, which cannot be described by equations. Our approach will allow us to solve complex multidimensional nonlinear problems without the necessity of fully understanding them and the necessity of finding mathematical formulas. The proposed approach takes a different path: at first we create very complex artificial system trainable weights, and then the system is trained for our need. This approach relieves us, as humans, from a full understanding of the problem under investigation, but still the problem can be solved. Successful completion of the project may have a significant impact on our civilization because it will allow us to solve many practical problems, which we have difficulties to understand. One of many examples would be the elimination of many sensors in control systems. By measuring easy accessible values and using our nonlinear systems capable to estimate values, which could be measured by non existing sensors.

References

1. Wilamowski, B.M.: Neural Network Architectures and Learning algorithms – How Not to Be Frustrated with Neural Networks. IEEE Industrial Electronics Magazine 3(4), 56–63 (2009) (best paper award)
2. Hecht-Nielsen, R.: Theory of the Back Propagation Neural Network. In: Proc. 1989 IEEE IJCNN, pp. 1593–1605. IEEE Press, New York (1989)
3. Peng, J., Li, K., Irwin, G.W.: A New Jacobian Matrix for Optimal Learning of Single-Layer Neural Networks. IEEE Trans. on Neural Networks 19(1), 119–129 (2008)
4. Wilamowski, B.M., Yu, H.: Improved Computation for Levenberg Marquardt Training. IEEE Trans. on Neural Networks 21(6), 930–937 (2010)
5. Wilamowski, B.M., Hunter, D., Malinowski, A.: Solving parity-N problems with feedforward neural networks. In: Proc. 2003 IEEE IJCNN, pp. 2546–2551. IEEE Press (2003)
6. Wilamowski, B.M., Yu, H., Chung, K.T.: Parity-N Problems as a Vehicle to Compare Efficiency of Neural Network Architectures. In: Industrial Electronics Handbook, 2nd edn. Intelligent Systems, vol. 5, ch. 10, pp. 10-1–10-8. CRC Press (2011)
7. Rumelhart, D.E., Hinton, G.E., Williams, R.J.: Learning representations by back-propagating errors. Nature 323, 533–536 (1986)

8. Levenberg, K.: A method for the solution of certain problems in least squares. Quarterly of Applied Mathematics 2(2), 164–168 (1944)
9. Hagan, M.T., Menhaj, M.B.: Training feedforward networks with the Marquardt algorithm. IEEE Trans. on Neural Networks 5(6), 989–993 (1994)
10. Zadeh, L.A.: Fuzzy Sets. Information and Control 8, 338–353 (1965)
11. Mamdani, E.H.: Application of Fuzzy Algorithms for Control of Simple Dynamic Plant. IEEE Proceedings 121(12), 1585–1588 (1974)
12. Sugeno, M., Kang, G.T.: Structure Identification of Fuzzy Model. Fuzzy Sets and Systems 28(1), 15–33 (1988)
13. Roger, J.S., Sun, C.T.: Functional Equivalence Between Radial Basis Function Networks and Fuzzy Inference Systems. IEEE Trans. on Neural Networks 4(1), 156–159 (1993)
14. Jin, Y., Sendhoff, B.: Extracting Interpretable Fuzzy Rules from RBF Networks. Neural Process. Lett. 17(2), 149–164 (2003)
15. Li, W., Hori, Y.: An Algorithm for Extracting Fuzzy Rules Based on RBF Neural Network. IEEE Trans. on Industrial Electronics 53(4) (August 2006)
16. Moody, J., Darken, C.J.: Learning with Localized Receptive Fields. In: Touretzky, D., Hinton, G., Sejnowski, T. (eds.) Proc. 1988 Connectionist Models Summer School, Carnegie Mellon University. Morgan Kaufmann Publishers (1988)
17. Hecht-Nielsen, R.: Counterpropagation networks. Applied Optics 26(23), 4979–4984 (1987)
18. Pao, Y.H.: Adaptive Pattern Recognition and Neural Networks. Addison-Wesley Publishing Co., Reading (1989)
19. Vapnik, V.N.: The Nature of Statistical Learning Theory. Springer (1995)
20. Sch´olkopf, B., Burges, C.J.C., Smola, A.J. (eds.): Advances in Kernel Methods: Support Vector Learning. MIT Press, Cambridge (1999)
21. Arel, I., Rose, D.C., Karnowski, T.P.: Deep Machine Learning – A New Frontier in Artificial Intelligence Research. IEEE Computational Intelligence Magazine 5(4), 13–18 (2010)
22. Chen, K., Salman, A.: Learning Speaker-Specific Characteristics with a Deep Neural Architecture. IEEE Trans. on Neural Networks 22(11), 1744–1756 (2011)
23. Binfet, J., Wilamowski, B.: Microprocessor Implementation of Fuzzy Systems and Neural Networks. In: International Joint Conference on Neural Networks (IJCNN 2001), Washington, DC, pp. 234–239 (2001)
24. Xie, T., Yu, H., Wilamowski, B.: Replacing fuzzy systems with neural networks. In: HSI 2010, May 13-15, pp. 189–193 (2010)
25. Rutkowska, D., Hayashi, Y.: Neuro-fuzzy systems approaches. International Journal of Advanced Computational Intelligence 3(3), 177–185 (1999)
26. Yu, H., Xie, T., Wilamowski, B.M.: Neuro-Fuzzy System. In: Industrial Electronics Handbook, 2nd edn. Intelligent Systems, vol. 5, ch. 20, pp. 20-1–20-9. CRC Press (2011)
27. Cover, T.M.: Geometrical and Statistical Properties of Systems of Linear Inequalities with Applications in Pattern Recognition. IEEE Trans. on Electronic Computers EC–14, 326–334 (1965)
28. Wilamowski, B.M., Jaeger, R.C.: Implementation of RBF Networks by Feedforward Sigmoidal Neural Networks. In: Dagli, C.H., et al. (eds.) Intelligent Engineering Systems Through Artificial Neural Networks, New York, vol. 7, pp. 183–188 (1997)
29. Park, J., Sandberg, I.W.: Universal Approximation Using Radial-Basis-Function Networks. Neural Computation 3(2), 246–257 (1991)

30. Hunter, D., Yu, H., Pukish, M.S., Kolbusz, J., Wilamowski, B.M.: Selection of Proper Neural Network Sizes and Architectures - Comparative Study. IEEE Trans. on Industrial Informatics 8, 228–240 (2012)
31. Alvarez-Sanchez, J.R.: Injecting knowledge into the solution of the two-spiral problem. Neural Computing and Applications 8, 265–272 (1999)
32. Wilamowski, B.M., Cotton, N.J., Kaynak, O., Dundar, G.: Computing Gradient Vector and Jacobian Matrix in Arbitrarily Connected Neural Networks. IEEE Trans. on Industrial Electronics 55(10), 3784–3790 (2008)
33. Wilamowski, B.M., Yu, H.: Neural Network Learning without Backpropgation. IEEE Trans. on Neural Networks 21(11), 1793–1803 (2010)
34. Demuth, H.B., Beale, M.: Neural Network Toolbox: for use with MATLAB: Mathworks Natick, MA, USA (2000)
35. Yu, H., Xie, T., Paszczynski, S., Wilamowski, B.M.: Advantages of Radial Basis Function Networks for Dynamic System Design. IEEE Trans. on Industrial Electronics 58(12), 5438–5450 (2011)
36. Yu, H., Reiner, P.D., Xie, T., Bartczak, T., Wilamowski, B.M.: An Incremental Design of Radial Basis Function Networks. IEEE Trans. on Neural Networks and Learning Systems 25 (2014)
37. Xie, T., Yu, H., Hewlett, J., Rozycki, P., Wilamowski, B.M.: Fast and Efficient Second-Order Method for Training Radial Basis Function Networks. IEEE Trans. on Neural Networks and Learning Systems 23(4), 609–619 (2012)

A Greedy Incremental Algorithm for Universal Approximation with RBF Newtorks

Xing Wu and Bogdan M. Wilamowski

Department of Electrical and Computer Engineering
Auburn University, Alabama, USA
{xzw0015,wilambm}@tigermail.auburn.edu

Abstract. Radial basis function(RBF) networks have been proved to be a universal approximator when enough hidden nodes are given and proper parameters are selected. Conventional algorithms for RBF networks training, including two-stage methods and gradient-based algorithms, cost much computation and have difficulty to determine the network size. In this paper, a new greedy incremental(GI) algorithm is proposed which constructs the RBF network by adding hidden node one by one; Each added hidden node is trained once and then fixed. The parameters of each added hidden node are trained in a greedy way to approximate the local area around the pattern with the biggest error magnitude. The center and weight are determined by local regression, the width is tuned iteratively with a simple rule. The proposed greedy incremental algorithm is tested on some practical experiments and compared with other popular algorithms. The experiments results illustrated the GI algorithm could approximate the function universally with high efficiency and robustness.

Keywords: radial basis function networks, constructive learning, greedy incremental algorithm.

1 Introduction

Because of the simple topology structure and the ability to approximate complex nonlinear mappings from the input-output data, radial basis function(RBF) network was broadly used in classification and function approximation area [1,2,3]. It has been proved to be a universal approximator for any continuous target function when sufficient hidden nodes are provided [4]. As analyzed and compared with other neural networks and fuzzy systems, RBF networks have better generalization ability and tolerance to input noiseand perform better in regular function approximation [5,6]. Based on these properties and the simple topology structure, RBF networks are widely applied for solving various industrial application problems, such as fault diagnosis [7,8] and image processing [9,10].

A typical RBF network consists of a hidden layer with non-linear RBF activation function and a linear output layer (Fig. 1). Adjustable parameters of RBF networks include hidden layer parameters (centers and widths) and output weights connecting hidden layer and output layer.

J. Fodor and R. Fullér (eds.), *Advances in Soft Computing, Intelligent Robotics and Control,* Topics in Intelligent Engineering and Informatics 8,
DOI: 10.1007/978-3-319-05945-7_9,

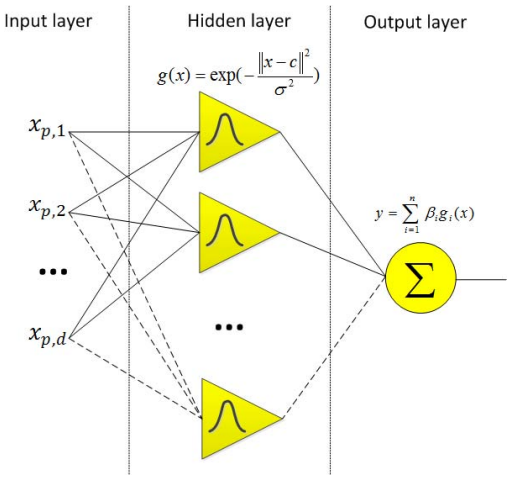

Fig. 1. Architecture of RBF network

Original approach for training RBF networks is to take all the training samples as centers and preset the width of all the hidden nodes. Only the output weights are trained with least squares regression or gradient-based methods. However, this algorithm could lead to overfitting and is also not practical for real world approximation problems. In order to achieve high accuracy with compact RBF networks, centers and widths are further selected or adjusted with different algorithms. Moody and Darken [2] used unsupervised self-organized selection to determine the centers and widths. Support vector machines [11] selected support vectors from training sets as centers. However, the search space is too restricted since the widths are fixed and centers are subset of the discrete training samples.

Alternative method is to train all the parameters simultaneously. Some gradient based optimization algorithms were proposed for RBF networks training [12,13]. To improve the slow convergence rate of first order gradient, recently, T. Xie et al. presented an improved second order(ISO) algorithm [15] based on an improved Levenber-Marquardt algorithm [14]. Though more compact network is reached with this algorithm, it costs more time due to expensive gradient computation.

While most algorithms have to specify the size of the RBF network before training, it is difficult to determine the network size. To determine the network size during training, some constructive algorithms were proposed by adding hidden node one by one, or batch by batch. T.-Y. Kwok and D.-Y. Yeung trained each added hidden node with modified Quickprop algorithm by minimizing some objective functions [21]. Huang et al. proposed a family of extreme learning machines (ELM) by adding random hidden nodes and training weight only. The algorithms were shown to be much faster than other general algorithms. However, much larger network was achieved with these ELMs.

In this paper, a new greedy incremental (GI) algorithm is proposed to construct the RBF network by adding hidden nodes one by one. Each added hidden node is trained once and then fixed. The parameters of each added hidden node are trained in a greedy way to approximate the local area around the pattern with the biggest error magnitude. The center and weight are determined by local regression; the width is tuned iteratively with a simple rule. The proposed algorithm is very simple and can construct a compact RBF network for approximation speedily.

The paper is organized as following. In Section 2, computation fundamentals of RBF networks are briefly introduced. Section 3 presents the proposed GI algorithm for the RBF networks training. Section 4 gives several practical benchmarks for function approximation. Experiment results are compared with other popular algorithms. In section 5, a brief conclusion is given and future work is introduced.

2 Computational Fundamentals

Since an approximation problem with multiple outputs can be divided into several independent approximation task with unique output, in this paper, we are focusing on the function approximation with single output. Before describing the algorithm details, several common indices and notations are introduced. Assume the algorithms discussed in this paper are all aiming at approximating a training set $\{(\mathbf{x}_p, y_p) \mid \mathbf{x}_p \in R^D, y_p \in R, p = 1, 2, \ldots, P\}$, where there are P training patterns with D-dimension input and scalar output, $(\mathbf{x}_p, y_p)$ denote the p_{th} input and output.

As shown in figure 1, a conventional RBF network has fixed architecture with three layers: an input layer, a hidden layer with RBF activation function and a linear output layer. Activation function of RBF networks can be different radial basis functions, including multiquadric, inverse quadratic function, etc. In this paper, we used the popular gaussian function as activation function of the RBF network.

$$g(x) = \exp\left(-\frac{\|\mathbf{x} - \mathbf{c}\|^2}{\sigma^2}\right), \qquad \mathbf{x}, \mathbf{c} \in R^D, \sigma \in R^+ \tag{1}$$

in which, $\|\cdot\|$ represents Euclidean distance, $\mathbf{c}, \sigma$ are center and width of the RBF node.

The output of the RBF network is calculated by summing multiplication of hidden layer and output weights. The output of a RBF network with n hidden nodes can be described as,

$$y = \sum_{i=1}^{n} \beta_i g_i(\mathbf{x}) \tag{2}$$

in which, β_i is the weight connecting the i_{th} hidden node and the output node.

3 The Greedy Incremental Algorithm

In this section, the proposed Greedy Incremental(GI) algorithm is introduced.

3.1 Constructive algorithm

The proposed GI algorithm is a constructive algorithm for RBF network training. The constructive algorithm is a general method for a single layer feedforward network (SLFN) with any kernels. One advantage of constructive algorithms is that the network size can be determined while training. The algorithm starts from a SLFN with zero hidden neuron and constructs the SLFN by adding hidden nodes one by one. Each hidden node is trained supervised according to errors of previous SLFN and then fixed. Thus the training of whole SLFN is simplified into a sequence of single neuron training.

Assume the current SLFN has n hidden nodes, the errors of current SLFN are $\mathbf{E} = [e_1, e_2, \ldots, e_P]^T$. To approximate the errors with the new added neuron $g_{n+1}(\alpha, \mathbf{x})$, one is trying to tune its parameters α and output weight β to minimize the sum squared error(SSE).

$$S(\alpha, \beta_{n+1}) = \sum_{p=1}^{P} (e_p - \beta_{n+1} g_{n+1}(\alpha, \mathbf{x}_p))^2 \tag{3}$$

in which, $S(\cdot)$ is the SSE, α are parameters of the neurons to be tuned.

In order to minimize the objective function SSE, the neuron's parameters α and its output weight β can be optimized independently. From equation (3), one can observe that SSE is a convex function of output weight β, it achieves its minima while α is fixed and,

$$\beta_{n+1} = \frac{\sum_{p=1}^{P} e_p g_{n+1}(\mathbf{x}_p)}{\sum_{p=1}^{P} g_{n+1}^2(\mathbf{x}_p)}. \tag{4}$$

For other parameters (α) tuning, T.-Y. Kwok and D.-Y. Yeung [21] proposed a modified Quickprop algorithm to minimize the objective function. However, gradient computatoin still cost much time. Huang et al. presented an incremental extreme learning machine (I-ELM) [17] which generated random parameters for the single neuron and only determined output weight using (4). Though it is very fast, the I-ELM algorithm also resulted in a very large SLFN. Taking advantage of local property of RBF node, the proposed GI algorithm tuned the new added node in a greedy way to approximate a local area around the pattern with biggest error magnitude. The parameters of the added node and the output weight are all tuned in simple method.

3.2 Center and Weight

The proposed GI algorithm is a greedy process. In order to make each added new hidden node contribute most to the network, each time the new node was attempt to approximate the local area around the pattern with biggest error magnitude. The center and weight of the new node can be determined by simple regression with the local training sets.

Filter the local sets. While approximating the previous RBF network's residual error $\mathbf{E} = [e_1, e_2, \ldots, e_P]^T$ with a single RBF node, it is not necessary to consider all the training patterns. Because of the local property of gaussian function, one only need consider a local area in the input space for the single RBF training. The GI algorithm in this paper focuses on the local area around the pattern with biggest residual error magnitude. To filter these local sets, one can preset parameters K and τ and do the following process:

1. find the pattern with biggest error magnitude $|e_k|$, note the pattern as $A(\mathbf{x}_A, e_A)$;
2. find the subset(T) of the training set, whose elements are K nearest neighbors of A.
3. In subset T, filter a subset S, whose residual errors are in the range $(\tau e_A, e_A)$.

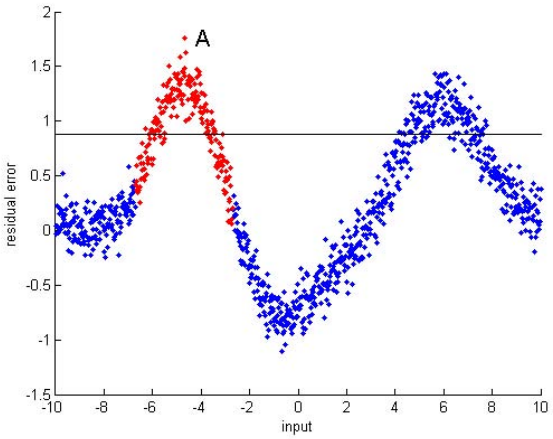

Fig. 2. A 1 dimension example of filtering the local set, $K = 200, \tau = 0.5$. (1) Find point with biggest error magitude A. (2) Filter K nearest neighbors of max point A.(red points) (3) Among red points, filter the points with residual error bigger than τe_A. (above the horizon line)

Local Regression. After above 3 steps, local set around the max point is filtered as S, assume the indices of S are $\{j_1, j_2, \ldots, j_S\}$. Using these patterns, we can determine optimal center and weight for the new node directly with local regression.

In order to approximate the previous RBF network's residual error $\mathbf{E}_S = [e_{j_1}, e_{j_2}, ..., e_{j_S}]^T$ with (1) multiplied by its output weight β_{n+1}, we are actually solving the following equations,

$$\beta_{n+1} \exp\left(-\frac{\|\mathbf{x}_p - \mathbf{c}\|^2}{\sigma^2}\right) = e_p, \qquad p = j_1, j_2, \ldots, j_S \tag{5}$$

Since the residual errors of local set S are in the range $(\tau e_A, e_A)$, which means they are with the same sign, β_{n+1} should also be the same sign. So for each pattern in the local set S, we can derive (5) as,

$$-\frac{1}{\sigma_2}\sum_{d=1}^{D} x_{p,d}^2 + \frac{2}{\sigma^2}\sum_{d=1}^{D} c_d x_{p,d} - \frac{1}{\sigma^2}\sum_{d=1}^{D} c_d^2 + \ln|\beta_{n+1}| = \ln|e_p| \tag{6}$$

in which, $x_{p,d}$ denotes the d^{th} dimension of the p^{th} pattern, c_d is the d^{th} dimension of the center $\mathbf{c}$. The equation is actually a standard linear regression format,

$$\mathbf{X}\mathbf{w} = \mathbf{b}, \tag{7}$$

in which

$$\mathbf{X} = \begin{bmatrix} \sum_{d=1}^{D} x_{j_1,d}^2 & x_{j_1,1} & x_{j_1,2} & \cdots & 1 \\ \sum_{d=1}^{D} x_{j_2,d}^2 & x_{j_2,1} & x_{j_2,2} & \cdots & 1 \\ \vdots & \vdots & \vdots & \ddots & 1 \\ \sum_{d=1}^{D} x_{j_S,d}^2 & x_{j_S,1} & x_{j_S,2} & \cdots & 1 \end{bmatrix} \tag{8}$$

$$\mathbf{w} = \left[-\frac{1}{\sigma^2},\ 2\frac{c_1}{\sigma^2},\ 2\frac{c_2}{\sigma^2},\ \ldots,\ 2\frac{c_D}{\sigma^2},\ -\frac{1}{\sigma^2}\sum_{d=1}^{D} c_d^2 + \ln|\beta| \right]^T \tag{9}$$

$$\mathbf{b} = [\ln|e_{j_1}|,\ \ln|e_{j_2}|,\ \ldots,\ \ln|e_{j_S}|]^T \tag{10}$$

For the linear regression (7), we can easily get the optimal $\mathbf{w}$,

$$\mathbf{w} = \left(\mathbf{X}^T\mathbf{X}\right)^{-1}\mathbf{X}^T\mathbf{b} \tag{11}$$

Combined with (9), we can determine all the parameters of the new hidden nodes (center $\mathbf{c}$, width σ and output weight β). However, because the above approximation only used filtered local set S, global convergence of the entire RBF network is not guaranteed. On the other hand, for a gaussian function, parameters determining peak location (center and height) are local parameters while the width is more related to its global character. So the proposed GI algorithm used the center $\mathbf{c}$ and output weight β from above computation and tunes the width in another simple rule.

3.3 Width

As center and weight are determined by local regression, width of the added hidden node is also necessary to be tuned. As presented by N. Benoudjit et al. [22], widths play an important role in the RBF networks approximation. The fast extreme learning machine was also shown to be improved significantly by

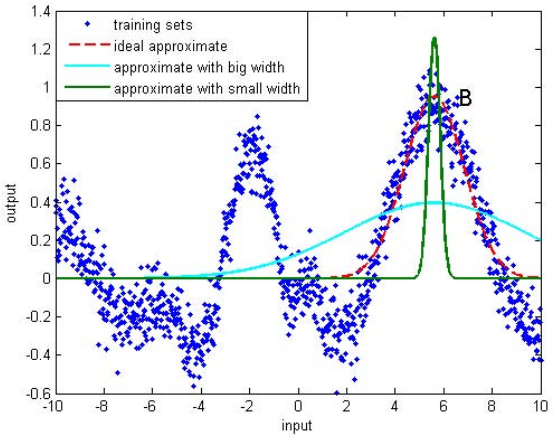

Fig. 3. Approximation result comparison of a 1-dimension example while using different width. With the optimal center determined in previous section, all the three cases use (4) to determine output weight. The red line used the ideal width; the green line selected a small width; the cyan line picked a big width.

tuning width [20]. The proposed GI algorithm tunes the width of the new added RBF node using an efficient iterative rule.

As mentioned in section 3.1, output weight is quite easy to determine by (4) once center and width are fixed. Since sum squared error (SSE) shown in (3) is a convex function of weight (β_{n+1}), the optimal weight can also guarantee SSE to be decreasing while adding more hidden nodes. That means, formula (4) could guarantee the constructive algorithm's global convergence. However, given a bad width, approximation result is still far from optimal. Fig. 3 shows a 1-dimension example.

From the figure, one can observe that the optimal approximation results from a proper width which makes the weight calculated by (4) match the optimal weight we get by local regression (point B in the figure). Though the three cases' approximation results look very different, the area under them are similar. In fact, to minimize SSE, a thinner gaussian with a bigger height would always be better than a thinner gaussian with a smaller height; a fatter gaussian with a smaller height would always be better than the one with a bigger height. So the proposed GI algorithm approaches a start width to optimal by equaling its area to the new gaussian with a new width and our optimal weight.

Lemma 1. *The area or integration of a D-dimension gaussian function with width σ, output weight β is,*

$$\text{Area} = \sqrt{\pi^D}\beta\sigma^D \tag{12}$$

Assume in previous section, we get the optimal center $\mathbf{c}_{\text{opt}}$ and weight β_{opt}. Given the width in the t^{th} iteration σ_t, the weight calculated from (4)

using σ_t notes as β_t, for the $(t+1)^{\text{th}}$ iteration, we equal the new gaussian's area whose $\{\text{width}, \text{weight}\} = \{\sigma_{t+1}, \beta_{\text{opt}}\}$ to the old gaussian's area whose $\{\text{width}, \text{weight}\} = \{\sigma_t, \beta_t\}$,

$$\sqrt{\pi^D}\beta_{\text{opt}}\sigma_{t+1}^D = \sqrt{\pi^D}\beta_t\sigma_t^D \tag{13}$$

from which, we can get the update rule of width,

$$\sigma_{t+1} = \sqrt[D]{\frac{\beta_t}{\beta_{\text{opt}}}}\sigma_t \tag{14}$$

While updating width of the added RBF node with (4) (14), it is approaching to the optimal one.

3.4 Pseudo Code

Since all the parameters (center, width, weight) are trained in simple process, the proposed GI algorithm could approximate functions very efficiently. The pseudo code of the whole training process can be seen below.

```
Given a D-dimension training set with P patterns {X,Y}.
Desired error is d, maximum number of RBF nodes is N.
Initialize n = 0.

while n<N and SSE>d
     1. n = n + 1
     2. pick max point A
     3. filter local set around A as S
     4. use points in S following (7)-(11) do regression, get
         optimal center(c) and weight(ww)
     5. fix center as c, initialize width as sgm0, calculate new
         weight ww0 with (4), set a threshold th
         while |ww0-ww|>th
               (1) update new width sgm1 with (14)
               (2) use sgm1 to calculate weight ww1 with (4)
               (3) sgm0 = sgm1
               (4) ww0 = ww1
         endwhile     // optimal width is sgm0
     6. calculate output y of the new RBF node
          (center=c, width=sgm0, weight=ww)
     7. update error: err = err - y, calculate SSE
endwhile
```

4 Experiments

In this section, several highly nonlinear functions with noise are given to test the efficiency of the proposed GI algorithm. The experiments results are compared

with other popular RBF algorithms, including support vector regression (SVR) [11], extreme learning machines (ELM) [17,18,19].

The testing environment consists of: Windows 7 Enterprise 64-bit operating system, Intel® Core™ 2 Quad CPU Q8400 2.67GHz processor, 4.00GB RAM, MATLAB R2012a platform.

4.1 Peaks Function

Peaks function is a popular 2-dimension nonlinear benchmark for approximation test. In this paper, we used normalized format of peaks function (15). Fig. 4 shows the mesh plot of the peaks function.

$$\begin{aligned} z =& (0.3 + 1.8x + 2.7x^2)\exp(-1 - 6y - 9x^2 - 9y^2) - \\ & (0.6x - 27x^3 - 243y^5)\exp(-9x^2 - 9y^2) - \\ & \frac{1}{30}\exp(-1 - 6x - 9x^2 - 9y^2) \end{aligned} \tag{15}$$

In the experiment, 2000 points were generated randomly in the range $[-1, 1]$ as training sets and another 1000 points generated in the same way as testing sets. All the patterns were added a guassian noise with variance Var = 0.01. The RBF network was trained with the given training set by the GI algorithm and some other popular RBF algorithms, including extreme learning machines (ELM) and support vector machine (SVM) for regression.

For the proposed GI algorithm, we set parameters $K = 200$, $\tau = 0.5$ for filtering local set, threshold $th = 0.01$ for width tuning. We used four versions of extreme learning machines: batch Extreme Learning Machine (ELM) [16] and try different architecture, Incremental Extreme Learning Machine (I-ELM)

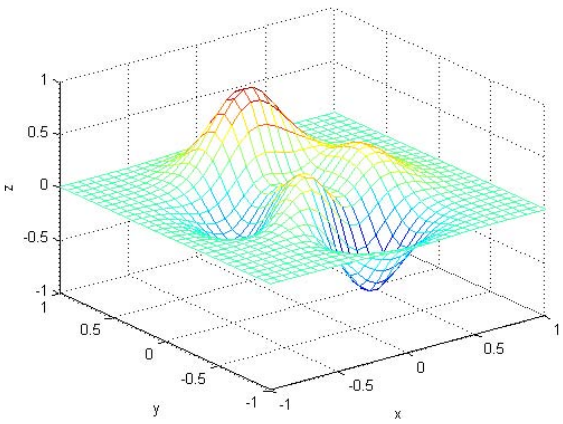

Fig. 4. Peaks function

Table 1. Comparison of RBF algorithms while approximating peaks function

Algorithm	GI	ELM	I-ELM	EI-ELM	CI-ELM	SVR
training error (RMSE)	0.114	0.1117	0.1966	0.1916	0.1963	0.1142
testing error (RMSE)	0.109	0.1089	0.1912	0.2116	0.1908	0.1107
training time (s)	0.0622	0.801	0.094	0.9206	0.1205	193.7296
# hidden nodes	10	48	200	200	200	764

[17], Enhanced Incremental Extreme Learning Machine (EI-ELM) [18], Convex Incremental Extreme Learning Machine (CI-ELM) [19]. All the ELMs used RBF kernel with following format,

$$g(x) = \exp(-\lambda \|\mathbf{x} - \mathbf{c}\|^2), \qquad \mathbf{x}, \mathbf{c} \in R^D, \lambda \in R^+ \tag{16}$$

in which, λ is called impact factor. All the ELMs generated random centers in the range $[-1, 1]$, random impact factors in the range $(0, 0.5]$. For batch ELM, we added hidden node one by one from zero and each time did the pseudo inverse. The EI-ELM algorithm used parameter $k = 20$.

The paper used LIBSVM [26] to train support vector machine for peaks approximation. Parameters of SVR (penalty C, impact factor γ) are grid searched where $C \in \{1, 10, 100, 1000\}$, $\gamma \in \{0.001, 0.01, 0.1, 1\}$. The optimal option was $C = 1000$, $\gamma = 1$, whose result was shown in Table 1. From the comparison table, one can see that the proposed GI algorithm worked very efficient to construct a compact RBF network.

4.2 Control Robot Arm Kinematics

The kinematics problem is a classic industrial application of function approximation [27]. The purpose of this problem is to simulate the movement of robot's end effectors and locate the position when joint angles change. Fig. 5 shows a 2-link planar manipulator.

From the figure, one can calculate the coordinates of the end effector by the following formula,

$$x = L_1 cos(\alpha) + L_2 cos(\alpha + \beta) \tag{17}$$

$$y = L_1 sin(\alpha) + L_2 sin(\alpha + \beta) \tag{18}$$

In this paper, we fix the two arm lengths (L_1, L_2) to be 1 and just give the approximation of the x-coordinate. The y-coordinate can be approximated in a same way. The surface of x-coordinate is shown in fig. 6.

We generated 40×40 points uniformly in the range $[-\pi, \pi]$ as training set. Another 1000 points were generated randomly in the same range for testing. Both training and testing sets were added white gaussian noise with variance Var = 0.01. All the algorithms were used in a similar setting to construct an RBF network for the approximation task. The comparison results are shown in Table 2. This experiment also illustrated the efficiency of the proposed GI algorithm.

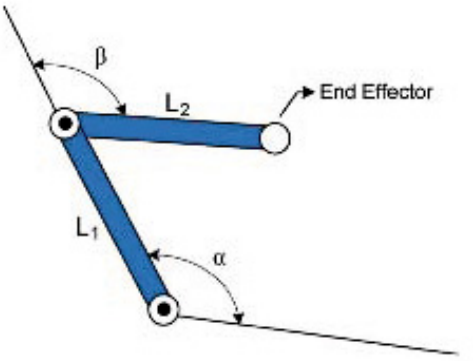

Fig. 5. The 2-link planar manipulator

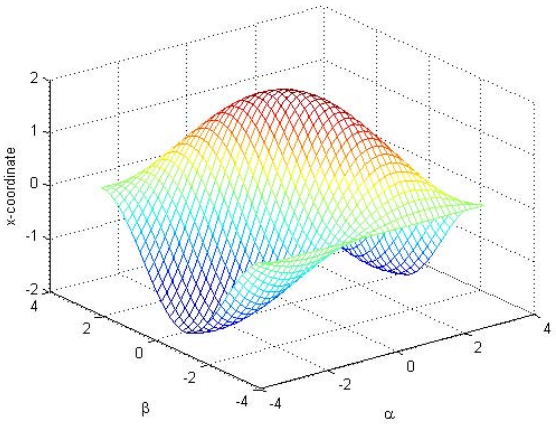

Fig. 6. Mesh plot of x-coordinate versus the two angles α and β

Table 2. Comparison of RBF algorithms while solving kinematics problem

Algorithm	GI	ELM	I-ELM	EI-ELM	CI-ELM	SVR
training error (RMSE)	0.2152	0.1245	0.4925	0.3065	0.5537	0.0796
testing error (RMSE)	0.2074	0.1275	0.4883	0.9984	0.5516	0.1233
training time (s)	0.1581	0.3141	0.1035	0.7888	0.1035	498.0173
# hidden nodes	6	33	200	200	200	738

5 Conclusion

In this paper, a simple greedy incremental(GI) algorithm was proposed for RBF network construction. The proposed algorithm is similar to other constructive algorithm: adding hidden node one by one, each added node is trained once and then fixed. The training of each added hidden node is divided into 2 steps:

1. filter the training set into a local set S around the pattern with biggest error magnitude and do local regression to determine optimal center and weight;
2. tune width iteratively using a simple update rule.

Several highly nonlinear practical experiments were given and presented the efficiency of the proposed GI algorithm, by comparing with other popular RBF algorithms.

Though the GI algorithm could achieve a compact RBF network efficiently, a big disadvantage exists. The mechanism of the construcitve algorithm that training each hidden node once and then fixed is not quite reasonable. The GI algorithm alone can not achieve high accuracy, either. So further research will focus on the fine-tuning of the RBF network after training with GI algorithm.

References

1. Broomhead, D.S., Lowe, D.: Multivariable functional interpolationand adaptive networks. Complex Syst. 2, 321–355 (1988)
2. Moody, J., Darken, C.J.: Fast learning in networks of locally-tuned processing units. Neural Comput. 1(2), 281–294 (1989)
3. Chen, S., Cowan, C.F.N., Grant, P.M.: Orthogonal least squares algorithm for radial basis funtion networks. Int. J. Control 2(2), 302–309 (1991)
4. Park, J., Sandberg, I.: Universal approximation using radial-basis function networks. Neural Comput. 3, 246–257 (1991)
5. Yu, H., Xie, T.T., Paszczynski, S., Wilamowski, B.M.: Advantages of radial basis function networks for dynamic system design. IEEE Trans. Ind. Electron. 58(12), 5438–5450 (2011)
6. Xie, T.T., Yu, H., Wilamowski, B.M.: Comparison of traditional neural networks and radial basis function networks. In: Proc. 20th IEEE Int. Symp. Ind. Electron., ISIE 2011, Gdansk, Poland, June 27-30, pp. 1194–1199 (2011)
7. Meng, K., Dong, Z.Y., Wang, D.H., Wong, K.P.: A self-adaptive RBF neural network classifier for transformer fault analysis. IEEE Trans. Power Syst. 25(3), 1350–1360 (2010)
8. Huang, S., Tan, K.K.: Fault detection and diagnosis based on modeling and estimation methods. IEEE Trans. Neural Netw. 20(5), 872–881 (2009)
9. Lee, Y.J., Yoon, J.: Nonlinear image upsampling method based on radial basis function interpolation. IEEE Trans. Image Process. 19(10), 2682–2692 (2010)
10. Ferrari, S., Bellocchio, F., Piuri, V., Borghese, N.A.: A hierarchical RBF online learning algorithm for real-time 3-D scanner. IEEE Trans. Neural Netw. 21(2), 275–285 (2010)
11. Vapnik, V.N.: Statistical Learning Theory, 1st edn. Wiley Interscience (1998)

12. Chng, E.S., Chen, S., Mulgrew, B.: Gradient radial basis function networks for nonlinear and nonstationary time series prediction. IEEE Trans. Neural Netw. 7(1), 190–194 (1996)
13. Karayiannis, N.B.: Reformulated radial basis neural networks trained by gradient descent. IEEE Trans. Neural Netw. 10(3), 657–671 (2002)
14. Wilamowski, B.M., Yu, H.: Improved computation for Levenberg–Marquardt training. IEEE Trans. Neural Netw. 21(6), 930–937 (2010)
15. Xie, T., Yu, H., Hewlett, J., Rozycki, P., Wilamowski, B.M.: Fast and efficient second-order method for training radial basis function networks. IEEE Trans. Neural Netw. Learn. Syst. 23(4), 609–619 (2012)
16. Huang, G.B., Zhu, Q.Y., Siew, C.K.: Extreme learning machine: Theory and applications. Neurocomputing 70(1-3), 489–501 (2006)
17. Huang, G.B., Chen, L., Siew, C.K.: Universal approximation using incremental constructive feedforward networks with random hidden nodes. IEEE Trans. Neural Netw. 17(4), 879–892 (2006)
18. Huang, G.B., Chen, L.: Enhanced random search based incremental extreme learning machine. Neurocomputing 71(16-18), 3460–3468 (2008)
19. Huang, G.B., Chen, L.: Convex incremental extreme learning machine. Neurocomputing 70, 3056–3062 (2007)
20. Reiner, P., Wilamowski, B.M.: Nelder-Mead Enhanced Extreme Learning Machine. In: INES 2013, Costa Rica, June 19-21 (2013)
21. Kwok, T.-Y., Yeung, D.-Y.: Objective functions for training new hidden units in constructive neural networks. IEEE Trans. Neural Netw. 8(5), 1131–1148 (1997)
22. Benoudjit, N., Verleysen, M.: On the Kernel widths in radial-basis function networks. Neural Process. Lett. 18, 139–154 (2003)
23. Huang, G.B., Saratchandran, P., Sundararajan, N.: An Efficient Sequential Learning Algorithm for Growing and Pruning RBF (GAP-RBF) Networks. IEEE Trans. on System, Man, and Cybernetics, Part B 34(6), 2284–2292 (2004)
24. Rousseeuw, P., Leroy, A.: Robust Regression and Outlier Detection, 3rd edn. John Wiley & Sons (1996)
25. Blake, C., Merz, C.: UCI repository of machine learning databases. Dept. Inf. Comp. Sci., Univ. California, Irvine (1998), `http://www.ics.uci.edu/~mlearn/MLRepository.html`
26. Chang, C.-C., Lin, C.-J.: $LIBSVM$: a library for support vector machines (2001), `http://www.csie.ntu.edu.tw/~cjlin/libsvm`
27. Malinowski, A., Yu, H.: Comparison of embedded system design for industrial applications. IEEE Trans. Ind. Informat. 7(2), 244–254 (2011)

A Note on Hamacher-Operators

László T. Kóczy

Széchényi István University, Győr, Hungary
Budapest University of Technology, Budapest, Hungary

1 Introduction

In his crucial paper Zadeh defined fuzzy operations in the "standard" way, by minimum and maximum [1]. However, in the same paper in a footnote he mentioned "intereractive operations" as an alternative, which were later known under the name "algebraic":

$$\begin{aligned} x \cap y &= xy, \\ x \cup y &= x + y - xy. \end{aligned} \tag{1}$$

Some time later Hamacher gave a much general form for this type of operations [2]:

$$\begin{aligned} x \cap y &= \frac{\lambda xy}{1 - (1-\lambda)(x + y - xy)}, \\ x \cup y &= \frac{\lambda (x + y) + xy (1 - 2\lambda)}{\lambda + xy (1 - \lambda)}, \end{aligned} \tag{2}$$

where $\lambda \geq 0$. (1) is given when $\lambda = 1$.

Later it was shown by various authors that these parametric operators may be generated in a much more general form, see e.g. [3]. The importance of Hamacher-operations cannot be neglected (cf. e.g. Fullér et al. [4], Batyrshin, Rudas et al. [5]), and some time ago we also proposed some applications [6]. In the next an interesting property will be discussed.

2 Inverse Set Operations?

It sounds a bizarre question int he context of Boolean sets. However, in [6] it was proposed that fuzzy set/logical operations being strictly monotonic (and continuous) in $(0, 1)$ are conditionally invertible. Inverse operations were introduced in a somewhat similar way as they are in algebraic fields, where both the addition and multiplication do have inverses. Similarities with fields are still limited, as in monotonic fuzzy algebras not all non-zero elements do have an inverse (in respect to both binary operations mentioned), except if the concept of membership function is extended to the real line (cf. R-fuzzy algebra, in [6]). Nevertheless, under conditions this inverse exists and thus inverse union and inverse intersection may also be defined. As Hamacher's operations are well known as being monotonic and continuous, the following may be stated:

J. Fodor and R. Fullér (eds.), *Advances in Soft Computing, Intelligent Robotics and Control,* Topics in Intelligent Engineering and Informatics 8,
DOI: 10.1007/978-3-319-05945-7_10,

If membership values are restricted to $(0,1)$ (thus excluding both the "additive" and "multiplicative" zeroes), the operations $x -\cap y$ and $z -\cup u$ denoting inverse intersection and union of x and y, respectively, do exist, whenever $x \leq y$, and $z \geq u$, and are defined through the basic properties:

$$\begin{aligned} x \cap y -\cap y &= x, \\ z \cup u -\cup u &= z. \end{aligned} \tag{3}$$

Obviously, if the arguments might assume the extreme values 0 or 1, several problems may occur. So, if $x = y = 0$, any value $a \in (0,1)$ satisfies $x \cap a = y$, and also, if $z = u = 1$, arbitrary $b \in (0,1)$ fulfils $b \cup u = z$. This is why inverse operations are pointless in the Boolean world.

Some of the properties of these inverse operations are the following (cf. [6]):

1. *Monotonicity.* Both $-\cap$ and $-\cup$ are strictly monotonic in $(0,1)$.
2. *Non-commutativity.* Obviously $x -\cap y \neq y -\cap x$ and $x -\cup y \neq y -\cup x$, when $x \neq y$ even, if the expressions on the left do exist, the expressions on the right have no meaning.
3. *Associativity and inter-commutativity.* Both inverse operations are associative combined with their respective straightforward operations, further, the sequence of $\cap$ and $-\cap$, further of $\cup$ and $-\cup$ may be changed.

   $$(x \cap y) -\cap z = x \cap (y -\cap z) = (x -\cap z) \cap y$$

   and

   $$(x \cup y) -\cup z = x \cup (y -\cup z) = (x -\cup z) \cup y,$$

   thus, it can be written that

   $$(x \cap y) -\cap z = x \cap y -\cap z = x -\cap z \cap y$$

   and similarly

   $$(x \cup y) -\cup z = x \cup y -\cup z = x -\cup z \cup y,$$

   provided that the ordering conditions apply. For short hand expressions, even $-\cup x$ is interpretable, whenever there is an $\cup y$ following it, where $x \leq y$ holds. Thus in practice, $-\cap$ and $-\cup$ may be treated as "signs", assuming again that the result is within $(0,1)$. (These properties lead straightforwardly to the introduction of the R-fuzzy extension of fuzzy sets, for $\mu\colon X \to R^1$; while $-\cap 0$ and $-\cup 1$ have to be still excluded from the inverse operations' range, in a very similar manner as division by 0 is prohibited.)
4. *De Morgan's Laws.* Very interesting pair of properties are the "inverse De Morgan properties". With proper negations the Hamacher-norms form a De Morgan triplet. This is preserved for the inverse operations.

   $$\begin{aligned} \text{If } \neg(x \cap y) = \neg x \cup \neg y, \text{ then } \neg(x -\cap y) &= \neg x -\cup y \\ \text{and consequently also } \neg(x -\cup y) &= \neg x -\cap y. \end{aligned}$$

5. *Distributive laws.* Similarly to other "unbalanced" equations, where the number of symbols is different on the two sides of the equation in Boolean algebra, monotonic operations never yield valid properties. Instead, strict inequalities hold (within $(0,1)$, of course), such as

$$x \cap (y \cup z) > (x \cap y) \cup (x \cap z)\,,$$

and

$$x \cup (y \cap z) < (x \cup y) \cap (x \cup z)\,.$$

A series of further similar properties might be easily deducted, such as the idempotency inequalities, and absorption inequalities, but these essentially follow the same logic mentioned under 5.

3 The Properties of Inverse Hamacher Operations

In the next the above definitions and properties will be illustrated by the general Hamacher-operations and the most popular special case, algebraic operations.

From (2) the inverse operations may be determined:

– *Inverse intersection* is given by

$$x = z -\cap y = z\frac{1-(1-\lambda)\,y}{(1-\lambda)\,(1-y)\,z+\lambda y}; \tag{4}$$

in the special algebraic case

$$x = \frac{z}{y}.$$

– Similarly, the *inverse union* is given by

$$x = z -\cup y = \frac{\lambda\,(z-y)}{\lambda+(1-2\lambda-z+z\lambda)\,y}. \tag{5}$$

And the algebraic case

$$x = \frac{z-y}{1-y}.$$

– *Monotonicity* is obvious.

In order to skip boring and lengthy calculations without any mathematical points, properties will be illustrated in the simplified algebraic cases.

– *Associativity* and *inter-commutativity* mean in the algebraic case

$$\frac{(xy)}{z} = \frac{x}{z}y = \frac{(yx)}{z} = \frac{xy}{z}$$

and

$$\left(\frac{x-y}{1-y}\right)+z-\left(\frac{x-y}{1-y}\right)z = \frac{(x+z-xz)-y}{1-y} = \frac{x-y+z-xz}{1-y}.$$

In the sense of applying $-\cup$ and $-\cap$ as "signs", the operators $\frac{[\,]-x}{1-x}$ and $\frac{[\,]}{x}$ must be understood, never in themselves, when traditional fuzzy is considered, but $[\,]=0$ and $[\,]=1$, respectively, in R-fuzzy.

– *De Morgan's Laws* appear with standard negation as

$$\neg\left(x -\cap y\right) = 1 - \frac{x}{y} = \frac{y-x}{y} = \frac{(1-x)-(1-y)}{1-(1-y)} = \neg x -\cup \neg y,$$

and as a matter of course, similarly,

$$\neg\left(x -\cup y\right) = 1 - \frac{x-y}{1-y} = \frac{1-x}{1-y} = \neg x -\cap \neg y.$$

– The *distributive inequlities* hold, as

$$\begin{aligned} x \cup (y \cap z) &= x\left(y + z - yz\right) = xy + xz - xyz < xy + xz - x^2yz = \\ &= (xy) + (xz) - (xy)\,(xz)\,, \end{aligned}$$

as $x < 1$, thus $-xyz < -x^2yz$. Similarly,

$$\begin{aligned} x \cup (y \cap z) &= x + yz - xyz > x^2 + xz - x^2z + xy - x^2y - xyz + x^2yz = \\ &= (x \cup y) \cap (x \cup z)\,, \end{aligned}$$

because the inner inequality can be reduced to

$$(1 - y - z + yz)\,x^2 < (1 - y - z + yz)\,x,$$

but $(1 - y - z + yz) = \neg\,(y \cup z) > 0$ and $x > 0$ both hold because of the $(0, 1)$ condition.

– Also, the *inverse distributive inequalities* are true:

$$\begin{aligned} (x \cup y) -\cap z &= \frac{x + y - xy}{z} = \frac{xz + yz - xyz}{z^2} > \\ &> \frac{xz + yz - xy}{z^2} = \frac{x}{z} + \frac{y}{z} - \frac{xy}{z^2} = (x -\cap z) \cup (y -\cap z)\,, \end{aligned}$$

because $z < 1$, thus $xyz < xy$. Similarly,

$$\begin{aligned} (x \cap y) -\cup z &= \frac{xy - z}{1 - z} = \frac{(1-z)\,(xy - z)}{(1-z)^2} = \frac{xy - xyz - z + z^2}{(1-z)^2} < \\ &< \frac{\left(xy - yz - zx + z^2\right)}{(1-z)^2} = \frac{x-z}{1-z} \cdot \frac{y-z}{1-z} = (x -\cup z) \cap (y -\cup z)\,, \end{aligned}$$

because

$$z\left(1 - (x + y - xy)\right) = z \cap \neg\,(x \cup y) > 0.$$

– The other similar properties are easy to illustrate, such as

$$\begin{matrix} x \cap x < x, \\ x \cup x > x, \end{matrix} \quad \text{and} \quad \begin{matrix} x \cap (x \cup y) < x, \\ x \cup (x \cap y) > x \end{matrix}$$

are obvious for algebraic norms because of the definitions, and not too complicated in case of the general Hamacher operations.

4 Open Questions

The properties presented above are rather straightforward, once the inverse operations are introduced, and may be nicely illustrated with help of both the general Hamacher and the algebraic norms. Several questions are however open. Among others:

1. What properties should fulfil the negations satisfying the inverse De Morgan Laws for the general Hamacher operations?
2. Are there any other meaningful and interesting properties in connection with the inverse operations?
3. Do the general operations obtained by generator functions satisfy all the above?
4. What are the conditions for the negations in the latter case?

Further similar problems may be found...

At this point nothing else remains but to express my best wishes to my good friend Imre Rudas on the occasion of his 65th birthday, and my wish that he may contribute to solving some of these open problems during the next years in good health and a vigorous mood!

Acknowledgement. This paper was supported by the National Scientific Research Fund grants OTKA K105559 and K108405, further by EU grant TÁMOP 4.2.2./B-10/1-2010-0010.

References

1. Zadeh, L.A.: Fuzzy sets, Information and Control, pp. 338–353 (1965)
2. Hamacher, H.: Über logische Vernupfungen unscharfer Aussagen und deren Zugehörige Bewertungsfunctionen. In: Trappl, R., Klir, G.J., Ricciardi, L. (eds.) Progress in Cybernetics and Systems Research, Hempisphere, Washington, vol. 3, pp. 276–288 (1978)
3. Fodor, J.C., Keresztfalvi, T.: A characterization of the Hamacher family of t-norms. FSS 65, 51–58 (1994)
4. Fullér, R., Keresztfalvi, T.: t-Norm-based addition of fuzzy intervals. FSS 51, 155–159 (1992)
5. Batyrshin, I.Z., Rudas, I.J., Villa, L.A., Cortés, A.P.: On the monotone sum of basic t-norms in the construction of parametric families of digital conjunctors for fuzzy systems with reconfigurable logic. Knowledge-Based Systems, 27–36 (2013)
6. Kóczy, L.T.: Interactive-algebras and fuzzy objects of type N. J. of Cybernetics, 273–290 (1978)

Practical Aspects of Fuzzy Rule Interpolation

Szilveszter Kovács

Department of Information Technology,
University of Miskolc Miskolc-Egyetemváros, Miskolc, Hungary, H-3515
szkovacs@iit.uni-miskolc.hu

Abstract. The number of the Fuzzy Rule Interpolation (FRI) applications in engineering tasks is still insignificant compared to the classical fuzzy reasoning methods. The main goal of this paper is to emphasize the benefits of the direct (embedded) applicability of fuzzy rule interpolation and the related sparse rule-based knowledge representation through demonstrative examples in rather different areas. As a prerequisite of sparse rule-base application in fuzzy system the FRI methods have the benefit of providing reasonable (interpolated) conclusions even if none of the existing rules matches the current observation. In spite of the classical fuzzy reasoning methods this feature enables FRI systems to have knowledge representation similarly constructed as expert systems, built upon the definition of cardinal rules only. On the other hand, thanks to the fuzzy concept, the fuzzy set symbol representation and the fuzzy reasoning, the discretely defined rules can act on continuous universes and continuous states. After a short discussion of FRI methods the paper will briefly introduce four FRI embedded application example of rule-based knowledge representation acting on continuous domain problems selected from the last 15 years work of our research group.

Keywords: Fuzzy Rule Interpolation (FRI), Embedded FRI Applications.

1 Introduction

Classical fuzzy reasoning methods (e.g. the Zadeh-Mamdani-Larsen compositional rule of inference [1,2,3] or the Takagi-Sugeno fuzzy inference [4,5]) are demanding complete rule bases, a special care of filling all the possible rules during the rule-base construction. In case if there are some rules missing (i.e. the rule base is "sparse"), observations may exist which matches no rule in the rule base and therefore no conclusion is obtained. Having no conclusion in fuzzy reasoning could have deliberate meaning. On the other hand if it is accidental e.g. in a control application, it could cause unpredictable side effects. Moreover the size of a complete fuzzy rule base is exponential with the number of the input dimensions. Having higher input dimensions the demand of complete rule-base is hardly tackleable.

One solution for handling the incomplete (sparse) fuzzy rule-base is the application of the fuzzy rule interpolation (FRI) methods. In case of FRI rule-base

J. Fodor and R. Fullér (eds.), *Advances in Soft Computing, Intelligent Robotics and Control,* Topics in Intelligent Engineering and Informatics 8,
DOI: 10.1007/978-3-319-05945-7_11,

representation the derivable rules are deliberately missing, since they can provide interpolated conclusions even if none of the existing rules matches the observation.

2 A Brief Overview of Some FRI Techniques

One of the first FRI techniques was published by Kóczy and Hirota [6]. It is usually referred as KH method. It is applicable to convex and normal fuzzy (CNF) sets. It determines the conclusion by its α-cuts in such a way that the ratio of distances between the conclusion and the consequents should be identical with the ones between the observation and the antecedents for all important α-cuts. The applied formula

$$\operatorname{dist}(A_1, x) : \operatorname{dist}(x, A_2) = \operatorname{dist}(B_1, y) : \operatorname{dist}(y, B_2), \tag{1}$$

where $A_1 \prec x \prec A_2$ and $B_1 \prec B_2$. $R_i \colon A_i \to B_i$, $i \in [1, 2]$ are the two fuzzy rules flanking the observation x, can be solved for the conclusion y for relevant α-cuts after decomposition.

It is shown e.g. in [7,8] that the conclusion of the KH method is not always directly interpretable as fuzzy set. This drawback motivated many alternative solutions. A modification was proposed by Vass, Kalmár and Kóczy [9] (VKK method), where the conclusion is computed based on the distance of the centre points and the widths of the α-cuts, instead of lower and upper distances. VKK method decreases the applicability limit of KH method, but does not eliminate it completely. The technique cannot be applied if any of the antecedent sets is singleton (the width of the antecedent's support must be nonzero). In spite of the disadvantages, KH is popular because its simplicity that infers its advantageous complexity properties. It was generalized in several ways. Among them the stabilized KH interpolator is emerged, as it is proved to hold the universal approximation property [10,11]. This method takes into account all flaking rules of an observation in the calculation of the conclusion in extent to the inverse of the distance of antecedents and observation. The universal approximation property holds if the distance function is raised to the power of the input's dimension.

Another modification of KH is the modified alpha-cut based interpolation (MACI) method [12], which alleviates completely the abnormality problem. MACI's main idea is the following: it transforms fuzzy sets of the input and output universes to such a space where abnormality is excluded, then computes the conclusion there, which is finally transformed back to the original space. MACI uses vector representation of fuzzy sets and originally applicable to CNF sets [13]. These latter conditions (CNF sets) can be relaxed, but it increases the computational need of the method considerably [14]. Another fuzzy interpolation technique was proposed by Kóczy et al. [15]. It is called conservation of "relative fuzziness" (CRF) method, which notion means that the left (right) fuzziness of the approximated conclusion in proportion to the flanking fuzziness of the neighboring consequent should be the same as the (left) right fuzziness of the observation in proportion to the flanking fuzziness of the neighboring

antecedent. The technique is applicable to CNF sets. An improved fuzzy interpolation technique for multidimensional input spaces (IMUL) was proposed in [16], and described in details in [17]. IMUL applies a combination of CRF and MACI methods, and mixes advantages of both. The core of the conclusion is determined by MACI method, while its flanks by CRF. The main advantages of this method are its applicability for multi-dimensional problems and its relative simplicity.

Conceptually different approaches were proposed by Bouchon-Meunier et al. [18,19]. The suggested "analogy-based interpolation" first interpolates the reference point position of the conclusion, then constructs the shape of conclusion fuzzy sets based on the similarity (distinguishability) relation of the rule antecedents and observation with respect to the similarity of the corresponding rule consequents and the conclusion. A similar two step method idea is appearing in the work of Baranyi et al. [20]. The suggested two step "General Methodology" (GM) first generate an interpolated "intermediate rule" in the reference point position of the observation, then in the second step a single rule reasoning method (revision function) is applied to determine the final fuzzy conclusion based on the similarity of the fuzzy observation and an "interpolated" observation. Practical application of the GM appears in the work of Johanyák et al. [21,22]. An extension of the GM is also appearing in the work of Shen et al. [23]. The suggested "scale and move transformation" can extend the original method to extrapolation.

A rather different application oriented aspect of the fuzzy rule interpolation emerges in the concept of "FIVE". The fuzzy reasoning method "FIVE" (Fuzzy Interpolation based on Vague Environment, originally introduced in [24,25,26]) was developed to fit the speed requirements of direct fuzzy control, where the conclusions of the fuzzy controller are applied directly as control actions in a real-time system.

The main idea of the FIVE is based on the fact that most of the control applications serves crisp observations and requires crisp conclusions from the controller. Adopting the idea of the vague environment (VE) [27], FIVE can handle the antecedent and consequent fuzzy partitions of the fuzzy rule base by scaling functions [27] and therefore turn the fuzzy interpolation to crisp interpolation. Because of its simple multidimensional applicability, in FIVE the Shepard operator based interpolation (first introduced in [28]) is adapted.

Because of the simple adaptivity to embedded applications, in the rest of the paper all the numerical examples of the applications are based on the FIVE FRI calculations. The code of the FIVE FRI together with other FRI methods as a freely available FRI Toolbox can be downloaded at [29,30].

3 Application Examples

For introducing some of the possible embedded application areas of the FRI methods, a vehicle control, a fault tolerant control application, a user adaptive emotion-based selection system and a human-robot interaction model example are shortly introduced in the followings.

3.1 Vehicle Navigation Control Example

The first application example is a simulated steering control of an automated guided vehicle (AGV) [31,32,33,34]. In the example application the goal of the path tracking strategy is to follow the guide path by the guide zone with minimal path tracking error on the whole path (see Fig. 1).

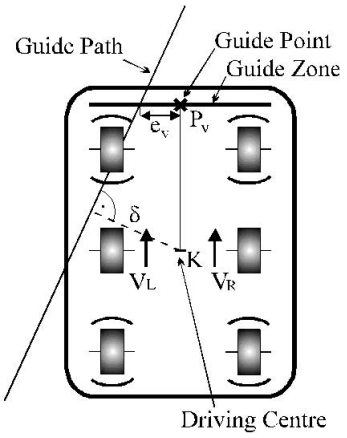

Fig. 1. Differential steered AGV with guide zone, δ is the path tracking error, e_v is the distance of the guide path and the guide point, P_v is the guide point, K is the driving centre

The simplest way of defining the fuzzy rules for the steering control is based on stud-ying the operator's control actions in relevant situations. These control actions could form the later rule-base. The basic idea of the path tracking strategy is very simple: keep the driving centre K of the AGV as close as it is possible to the guide path, and than simply turn the AGV into the new direction. This strategy needs two observations: the measured distance between the guide path and the guide point (e_v), and the estimated distance between the guide path and the driving centre (δ) (see Fig. 2 for the notation). Based on these observations, as a conclusion, the level of steering ($V_d = V_L - V_R$) needed to be calculated. Collecting the operator's control actions, the path tracking strategy can be characterized by five relevant situations, collected on Fig. 2.

Having the relevant control actions and the linguistic term fuzzy sets (fuzzy partitions) of the two antecedent and one consequent universes, the fuzzy rule base can be simply constructed. The i^{th} rule of the rule base has the form:

$$\mathtt{R_{Vd(i)}}: \quad \mathtt{If}\ \ e_v = A_{1,i}\ \ \mathtt{And}\ \ \delta = A_{2,i}\ \ \mathtt{Then}\ \ V_d = B_i$$

Let us have the linguistic term fuzzy partitions built up five fuzzy sets, namely: negative large (NL), negative middle (NM), zero (Z), positive middle (PM),

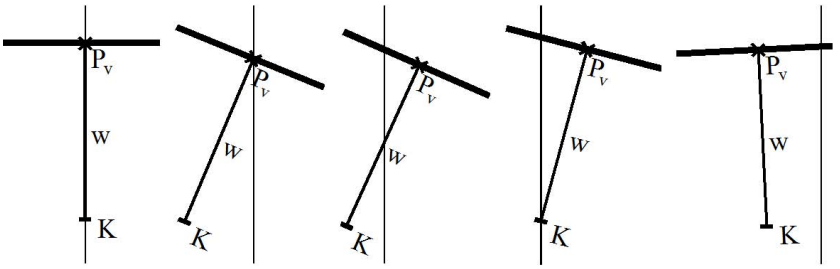

Fig. 2. Relevant control actions (V_d: steering) characterizing the path tracking strategy (see Fig. 1 for the notation)

positive large (PL) for the two antecedents universes (e_v, δ), and negative large (NL), negative small (NS), zero (Z), positive small (PS), positive large (PL) for the consequent universe (V_d). Building a complete fuzzy rule-base first, according to the antecedent terms, we have to set up an antecedent grid of all possible fuzzy rules, and then fill it with the corresponding rule consequents (see Table 1). First we can fill the rule consequents already known as relevant situations from the knowledge acquisition phase (noted by underline in Table 1.), then to make the rule base complete, the "filling" rules too.

Table 1. Path tracking, complete rule base

R_{Vd}:

$\delta \setminus e_v$	NL:	NM:	Z:	PM:	PL:
NL:	$\underline{PL}$	PS	Z	NS	$\underline{NL}$
NM:	$\underline{PL}$	PS	$\underline{PS}$	$\underline{Z}$	$\underline{NL}$
Z:	$\underline{PL}$	$\underline{PL}$	$\underline{Z}$	$\underline{NL}$	$\underline{NL}$
PM:	$\underline{PL}$	$\underline{Z}$	$\underline{NS}$	NS	$\underline{NL}$
PL:	$\underline{PL}$	PS	Z	NS	$\underline{NL}$

In most cases, the "filling" rules have the only task to get "smooth transient" between the relevant rules. Selecting a fuzzy reasoning method, e.g. the max-min composition, and center of gravity defuzzification, the control surface of the steering can be directly calculated (see Fig. 3).

The design of the path tracking steering control rule-base for FRI is very similar to the complete rule-base situation. The main difference is the lack of the "filling" rules. The rule base contains the rules of the relevant situations, known from the knowledge acquisition phase, only (see Table 2). Introducing single antecedent rules, rules which have the same conclusion independently from some of the antecedents can be merged to single rules i.e. according to our

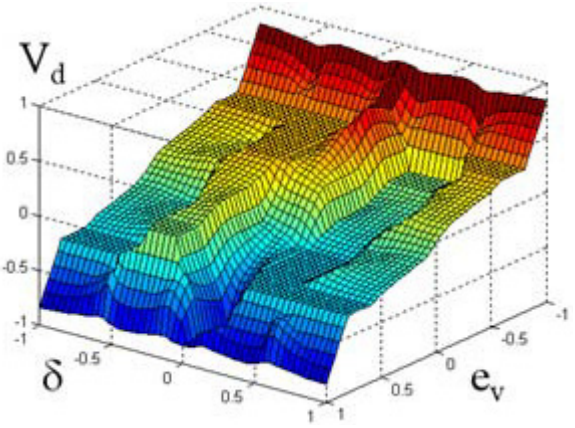

Fig. 3. Control surface of the path tracking steering strategy, max-min CRI, centre of gravity defuzzification, 25 rules, complete rule base according to Table 1 [31]

Table 2. Path tracking, sparse rule base

R_{Vd}:

$\delta \setminus e_v$	NL:	NM:	Z:	PM:	PL:
NL:	PL				NL
NM:	PL		PS	Z	NL
Z:	PL	PL		NL	NL
PM:	PL	Z	NS		NL
PL:	PL				NL

Table 3. Path tracking, sparse rule base

R_{Vd}	e_v	δ	V_d
Rule 1:	NL		PL
Rule 2:	PL		NL
Rule 3:	NM	Z	PL
Rule 4:	PM	Z	NL
Rule 5:	NM	PM	Z
Rule 6:	PM	NM	Z
Rule 7:	Z	PM	NS
Rule 8:	Z	NM	PS

example the rule base of Table 2 can be simplified to Table 3. Selecting a fuzzy reasoning method suitable for sparse rule bases, i.e. in our case the "FIVE" FRI, introduced briefly in Section 2, the control surface of the steering can be directly calculated (see Fig. 4).

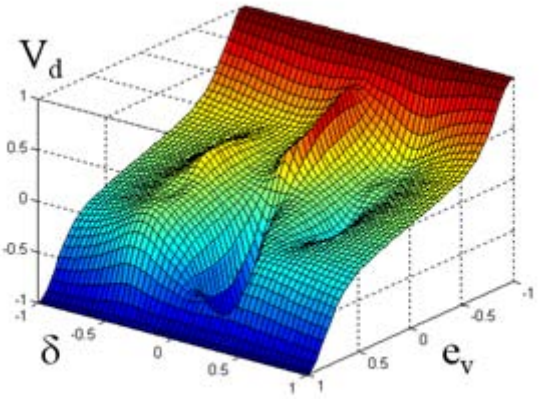

Fig. 4. Control surface of the path tracking steering strategy, "FIVE" FRI, 8 rules, sparse rule base, according to Table 3 [31]

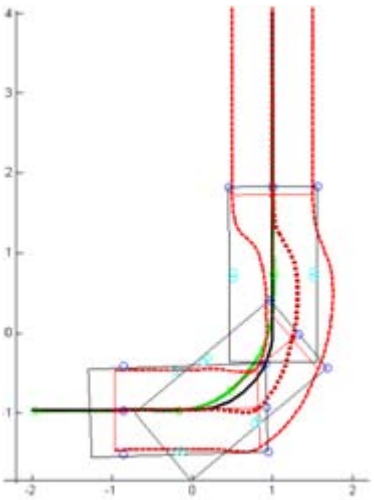

Fig. 5. Track of the optimized FIVE FRI AGV steering control [31]

Conclusions of the Example. The simulated results show (see e.g. Fig. 5), that in the tested situation the suggested embedded FRI control was able to follow the guide path in the expected manner. (See the example more detailed in [31].)

3.2 Fault Tolerant Control Example

The second simple application example of the embedded FRI control is the fault diagnosis and reconfiguration of the three tank benchmark in a simplified configuration (two tanks only) [35,36,33] (see Fig. 6).

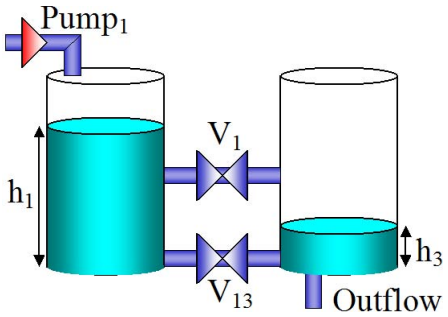

Fig. 6. Simplified configuration of the three tank benchmark

The goal of the control system is to keep the water levels in $tank_1$ and $tank_3$ to be $h_1 = 0.5$ and $h_3 = 0.1$ by controlling the $valve_{13}$ and the $pump_1$ at a constant value of outflow from $tank_3$ (*normal* behaviour of the system).

The example is concentrating of the faults of the $valve_{13}$. Were this valve opened and blocked, the water level in $tank_3$ $h_3 = 0.1$ could be controlled by $pump_1$ (this case h_1 is changed) – this is the *fault condition no.1.* Were this valve closed and blocked, the water levels in $tank_1$ and $tank_3$ $h_1 = 0.5$ and $h_3 = 0.1$ could be controlled by the $valve_1$ and the $pump_1$ – this is the *fault condition no.2.*

The way of the implementation is adapting the fuzzy behaviour-based control structure introduced in [35,36,33] (see Fig. 7).

The suggested solution contains three component behaviours, i.e. three controllers are handling the three separate situations, one controller is set for handling the "normal", one for the "Fault 1" and one for the "Fault 2" system behaviours. In this example for symptom evaluation the fuzzy clustering was applied. The symptom evaluation module has to be able to characterize all the state-transitions in all the studied behaviours. The state-transition diagram for the studied states of the FRI automaton is shown in Fig. 8. (The states are fuzzy membership values.) The basic structure of the rule-base applied for the state-transitions of the FRI fuzzy automaton (rules for FRI) for the ith state Si (RAi) are the following:

$$\texttt{If } S_i = \texttt{One And } S_i - S_i = \texttt{One} \quad \texttt{Then } S_i = \texttt{One}$$
$$\texttt{If } S_i = \texttt{One And } S_i - S_k = \texttt{One} \quad \texttt{Then } S_i = \texttt{Zero}$$
$$\texttt{If } S_k = \texttt{One And } S_k - S_i = \texttt{One} \quad \texttt{Then } S_i = \texttt{One}$$
$$\texttt{If } S_k = \texttt{One And } S_k - S_i = \texttt{Zero} \quad \texttt{Then } S_i = \texttt{Zero}$$

where $S_i - S_k$ is the conclusion of the symptom evaluation about the state-transition from state i to k, $\forall k \in [1, N]$, N is the number of the component behaviours (state variables). The structure of the state-transition rules is similar for all the state variables. `Zero` and `One` are linguistic labels of fuzzy sets

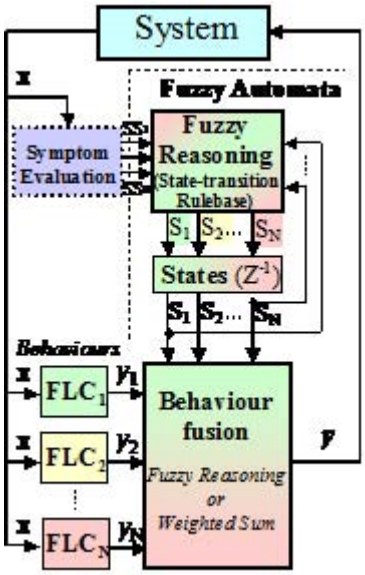

Fig. 7. The applied behaviour-based control structure

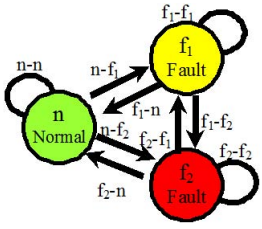

Fig. 8. State-transition diagram of the fuzzy automaton, where e.g. $f_1 - f_2$ is the conclusion of the symptom evaluation related to the "from f_1 to f_2" state-transition

(linguistic terms) representing high and low similarity. The interpretations of the `Zero` and `One` fuzzy sets can be different in each S_i, $S_i - S_k$ universes.

The applied behaviour fusion is a convex combination of the conclusions of the component behaviours with the membership values of the corresponding states act as weights.

Conclusions of the Example. The simulated example application demonstrated that the FRI fuzzy automaton is able to follow the studied relevant states and state-transitions (e.g. Normal–Fault1–Normal in Fig. 9). Moreover, because of the fuzzy state approximation and the convex combination behaviour fusion in some cases the system is also able to handle unknown (unstudied) fault

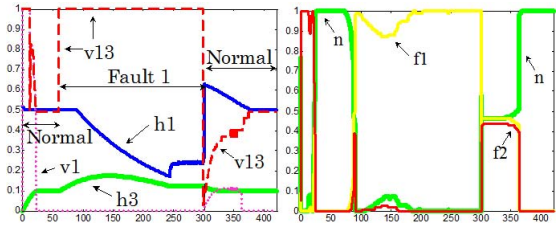

Fig. 9. The simulated results and the approximated fuzzy states of the complete control system (Normal – Fault 1 – Normal behaviour) [35]

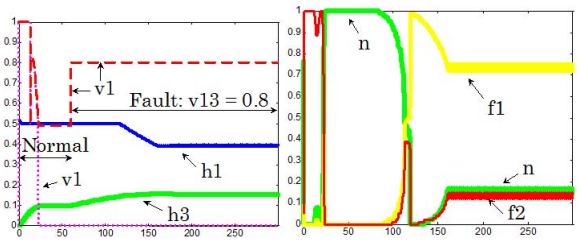

Fig. 10. The simulated results and the approximated fuzzy states of the complete control system (Normal – Fault: v13 = 0.8 unstudied situation) [35]

situations too (see e.g. in Fig. 10, where v13 = 0.8 open is an unstudied fault situation). (See the example more detailed in [35].)

3.3 User Adaptive Emotion-Based System Example

The third example of the embedded FRI application is a user adaptive emotion-based system, an interactive selection system [37,33]. The example application is based on the idea, that from the viewpoint of the application, the user adaptivity is similar task as the situation adaptivity, introduced in the previous example. Forming the emotional user model as on-line variable fusion of some fixed existing (off-line collected) models. In this case the user adaptation itself is handled as a kind of adaptive fusion of existing emotional models in the manner of "the more similar the actual user to one of the existing emotional model, the more similar must be the actual emotional model to that model". In other words, instead of identifying the actual emotional model itself, the user is classified in the manner of existing emotional models. As an analogy to the previous applications, the different known behaviours are the different known emotional models, and the actual situation is the similarity of the actual user to the evaluators, gave the known emotional models. The main benefit of this view is quick convergence, as in the most cases the problem of user classification related to some existing emotional models is much simpler than the identification of the complicated

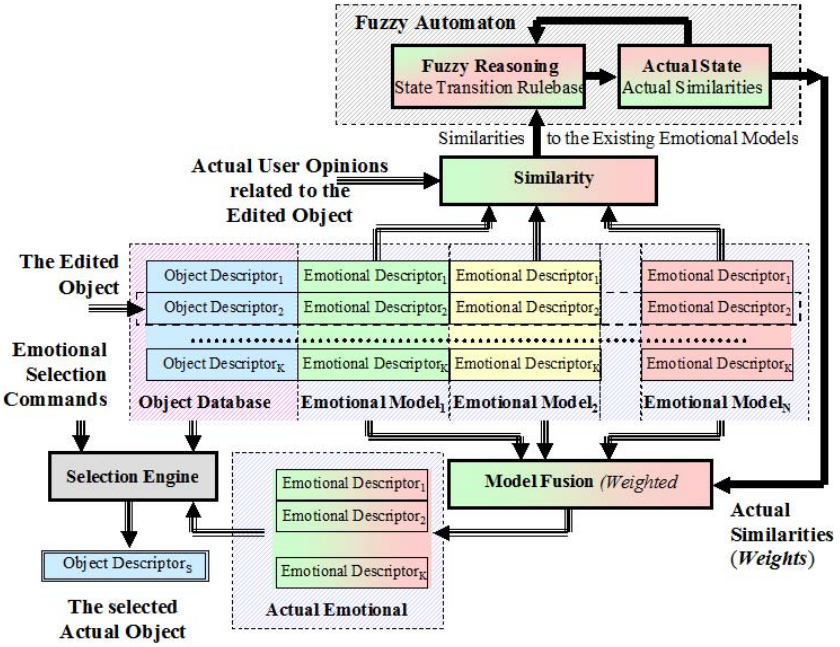

Fig. 11. Structure of the proposed adaptive emotional model generation [37]

emotional model itself. The ability of proper depiction of user emotion is highly dependent on the number and diversity of the known models available in the system. The implementation of the suggested embedded FRI behaviour-based control model is very similar to the previous example. The main differences (Fig. 7, Fig. 11) are the substitution of the known behaviour controllers (FLCi) by the known emotional models (Object Descriptor – Emotional Descriptors), and the direct similarity checking (similarities of the actual user opinions to the content of the existing models) instead of symptom evaluation.

Using the selection system, the user can search the object database by giving emotion-related requests (like "friendly" or "convenient"). These requests are translated to physical parameters (characterising the real objects) by the actual emotional model. The user adaptivity of the actual emotional model (see Fig. 11) (since the physical meanings of the emotional words are highly user dependent) is provided by the suggested FRI behaviour-based control model. This case the state of the fuzzy automaton (actual similarities, see Fig. 11) is interpreted as the actual approximated similarities of the actual user opinions and the known emotional models.

Conclusions of the Example. The goal of the actual user model modifications from the user side is to tune the system to be closer to his/her opinions. Practically the system is starting from an initial stage (where the similarities to the existing

models are equal), and in the case if the user is disagreeing with the evaluation of the actual object given by the system, he/she has the possibility to modify the actual user model by giving his/her opinions. In most cases the given opinions are related to one or a few emotional descriptors of the edited object (see Fig. 11). But because of the suggested structure, all the changes are done globally (all the emotional descriptors of known model has the same weights "globally" in the actual model – not only the descriptor weights related directly to the given user opinion are "locally" modified). Hopefully that this kind of adaptation strategy keeps the actual user model coherent, and able to avoid incoherence could caused by step by step partial modifications. E.g. if one of the users have exactly the same opinions as one of the known model (even his/her opinions were given through some of the emotional parameters only), then (after a few modification, detection steps) as the best fitting known model, the system will use it exactly. Basically the "adaptive knowledge" of the system related to the actual user is not a new adapted emotional model, but the actual system state, a set of approximated similarities of the actual user opinions to the known emotional models. Because of the convex combination way of the emotional model combination, the suggested structure is unable to follow user requirements outside the area covered by the known models. In other words, the system cannot go beyond its existing "knowledge". The only solution of this problem is extending the number and the variety of the known emotional models, to cover the model space as much as it is possible. (See the example more detailed in [37].)

3.4 Human-Robot Interaction Model Example

The last example is supporting the idea, that a novel aspect of Human-Robot Interaction (HRI) can be put on the basis, that the robot side is implemented on a state-machine (FRI embedded fuzzy automaton), which reacts the human intervention as a function of the robot state and the human action (suggested in [38,39,40]). This platform is suitable for implementing quite complicated action-reaction sequences, like the interaction of human and an animal, e.g. the behaviour of an animal companion to the human. According to this paradigm the robot can follow the existing biological examples and form inter-species interaction. The 20,000 year old human-dog relationship, as interaction of different species, could be a good example for this relation.

The actual example is a tiny fragment of a more complex ethological model of an RDog behaving in an unfamiliar room in interaction with its owner and an unknown human ("Owner" and "Human2" in Fig. 12). In the name of "RDog" the "R" stands for "Robot" i.e. the dog in question is a Robot. According to the structure of the embedded FRI behaviour-based control model introduced in Fig. 7, the example behaviour is built upon two component behaviours, namely "`RDogExploresTheRoom`" and "`RDogGoesToDoor`". The "`RDogExploresTheRoom`" is an exploration dog activity, in which the dog "looks around" in an unknown environment (see the "ellipsoid" track in Fig. 12). The "`RDogGoesToDoor`" is a simple dog activity, in which the dog goes to the door, and then stands (sits) in front of it.

The example is the definition of the related state-transition FRI rules of the fuzzy automaton acts as behaviour coordination. The states concerned in the example are the following:

"Missing the owner mood of the RDog" (`RDogMissTheOwner`) and "Anxiety level of the RDog" (`RDogAnxietyLevel`): "hidden" states, which have no direct task in controlling any of the above mentioned behaviours, but has an importance in the state-transition rule-base.

"Going to the door mood of the RDog" (`RDogGoesToDoor`) and "Room exploration mood of the RDog" (`RDogExploresTheRoom`): states, which have also direct task in controlling the corresponding "RDogExploresTheRoom" and "RDogGoesToDoor" behaviours.

As a possible rule base structure for the state-transitions of the fuzzy automaton, the following is defined (a tiny fragment of a more complex rule-base):

State-transition rules related to the missing the owner mood (state) of the RDog:

`If OwnerInTheRoom=`*`False`* `Then RDogMissTheOwner=`*`Increasing`*
`If OwnerInTheRoom=`*`True`* `Then RDogMissTheOwner=`*`Decreasing`*

State-transition rules related to the anxiety level (state) of the RDog:

`If OwnerToDogDistance=`*`Small`* `And Human2ToDogDistance=`*`High`*
`Then RDogAnxietyLevel=`*`Decreasing`*
`If OwnerToDogDistance=`*`High`* `And Human2ToDogDistance=`*`Small`*
`Then RDogAnxietyLevel=`*`Increasing`*

State-transition rules related to the going to the door mood (state) of the RDog:

`If OwnerInTheRoom=`*`False`* `And RDogMissTheOwner=`*`High`*
`Then RDogGoesToDoor=`*`High`*
`If OwnerInTheRoom=`*`True`* `Then RDogGoesToDoor=`*`Low`*

State-transition rules related to the room exploration mood (state) of the RDog:

`If RDogAnxietyLevel=`*`Low`* `And OwnerStartsGame=`*`False`*
`And ThePlaceIsUnknown=`*`High`* `Then RDogExploresTheRoom=`*`High`*
`If ThePlaceIsUnknown=`*`Low`* `Then RDogExploresTheRoom=`*`Low`*
`If RDogAnxietyLevel=`*`High`* `Then RDogExploresTheRoom=`*`Low`*

where the text in Italic are the linguistic terms (fuzzy sets) of the FRI rule base.

A sample run of the example is introduced in Fig. 12 and Fig. 13. At the beginning of the scene, the owner is in the room and the Human2 is outside. The place is unknown for the dog ("`ThePlaceIsUnknown=`*`High`*" in the rule base). According to the above rule base, the dog starts to explore the room. At around the step count 17, the owner of the dog left the room, than "Human2" enters and stay inside. As an effect of the changes (according to the above state-transition rule base), the anxiety level of the dog and the "missing the owner" is increasing, and as a result, the dog goes and stays at the door, where the owner has left the room. See example run tracks in Fig. 12 and state changing in Fig. 13. (See the example more detailed in [38].)

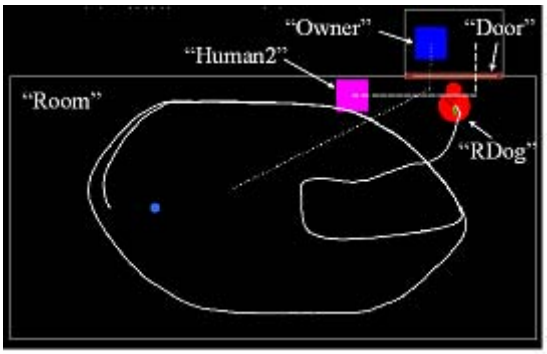

Fig. 12. Tracks of a sample run; continuous line for the dog, dotted for the Owner and dashed for the Human2 [38]

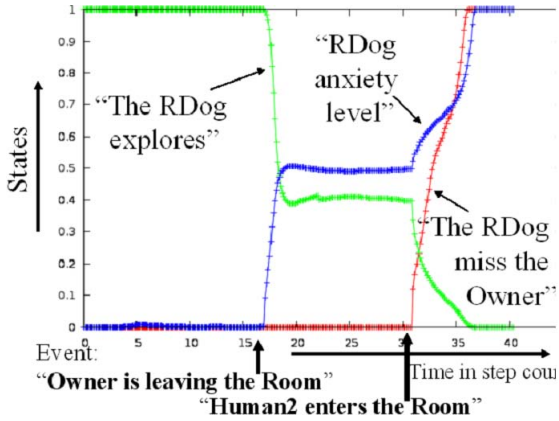

Fig. 13. Some state changes during the sample run introduced in Fig. 12 [38]

4 Conclusion

The main goal of this paper was to emphasize the practical, application oriented aspects of Fuzzy Rule Interpolation (FRI) techniques. Supporting the sparse rule-base knowledge representation, FRI methods can dramatically simplify the way of fuzzy rule base creation. Keeping the convenience of fuzzy knowledge representation FRI techniques can give solutions for problems hardly tackleable by classical fuzzy reasoning.

Acknowledgment. The author would like to express his greatest gratitude to **Professor Imre J. Rudas** for his highly respected unselfish work in inspiring and supporting young researchers and the computational intelligence related research in Hungary.

References

1. Zadeh, L.A.: Outline of a new approach to the analysis of complex systems and decision processes. IEEE Trans. on SMC (3), 28–44 (1973)
2. Mamdani, E.H., Assilian, S.: An experiment in linguistic synthesis with a fuzzy logic controller. Int. J. of Man Machine Studies (7), 1–13 (1975)
3. Larsen, P.M.: Industrial application of fuzzy logic control. Int. J. of Man Machine Studies 12(4), 3–10 (1980)
4. Sugeno, M.: An introductory survey of fuzzy control. Information Science (36), 59–83 (1985)
5. Takagi, T., Sugeno, M.: Fuzzy identification of systems and its applications to modeling and control. IEEE Trans. on SMC (15), 116–132 (1985)
6. Kóczy, L.T., Hirota, K.: Rule interpolation by α-level sets in fuzzy approximate reasoning. J. BUSEFAL, Automne, URA-CNRS 46, 115–123 (1991)
7. Kóczy, L.T., Kovács, S.: On the preservation of the convexity and piecewise linearity in linear fuzzy rule interpolation. Tokyo Inst. Technol., Yokohama, Japan, Tech. Rep. TR 93-94/402, LIFE Chair Fuzzy Theory (1993)
8. Kóczy, L.T., Kovács, S.: Shape of the Fuzzy Conclusion Generated by Linear Interpolation in Trapezoidal Fuzzy Rule Bases. In: Proceedings of the 2nd European Congress on Intelligent Techniques and Soft Computing, Aachen, pp. 1666–1670 (1994)
9. Vass, G., Kalmár, L., Kóczy, L.T.: Extension of the fuzzy rule interpolation method. In: Proc. Int. Conf. Fuzzy Sets Theory Applications (FSTA 1992), Liptovsky M., Czechoslovakia, pp. 1–6 (1992)
10. Tikk, D., Joó, I., Kóczy, L.T., Várlaki, P., Moser, B., Gedeon, T.D.: Stability of interpolative fuzzy KH-controllers. Fuzzy Sets and Systems 125(1), 105–119 (2002)
11. Tikk, D.: Notes on the approximation rate of fuzzy KH interpolator. Fuzzy Sets and Systems 138(2), 441–453 (2003)
12. Tikk, D., Baranyi, P.: Comprehensive analysis of a new fuzzy rule interpolation method. IEEE Trans. Fuzzy Syst. 8(3), 281–296 (2000)
13. Yam, Y., Kóczy, L.T.: Representing membership functions as points in high dimensional spaces for fuzzy interpolation and extrapolation. Dept. Mech. Automat. Eng., Chinese Univ. Hong Kong, Tech. Rep.CUHK-MAE-97-03 (1997)
14. Tikk, D., Baranyi, P., Gedeon, T.D., Muresan, L.: Generalization of a rule interpolation method resulting always in acceptable conclusion. Tatra Mountains Math. Publ. 21, 73–91 (2001)
15. Kóczy, L.T., Hirota, K., Gedeon, T.D.: Fuzzy rule interpolation by the conservation of relative fuzziness. Technical Report TR 97/2. Hirota Lab, Dept. of Comp. Int. and Sys. Sci., Tokyo Inst. of Techn., Yokohama (1997)
16. Wong, K.W., Gedeon, T.D., Tikk, D.: An improved multidimensional α-cut based fuzzy interpolation technique. In: Proc. Int. Conf Artificial Intelligence in Science and Technology (AISAT 2000), Hobart, Australia, pp. 29–32 (2000)
17. Wong, K.W., Tikk, D., Gedeon, T.D., Kóczy, L.T.: Fuzzy Rule Interpolation for Multidimensional Input Spaces With Applications. IEEE Transactions on Fuzzy Systems 13(6), 809–819 (2005) ISSN 1063-6706
18. Bouchon-Meunier, B., Delechamp, J., Marsala, C., Mellouli, N., Rifqi, M., Zerrouki, L.: Analogy and fuzzy interpolation in case of sparse rules. In: Proceedings of the EUROFUSE-SIC Joint Conference, pp. 132–136 (1999)
19. Bouchon-Meunier, B., Marsala, C., Rifqi, M.: Interpolative reasoning based on graduality. In: Proceedings of FUZZ-IEEE 2000, International Conference, San Antonio, pp. 483–487 (2000)

20. Baranyi, P., Kóczy, L.T., Gedeon, T.D.: A Generalized Concept for Fuzzy Rule In-terpolation. IEEE Trans. on Fuzzy Systems 12(6), 820–837 (2004)
21. Johanyák, Z.C., Kovács, S.: Fuzzy rule interpolation based on polar cuts. In: Reusch, B. (ed.) Computational Intelligence, Theory and Applications, pp. 499–511. Springer (2006)
22. Johanyák, Z.C.: Fuzzy Rule Interpolation based on Subsethood Values. In: Proceedings of 2010 IEEE Interenational Conference on Systems Man, and Cybernetics (SMC 2010), October 10-13, pp. 2387–2393 (2010) ISBN 978-1-424-6587-3
23. Huang, Z., Shen, Q.: Fuzzy interpolative reasoning via scale and move transformations. IEEE Trans. Fuzzy Syst. 14(2), 340–359 (2006)
24. Kovács, S.: New Aspects of Interpolative Reasoning. In: Proceedings of the 6th International Conference on Information Processing and Management of Uncertainty in Knowledge-Based Systems, Granada, Spain, pp. 477–482 (1996)
25. Kovács, S., Kóczy, L.T.: Approximate Fuzzy Reasoning Based on Interpolation in the Vague Environment of the Fuzzy Rule base as a Practical Alternative of the Classical CRI. In: Proceedings of the 7th International Fuzzy Systems Association World Congress, Prague, Czech Republic, pp. 144–149 (1997)
26. Kovács, S., Kóczy, L.T.: The use of the concept of vague environment in approximate fuzzy reasoning. In: Fuzzy Set Theory and Applications, vol. 12, pp. 169–181. Tatra Mountains Mathematical Publications, Mathematical Institute Slovak Academy of Sciences, Bratislava, Slovak Republic (1997)
27. Klawonn, F.: Fuzzy Sets and Vague Environments. Fuzzy Sets and Systems 66, 207–221 (1994)
28. Shepard, D.: A two dimensional interpolation function for irregularly spaced data. In: Proc. 23rd ACM Internat. Conf., pp. 517–524 (1968)
29. FRI Toolbox available at: `http://fri.gamf.hu`
30. FRI applications are available at: `http://www.iit.uni-miskolc.hu/~szkovacs`
31. Kovács, S., Kóczy, L.T.: Application of the Approximate Fuzzy Reasoning Based on Interpolation in the Vague Environment of the Fuzzy Rulebase in the Fuzzy Logic Controlled Path Tracking Strategy of Differential Steered AGVs. In: Reusch, B. (ed.) Fuzzy Days 1997. LNCS, vol. 1226, pp. 456–467. Springer, Heidelberg (1997)
32. Kovács, S., Kóczy, L.T.: Path Tracking and Collision Avoidance Strategy of an AGV Implemented on Interpolation-based Fuzzy Logic Controller. In: Proceedings of the INES 1998 IEEE International Conference on Intelligent Engineering Systems, Vienna, Austria, pp. 67–72 (1998)
33. Kovács, S.: Fuzzy Behaviour-based Control Techniques in Adaptive System Applications. In: Proceedings of the IEEE International Conference on Computational Cybernetics, ICCC 2003, Siófok, Hungary, August 29-31, p. 6 (2003)
34. Kovács, S.: Fuzzy Rule Interpolation in Practice. In: Proceedings of the Joint 3rd International Conference on Soft Computing and Intelligent Systems and 7th International Symposium on advanced Intelligent Systems (SCIS & ISIS 2006), September 20-24. O-okayama Campus West Bldg, 9, p. 6. Tokyo Institute of Technology, Tokyo (2006)
35. Kovács, S., Kóczy, L.T.: Interpolative Fuzzy Reasoning in Similarity based System Reconfiguration. In: Proceedings of IEEE SMC 1999, IEEE International Conference on Systems, Man, and Cybernetics, Tokyo, Japan, vol. V, pp. 226–231 (1999)
36. Kovács, S.: Similarity Based System Reconfiguration by Fuzzy Classification and Hierarchical Interpolate Fuzzy Reasoning. In: Reusch, B. (ed.) Fuzzy Days 1999. LNCS, vol. 1625, pp. 12–19. Springer, Heidelberg (1999)

37. Kovács, S., Kubota, N., Fujii, K., Kóczy, L.T.: Behaviour based techniques in user adaptive Kansei technology. In: Proceedings of the 6th International Conference on Virtual Systems and Multimedia, VSMM 2000, Ogaki, Gifu, Japan, October 3-6, pp. 362–369 (2000)
38. Sz. Kovács, D., Vincze, M., Gácsi, Á., Miklósi, P.: Korondi, Ethologically inspired robot behavior implementation. In: 4th International Conference on Human System Interactions (HSI 2011), Yokohama, Japan, May 19-21, pp. 64–69 (2011)
39. Kovács, S., Vincze, D., Gácsi, M., Miklósi, Á., Korondi, P.: Fuzzy automaton based Human-Robot Interaction. In: IEEE 8th International Symposium on Applied Machine Intelligence and Informatics (SAMI), Herľany, Slovakia, January 28-30, pp. 165–169 (2010)
40. Vincze, D., Kovács, S., Gácsi, M., Korondi, P., Miklósi, Á., Baranyi, P.: A Novel Appli-cation of the 3D VirCA Environment: Modeling a Standard Ethological Test of Dog-Human Interactions. Acta Polytechnica Hungarica 9(1), 107–120 (2012)

On Generalization of Nguyen's Theorem: A Short Survey of Recent Developments

Robert Fullér

Institute of Applied Mathematics
John von Neumann Faculty of Informatics
Óbuda University
Bécsi út 96/b, 1034 Budapest, Hungary,
fuller.robert@nik.uni-obuda.hu

Abstract. One of the most important principles in fuzzy set theory is Zadeh's sup-min extension principle. Nguyen's classical theorem expressed sup-min extensions of continuous functions in terms of alpha-cuts of fuzzy sets. In 1991 Fullér and Keresztfalvi computed the alpha-cuts of extended functions defined via sup-t-norm composition. In 2004 Carlsson, Fullér and Majlender gave a closed formula for α-cuts of extended functions using the concept of joint possibility distributions. In this paper we give a short survey of some later works that extend and develop these models.

1 Concepts and Issues

One of the basic concepts in the fuzzy set is the extension principle, where one extends crisp domains of mathematical expressions (concepts, functions, operators, etc) to fuzzy domains.

Definition 1.1. *A fuzzy (sub)set A in a classical set X is defined by its membership function*

$$A\colon X \to [0,1],$$

where $A(x)$ denotes the degree of membership of $x \in X$ in fuzzy set A. In the following we shall use the same notation for the fuzzy set and for its membership function. The symbol $\mathcal{F}(X)$ denotes the family of all fuzzy (sub)sets of X.

Definition 1.2. *A α-level set of a fuzzy set A in X is defined by*

$$[A]^{\alpha} = \{t \in X \mid A(t) \geq \alpha\},$$

if $\alpha > 0$ and

$$[A]^{0} = \mathrm{cl}\{t \in X \mid A(t) > 0\},$$

is defined as the closure of the support of A.

J. Fodor and R. Fullér (eds.), *Advances in Soft Computing, Intelligent Robotics and Control,* Topics in Intelligent Engineering and Informatics 8,
DOI: 10.1007/978-3-319-05945-7_12,

A fuzzy number is a fuzzy set of the real line with a normal, fuzzy convex and upper semi-continuous membership function of bounded support [3]. Fuzzy numbers can be considered as possibility distributions. If A and B are fuzzy numbers then we say that they are equal in membership function, and write $A = B$, if $A(x) = B(x)$ for all $x \in \mathbb{R}$. The family of fuzzy numbers will be denoted by $\mathcal{F}$ [4]. Let us recall the concept and some basic properties of joint possibility distribution introduced by Fullér and Majlender in [5].

Definition 1.3 (Fullér and Majlender in [5]). *If $A, B \in \mathcal{F}$ then C is said to be their joint possibility distribution if $\max\{C(x,t) \mid t \in \mathbb{R}\} = A(x)$ and $\max\{C(t,y) \mid t \in \mathbb{R}\} = B(y)$, for all $x, y \in \mathbb{R}$. Furthermore, A is called the first marginal possibility distribution of C, and B is called the second marginal possibility distribution of C.*

Definition 1.4 (Schweizer and Sklar [7]). *A function*

$$T\colon [0,1] \times [0,1] \to [0,1],$$

is said to be a triangular norm if T is symmetric, associative, non-decreasing in each argument, and $T(x,1) = x$ for each $x \in [0,1]$.

Often we will simple write t-norm instead of triangular norm [8]. Let C be the joint possibility distribution of $A, B \in \mathcal{F}$. Then we have,

$$C(x,y) \leq \min\{A(x), B(y)\},$$

for all $x, y \in \mathbb{R}$ and $\alpha \in [0,1]$.

Definition 1.5 (Fullér and Majlender in [5]). *Fuzzy numbers A and B, are said to be non-interactive if their joint possibility distribution is given by*

$$C(x,y) = \min\{A(x), B(y)\},$$

for all $x, y \in \mathbb{R}$.

In other words, $A, B \in \mathcal{F}$ are non-interactive then their joint possibility distribution is defined by $A \times B$ [9].

We shall recall now *Zadeh's sup-min extension principle* which plays a fundamental role in extending crisp functions to fuzzy functions.

Definition 1.6 (Zadeh [14]). *Suppose that X and Y are crisp sets and let f be a mapping from X to Y,*

$$f\colon X \to Y.$$

Let $A \in \mathcal{F}(X)$. Then using the sup-min extension principle, we can define $f(A)$ as a fuzzy subset of Y such that

$$f(A)(y) = \sup_{x \in f^{-1}(y)} A(x) \tag{1}$$

if $f^{-1}(y) \neq \emptyset$ and $f(A)(y) = 0$ if $f^{-1}(y) = \emptyset$ (the supremum is set to zero).

It should be noted that we use thy same notation for function and for its extension. The sup-min extension principle can be generalized to two-place (or more generally to n-place) functions.

Definition 1.7 (Zadeh [14]). *Let f be a function,*

$$f\colon X \times X \to Y.$$

Let $A, B \in \mathcal{F}(X)$ be fuzzy, then the sup-min extension defines $f(A,B) \in \mathcal{F}(Y)$ as,

$$f(A,B)(z) = \sup_{(x,y)\in f^{-1}(z)} \min\{A(x), B(y)\}, \tag{2}$$

if $f^{-1}(z) \neq \emptyset$ and $C(z) = 0$ if $f^{-1}(z) = \emptyset$ (the supremum is set to zero).

The following two theorems (Nguyen, 1978) show that similar representations are valid for any extended continuous function.

Theorem 1.1 (Nguyen, [10]). *Let X be a locally compact topological space, let*

$$f\colon X \to X$$

be a continuous function and let $A \in \mathcal{F}(X)$. Then

$$[f(A)]^\alpha = f([A]^\alpha)$$

where $f(A)$ is defined by the extension principle (1) and

$$f([A]^\alpha) = \{f(x) \mid x \in [A]^\alpha\}.$$

Example 1.1. If A is a fuzzy number and

$$[A]^\alpha = [a_1(\alpha), a_2(\alpha)],$$

and, furthermore, f is monotone decreasing then from Theorem 1.1 we get

$$\begin{aligned} {}^\alpha &= f([A]^\alpha) \\ &= f([a_1(\alpha), a_2(\alpha)]) \\ &= [f(a_2(\alpha)), f(a_1(\alpha))]. \end{aligned}$$

Theorem 1.2 (Nguyen,[10]). *Let X, Y be locally compact topological spaces and let $f\colon X \times Y \to X$ be a continuous function and let $A \in \mathcal{F}(X)$ and $B \in \mathcal{Y}(Y)$ be fuzzy sets. Then*

$$[f(A,B)]^\alpha = f([A]^\alpha, [B]^\alpha)$$

where

$$f([A]^\alpha, [B]^\alpha) = \{f(x,y) \mid x \in [A]^\alpha, y \in [B]^\alpha\}.$$

Let $f\colon \mathbb{R}^2 \to \mathbb{R}$ be defined as

$$f(x,y) = x + y,$$

i.e. f is the addition operator on the real line.

Example 1.2. Suppose $[A]^\alpha = [a_1(\alpha), a_2(\alpha)]$ and $[B]^\alpha = [b_1(\alpha), b_2(\alpha)]$ are fuzzy numbers. Then using the sup-min extension principle we get

$$(A + B)(z) = \sup_{x+y=z} \min\{A(x), B(y)\}$$

Then,

$$[A + B]^\alpha = [a_1(\alpha) + b_1(\alpha), a_2(\alpha) + b_2(\alpha)] = [A]^\alpha + [B]^\alpha,$$

for all $\alpha \in [0, 1]$.

Definition 1.8 (Fullér and Keresztfalvi [11]). *If T is a t-norm, $f : X \times Y \to Z$, $A \in \mathcal{F}(X)$ and $B \in \mathcal{F}(Y)$ then the fuzzy set $f(A, B) \in \mathcal{F}(Z)$ is defined via the extension principle by*

$$f(A, B)(z) = \sup_{f(x,y)=z} T(A(x), B(y)), \ z \in Z. \tag{3}$$

In 1991 Fullér and Keresztfalvi [11] generalized Theorems 1.1 and 1.2 to sup-t-norm extended functions.

Theorem 1.3 (Fullér and Keresztfalvi [11]). *Let $X \neq \emptyset$, $Y \neq \emptyset$, $Z \neq \emptyset$ be sets and let T be a t-norm. If $f : X \times Y \to Z$ is a two-place function and $A \in \mathcal{F}(X)$, $B \in \mathcal{F}(Y)$ then a necessary and sufficient condition for the equality*

$$[f(A, B)]^\alpha = \bigcup_{T(\xi,\eta)\geq\alpha} f([A]^\xi, [B]^\eta), \ \alpha \in (0, 1], \tag{4}$$

is, that for each $z \in Z$,

$$\sup_{f(x,y)=z} T(A(x), B(y))$$

is attained.

The next theorem shows that the equality (4) holds for all upper semi-continuous triangular norm T and continuous function f in the class of upper semi-continuous fuzzy sets of compact support. When X is a topological space, we denote by $\mathcal{F}(X, \mathcal{K})$ the set of all fuzzy sets of X having upper semi-continuous, membership function of compact support.

Theorem 1.4 (Fullér and Keresztfalvi, [11]). *If $f : X \times Y \to Z$ is continuous and the t-norm T is upper semi-continuous, then*

$$[f(A, B)]^\alpha = \bigcup_{T(\xi,\eta)\geq\alpha} f([A]^\xi, [B]^\eta), \ \alpha \in (0, 1], \tag{5}$$

holds for each $A \in \mathcal{F}(X, \mathcal{K})$ and $B \in \mathcal{F}(Y, \mathcal{K})$.

Equation (5) is known in the literature as Nguyen-Fullér-Keresztfalvi (NFK) formula [21].

Let $f\colon \mathbb{R}^2 \to \mathbb{R}$ be defined as

$$f(x, y) = x + y,$$

i.e. f is the addition operator on the real line.

Example 1.3. Suppose $[A]^\alpha = [a_1(\alpha), a_2(\alpha)]$ and $[B]^\alpha = [b_1(\alpha), b_2(\alpha)]$ are fuzzy numbers. Then using the sup-product-t-norm extension principle we get

$$(A+B)(z) = \sup_{x+y=z} A(x)B(y)$$

Then,

$$[A+B]^\alpha = \bigcup_{\xi\eta\geq\alpha} \left([A]^\xi + [B]^\eta\right)$$

for all $\alpha \in [0,1]$.

2 The Extension Principle for Interactive Fuzzy Numbers

Using the concept of joint possibility distribution Carlsson, Fullér and Majlender [12] introduced the following sup-C extension principle in 2004.

Definition 2.9 (Carlsson, Fullér and Majlender [12]). *Let C be the joint possibility distribution with marginal possibility distributions $A, B \in \mathcal{F}$, and let $f\colon \mathbb{R}^2 \to \mathbb{R}$ be a continuous function. Then $f(A,B)$ the sup-C extension of f is defined by,*

$$f(A,B)(z) = \sup_{z=f(x,y)} C(x,y). \tag{6}$$

It can be shown (Carlsson, Fullér and Majlender [12] for details) that $f(A,B)$ will be a fuzzy number for any continuous function f.

Note 1. If A, B are non-interactive then (6) turns into Zadeh's sup-min extension principle [14]. And, if

$$C(x,y) = T(A(x), B(y)), \tag{7}$$

where T is a t-norm then we get the t-norm-based extension principle (3).

In 2004 Carlsson, Fullér and Majlender [12] proved the following theorem, which can be considered as the most general form of NFK theorem for fuzzy numbers.

Theorem 2.5 (Carlsson, Fullér and Majlender [12]). *Let $A, B \in \mathcal{F}$ be fuzzy numbers, let C be their joint possibility distribution, and let*

$$f\colon \mathbb{R}^2 \to \mathbb{R}$$

be a continuous function. Then, $f(A,B)$ is a fuzzy number and furthermore,

$$[f(A,B)]^\alpha = f([C]^\alpha),$$

for all $\alpha \in [0,1]$.

We will show now an interesting example (based on Fullér [13]) for the extension principle with interactive fuzzy numbers.

If A is a fuzzy number then,

$$C(x,y) = A(x)\chi_{\{x-y=0\}}(x,y), \tag{8}$$

where,

$$\chi_{\{x-y=0\}}(x,y) = \begin{cases} 1, \text{ if x=y;} \\ 0, \text{ otherwise;} \end{cases}$$

defines a joint possibility distribution with marginal possibility distributions A and B, where $B = A$. Now let $f(x,y) = x - y$. Then,

$$\begin{aligned} f(A,B)(z) &= (A-B)(z) \\ &= \sup_{z=x-y} A(x) \cdot \chi_{\{x=y\}}(x,y). \end{aligned}$$

Then we get

$$(A-B)(z) = \begin{cases} 1, \text{ if z=0;} \\ 0, \text{ otherwise.} \end{cases}$$

In other words, if A is a fuzzy number and C is defined by (8) then its marginal possibility distributions A and B have identical membership function, and furthermore, we have,

$$A - B = \bar{0},$$

where

$$\bar{0}(z) = \begin{cases} 1, \text{ if z=0;} \\ 0, \text{ otherwise.} \end{cases}$$

This case is very similar to the definition of $X - Y$, where X and Y are random variables. If $Y = X$ we get

$$X - Y = 0,$$

and in this case their joint probability density function is defined by $f_{X,Y}(x,y) = f_X(x)\delta(x-y)$.

3 Recent Developments

In 2001 Wagenknecht, Hampel and Schneider [15] used the NFK theorem (5) to compute the α-level sets of extended addition and multiplication of fuzzy numbers of type LR. In 2005 Carlsson and Fullér [16] summarized some properties of the extended addition operator on fuzzy numbers, where the interactivity relation between fuzzy numbers is given by their joint possibility distribution. In 2008 Gera and Dombi [17] discussed extended t-norms and t-conorms on continuous and interactive fuzzy truth values and using the NFK theorem they showed that complex convolutions of the extended operations are equivalent to simple point-wise expressions for several special cases. Their computation method can also be applied immediately to type-2 fuzzy set operations. In 2008 Chalco-Cano

[18] proposed a decomposition of large ranges of uncertainty associated with the Cartesian product of two fuzzy intervals. Then computed an approximation of the fuzzy set obtained by applying extension principle to a real function by means of this decomposition and piecewise linearization of the function. In 2010 Wu [19] extended the NFK theorem to a wider class of aggregation functions. In 2012 Scheerlinck, Vernieuwe, and De Baets [20] considered Zadeh's sup-min extension principle for continuous functions, where both the input variables and the output variable are fuzzy intervals. Using a parallel optimization approach they designed a Fuzzy Calculator to efficiently compose the membership function of the output. In 2013 Bzowski and Urbański [21] formulated the general NFK theorem, which does not require assumptions on the shape of fuzzy sets, t-norms, nor topology of underlying spaces. They also showed that NFK theorem (5) can be extended to the class of fuzzy sets with unbounded supports. Using the NFK theorem in 2013 Hong [22] obtained some interesting results of the strong laws of large numbers for triangular norm-based addition of fuzzy set-valued random variables.

Acknowledgment. This works has been partially supported by the Hungarian Scientific Research Fund OTKA K-106392.

References

1. Fullér, R.: Fuzzy Reasoning and Fuzzy Optimization. TUCS General Publications, No. 9, Turku Centre for Computer Science, Åbo (1998)
2. Fullér, R.: Neural Fuzzy Systems, Åbo Akademis tryckeri, Åbo, ESF Series A:443 (1995)
3. Carlsson, C., Fullér, R.: Concepts and issues. In: Carlsson, C., Fullér, R. (eds.) Possibility for Decision. STUDFUZZ, vol. 270, pp. 7–25. Springer, Heidelberg (2011)
4. Hong, D.H., Moon, E.L., Kim, J.D.: Remarks on possibilistic variances of fuzzy numbers. Journal of Applied Mathematics and Computing 36, 163–171 (2011), doi:10.1007/s12190-010-0394-7
5. Fullér, R., Majlender, P.: On interactive fuzzy numbers. Fuzzy Sets Systems 143, 355–369 (2003), doi:10.1016/S0165-0114(03)00180-5
6. Fullér, R., Mezei, J., Várlaki, P.: An improved index of interactivity for fuzzy numbers. Fuzzy Sets and Systems 165, 56–66 (2011), doi:10.1016/j.fss.2010.06.001
7. Schweizer, B., Sklar, A.: Associative functions and abstract semigroups. Publ. Math. Debrecen 10, 69–81 (1963)
8. Hong, D.H., Ro, P.I.: The law of large numbers for fuzzy numbers with unbounded supports. Fuzzy Sets and Systems 116, 269–274 (2000), doi:10.1016/S0165-0114(98)00188-2
9. Carlsson, C., Fullér, R.: A Normative View on Possibility Distributions. In: Carlsson, C., Fullér, R. (eds.) Possibility for Decision. STUDFUZZ, vol. 270, pp. 27–76. Springer, Heidelberg (2011)
10. Nguyen, H.T.: A note on the extension principle for fuzzy sets. Journal of Mathematical Analysis and Applications 64, 369–380 (1978), doi:10.1016/0022-247X(78)90045-8

11. Fullér, R., Keresztfalvi, T.: On generalization of Nguyen's theorem. Fuzzy Sets and Systems 41, 371–374 (1991), doi:10.1016/0165-0114(91)90139-H
12. Carlsson, C., Fullér, R., Majlender, P.: Additions of Completely Correlated Fuzzy Numbers. In: FUZZY IEEE 2004, Budapest, Hungary, pp. 535–539 (July 2004), doi:10.1109/FUZZY.2004.1375791
13. Fullér, R.: Some Criteria for Equality of Possibilistic Variables. In: Seventh International Symposium on Intelligent Systems and Informatics, Subotica, Serbia, pp. 17–20 (September 2009), doi:10.1109/SISY.2009.5291175
14. Zadeh, L.: The concept of a linguistic variable and its application to approximate reasoning - I. Information Sciences 8, 199–249 (1975), doi:10.1016/0020-0255(75)90036-5
15. Wagenknecht, M., Hampel, R., Schneider, V.: Computational aspects of fuzzy arithmetics based on Archimedean t-norms. Fuzzy Sets Systems 123, 49–62 (2001), doi:10.1016/S0165-0114(00)00096-8
16. Carlsson, C., Fullér, R.: On additions of interactive fuzzy numbers. Acta Polytechnica Hungarica 2, 59–73 (2005)
17. Gera, Z., Dombi, J.: Exact calculations of extended logical operations on fuzzy truth values. Fuzzy Sets Systems 159, 1309–1326 (2008), doi:10.1016/j.fss.2007.09.020
18. Chalco-Cano, Y., Jimenez-Gamerob, M., Roman-Floresc, H., Rojas-Medard, M.A.: An approximation to the extension principle using decomposition of fuzzy intervals. Fuzzy Sets Systems 159, 3245–3258 (2008), doi:10.1016/j.fss.2008.06.011
19. Wu, H.-C.: Generalized Extension Principle. Fuzzy Optimization Decision Making 9, 31–68 (2010), doi:10.1007/s10700-010-9075-0
20. Scheerlinck, K., Vernieuwe, H., De Baets, B.: Zadeh's Extension Principle for Continuous Functions of Non-Interactive Variables: A Parallel Optimization Approach. IEEE Transactions on Fuzzy Systems 20, 96–108 (2012), doi:10.1109/TFUZZ.2011.2168406
21. Bzowski, A., Urbański, M.K.: A note on Nguyen-Fullér-Keresztfalvi-theorem and Zadeh's extension principle. Fuzzy Sets Systems 213, 91–101 (2013), doi:10.1016/j.fss.2012.09.004
22. Hong, D.H.: Strong laws of large numbers for t-norm-based addition of fuzzy set-valued random variables. Fuzzy Sets and Systems 223, 26–38 (2013), doi:10.1016/j.fss.2013.01.011

Towards Knowledge Driven Adaptive Product Representations

László Horváth

Óbuda University, John von Neumann Faculty of Infomatics,
Institute of Applied Mathematics
1034 Budapest, Bécsi út 96/B, Hungary
horvatth.laszlo@nik.uni-obuda.hu

Abstract. Highly integrated engineering models are developed for lifecycle of industrial products towards increased self-development capabilities. Adaptive model has the capability to change itself in accordance with changed circumstances and events. Knowledge content in product model gives this capability for the modification of affected model entities as a result of changed parameters in the modeled product objects or the environment of the modeled product. This capability of the model is based among others on the well proven feature principle. According to this principle, product model is developed in the course of a series modification feature definitions. Modification by a feature is propagated through contextual connection chains of parameters of the modifying and modified features. Considering the recent development history of product modeling, product object feature driven models have been developed towards knowledge feature driven models where product object representations are generated and modified by active knowledge features. At the same time, lifecycle models of products are more and more interdisciplinary where product objects from mechanical, electrical, electronic, computer and other areas of engineering are included in a single model and handled by the same mechanism of modeling. However, interdisciplinary product model needs representations on higher abstraction levels than product object features. This chapter introduces some works and results from recent research activities contributing to the above sketched development history. It starts with scenario of current product modeling and the self-development capability of product models. Following this, the concept of product model affect zone and method to organize context definitions are proposed. The main contribution in the chapter includes introduction of different concepts for the abstraction levels in product model as well as abstraction levels and the related knowledge representations in the proposed coordinated request driven product model (CRPM). Finally, possible integration of the CRPM method into PLM systems is discussed.

Keywords: Product lifecycle management (PLM), feature driven product model, adaptive product representations, abstraction levels in product model.

J. Fodor and R. Fullér (eds.), *Advances in Soft Computing, Intelligent Robotics and Control,* Topics in Intelligent Engineering and Informatics 8,
DOI: 10.1007/978-3-319-05945-7_13,

1 Introduction

The history of computer application in product development started with urgent need for mathematically represented shapes in aircraft and rocket industries during the 50s of the past century. Starting from this point, a fantastic development started with computer assisted engineering in the past century and resulted computer centered engineering in the beginning of this century. The author of this chapter participated in this history and knows that it is not easy to understand results of advanced mathematics, physics, computational intelligence, object modeling, and other leading research results in the every day industrial engineering processes. Similarly to other high technology intensive areas of industry, advanced solutions are needed to establish quick and reliable product prototyping in virtual space replacing the restricted, time consuming, and expensive conventional methods of product development. Engineering oriented virtual spaces have the capabilities to accommodate and apply accumulated expertise and experience at companies.

Recent and future development of industrial product modeling is determined by four critical market demands. They are extensive info-communication during the entire lifecycle of product, representation of objects for different engineering areas in a single model, quick response of the model for changed situations and events, and representation of active corporate knowledge in product model. This chapter is organized around recent advanced product modeling theories, concepts, and methods to fulfill the above four demands. Because integration is one of the main issues in product modeling, own results in integration are discussed together with recent achievements in leading product lifecycle management (PLM) system development. Beyond classical problems and solutions in product modeling, higher level knowledge driven product definition and modeling on higher level of abstraction are emphasized. In close connection with abstraction and its knowledge background, application of soft computing methods and methods from systems engineering are also discussed in this chapter.

It is important to avoid the common mistake of considering the proposed methods as part of new methodology for a stand alone new modeling system. The currently representative product modeling is result of more than sixty years research and development work at the competitive edge in the world. It would be impossible to develop appropriate and enough precise experimental environment for our modeling methods. This is why we consider application of theoretically and methodically appropriate and enough high level modeling in a PLM system product for the experimental purpose. In this view, development of the proposed methods in order to prepare a laboratory for verification and application purpose needs only implementation. Open PLM architectures provide integrated means to define new object classes together with the required parameter, relationship, and procedure definitions. At the same time, recent PLM systems inherently provide features for the representation of wide range knowledge and other abstraction content.

2 Developing Product Representations

Understanding recent quick changes of concepts and methods in product representations is often made more difficult by a mistake that the current advanced PLM systems are the advanced versions of the computer aided (CAD/CAM/-CAE, etc.) systems from the past century. At the same time, it is inevitable that the currently representative PLM technology was developed on the basis of these pioneer engineering technologies. However, current PLM technology represents a new age of engineering and includes dozens of new concepts, principles, approaches, and methodologies. In the opinion of the author of [3], PLM is a new paradigm for product manufacturing industry which improves all product related activities at companies.

Research in product representations is concentrated on feature definitions, corporate knowledge representations, human-computer interactions, and application of methods from systems engineering. Lifecycle management of product data needs feature which can be applied at more or less downstream engineering activities [6]. In [6], extended life cycle definition of feature is proposed and defined. Application of soft computing in engineering design facilitates fuzzy logic, genetic algorithm, and artificial neural network representation capabilities for numerous hard-to-solve engineering tasks [9]. Methods from systems engineering help the development of abstraction in product model. In [12], application of the requirements, functions, logical connections, and physical representations (RFLP) structure is introduced for abstract product representation as baseline for systems engineering supported PLM. This enhances interaction and collaboration between disciplines in product engineering. It seems that application of system of systems engineering (SoSE) methods can not be avoided in PLM developments where independent systems are to be handled [17]. Authors of [10] emphasize importance of standards in systems engineering and SoSE and introduces activities about management of the related standards.

Long research work accumulated results achieved by the authors of the publications cited below during the past twenty years in order to produce a vast of preliminaries to the work which is introduced in this chapter. Paper [18] introduces a new method for the application of machine learning methods at manufacturing process planning in order to knowledge based integration of this group of engineering activities with other activities of product engineering. In [19], the above engineering activity group is analyzed for the efficiency of computer interactions at decision making and knowledge acquisition in engineering modeling. On the way to multilevel abstraction, an early work in [20] resulted multilevel modeling of manufacturing processes. For this purpose, application of Petri Net was considered together with advanced knowledge representation. Method is conceptualized in [21] for Petri Net generation for representation of manufacturing process model entities. Process of this modeling is outlined in [22]. Importance of human intent modeling is emphasized and methodology is introduced in [23] in order to realize intelligent modeling of manufacturing processes. The simultaneous modeling aspect is analyzed in [24] where manufacturing process is modeled in collaborative environment. Feature based integration of machining process

model with part model is conceptualized and manufacturing process features are defined in [25]. Strengthened virtual engineering methodology motivates application of virtual technology for integration of associative representations around mechanical parts in [26]. As result of research for the application of the feature principle in model integration, a method is given in [27] for the generation of robot assembly paths using form features and considering product variants. In close connection with this work, shape and robot process model features are connected by relationships in [28]. Product model information structure is analyzed and discussed, and engineering modeling methods for problem solving are organized in the monograph [2]. In [29], change management is analyzed in industrial engineering model considering application of intelligent computing. Human intent and knowledge are analyzed in order to establish improved means for the management of changes at product modeling in [30]. Emerging PLM technology motivates a new approach to knowledge intensive PLM product modeling in [31]. An early research result in multi-level abstraction based product representation is introduced in [7] as a new method for information content driven product definition. Paper [16] introduces new processes in order to realize global level human interaction at knowledge based product definition. Earlier findings and definitions in application of knowledge technology at product definition are summarized in a chapter of the book [4]. Issues of systems engineering are mixed with issues in product model representation in [32] for better decision making in engineering systems. As a contribution to the new trend of request driven modeling in PLM systems requested behavior driven control of product definition with initial methodology is introduced in [11]. In paper [8], methodology is introduced for the situation driven control using active knowledge at the definition of product.

In order to establish a comprehensive conceptual basis for product modeling in this chapter, Fig. 1 introduces the current representative scenario. The result of product definition consists of contextually connected features. Features are included in an object model where object classes and taxonomy serve the information technology background. Methodology of feature definitions in object oriented environments was grounded by the product model standard ISO 10303. International efforts in order to establish product model standard by International Organization for Standardization (ISO) during eighties and nineties produced connectional and methodological basics of model construction resource based and feature driven object model which can be implemented by using of engineering area specific application protocols. The AP203 for configuration controlled 3D designs of mechanical parts and assemblies, the AP214 for automotive mechanical design, and the AP212 for electrotechnical design and installation were developed in close connection strengthening the integration of product modeling areas. Many researches aimed at handling advanced knowledge representations in ISO 10303 based models. Authors of [5] state that the above standard is focused on representation of product data. They propose a framework to integrated data and knowledge models assuring reuse of expertise in product modeling environments.

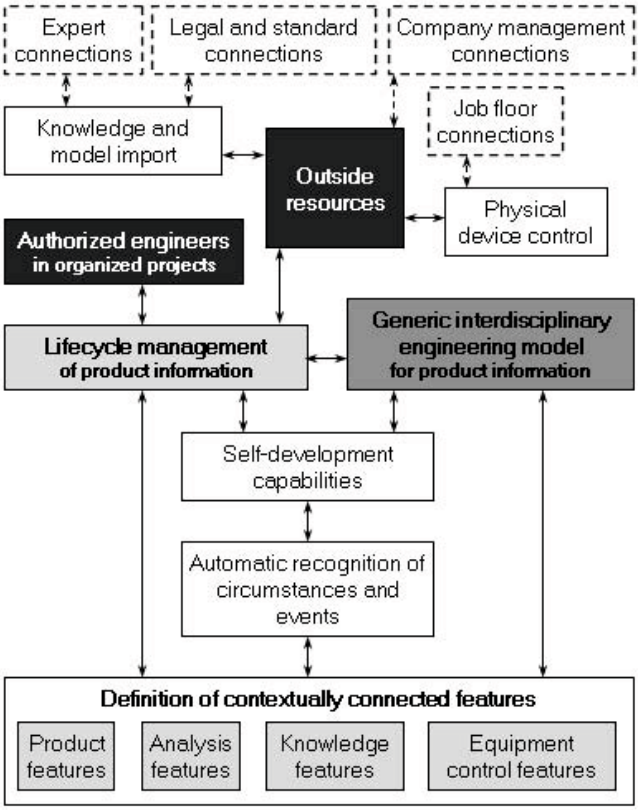

Fig. 1. Scenario of current product modeling

Product modeling processes use outside resources in less or more integration. Knowledge and model import comes from expert, legal, and standard connections. Company management connections communicate company strategies, decisions, and the related company information. Job floor connections are mainly related with physical device control.

Authorized engineers work in organized projects. Wide range of less or more integrated function sets serve group work of engineers who are in task and role specific contexts. Hundreds even thousands of engineers work on product ranges in organizations at companies and their subsidiaries. Various virtual company management methods are applied. Recently, integration of features from this area into product model is one of the main promising developments in engineering.

Engineering activities for a range or family of products are concentrated in lifecycle management of product information. For these activities, PLM systems provide development environments in order to facilitate third party and application developments. This is important because knowledge is available at the companies. Knowledge in the product model is property of companies and it is protected.

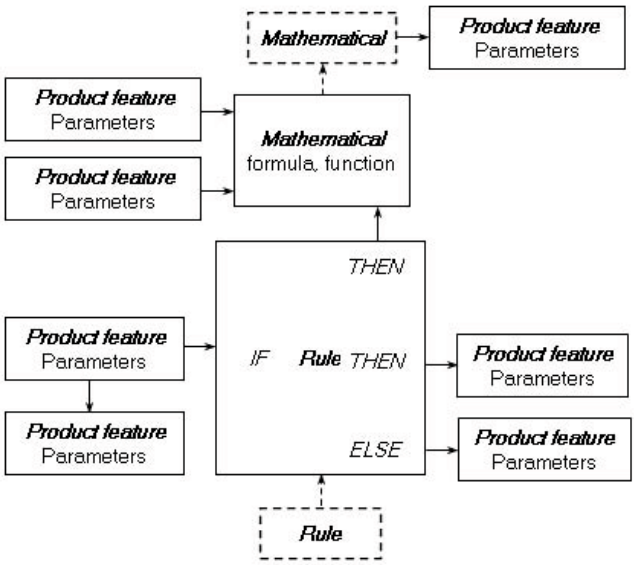

Fig. 2. Self-development capability

Generic interdisciplinary engineering model (Fig. 1) accommodates product information. Definition of product features from the viewport of the modeling system is important mainly at the beginning of a product development. It is gradually replaced by self-development capabilities of the product model. These capabilities take the control from humans and utilize active knowledge in product model. Knowledge is activated by automatic recognition of circumstances and events.

As it is explained above, contextually connected features are defined by human interaction or knowledge activation. Product features represent product units and elements together with their relationships. Analysis features describe analysis activities and results in order to representation of actual product behavior in the application environment. Equipment control features represents control programs and specific objects of production systems, equipment, and devices. Recently, production environment is considered as organic part of PLM systems providing physical end users. Knowledge features represent relationships and other knowledge items for the definition of the other three groups of features.

Self-development capabilities of the product model utilize knowledge at the definition of contextual parameter connections amongst product features. The example in Fig. 2 is a typical configuration in current product models. Parameters of a product feature are selected as conditions for a rule. At the same time, these parameters are in direct connection with some parameters of other product feature. Direct connection is defined where a feature or its parameters are applied at the definition of other feature. For example, a curve is a parameter of a surface shape of which is controlled by the curve. On the THEN branch

of rule product feature parameters are defined and mathematical formula or function is connected to other mathematical entity which controls parameters of other product feature. On the ELSE branch, product parameters are defined. The above rule is controlled by other rule. This is the case, for example, when different situations require different rules.

3 Organizing Contextual Connections in Product Model

Increasing number of product features and associated unarranged contextual connections makes handling of model changes including definition of new product features more and more difficult. This is one of the problems in modeling for extensive product development products and motivates important researches. First problem is finding organized means for tracking change propagation. In [29], change affect zone (CAZ) was defined as entity to record connections of a product object in the product model. Recently, this method was evaluated and revised considering actually representative PLM models. The revised method is sketched in Fig. 3.

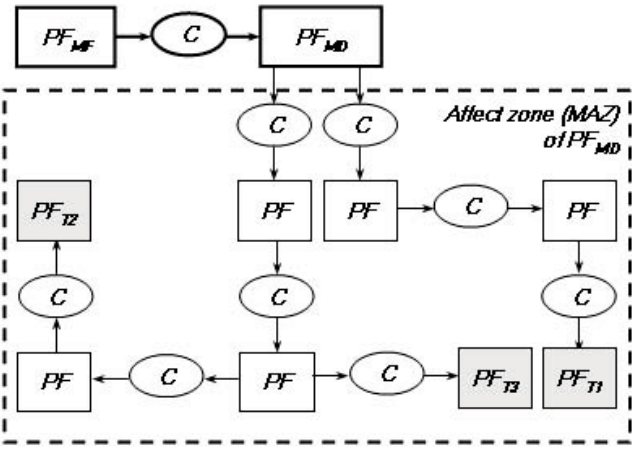

Fig. 3. Affect zone of a modification by feature

Fig. 3 shows an example for affect zone of product feature PF_{MD}. PF_{MD} modifies the product model detail of which is shown in Fig. 3. PF_{MD} is defined in the context of product feature PF_{MF}. C is for an arbitrary contextual connection. Modification by PF_{MD} is propagated along three branches of product features. The product features PF_{T1}, PF_{T2}, and PF_{T3} have special role. The propagation is terminated at these features. This as the modification affect zone (MAZ) referring to the application of mod-ification of model on the principle of contextual features.

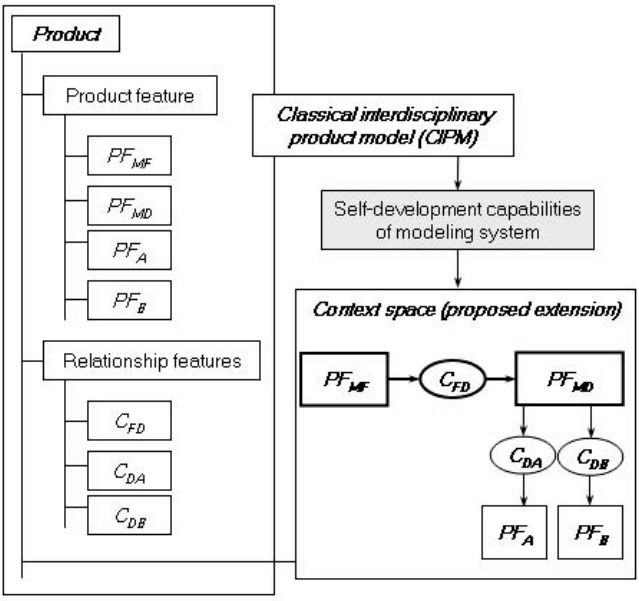

Fig. 4. Organizing context definitions

The next question is how organizing entities can be included in a product model as features. For this purpose, the classical product model (CPM) was defined in [7]. At the time of that publication, CPM was considered as a representative state-of-the-art product model which serves as starting point for the research in organized relationships within product model. By now, product models include features for the representation of active knowledge and abstraction levels. In order to develop the CPM idea, classical interdisciplinary feature driven product model (CIPM) was defined (Fig. 6).

The main principle of organizing context definitions is sketched in Fig. 4. Detail of a CIPM includes four product (PF) and three relationship (C) features. In a typical CIPM, these features are included in two groups. Position within the groups represents the place at which the model is modified by the actual feature. While this information in essential in a feature derive product model, it does not assist tracking of indirect modification affects. As a possible solution, Fig. 4 introduces the feature context space (CS) which is proposed to extend the CIPM. Really, CS is a map of contexts in which product features PF_{MF}, PF_{MD}, PF_A, and PF_B are connected by relationship features C_{FD}, C_{DA}, and C_{DB}. Relationship features act as contextual connections in the product model. CP is connected to the product model by using of self-development capabilities of the CIPM modeling system.

4 Abstraction Levels in Product Model

The need for more advanced decision assistance, the advances in integration of knowledge driven model definition, the increasing emphasis on handling of product behaviors and nonlinear problems, and the need for multidisciplinary product model motivate researches to establish abstraction levels in the product model.

As an early contribution to efforts in establishment of abstraction levels, a new concept and method was introduced to include content which is behind CPM object information in product model [7]. The main objective was to produce interactive knowledge transfer from humans to information based modeling procedures in order to better explanation and evaluation of engineering objects at decision making during product definition.

Information content facilitated new adaptive characteristics in product model [7]. Information content was placed in an abstraction structure which included five levels (Fig. 5). Intent of humans included knowledge to fulfill engineering objectives. Meaning of new concepts which were unknown for the modeling system was introduced on the second level. Engineering objectives were modeled by expected product behavior on the third level. A suitable extended definition of product behavior was published in [31]. The fourth level included contextual connections. Decisions on features as engineering objects were placed on the fifth level. It is obvious that all levels must be mapped to feature definitions in the CPM model. For this purpose, intent, behavior, and decision contextual spaces were defined. Spaces and their contextual connections were published in [16]. In the recent years, the most advanced PLM systems started to involve abstraction levels mainly for unified handling of abstract features in multidisciplinary product models. These systems apply integrated feature driven adaptive product model abstraction which is based on the RFLP [12] structure. RFLP structure is well known in systems engineering. Consequently, it can be stated that abstraction is a step towards enhanced application of systems engineering in PLM product definitions. The RFLP [12] structure consists of requirements against the product, functions to fulfill requirements, structure of logical components, and representations of real world product (Fig. 5). In other words, the abstraction is done on the requirement, function, logical, and physical levels. In Fig. 5, the dashed lines show logical connections of pairs of levels. The real connection is realized through the integrated product model.

Because the modeling methods which are proposed in this chapter are devoted to integrate in PLM environments, equivalence of levels in the two abstraction of the Fig. 5 is important. Equivalences are illustrated by dotted lines. Requirements for the RFLP structure can be produced by the levels of intent of humans and meaning of concepts. Engineering objectives are represented by behaviors considering product functions. Structure of logical connections are covered by appropriately defined contexts. Finally, decisions include information for product features so that this level can be connected to the physical level.

Development of the above introduced abstraction by using of five levels of information content was applied at the concept and method of coordinated request

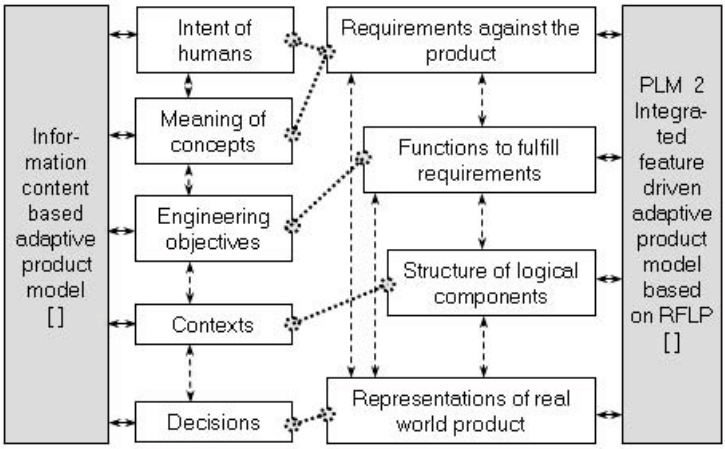

Fig. 5. Comparison of the information content based and the RFLP concepts

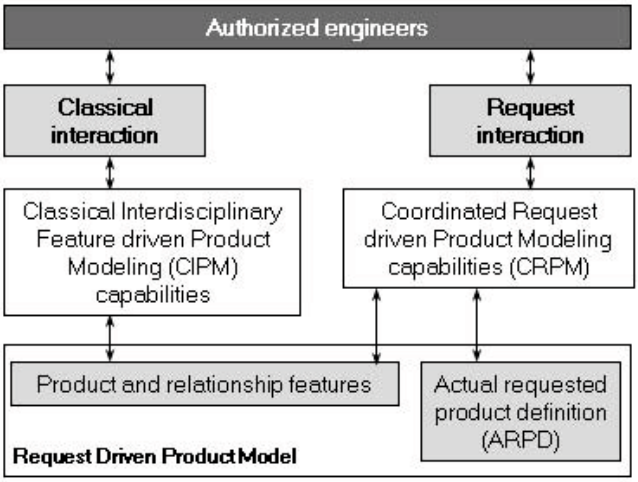

Fig. 6. Coordinated Request driven Product Modeling

driven product modeling (CRPM). Fig. 6 explains the cooperation of CIPM and CRPM. Authorized engineers must have the choice of classical and request interaction. CIPM capabilities generate product and relationship features on the basis of interacted feature definitions. Capabilities for CRPM are in communication with CIPM capabilities through product and relationship features. At he same time, they generate abstraction level features in the actual requested product definition (ARPD) extending the CIPM model to request driven product model.

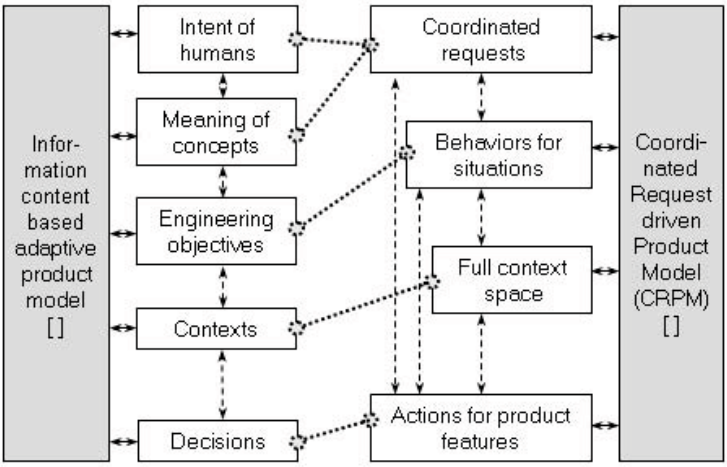

Fig. 7. Comparison of the information content based and the CRPM concepts

Establishment of the CIPM-CRPM connection requires extensive research in the future especially for the features through which the communication is done in case of various representative professional industrial PLM modeling methodologies.

The abstraction levels of the information content based adaptive product model had to be modified in order to integration with PLM product models. The modified sequence of levels is applied in the coordinated request driven product model (CRPM). Levels are shown in Fig. 7 in comparison with the original information content based levels. Equivalences are illustrated by dotted lines. Levels of intent of humans and meaning of concepts are merged in coordinated request. Engineering objectives are represented as behaviors for situations. Contexts are represented in full context space in order to facilitate any structure of logical connections to include. Finally, decisions are represented as actions for product features.

5 Coordinated Request Driven Product Modeling

Main capabilities of the modeling by using of the CRPM together with the main connections are introduced in Fig. 8. Request interaction drives request definition. The defined request features are generated and placed in the actual requested product definition (ARPD). At the same time, request interaction communicates with the request feature generation directly. Request interaction by authorized engineers can define features in the CIPM model. Regardless the level of abstraction and automation of product definition, the project leaders may allow this direct feature definition. Requests are coordinated. This coordination is supported by consequence analysis. Method of consequence analysis was published in [30]. Coordinated requests drive behavior feature generation.

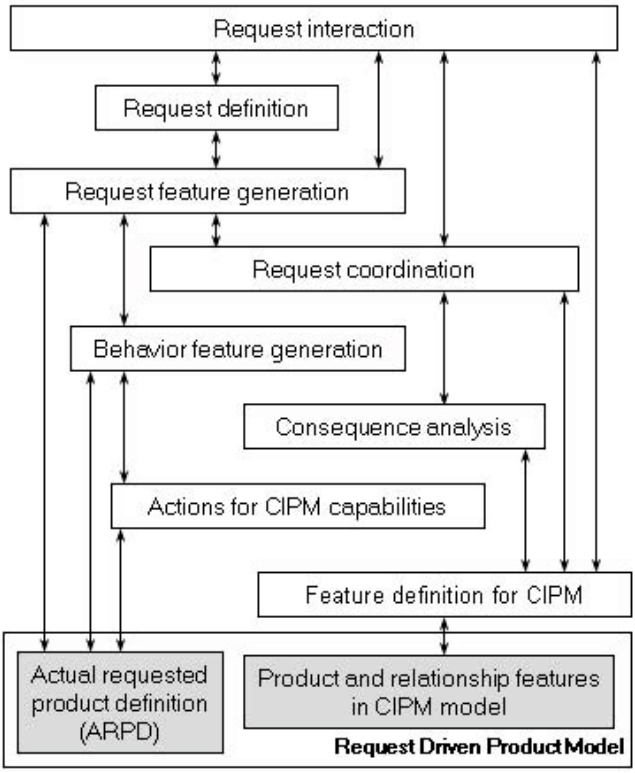

Fig. 8. Coordinated request driven product modeling (CRPM) capabilities

Behavior includes actions. These actions are configured to drive CIPM capabilities. Request coordination and consequence analysis also can communicate with the feature definition for CIPM directly.

PLM systems provide very flexible means of feature and contextual connection definitions. However, threshold knowledge can not be broken. Threshold knowledge is defined in [4] as the knowledge which inevitably applies to avoid definite deterioration in the quality of model or product.

Request consists of product function, specification, procedure, and configuration features. Product function is defined individually, in a set, or in product or product unit specific structure. Specification may be independent of function or function related. It may be defined in set or structure. Configuration is a pattern of product features. Procedure carries knowledge and process for the definition of function, specification, and configuration. Request definition utilizes the contextual feature drive principle. Request may be arbitrary incomplete. When a coordinated request is mapped in a behavior, it is completed by stored corporate knowledge and knowledge assisted human decision. At the same time, feature generations are done by knowledge in procedures.

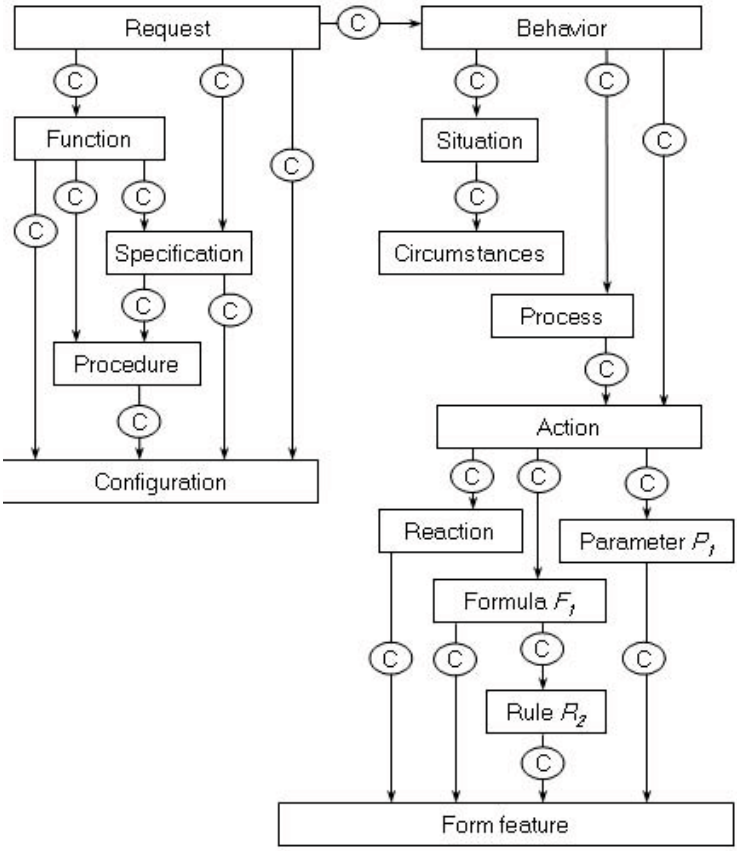

Fig. 9. Contextual connections in the request driven product model

Fig. 8 shows an inherently configured contextual structure of request driven product model features. Product function, specification, procedure, and configuration features are defined in the context of request. At the same time, these features also have contextual connection definitions. Behavior is defined in the context of request. Situation is defined in the context of behavior while circumstances are defined in the context of situation. Circumstances for a situation are mapped to features in the relevant request. However, this can be done only through the request-behavior contextual connection.

Fig. 9 shows the contextual connection between action feature in the CRPM and the knowledge carrier features in the CIPM. In the example in Fig. 9, a reaction, parameter P_1, and formula F_1, features are generated in the context of the definition carried by the action feature. Rule R_2 is generated in the context of formula F_1. The above knowledge features drive appropriate features in the CIPM.

6 Knowledge in the CRPM Model

As it was explained and discussed above, knowledge is defined by authorized engineers and communicated with the model generation environment in the course of request interaction (Fig. 10). At the decisions for product definition human applies stored engineering experience and add personal experience and expertise. In a simplified schema, human communicates with problem solution method. This method is strongly supported by corporate knowledge representations. Most of these representations can be included in the CIPM. However, definition of knowledge content requires research on its various levels. PLM systems are being increasingly prepared for this work. Virtual prototyping simulations are organized by planned experiments. Numerical methods are widely applied at shape representations, finite element analysis, etc. Rules, checks are applied at situation, while reactions are applied at event driven product feature definition as it is illustrated in Fig. 9. Main optimization algorithms are available in PLM systems and new algorithms can be defined in application environments.

Individual and mixed application of fuzzy logic, genetic algorithms, and neural networks is an important way towards more intelligent product models. Because their integration in CIPM model is presently at its initial stage, more attention is advised to devote their integration into CRPM model as method.

The success story of soft computing motivates its application in product definition where the problem solving often requires strengths and features of soft computing [1]. Tolerance for imprecision and uncertainty is often necessary in engineering problem solving. Consequently, fuzzy logic, neuro-computing, and probabilistic reasoning must be considered at definition of methods for CRPM modeling.

Problem solving processes often can utilize fuzzy rule base and the associated reasoning at product development. The most important processes are for decision support, expert knowledge processing, and definition of equipment and device control. However, known operators are often not able to follow the modeled phenomena. Authors of [13] propose generalization of conventional operators to include them in the sophisticated intelligent engineering systems.

Information aggregation well fits into numerous problem-solving processes in engineering where various types of information items must be handled [14]. In order to solve the problem caused by information types, authors of [14] propose an extension of fuzzy set membership functions for the reinterpretation information items in approximate formal setting using profiles. Consequently, appropriate profile aggregation is applied at modeling.

Authors of [15] concentrate on study of information aggregation in engineering related intelligent systems. Considering characteristics of problems in the engineering practice, they propose procedures to identify aggregation function in order to best fit to empirical data.

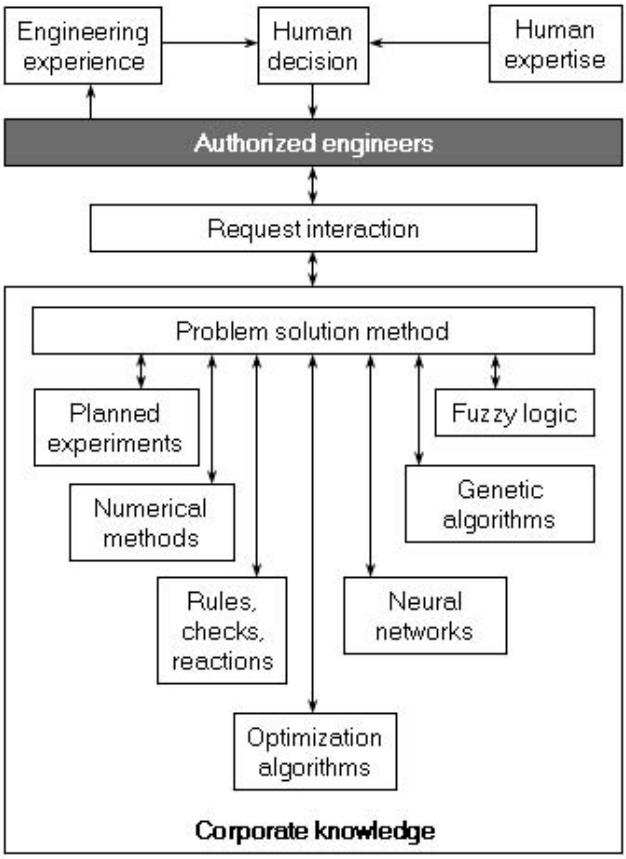

Fig. 10. Knowledge in the CRPM model

7 Integration CRPM into PLM System

In the above introduced request driven product model includes the proposed actual requested product definition (ARPD) in integration with the CIPM model (Fig. 11). CIPM represents the current PLM modeling technology. The ARPD includes request, behavior, and action features, while CIPM consists of product, analysis, knowledge, and equipment control features.

The main question is that how can the above integration be realized in an industrial PLM system. The generally applicable solution is seen in Fig. 11. Besides this solution, more engineer friendly means are being developed for direct extension by using of normal feature definition within a PLM system.

In case of the generally applicable solution of integration, request driven modeling procedures communicate through application programming interface (API) services of the PLM system. This means communication with product and rela-

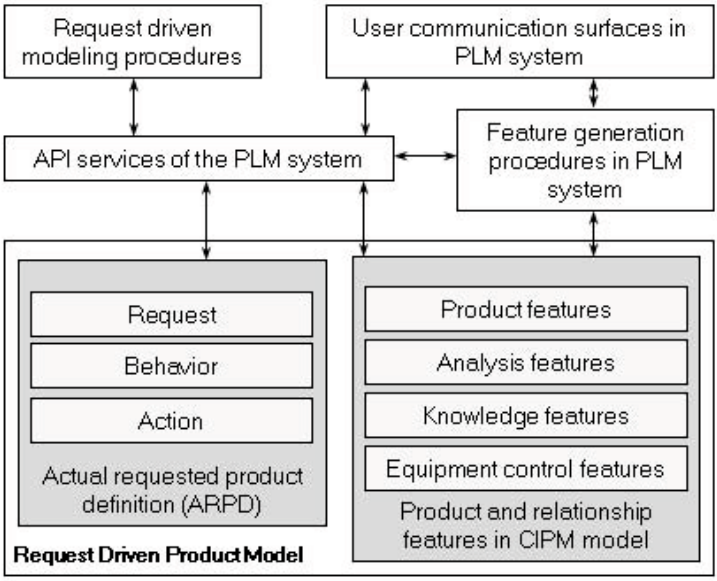

Fig. 11. Integration in PLM model

tionship features in CIPM model, ARPD features, as well as feature generation procedures and user communication surfaces in the actual PLM system.

8 Conclusions

Definition processes and means for representation of product information were undergone essential development during the past decade. This chapter introduces this development and emphasizes improvements in product definition capabilities of PLM systems. Former publications are cited in order to give a survey on the grounding of the recent results in knowledge supported modeling which are introduced in this chapter.

On the way towards smart self-development product model, adaptive capabilities must be strengthened. This work utilizes organized contextual connections of features, application of abstraction levels, and typical contextual connection chains in product model. The contributions in this chapter are aimed to solve these problems.

The classical interdisciplinary feature driven product model (CIPM) was defined in order to distinct it from the proposed coordinated request driven product model (CRPM). CIPM represents the currently representative product model and is extended by the CRPM. New abstraction levels are proposed in order to support this extension.

A former result for abstraction levels in product model was defined as content of product information. These levels are compared with RFLP structure which

is well known in systems engineering and recently applied at PLM modeling practice. In order to facilitate connection of the CRPM based modeling to the modeling systems with RFLP structure, a modified set of abstraction levels is proposed as a revision of the abstraction by product information content.

The proposed CRPM modeling requires representative PLM system environment which is suitable for the integration with the CRPM extension. For this purpose, PLM research environment is under development. In this installation, a suitable PLM system will serve the work of the Laboratory of Intelligent Engineering System (LIES). Mission of this laboratory of the Institute of Applied Mathematics, John von Neumann Faculty of Informatics, Óbuda University is bridging theory, methodology, and industrial practice.

Acknowledgment. The author gratefully acknowledges the financial support by the Óbuda University research fund.

References

1. Zadeh, L.A.: Soft computing and fuzzy logic. Software 11(6), 48–56 (1994)
2. Horváth, L., Rudas, I.J.: Modeling and Problem Solving Methods for Engineers. Elsevier, Academic Press (2004)
3. Stark, J.: Product Lifecycle Management: 21st Century Paradigm for Product Realisation. Birkhäuser (2004)
4. Horváth, L., Rudas, I.J.: Knowledge Technology for Product Modeling. In: Knowledge in Context – Few Faces of the Knowledge Society, ch. 5, pp. 113–137. Walters Kluwer (2010)
5. Jardim-Goncalves, R., Figay, N., Steiger-Garcao, A.: Enabling interoperability of STEP Application Protocols at meta-data and knowledge level. International Journal of Technology Management 36(4), 402–421 (2006)
6. Sy, M., Mascle, C.: Product design analysis based on life cycle features. Journal of Engineering Design 22(6), 387–406 (2011)
7. Horváth, L.: A New Method for Enhanced Information Content in Product Model. WSEAS Transactions on Information Science and Applications 5(3), 277–285 (2008)
8. Horváth, L., Rudas, I.J.: Active Knowledge for the Situation-driven Control of Product Definition. Acta Polytechnica Hungarica 10(2), 217–234 (2013)
9. Saridakis, K.M., Dentsoras, A.J.: Soft computing in engineering design. A review. Advanced Engineering Informatics 22(2), 202–221 (2008)
10. Clark, J.O.: System of Systems Engineering and Family of Systems Engineering From a Standards Perspective. In: Proc. of the Third IEEE SMC International Conference on System of Systems Engineering (SoSE), Monterey, California, USA, pp. 1–6 (2008)
11. Horváth, L., Rudas, I.J.: Requested Behavior Driven Control of Product Definition. In: Proc. of the 38th Annual Conference on IEEE Industrial Electronics Society, Montreal, Canada, pp. 2821–2826 (2012)
12. Kleiner, S., Kramer, C.: Model Based Design with Systems Engineering Based on RFLP Using V6. In: Abramovici, M., Stark, R. (eds.) Smart Product Engineering. LNPE, vol. 5, pp. 93–102. Springer, Heidelberg (2013)

13. Rudas, I.J., Fodor, J.: Information Aggregation in Intelligent Systems Using Generalized Operators. International Journal of Computers Communications & Control 1(1), 47–57 (2006)
14. Rudas, I.J., Fodor, J.: Non-conventional Interpretation of Fuzzy Connectives. In: Proc. of the 14th WSEAS International Conference on Applied Mathematics, Puerto de la Cruz, Spain, pp. 294–299 (2009)
15. Rudas, I.J., Pap, E., Fodor, J.: Information aggregation in intelligent systems: An application oriented approach. Knowledge-Based Systems 38, 3–13 (2013)
16. Horváth, L., Rudas, I.J.: Processes for Improved Human Control over Definition of Product Models. In: Proc. of the 35th Annual Conference of the IEEE Industrial Electronics Society, Porto, Portugal, pp. 2491–2496 (2009)
17. Horváth, L., Rudas, I.J.: Towards interacting systems in product lifecycle management. In: Proc. of the 8th International Conference on System of Systems Engineering (SoSE), Maui, Hawaii, USA, pp. 267–272 (2013)
18. Horváth, L., Rudas, I.J.: A Machine Learning Based Approach to Manufacturing Process Planning. In: Proc. of the IEEE International Symposium on Industrial Electronics (ISIE 1993), Budapest, pp. 429–433 (1993)
19. Horváth, L., Rudas, I.J.: Human-Computer Interactions at Decision Making and Knowledge Acquisition in Computer Aided Process Planning Systems. In: Proc. of the 1994 IEEE International Conference on Systems, Man and Cybernetics, San Antonio, Texas, USA, pp. 1415–1419 (1994)
20. Horváth, L., Rudas, I.J.: Multilevel Modeling of Manufacturing Processes Using Object Oriented Petri Nets and Advanced Knowledge Representation. In: Proc. of the 1995 IEEE 21st International Conference on Industrial Electronics, Control, and Instrumentation (IECON 1995), Orlando, Florida, USA, pp. 133–137 (1995)
21. Horváth, L., Rudas, I.J.: Knowledge Based Generation of Petri Net Representation of Manufacturing Process Model Entities. In: Proc. of the 1996 IEEE International Conference on Systems, Man and Cybernetics, Beijing, China, pp. 2957–2962 (1996)
22. Rudas, I.J., Horváth, L.: Modeling of Manufacturing Processes Using Petri Net Representation. Engineering Applications of Artificial Intelligence 10(3), 243–255 (1997)
23. Rudas, I.J., Horváth, L.: Intelligent Computer Methods for Modeling of Manufacturing Processes and Human Intent. Journal of Advanced Computational Intelligence and Intelligent Informatics 2(3), 111–119 (1998)
24. Horváth, L., Rudas, I.J.: Modeling of Manufacturing Processes in Simultaneous Engineering Using Collaborative Methods and Tools. In: Simultaneous Engineering: Methodologies and Applications (Automation and Production Systems), pp. 321–357. Gordon and Breach Science Publisher, New York (1999)
25. Horváth, L., Rudas, I.J., Hancke, G.: Associative Modeling of Machining Processes Using Feature Based Solid Part Models. In: Proc. of the 2006 26th Annual Conference of the IEEE Industrial Electronics Society, Nagoya, Japan, pp. 1267–1273 (2000)
26. Horváth, L., Rudas, I.J.: Virtual technology based associative integration of modeling of mechanical parts. Journal of Advanced Computational Intelligence and Intelligent Informatics 5(5), 269–278 (2001)
27. Horváth, L., Rudas, I.J., Bitó, J.F.: Form Feature Based Generation of Robot Assembly Paths for Product Variants. In: Proc. of the 2002 IEEE Conference on Industrial Technology, Bangkok, Thailand, pp. 181–186 (2002)
28. Horváth, L., Rudas, I.J., Tzafestas, S.G.: Relating Shape and Robot Process Model Features. International Journal of Mechanics and Control 4(2), 27–31 (2003)

29. Horváth, L., Rudas, I.J., Bitó, J., Hancke, G.: Intelligent Computing for the Management of Changes in Industrial Engineering Modeling Processes. Computing and Informatics 24, 549–562 (2005)
30. Horváth, L., Rudas, I.J.: Emphases on human intent and knowledge in management of changes at modeling of products. WSEAS Transactions on Information Science and Application 3(9), 1731–1738 (2006)
31. Horváth, L., Rudas, I.J.: New approach to knowledge intensive product modeling in PLM systems. In: Proc. of the IEEE International Conference on Systems, Man and Cybernetics, Montreal, Canada, pp. 668–673 (2007)
32. Horváth, L., Rudas, I.J.: New Product Model Representation for Decisions in Engineering Systems. In: Proc. of the 2011 International Conference on System Science and Engineering (ICSSE), Macau, China, pp. 546–551 (2011)

Interrelationship of Fuzzy Decision System Parameters

Márta Takács

Óbuda University, John von Neumann Faculty of Infomatics,
1034 Budapest, Bécsi út 96/B, Hungary
takacs.marta@nik.uni-obuda.hu

Abstract. The fuzzy decision systems contain fuzzified input and outputs parameters sequentially in premises and consequences of the decisions rules. The interrelationship of those can be very different from the basic relations described with if... then rules till the correlations of input parameters described with cognitive maps. The paper gives a summary of the fuzzy parameters' inter-relationship investigated by the authors in recent years based on fundamental results published by Imre J. Rudas, or investigated in joint works with him.

Keywords: fuzzy decision making, distance based operators, AHP, risk management.

1 Introduction

The interrelationship of the system parameters of fuzzy decision making system can be very different from the basic relations between parameters of premises and parameters of consequences of the if... then rules till the correlations and quantitative representation of relationships of input parameters from the set of premises.

Fuzzy decision making systems can be constructed from if A then B types of rules, where A and B are fuzzified system parameters and the mathematical background of the calculation is based on the definition of fuzzy relations and basic binary opera-tions of t-norms and conorms [9].

In the last few decades in fuzzy control systems the Mamdani type of decision model is widely used, and beyond the min and max operators others are also investigated in theoretical and practical environment in order to increase the efficiency of the system operation.

The basic interrelationship of the fuzzy system parameters is this one, the relationship between the t-norm or conorm operators or other aggregation operators applied in fuzzy based approximate reasoning methods. Uninorms, and especially generalized distance based operators, introduced by Rudas [1] continue to bring new possibilities in fuzzy systems models. Distance-based operators as the basic operators applied in approximate reasoning resulted investigation of similarity measures of fuzzy sets and residuum of those special operators [2].

J. Fodor and R. Fullér (eds.), *Advances in Soft Computing, Intelligent Robotics and Control*, Topics in Intelligent Engineering and Informatics 8,
DOI: 10.1007/978-3-319-05945-7_14,

Other investigations are focused on the representation of distance based operators in the group of uninorms and general aggregation operators. Considering that the uninorms are parameter-dependent norms, it is possible to investigate the behavior of the fuzzy decision making or control system by changing or sliding the parameter values [3].

In complex systems it is very important to recognize the measure of interaction and the measure of importance of the system parameters. This knowledge can help one to construct the structure of the decision system. The models investigated by the authors and summarized in this paper are related to the risk management systems, and the studied methods are the hierarchical construction of decision making model and the AHP model [4].

2 Distance Base Operators

2.1 Definition and Special Properties

The distance-based operators can be expressed by means of the min and max operators as follows [5]:

– the maximum distance minimum operator with respect to $e \in [0,1]$ is defined as

$$T_e^{\max} = \max_e^{\min} = \begin{cases} \max(x,y) & \text{if } \ y > 2e - x \\ \min(x,y) & \text{if } \ y < 2e - x \\ \min(x,y) & \text{if } \ y = 2e - x \end{cases} \tag{1}$$

– the minimum distance minimum operator with respect to $e \in [0,1]$ is defined as

$$T_e^{\min} = \min_e^{\min} = \begin{cases} \max(x,y) & \text{if } \ y > 2e - x \\ \min(x,y) & \text{if } \ y < 2e - x \\ \max(x,y) & \text{if } \ y = 2e - x \end{cases} \tag{2}$$

– the maximum distance maximum operator with respect to $e \in [0,1]$ is defined as

$$S_e^{\max} = \max_e^{\max} = \begin{cases} \max(x,y) & \text{if } \ y > 2e - x \\ \min(x,y) & \text{if } \ y < 2e - x \\ \max(x,y) & \text{if } \ y = 2e - x \end{cases} \tag{3}$$

– the minimum distance maximum operator with respect to $e \in [0,1]$ is defined as

$$S_e^{\min} = \min_e^{\max} = \begin{cases} \min(x,y) & \text{if } \ y > 2e - x \\ \max(x,y) & \text{if } \ y < 2e - x \\ \max(x,y) & \text{if } \ y = 2e - x \end{cases} \tag{4}$$

The modified distance based operators described above are changed in the boundary condition for neutral element e:

– the maximum distance minimum operator and the maximum distance maximum operator with respect to $e \in]0,1]$,

– the minimum distance minimum operator and the minimum distance maximum operator with respect to $e \in [0, 1[$.

The distance-based operators have the following properties :

– $\max_e^{\min}$ and $\max_e^{\max}$ are uninorms,
– the dual operator of the uninorm $\max_e^{\min}$ is $\max_{1-e}^{\max}$, and
– the dual operator of the uninorm $\max_e^{\max}$ is $\max_{1-e}^{\min}$.

Based on results from [6] we conclude:

Operator $\max_{0.5}^{\min}$ is a conjunctive left-continuous idempotent uninorm with neutral element $e \in]0, 1]$ with the super-involutive decreasing unary operator

$$g(x) = 2e - x = 2 \cdot 0.5 - x \quad \Rightarrow \quad g(x) = 1 - x.$$

Operator $\min_{0.5}^{\max}$ is a disjunctive right-continuous idempotent uninorm with neutral element $e \in]0, 1]$ with the sub-involutive decreasing unary operator [2]

$$g(x) = 2e - x = 2 \cdot 0.5 - x \quad \Rightarrow \quad g(x) = 1 - x.$$

2.2 Distance-Based Group of Operator in Fuzzy Inference Mechanism

In control theory much of the knowledge of a controller can be stated in the form of if-then rules, involving some variables. The fuzzy theory and fuzzy logic control has been carried out searching for different mathematical models in order to supply these rules. The Mamdani type of decision model is widely used in control problems. In this model the IF x is A THEN y is B rule is modeled just as an connection between so called rule premise: x is A, and rule consequence: y is B, where A and B are fuzzy sets, and sequentially x is the rule input variable from the universe X, and y is the rule output variable from universe Y. The connection is represented by t-norm types of operators. From set of if ... then ... rules the rule base system is constructed describing the system behavior. When the system works, the influence of the system input is investigated based on the given rule base. This influence is represented by the system output. The algorithm and mathematical calculation of the actual system output is the inference mechanism. One of the widely used methods for inference calculation in fuzzy control theory is the generalized modus ponens (GMP). The system output y is B' (similar to rule output) is obtained when the proposition are: the rule

$$\text{IF } x \text{ is } A \text{ THEN } y \text{ is } B,$$

and the system input x is A' (similar to rule premise).

In Mamdani type of inference the general rule consequence for the i-th rule from the rule base system is obtained by

$$B_i'(y) = \sup_{x \in X} \Big(T1\Big(A'(x), T2\big(A_i(x), B_i(y)\big)\Big)\Big), \quad x \in X, \quad y \in Y. \tag{5}$$

The connection $T1$ and $T2$ are generally defined, and they can be some type of fuzzy conjunctive operators.

If we use the same T operator instead of $T1$ and $T2$ operators, based on the t-norm operators' properties, from the above expression follows

$$B'_i(y) = \sup_{x \in X} \Big(T\Big(A'(x), T\big(A_i(x), B_i(y) \big) \Big) \Big). \tag{6}$$

Generally speaking, the consequence (rule output) is given with a fuzzy set $B'(y)$, which is derived from rule consequence $B(y)$, as a cut of the $B(y)$. This cut,

$$\mathrm{DOF}_i = \sup_{x \in X} T\big(A'(x), A_i(x) \big) \tag{7}$$

is the generalized degree of firing level of the rule, considering actual rule base input $A'(x)$, and usually depends on the covering over $A(x)$ and $A'(x)$. But first of all it depends on the sup of the membership function of $T\left(A'(x), A(x)\right)$. Rule base output B'_{out} is an aggregation of all rule consequences $B'_i(y)$ from the rule base. As aggregation operator a disjunctive operator (conorm) is usually used.

$$B'_{\mathrm{out}} = S\Big(B'_n(y), S\Big(B'_{n-1}(y), S\Big(\ldots S\big(B'_2(y), B'_1(y) \big) \ldots \Big) \Big) \Big). \tag{8}$$

If in the application a crisp output y_{out} is needed, it is constructed as a crisp value calculated with a defuzzification method, from rule base output, for example with the center of gravity method, given by

$$y_{\mathrm{out}} = \frac{\int\limits_Y B'_{\mathrm{out}} \cdot y \,\mathrm{d}y}{\int\limits_Y B'_{\mathrm{out}} \,\mathrm{d}y}. \tag{9}$$

It can be concluded, that in decision making approximate reasoning the (T, S) pair of operators are used.

Instead of the operators T and S an operator from the group of distance-based operators can be chosen. Considering the structure of distance based operators, namely that they are constructed by the min and max operators; it was worth trying to move away from the strictly applied max (disjunctive) and min (conjunctive) operator pair in approximate reasoning. Therefore, in a simulation systems different operators from the group of distance based operators were applied as disjunctive and conjunctive ones. Moreover, the distance based operators are parameterized by the parameter e, therefore the program, which performs the task of decision making in the simulation system, has global, optional, variables (Con, Dis, e), where Con is the operator applied by GMP, and the Dis is the aggregation operator for the calculation of the B'_{out}.

The neutral element of the Con operator is the parameter e, and the neutral element of the Dis operator is the parameter $1 - e$. Details about the simulation results can be found in [3]. Hence and because by the simulation the triple (Con,

Dis, e) can be chosen by even running of the simulation system, it enables the parameters to be set at every running of the system in order to achieve greater efficiency.

Although the minimum plays an exceptional role in fuzzy control theory, there are situations requiring new models. In system control one would intuitively expect: to make the powerful coincidence between fuzzy sets stronger, and the weak coincidence even weaker. The distance-based operators group satisfy these properties, but the covering over $A(x)$ and $A'(x)$ are not really reflected by the sup of the membership function for example if we use $\min_e^{\max}$ to calculate degree of firing as $\min_e^{\max}\big(A'(x), A_i(x)\big)$.

Hence, and because of the properties of distance-based operators, it was unreason-able to use the classical degree of firing (7), to give expression of the coincidence of the rule premise (fuzzy set A), and system input (fuzzy set A'), therefore a Degree of Coincidence (Doc) for those fuzzy sets has been initiated. This is actually the propor-tion of area under membership function of the distance-based intersection of those fuzzy sets, and the area under membership function of their union (using max as the fuzzy union).

$$\mathrm{Doc}_i = \frac{\int\limits_X \min_e^{\max}\big(A_i(x), A'(x)\big)\,\mathrm{d}x}{\int\limits_X \max\big(A_i(x), A'(x)\big)\,\mathrm{d}x} \tag{10}$$

This definition has two advantages:

- it considers the whole measure of coincidence of A_i and A', and not only the "height", the sup of the coincidence, and
- the rule output is weighted with a measure of coincidence of A_i and A' in each rule.

How to get the rule output?

The rule output can be the cut of the rule consequence, in this case

$$B_i'(y) = \min\big(\mathrm{Doc}_i, B_i(y)\big). \tag{11}$$

Despite the fact that Mamdani's approach is not entirely based on compositional rule of inference, it is nevertheless very effective in fuzzy approximate reasoning. Because of this it is possible to apply several t-norms, or, as in considered case, distance based operators. This leads to further tasks and problems. The problem of the measurement of covering over of the rule premise and rule input is partly solved with the degree of coincidence. But in any case there must be a system of conditions that is to be satisfied by the new model of inference mechanism in fuzzy systems [8].

For a given input fuzzy set $A'(x)$, in a mathematical-logical sense, the output fuzzy set $B_i'(y)$ in one rule, can be generated with the expression

$$B_i'(y) = \max\left(B_i(y), \sqrt{1 - \mathrm{Doc}_i}\right). \tag{12}$$

It is easy to prove, that $\mathrm{Doc}_i \in [0,1]$, and $\mathrm{Doc}_i = 1$ if A_i and A' cover over each other, and $\mathrm{Doc}_i = 0$ if A_i and A' have no point of contact.

Several pairs of distance-based operators have been tried out in a simulation system for a control problem, with special emphasis on the pairs $\left(T_e^{\max}, S_{1-e}^{\max}\right)$ and $\left(T_e^{\min}, S_{1-e}^{\min}\right)$.

The choosing of pairs $\left(T_e^{\max}, S_{1-e}^{\max}\right)$ and $\left(T_e^{\min}, S_{1-e}^{\min}\right)$ by the simulation, using the same e value, gives results with negligible difference. So it was sufficient trying out the pairs $\left(T_e^{\max}, S_{1-e}^{\max}\right)$ for example. The choosing of the pair $\left(T_e^{\max}, S_{1-e}^{\max}\right)$, where e is near zero, return in short time the desired state of the system, but it is not stable. If e is near 1, the situation is known, because it develops to choosing of pair $(\min, \max)$. The desired state is obtained easier, and the systems stay stable. It can be observed, that continual sliding of e from zero to 1 results continual improvement in stability, and continual increasing time of obtaining desired state in the system. The choosing of pair $(T_{0.5}^{\max}, S_{0.5}^{\max})$ gives acceptable result by both criteria [7].

3 Interrelationship of the Input Parameters in Complex Systems

A risk model is a multi-parameter and multi-criteria decision making system. The complexity of the systems increases the runtime factor by the decision, and the large system parameter set has not a user-friend transparency. The traditional well-known models work without management of the uncertainties. The complexity and uncertainties in those systems raise the necessity of soft computing based models. The use of fuzzy sets to describe the risk factors and fuzzy-based decision techniques to help incorporate inherent imprecision, uncertainties and subjectivity of available data, as well as to propagate these attributes throughout the model, yield more realistic results. The structural modeling of risk and disaster management is case-specific, but the hierarchical model is widely applied. The system characteristics are as follows: it is a multi-parametrical, multi-criteria decision process, where the input parameters are the measured risk factors, and the multi-criteria rules of the system behaviors are included in the decision process. The Analytical Hierarchy Process (AHP) expands this complex system with the pairwise comparison of the factors' importance and interaction [10].

The techniques used in risk management have been taken from other areas of system management. The first step is the identification of risks and potential risks to the system operation at all levels. Evaluation, the measure and structural systematization of the identified risks, is the next step. Measurement is defined by how serious the risks are in terms of consequences and the likelihood of occurrence. It can be a qualitative or quantitative description of their effects on the environment. Plan and control are the next stages to prepare the risk management system. This can include the development of response actions to these risks, and the applied decision or reasoning method. Monitoring and review will ensure that the risk management process is dynamic and continuous, with correct verification and validity control.

Generally, the risk management system in its preliminary form is a knowledge-based model, where objective and subjective knowledge is included in the decision process. Considering the possible uncertainties and imprecision, and the large number or quantitative description of the parameters, we can conclude that the fuzzy set theory extended with the AHP matrixes manage complexity [11].

Fuzzy-based risk management models assume that the risk factors are fuzzified (because of their uncertainties or linguistic representation); furthermore the risk man-agement and risk level calculation statements are represented in the form of *if premises then conclusion* rule forms, and the risk factor calculation or output decision (summarized output) is obtained using fuzzy approximate reasoning methods. Considering the fuzzy logic and fuzzy set theory results, there are further possibilities to extend fuzzy-based risk management models modeling risk factors with type-2 fuzzy sets, representing the level of the uncertainties of the membership values, or using special, problem-oriented types of operators in the fuzzy decision making process [4].

The hierarchical or multilevel construction of the decision process, the grouped structural systematization of the factors, with the possibility of gaining some subsystems, depending on their importance or other significant environment characteristics or on laying emphasis on risk management actors, is a possible way to manage the complexity of the system [12].

4 The Present and Planned Further Works

The recent works of the authors of this paper are related to the interrelationship of fuzzy decision system parameters based on the fuzzy cognitive maps of them. It is obvious that the AHP matrix and weights of fuzzy cognitive maps have a similar role in the relationship description of the system parameters, but the determination, and later the tuning of them offers new challenges for as the experts. Current active fields of investigation regarding interrelationship description of the fuzzy system parameters includes risk management, medical diagnostic problems and the student work evaluation.

Acknowledgements. The research was supported by the Hungarian OTKA projects 106392 and 105846, and project of the Vojvodina Academy of Sciences and Arts “Mathematical models of intelligent systems and theirs applications”.

References

1. Rudas, I., Kaynak, O.: New Types of Generalized Operations. In: Kaynak, O., Zadeh, L.A., Turksen, B., Rudas, I.J. (eds.) Computational Intelligence: Soft Computing and Fuzzy-Neuro Integration with Applications. Springer NATO ASI Series, Computer and Systems Sciences, vol. 162, pp. 128–156 (1998)
2. Takács, M.: Uninorm-based models for FLC systems. Journal of Intelligent and Fuzzy Systems 19(1), 65–74 (2008) ISSN: 1064-1246

3. Takács, M.: Parametrized Program-interface for Simulation-based Operator Evaluation. Studies in Informatics and Control with Emphasis on Useful Applications of Advanced Technology 15(3), 307–314 (2006) ISSN 1220-1766
4. Tóth-Laufer, E., Takács, M., Rudas, I.J.: Interactions Handling Between the Input Factors in Risk Level Calculation. In: IEEE 11th International Symposium on Applied Machine Intelligence and Informatics (SAMI 2013), pp. 71–76 (2013) ISBN 978-1-4673-5928-3
5. Takacs, M., Rudas, I.J.: Generalized Mamdani Type Fuzzy Controllers. In: Proceedings of Eurofuse-SIC 1999, pp. 162–165 (1999)
6. De Baets, B., Fodor, J.: Residual operators of uninorms. Soft Computing 3, 89–100 (1999)
7. Takacs, M.: Uninorm-based Approximate Reasoning Models. In: Linz Seminar on Fuzzy Sets and Systems, pp. 124–127 (2006)
8. Takács, M.: Axioms of the System Behavior in FLC Using Uninorms. In: Proc. of IEEE 4th International Symposium on Applied Computational Intelligence and Informatics (SACI 2007), Timisoara, Romania, May 17-18, pp. 35–39 (2007) ISBN 1-4244-1234-X
9. Klement, E.P., Mesiar, R., Pap, E.: Triangular Norms. Kluwer Academic Publishers (2000) ISBN 0-7923-6416-3
10. Saaty, T.L., Vargas, L.G.: Models, Methods, Concepts and Applications of the Analytic Hierarchy Process. Kluwer Academic Press (2001)
11. Takács, M.: Multilevel Fuzzy Approach to the Risk and Disaster Management. Acta Polytechnica Hungarica 7(4), 91–102 (2010)
12. Takacs, M.: Scaling tasks in a risk management system based on multilevel fuzzy decision making. In: Proc. of 2011 System Science and Engineering Conference (ICSSE), pp. 379–383 (2011) ISBN 978-1-61284-351-3

Swarm-Based Heuristics for an Area Exploration

Marek Masár and Ivana Budinská

Institute of Informatics, Slovak Academy of Sciences
Dubravska cesta 9, 845 07 Bratislava, Slovakia
budinska@savba.sk

Abstract. This paper describes design and implementation of biologically inspired heuristic for the purpose of motion coordination. Proposed method goes from known principles and methods, namely: particle swarm optimization, ant colony optimization, and simulation of virtual bird flocking methods. It combines several known features and also introduces some new approaches to create a new heuris-tics focused on an area exploration and surveillance. After promising simulation results, the approach was tested on Lego robots within simple environment in order to prove the concept.

1 Introduction

The concept of swarm intelligence is well-known and can be found in numerous applications in many different domains. Algorithms and methods are being modified, transformed or combined to meet specific requirements. A common application exploiting biological inspiration is in cooperative multi-robot system, where rules from biological systems are applied to the artificial systems, in order to achieve organized society with intelligent behavior.

This paper presents a new method for coordination of a group of mobile agents that can be used for unknown area exploration and monitoring. It is organized as follows: following section gives overview of basic biological inspiration and related work. Third section formulates the problem. Fourth section introduces proposal of our approach, following with fifth section which describes the implementation. Sixth and seventh section presents computer simulations and results achieved by comparison with other ap-proaches. Eighth section gives overview of multi-agent system created to test proposed heuristic method. Finally, last section summarizes achieved results.

2 Inspiration from Nature and Related Work

Nearly all of the work in cooperative mobile robotics began after the introduction of the new robotics paradigm of behavior-based control. This behavior-based paradigm has had a strong influence in much of the cooperative mobile robotics research. Because the behavior-based paradigm for mobile robotics is rooted in biological inspirations, many cooperative robotics researchers have also found it

J. Fodor and R. Fullér (eds.), *Advances in Soft Computing, Intelligent Robotics and Control,* Topics in Intelligent Engineering and Informatics 8,
DOI: 10.1007/978-3-319-05945-7_15,

instructive to examine the social characteristics of insects and animals, and to apply these findings to the design of multi-robot systems [9].

A typical example of this paradigm is an optimization method based on a swarming theory, discovered through simulation of a simplified social model, which was introduces in 1995 by Eberhart and Kennedy [6]. The authors proved an ability of the particle swarm optimization method (PSO) to solve complex optimization problems. The weakness of this method is its tendency to converge early to a suboptimal solution. Since then, several improvements and modifications have been made to adjust this method for different scenarios and to suppress its weaknesses. Hereford and Siebold [4] presented a version of PSO called Physically embedded PSO, which was designed to control robots in the process of finding a target in any environment. A PSO modification for the purpose of space exploration was introduced in [8].

Ant colony optimization (ACO), proposed by Dorigo and Stützle in [1] is a probabilistic technique for solving computational problems, which can be reduced to finding good paths through graphs. The keystone was the deposition of virtual pheromones by virtual ants. The pheromones were used to select the next node in a graph as a waypoint.

A combination of PSO with digital pheromones for constrained optimization problems has been described in [5]. Virtual pheromone based communication mechanism to decrease communication cost in the map coverage task was introduced in [13]. Virtual pheromones and ant-exploration methods for robotics application are further described in [10,15].

C.W. Reynolds created a computer simulation of artificial bird flocking in 1986. Artificial birds (boids) were able to model the motion of a flock of birds following simple rules [11]. A group of artificial fish capable to exhibit schooling behavior, was evolved by Ward [16].

The swarm multi-agent system presented in this paper implements several features from the above mentioned basic methods – particle swarm optimization, ant colony optimization and virtual bird flocking.

3 Problem Statement

The goal is to create a swarm of mobile agents that can explore a two-dimensional space (a flat surface) and create a model of this environment. The agents should be able to coordinate their actions, to communicate, and to create the map of the environment interactively. After exploring the whole environment, agents should continue in a surveillance of the explored space. The robots are equipped with sensors, and are able to sense their surroundings and detect obstacles in the distance. The goal is not to visit every single bit of the two-dimensional area, but to cover the whole area with the sensors.

Mathematical formulation is as follows. Let us suppose a two-dimensional rectangular array $A_{m\times n}$ consisting of $m \times n$ square cells, where each square cell $s(i,j) \in A$ is uniquely determined and initialized with value 0. Position of the robot n is $R_n\,(x_n, y_n)$. The movement of the robot in the space is described by

changing its coordinates in time. If the range of the sensor is ε, we can define an operation radius O_ε of robot R_n as:

$$O_\varepsilon(R_n) = \{X \in A \colon \rho(R_n, X) < \varepsilon\}, \quad O_\varepsilon(R_n) \ll A, \tag{1}$$

where $X(i,j)$ is the middle of a square $s(i,j)$. When the middle of the square $s(i,j)$ occurs within the operation radius O_ε, its value is set to 1. The goal is to achieve the state where:

$$\forall A \in A_{m \times n},\ i < m,\ j < n \colon X(i,j) = 1. \tag{2}$$

This is the state, where each element of the array is set to 1, i.e. it has been explored by any of the group of robots.

4 Method Description

The behavior of each robot is influenced by two vectors in our approach. The first one is the influence vector, which is mostly responsible for coordination in a group and the second one is the vector denoting the position of a virtual pheromone in the surroundings.

As a symbolic representation of the environment, the proposed method uses grid maps. The space is divided into a grid containing m x n square cells. The grid itself does not restrict the movement of the robots to the edges or square centers. Robots move over the grid continuously. The square cells hold the information about virtual pheromone, which is distributed by the robots. In the case of real application, they hold information about the obstacles in real environment. From these reasons, the size of virtual square impacts the behavior of the system.

As a symbolic representation of the environment, the proposed method uses grid maps. The space is divided into a grid containing $m \times n$ square cells. The grid itself does not restrict the movement of the robots to the edges or square centers. Robots move over the grid continuously. The square cells hold the information about virtual pheromones, which is distributed by the robots. In the case of real application, they hold information about the obstacles in the real environment. For these reasons, the size of the virtual square impacts the behavior of the system.

4.1 Influence Vector

A circular zone of influence (Z1) is set around each agent. When other agent occurs within this zone, it influences the behavior of agent in the center (central agent). This influence is bilateral attraction or repulsion and it is determined by an influence function. Generally speaking, when the robots are very close each other, they tend to repel each other; when the distance is greater, they are attracted to each other. This influence is represented by a vector computed by the influence function. Fig. 1 depicts the influence function.

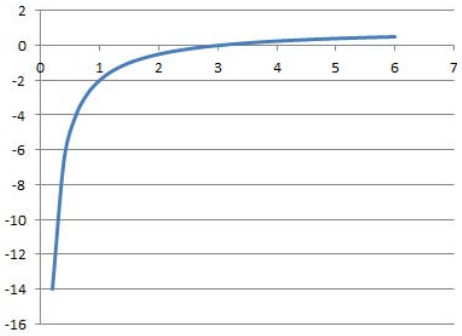

Fig. 1. The influence function. The equilibrium distance is defined by the spot, where the function crosses an x-axis

This figure shows that the closer the robots are, the greater the repulsion force is. With attractive force, the situation is similar. In fact, the influence function is designed in such a way, that for input variable (distance of two robots) it outputs the force vector with the magnitude which navigates the robot to the equilibrium position. Equilibrium position is the distance between two robots, when they do not attract or repel each other. In the case of influence function depicted in Fig. 1, the equilibrium distance is set to $e = 3$. The influence function crosses the x axis in the equilibrium distance and the magnitude of the output vector for input value three is zero. Mathematical formulation of influence function is:

$$t_a = \frac{\left|\overrightarrow{d_{an}}\right| - e}{\left|\overrightarrow{d_{an}}\right|}, \tag{3}$$

where $\overrightarrow{d_{an}}$ is the vector denoting the position of the robot R_n relative to the position of the central robot R_a. The output of this function is the transformation coefficient t_a, which transforms vector $\overrightarrow{d_{an}}$ to the vector that defines the shortest way from the current position to the equilibrium position of both robots. The size of vector $\overrightarrow{d_{an}}$ plus the size of transformed vector $\overrightarrow{d_{an}} \times t_a$ is equal to the parameter e.

$$\left|\overrightarrow{d_{an}}\right|_{t+1} = e + \left|\overrightarrow{d_{an}}\right|_t \cdot t_a. \tag{4}$$

Graphical interpretation of this equation is in Fig. 2.

The transformation coefficient is used to determine the influence vector $\overrightarrow{y_{an}}$ as follows:

$$\overrightarrow{y_{an}} = \frac{\overrightarrow{d_{an}} \cdot t_a}{2}. \tag{5}$$

The influence vector is computed using a relative vector $\overrightarrow{d_{an}}$ and a transformation coefficient t_a and it determines a trajectory to an equilibrium position of

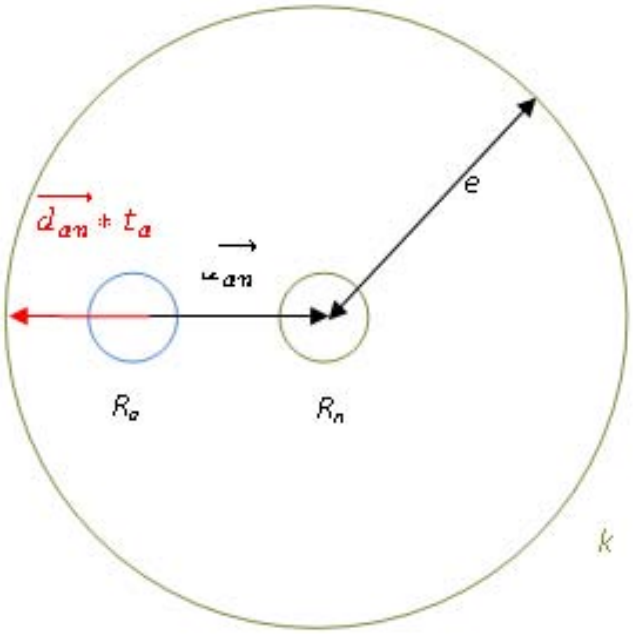

Fig. 2. A circle k with a radius e defines equilibrium distance between agent R_a and R_n

both agents. In order to achieve the equilibrium distance between two agents, it is required that each of the agents travels a half of the distance, therefore there is the number 2 in the denominator.

$\overrightarrow{y_{an}}$ represents the influence force from the agent R_n to the agent R_a. There could be more than one agent within the influence zone of the agent R_a. In this case each agent creates an influence vector and influences the central agent. The resulting vector is created using a vector sum of all such vectors.

$$\overrightarrow{y_a} = \sum_{t=1}^{z} \frac{\overrightarrow{d_{at}} \cdot \frac{\left|\overrightarrow{d_{at}}\right| - e}{\left|\overrightarrow{d_{at}}\right|}}{2}, \tag{6}$$

where z is total number of other agents within the influence zone $Z1$ of agent R_a.The range of the influence function is limited by the range of the influence zone. The robots outside this range do not influence the central robot.

4.2 Pheromone Vector

Robots deposit virtual pheromone markers while traveling in the environment. These pheromones are used to determine which square cell of the map has been

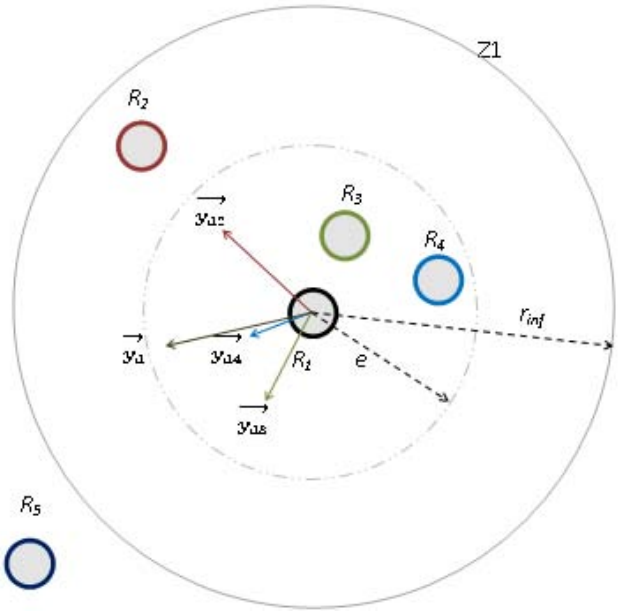

Fig. 3. A central agent R_1 influenced by other agents. Agents closer than the equilibrium distance (R_3, R_4) create repulsive forces. Agent R_2 is farther than the equilibrium distance, but still in $Z1$. It creates an attractive force. Agent R_5 is outside the zone of influence and has no influence on central agent R_1.

visited so far. If we implement pheromone evaporation, it is possible to determine how long it is since the last visit. Pheromone is deposited immediately when a robot reaches new square cell. This means, setting the highest value of the pheromone within the predefined radius. The previous pheromone values (pheromone strength) do not have any effect, since they are overwritten with new ones. The pheromones are not reinforced by multiple passes. The use of the pheromone is similar to the use in ACO method, but unlike virtual ants, the robots are searching for the square cell without any pheromone marks. Virtual pheromones are not used to construct paths, but to mark explored space. A circular zone $Z2$ of pheromone detection is defined around each robot. Robot searches for the closest unexplored square cell within this zone. When it is found, the second vector influencing behavior of the agent is created. A vector $\overrightarrow{ph}$ is called a pheromone vector. A perimeter of the pheromone detection zone may or may not be fixed. In the second case, when no unexplored square cell is found within this range, the perimeter is extended. The probability of selecting the square $s(i, j)$ is derived from its pheromone value τ_{ij}.

$$p_{ij} = 1 - \frac{\tau_{ij}}{\sum_{ij}^{z} \tau_{ij}} \quad \text{for} \quad (i - x_r)^2 + (j - y_r)^2 < r_p^2, \tag{7}$$

where x_r, y_r are the coordinates denoting position of an agent. Robots do not always select the square cell with the lowest pheromone value. The p_{ij} probability of selecting square cell $s(i,j)$ as a preferred square is higher for a low pheromone value. Denominator represents the sum of all pheromone values within pheromone detection range $Z2$. This rule is the same when robots are exploring the environment, but in a simpler form, because the probability of selecting any unrevealed square cell within range is the same. In this case the probability is as follows:

$$p_{ij} = \frac{1}{n_p}, \tag{8}$$

where n_p is the number of the pheromone marks within zone $Z2$. After selecting a pheromone, vector $\overrightarrow{p_h}$ is constructed. It determines a position of selected square relative to the position of the agent.

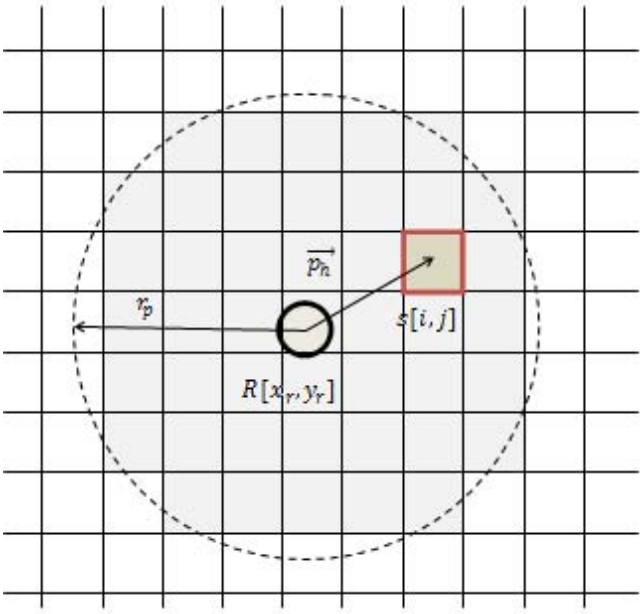

Fig. 4. A gray area represents squares that fit $(1 - x_r)^2 + (j - y_r)^2 < r_p^2$ in (7)

There is a limit for the length of the vector $\overrightarrow{p_h}$, in order to maintain influence balance between this vector and the first vector $\overrightarrow{y_a}$. Therefore, it is a good idea to set the same limit for the length of $\overrightarrow{p_h}$as the equilibrium distance. If pheromone evaporation is presented, it is not derived from the time. It is only dependent on the movement of the agents. All pheromone values are decreased when any agent crosses a border between two adjacent squares. So there is no need to use any synchronization tool and the communication requirements are lowered.

4.3 Movement

After specifying pheromone vector $\overrightarrow{p_h}$ and influence vector $\overrightarrow{y_a}$, the next position of the robot is computed using a vector sum:

$$\overrightarrow{v} = \overrightarrow{y_a} + \overrightarrow{p_h}. \tag{9}$$

Since the influence function outputs scaled influence vector, there is no need to adjust it with additional weights. We also use the limit $v_{\max}$ which defines maximum length of the vector $\overrightarrow{v}$. Adjusted vector $\overrightarrow{v_n}$ is the resulting vector determining the following movement of the agent (in the original PSO method, the vector $\overrightarrow{v_n}$ denoting following movement of the particle, is referred as a velocity vector, but referring it as a displacement vector is more intuitive). $v_{\max}$ is a parameter set by a user and determines the frequency of selecting the next action to be performed. The higher the frequency is, the higher is the decision rate. It is like having the higher sample rate of the environment changing in time to get more accurate response. Agents reflects the changes in environment more often, but high frequency may lead to the chaotic movement, because agents will not be even able to reach the destination square and the will be forced to select another one. Determining this parameter is therefore important process, which should reflect environmental aspects and the abilities of robotic platform (speed, reach of the sensors, etc.)

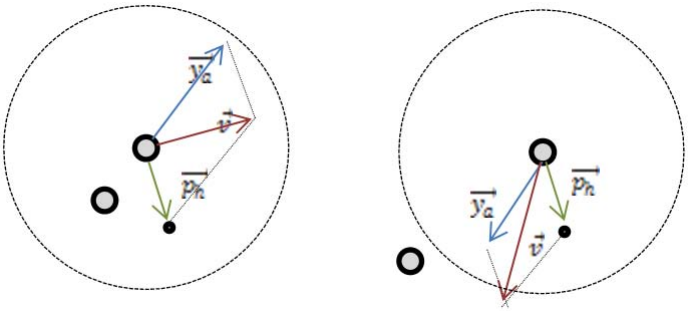

Fig. 5. The left figure shows the situation in which robots are too close and the influences vector (blue) causes repulsion. In the right figure robots are further away and the influence vector causes attraction. An outer circle shows the equilibrium distance. In case the second robot is directly on this circle, the influence vector has zero magnitude.

A fixation of the pheromone detection range and the pheromone evaporation are two parameters, which lead to two different behavior of a swarm as follows:

- if the pheromone does not evaporate and the perimeter of the zone of pheromone detection is not fixed, the behavior of the robots is aimed strictly towards space exploration,
- if the pheromone does evaporate and the perimeter is fixed, the behavior of the swarm resembles environment surveillance.

5 Implementation

The basic algorithm of proposed method in pseudo code showing the process of decision of the individual agent is as follows:

```
1  if (there is any agent in Z1){
2    select the closest agent;
3    determine influence vector y_an;}
4  else
5    set influence vector to y_an = 0;
6  if (the closest agent is not closer than allowed limit){
7    determine the square cell using equation (8);
8    determine vector p_h;}
9    compute vector v using v = y_an + p_h;
```

For the purpose of the simulation, control processes of the agents were ordered sequentially, but it is possible to parallelize it. A control process of an individual agent is in the diagram in Fig. 6.

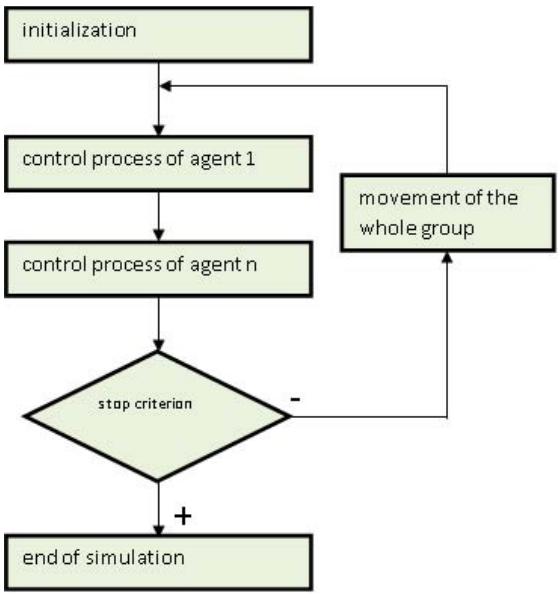

Fig. 6. A control process of an agent

6 Computer Simulations

We have created a simulation software VERA, which is able to simulate the behavior of the swarm according to the proposed method. The following figures are screenshots taken from the VERA tool. Fig. 7 illustrates the situation

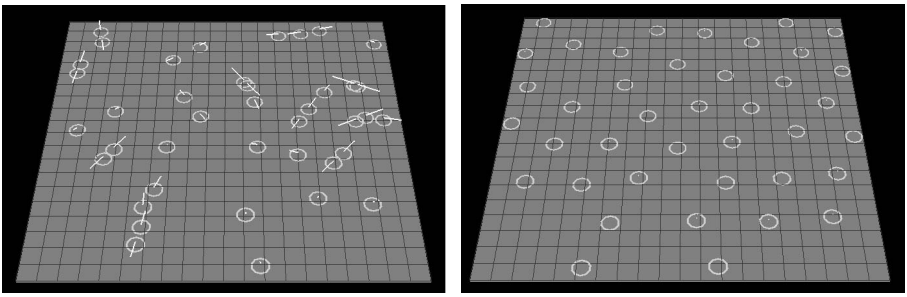

Fig. 7. A distribution of agents in a space. White lines represent influence vectors. There are no influence vectors in the figure on the right, because all robots are in equilibrium distance to each other.

where robots calculate influence vectors only. It is a demonstration example that shows that robots have tend to evenly distribute in the space and to hold their distances.

The question is how to set a limit for k, the number of robots influencing the focal robot. In the case with unlimited number, robots show the tendency to oscillate around equilibrium distances or to collide with each other, especially in the system where many robots (more than five) are influencing the focal robot. The reason is that resulting influence vector is confusing for the robot, because it includes irrelevant neighbors. Fig. 8 depicts this situation.

Top priority for the robot in this figure should be to avoid collision with the nearest neighbor; achieving the equilibrium distance with other robots is not important in this situation. By trials and errors we have set the limit for the

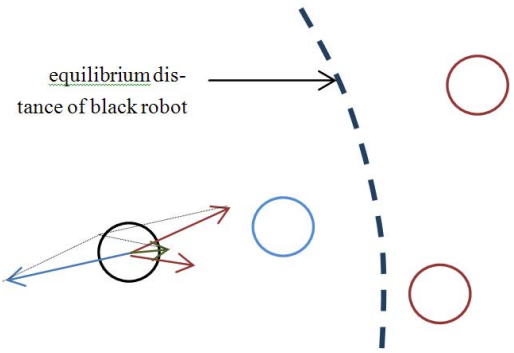

Fig. 8. Two brown robots are attracting the focal robot (brown vectors), while the blue robot is causing repulsion (the blue vector). The important thing is to avoid collision with the blue robot, but resulting green vector omits this.

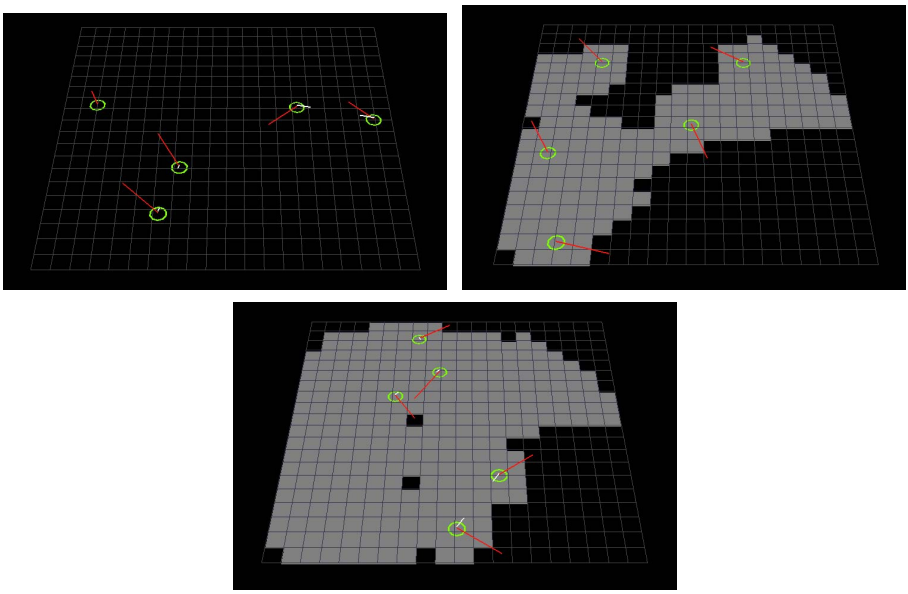

Fig. 9. Five robots exploring the environment. Red lines represent pheromone vectors. Simulation parameters: pheromone detection range = 4, pheromone deposit range = 2, $k = 1$, map dimension: 20×20 square cells.

variable k to 1. In other words, only the nearest neighbor influences the focal robot. This respects the fact that avoiding collision should have the highest priority. We have included this limit in all the simulations.

Sequence of pictures within Fig. 9 shows the case, where the behavior of the robots was set to follow the goal of space exploration (no pheromone evaporation, variable pheromone detection range).

Robots were attracted to the nearest unexplored square cell and influenced by each other. The result was that the whole space has been explored without any collision and with tendency of the robots to stay together in the equilibrium distance (this tendency is more evident in the map with larger scale).

We have also defined a critical minimum distance of two robots. When two robots are closer than this critical distance, they compute the influence vector only and the unexplored square cells are ignored. The reason for this is to avoid any unexpected situations which might lead to collision (failure of a robot). In the case of Fig. 10, robots were set to make surveillance in the area (pheromone evaporation, fixed pheromone detection range).

In this case, robots are mostly attracted to the space in their surroundings which was explored, but the longest time ago. Pheromone evaporation is illustrated by fading of the white color. The lower the pheromone value of a specific square cell, the longer this time is.

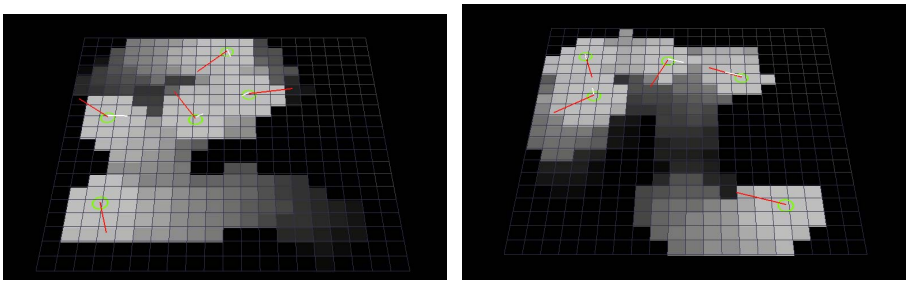

Fig. 10. Pheromone evaporation in time. Robots are attracted to the areas with the lowest pheromone values (dark areas).

7 Comparison with Other Methods

The proposed method was compared with other similar methods, namely:

- simplified ant colony optimization based on pheromone deposition and detection [1];
- modification of PSO for the purpose of the space exploration [8];
- modification of PSO for the purpose of the space exploration with additional influence vector denoting the unrevealed areas in the surroundings of agents;
- combination of ePSO method and the principles of virtual bird flocking.

The proposed method utilizes some of the features of these other methods. They were selected for comparison in order to see our improvement. All the simulations were done in simulation software VERA and statistically evaluated.

7.1 Space Exploration

The following simulation results show the effectiveness of the proposed method in the process of space exploration and surveillance. Each method has been tested using different number of agents (3, 10, and 20 agents) and for different number of iterations.

The results in Fig. 11 show, ePSO method has the lowest performance. The reason is the tendency of agents/particles to group together, what is the characteristic behavior of PSO. Modified PSO method and the modification using virtual bird flocking principles achieve better results. The best results were achieved by the proposed method and the simplified ACO. The reason is, they are both based on virtual pheromones. Even the results are very similar, it has to be mentioned that simplified ACO method does not incorporate any coordination mechanism, thus it is less suitable.

7.2 Surveillance

The following experiments illustrate the process of surveillance. The square element $s(i, j)$ directly within the sensor radius of any agent is marked as fully

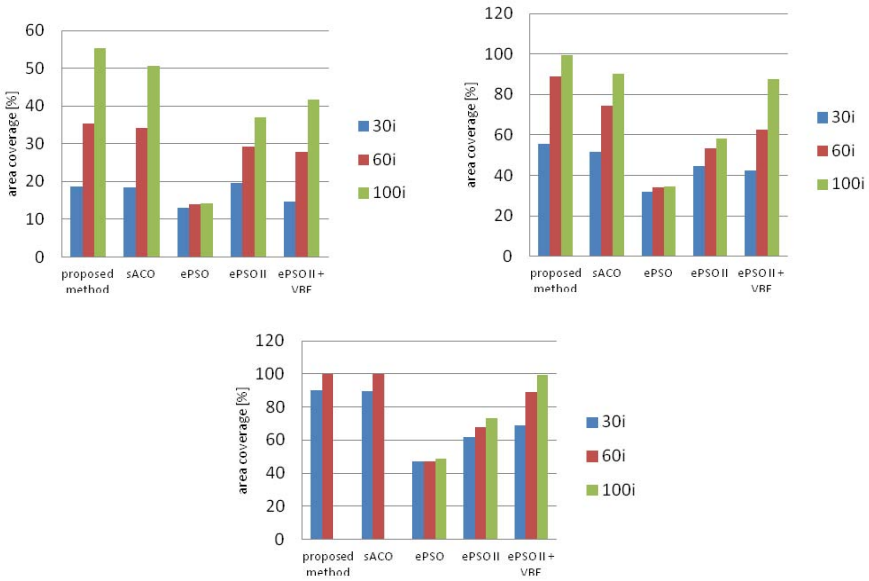

Fig. 11. The simulation results for 3, 10, and 20 agents

revealed $p_p = 100$ (100%). Unrevealed element was marked as $p_p = 0$ (0%). Value p_p of each square was lowering with every agent crossing between squares. Overall revealed volume of the whole area (with the size of $m \times n$ square cells) was computed using following equation.

$$p_p = \frac{\sum_{i=1}^{m} \sum_{j=1}^{n} p_p\,(i,j)}{mn}. \tag{10}$$

Following graphs in Fig. 12 show the dependence between P_p value and the number of iterations. The experiments were done using different number of agents.

The best results were achieved by the proposed method and the sACO method. Good results were achieved also by ePSO combined with principles of virtual bird flocking. The important fact is, that these methods maintain non-decreasing curve. That means the agents are not pointlessly grouping and overlapping their sensor radiuses. The best results were achieved by the proposed method.

20 agents were used in this simulation with the sensor radius of two square elements. The map dimension was 40×40 square elements. One agent alone is able to cover the amount of 0.8% of the whole environment. The maximum amount of space covered by 20 agents is 16%, if they do not overlap their sensor radiuses. The following graph in Fig. 13 shows the comparison of this ideal state and the real map coverage achieved by 20 agents. It can be seen, that the proposed method is close to this optimal value of 16% map coverage.

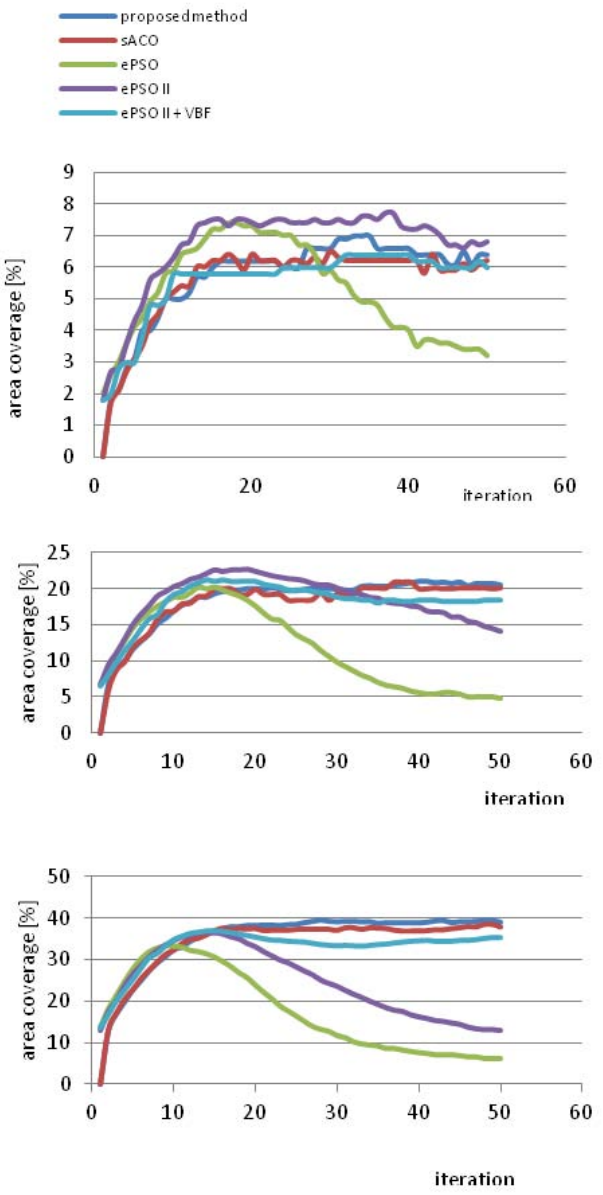

Fig. 12. Simulation results for 3, 10, and 20 agents

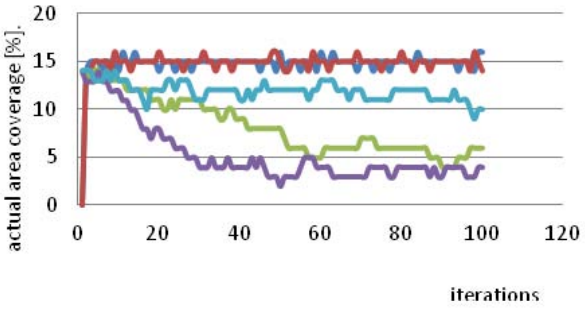

Fig. 13. The comparison of an ideal state of coverage and results achieved by 20 agents

8 Prove of the Concept

The proposed method was implemented and tested on real mobile agents. The goal was to show, that proposed method is usable in real environment.

The problem of area coverage – exploring and surveillance, encompasses many partial problems related to path planning, navigation and localization. The proposed method does not include optimization of path planning. In the future the method will be tested on a group of ardu-copters (quad copters based on an Arduino platform[1]). An algorithm for shortest path planning, e.g. in [2] will be applied.

Multi-agent system consisted of three autonomous mobile robots. A brief description of the robotic platform is given in the next section.

8.1 A Robotic Platform Description

A robotic platform LEGO NXT Mindstorm and differential wheeled robots that were able to move over a flat surface was used in these experiments. Robots were equipped with two angle sensors, digital compass, color sensor, ultrasonic sensor, and two touch sensors. Sensor equipment is crucial for robots navigation. There are many interesting methods used for robots navigation. An artificial potential field method is broadly used for those tasks. Simon et al. in [14] suggest using WSNs RSSI Parameters together with a potential field method for navigation of mobile robots. Recently Ambient Intelligence influences the robotics research, too. Rodić in [12] describes sensor based navigation and integrated control of ambient wheeled robots.

Indoor localization is a separate problem that can be handled e.g. by neural network [3]. In our case, an odometer was used for the localization task. Colored vertical and horizontal lines distributed periodically on a white surface helped robots to eliminate any accumulated and systematic errors of the

[1] `http://www.arducopter.co.uk/`

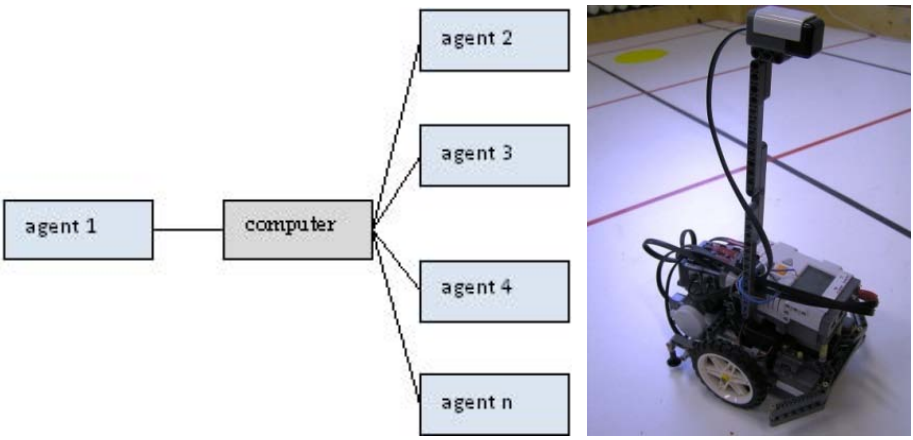

Fig. 14. Broadcasting simulated by PC and a Lego-robot used for testing in a laboratory

odometer method. Robots were able to sense obstacles with ultrasonic sensor, or with touch sensors. They were able to detect different color of the surface beneath them. This is later used to detect circle-shaped marks in the environment. Robots are able to avoid obstacles; we have implemented a low level control layer for this purpose. If the obstacle is detected, it is marked into the map of the robot. The communication is done via Bluetooth. NXT platform does not support broadcasting communication; therefore it is simulated using PC (see Fig. 14).

Agents communicate their actual positions. Pheromone deposition and pheromone evaporation is then derived from this information. In case of using real robots, the VERA tool works as a software agent, which collects all the information from all agents in a group. This software agent is responsible for the creation of the probabilistic model of the environment. Fig. 15 depicts the layers of behavior of the agents.

8.2 Testing

We have performed a lot of tests with many different obstacle layouts. The number of agents was ranging from one to three. First experiments were done using only one agent. The goal was to prove, that even only one agent is able to explore or monitor space. Behavior of the agent was based only on pheromone vector, since there were no other agents creating the influence vectors. This fact causes a drop in the efficiency, but beside this, one agent was able to carry out assigned task.

In the next tests, we have used three agents, but we have simulated a failure on two of them. The result was that remaining agent was able to continue in its task. If it detected other agents in the environment, it marked them as ob-

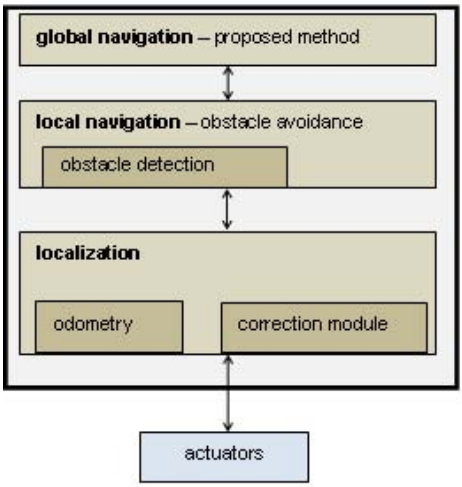

Fig. 15. A general agent's behaviour schema

stacles, because it had lost a communication with them. These tests proved the robustness of the proposed method.

The following experiments were focused mainly on creation of the model of probabilistic placement of the obstacles and free areas (further referred as probabilistic map). All the information about environment and obstacles were collected by software agent running on computer. When an agent detected an obstacle, it was send to the software agent. This software agent was creating a probabilistic model of the environment based on this information. The probability of the obstacle was raised when it was detected by other agent. The created probabilistic map of the environment was three dimensional, with the obstacle probability on the vertical axis. Therefore, the resulting graph had a wavy surface and the peaks represent places with the highest probability of the obstacle occurrence. An example of a probabilistic map created by the multi-agent system is given in Fig. 16 and 17.

The probabilistic map was in fact two-dimensional array. The visualization in the previous figures is done using Matlab software. As it was mentioned earlier, agents were able to detect also a circle-shaped yellow marks on the surface. The behavior of the agents was not aimed towards searching for these marks as targets, but the successful coverage of the environment resulted into full coverage of the yellow marks. The process of creating probabilistic map of the marks was the same as in the case with obstacles and the example is in the following figures.

The accuracy of created models depended from the accuracy of localization and the accuracy of ultrasonic sensor. The localization system was prone to systematic and random errors. Some improvement was achieved using correction mechanisms, but despite this fact there were cases of false obstacle detection resulting in obstacle misplacement within the virtual map.

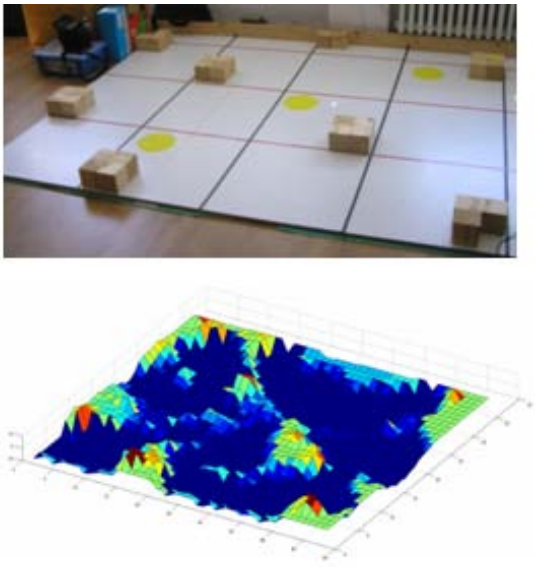

Fig. 16. A real environment and its model created by three agents

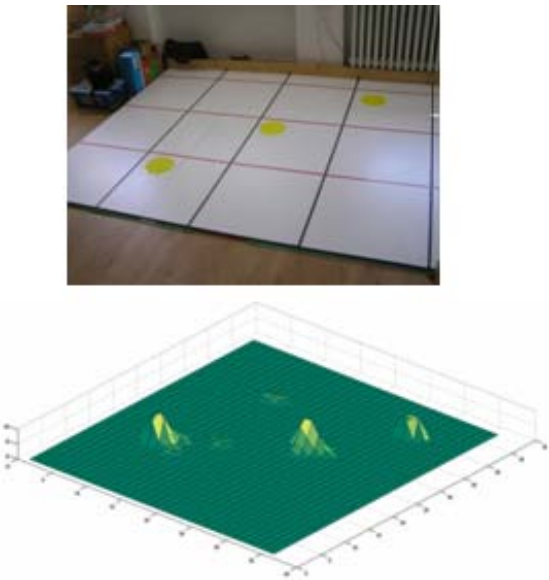

Fig. 17. Yellow spots detected by three agents

9 Conclusions

This paper proposed a new swarm-based method focused on autonomous multi-robot coordination, especially on space exploration and surveillance over the environment. The proposed method was tested by simulations and on real robots in the laboratory.

The simulation results prove that the proposed approach works well for space exploration and surveillance. Switching from exploration to surveillance mode is done via changing two features only. Effective map coverage was achieved, while still maintaining low communicational and computational costs. A virtual pheromone-based communication mechanism is adapted to decrease the communication cost and optimize the cooperation within the swarm. The most important features of the presented approach are:

flexibility – different parameters setting results in different behavior of the system,
scalability – the algorithm works for any number of robots. The only limitation is communicational ability of individual robots,
adaptability – the presented approach can be used in any environment, however it was tested on indoor robots moving over a flat surface. The adaptation of our approach depends on specific mobile agents realization,
robustness – a failure of a robot does not cause a failure of the whole system,
platform independence – can be used for different types of robotic platforms, such as mobile vehicles, flying quad-copters, etc.,
parallelism – (the algorithm is distributed, each agent performs its operations in parallel).

The possible application of this method is in the various scenarios such as monitoring, space exploration, searching for target in dangerous environment, map creation of the unknown environment, etc.

Acknowledgements. The research presented in this paper is partially supported by the national grant agency SRDA under the grant No. 0261-10 and VEGA 2/0194/13.

References

1. Dorigo, M., Stutzle, T.: Ant Colony Optimization. MIT Press (2004) ISBN 0-262-04219-3
2. Gao, X.-Z., Hou, Z.-X., Zhu, X.-F., Zhang, J.-T., Chen, X.-Q.: The Shortest Path Planning for Manoeuvres of UAV. Acta Polytechnica Hungarica 10(1), 222–239 (2013) ISSN 1785-8860
3. Gogolak, L., Pletl, S., Kukolj, D.: Neural Network-based Indoor Localization in WSN Environments. Acta Polytechnica Hungarica 10(6), 221–235 (2013) ISSN 1785-8860

4. Hereford, J.M., Siebold, M.A.: Bio-inspired search strategies for robot swarms. In: Martin, E.M. (ed.) Swarm Robotics From Biology to Robotics. InTech (2010) ISBN: 978-953-307-075-9
5. Kalivarapu, V., Winer, E.: Implementation of Digital Pheromones in Particle Swarm Optimization for Constrained Optimization Problems. In: 49th AIAA/-ASME/ASCE/AHS/ASC Structures, Structural Dynamics, and Materials Conference, Schaumburg, IL (2008)
6. Kennedy, J., Eberhart, R.: A new optimizer using particle swarm theory. In: Proceedings of the IEEE Sixth International Symposium on Micro Machine and Human Science, pp. 39–43 (1995) ISBN: 0-7803-2676-8
7. Masár, M.: A biologically inspired swarm robot coordination algorithm for exploration and surveillance. In: INES 2013: IEEE 17th Internetional Conference on Intelligent Engineering Systems (2013)
8. Masár, M., Zelenka, J.: Modification of PSO algorithm for the purpose of space exploration. In: SAMI 2012: Proceedings, pp. 223–226. IEEE, Piscataway (2012) ISBN 978-1-4577-0195-5
9. Parker, L.E.: Current State of the Art in Distributed Autonomous Mobile Robotics. In: Parker, L.E., Bekey, G., Barhen, J. (eds.) Distributed Autonomous Robotic Systems 4, pp. 3–12. Springer (2000)
10. Payton, D., Estkowski, R., Howard, M.: Pheromone robotics and the logic of virtual pheromones. In: Şahin, E., Spears, W.M. (eds.) Swarm Robotics WS 2004. LNCS, vol. 3342, pp. 45–57. Springer, Heidelberg (2005)
11. Reynolds, C.W.: Flocks, herds and schools: A distributed behavioral model. In: SIGGRAPH 1987: Proceedings of the 14th Annual Conference on Computer Graphics and Interactive Techniques, pp. 25–34. Association for Computing Machinery (1987), doi:10.1145/37401.37406 ISBN 0-89791-227-6
12. Rodić, A., Mester, G.: Sensor-based Navigation and Integrated Control of Ambient Intelligent Wheeled Robots with Tire-Ground Interaction Uncertainties. Acta Polytechnica Hungarica 10(3), 113–133 (2013) ISSN 1785-8860
13. Shang, L., Kai, C., Guan, H., Liang, A.: A Map-Coverage Algorithm Basing on Particle Swarm Optimization. In: 2009 International Conference on Scalable Computing and Communications; Eighth International Conference on Embedded Computing, pp. 87–91 (2009) ISBN 978-0-7695-3825-9
14. Simon, J., Martinović, G.: Navigation of Mobile Robots Using WSN's RSSI Parameter and Potential Field Method. Acta Polytechnica Hungarica 10(4), 107–118 (2013) ISSN 1785-8860
15. Svennebring, J., Koenig, S.: Building terrain covering ant robots: a feasible study. Autonomous Robots 16(3), 313–332 (2004)
16. Ward, C.R., Gobet, F., Kendall, G.: Evolving collective behavior in an artificial ecology. Artificial Life 7(2), 191–209 (2001)

Part III
Applied Mathematics

A Note on Perturbation Estimates for Invariant Subspaces of Hessenberg Matrices

Aurél Galántai

Óbuda University
Bécsi út 96/b, 1034 Budapest, Hungary
galantai.aurel@nik.uni-obuda.hu

Abstract. We give survey of polynomial and matrix perturbation results that are necessary to understand and develop the invariant subspace perturbation theorem we investigate in details. The main purpose of this note is to point out special features of that result such as computability and sharpness. We tested our perturbation estimate on several matrices. The numerical results indicate a high precision and also the possibility of further development for theory and applications.

Keywords: perturbation, polynomial, matrix, invariant subspace, angles between subspaces.

1 Introduction

The eigenvalue problem of matrices is very important in theory and applications and raises many questions. The eigenvalue problem and the polynomial equations are intertwined via the characteristic polynomial. The matrix and polynomial perturbations have been studied from many aspects and the subject has quite an enormous literature (see, e.g. [25], [37], [5], [1]).

Here we are seeking for numerically computable perturbation estimates for invariant subspaces. In Sections 2 and 3 we recall those basic results and concepts we need for our investigations and also provide comparisons as well. In Section 4 we present computable estimates for the perturbation of invariant subspaces of unreduced Hessenberg matrices. The last section contains the details of computation and examples of numerical testing with some conclusions.

2 Polynomial Perturbation Results

The first computable estimate for the perturbation of polynomial zeros was given by Ostrowski [28] in 1940. He later extended this result to matrices using the fact that their characteristic polynomials are sufficiently close for perturbations small enough [29],[30].

Theorem 1 (Ostrowski [28]). *Let* $p(z) = z^n + a_1 z^{n-1} + \cdots + a_n$ *and* $q(z) = z^n + b_1 z^{n-1} + \cdots + b_n$. *For any root* x_i *of* $p(z)$, *there exists a root* y_j *of* $q(z)$

J. Fodor and R. Fullér (eds.), *Advances in Soft Computing, Intelligent Robotics and Control,* Topics in Intelligent Engineering and Informatics 8,
DOI: 10.1007/978-3-319-05945-7_16,

such that

$$|x_i - y_j| \le \left\{ \sum_{k=1}^{n} |a_k - b_k| \gamma^{n-k} \right\}^{1/n}, \tag{1}$$

where $\gamma = 2 \max_{1 \le k \le n} \{ |a_k|^{1/k}, |b_k|^{1/k} \}$. *Furthermore, the roots of* p *and* q *can be enumerated as* $\alpha_1, \ldots, \alpha_n$ *and* $\beta, \ldots, \beta_n$, *respectively, in such a way that*

$$\max_i |\alpha_i - \beta_i| \le (2n-1) \left\{ \sum_{k=1}^{n} |a_k - b_k| \gamma^{n-k} \right\}^{1/n}. \tag{2}$$

If $|a_j - b_j| \le \varepsilon$, $j = 1, \ldots, n$, then $\max_i |\alpha_i - \beta_i| = O\left(\varepsilon^{1/n}\right)$. This basic result is widely used in the literature as a final state of the art (see, e.g. [34], [9]). However, Beauzamy significantly improved the estimate in 1999. For polynomial $p(z) = \sum_{j=0}^{n} a_j z^{n-j}$, define the Bombieri-norm as $[p]_B = \left(\sum_{j=0}^{n} |a_j|^2 / \binom{n}{j} \right)^{1/2}$.

Theorem 2 (Beauzamy [3]). *Let* $k \ge 1$ *be an integer,* $p(z)$ *and* $q(z)$ *be two polynomials of degree* n, *with* $[p-q]_B \le \varepsilon$. *If* x_i *is any zero of* $p(z)$ *with multiplicity* k, *there exists a zero* y_j *of* $q(z)$, *with*

$$|x_i - y_j| \le \left(\frac{n!}{(n-k)!} \frac{\left(1 + |x_i|^2\right)^{n/2}}{\left|q^{(k)}(x_i)\right|} \right)^{1/k} \varepsilon^{1/k}. \tag{3}$$

If

$$\varepsilon \le \frac{(n-k)!}{2n!} \frac{\left|p^{(k)}(x_i)\right|}{\left(1 + |x_i|^2\right)^{\frac{n-k}{2}}}, \tag{4}$$

then (3) implies

$$|x_i - y_j| \le \left(\frac{2n!}{(n-k)!} \frac{\left(1 + |x_i|^2\right)^{n/2}}{\left|p^{(k)}(x_i)\right|} \right)^{1/k} \varepsilon^{1/k}. \tag{5}$$

This result of local character implies that in the neighborhood of a zero x_i of multiplicity $k < n$ the order of perturbation is $O\left(\varepsilon^{1/k}\right)$, which is definitely better than $O\left(\varepsilon^{1/n}\right)$ $(\varepsilon \to 0)$, if $p(z)$ has at least two different zeros.

Inspired by Beauzamy's result we developed the following estimate in a different way [14].

Theorem 3 ([14]). *Assume that* $p(z) = z^n + a_1 z^{n-1} + \cdots + a_{n-1} z + a_n$ *has the distinct roots* $z_1, \ldots, z_k$ *with multiplicity* $n_1, \ldots, n_k$. *Let* $\widetilde{p}(z) = z^n + \widetilde{a}_1 z^{n-1} + \cdots + \widetilde{a}_{n-1} z + \widetilde{a}_n$ *be a perturbation of* p *with* $\widetilde{a}_i = a_i + \varepsilon_i$, $|\varepsilon_i| \le \varepsilon$, $i = 1, \ldots, n$.

For $0 < \varepsilon < \varepsilon'$, there exist constants γ_i $(i = 1, \ldots, k)$ depending only on $p(z)$ such that disk

$$|z - z_i| \leq r_i = \left(\frac{2\,(n_i)!\gamma_i \varepsilon}{|p^{(n_i)}(z_i)|} \right)^{1/n_i} \qquad (i = 1, \ldots, k) \tag{6}$$

contains exactly n_i zeros of the perturbed polynomial $\widetilde{p}(z)$ provided that $r_i < \frac{1}{2} \min_{\ell \neq j} |z_\ell - z_j|$.

Note that the order of perturbation bound is given by the multiplicity n_i of the nearest root z_i. It also follows that the perturbation of simple roots is of order $O(\varepsilon)$. The estimates of Theorems 2 and 3 are compared in [14].

3 Eigenvalue and Subspace Perturbations of Matrices

Ostrowski [29], [30] proved the first computable bound for the perturbations of matrix eigenvalues as well using Theorem 1.

Theorem 4 (Ostrowski [29], [30]). *Let $A = [a_{ij}]_{i,j=1}^n$, $B = [b_{ij}]_{i,j=1}^n$ be two matrices and*

$$\varphi(\lambda) \equiv |A - \lambda I| = 0, \quad \psi(\lambda) \equiv |B - \lambda I| = 0 \tag{7}$$

the corresponding characteristic polynomials and equations. Denote the zeros of $\varphi(\lambda)$ by λ_i and those of $\psi(\lambda)$ by μ_i. Put

$$M = \max(|a_{ij}|, |b_{ij}|) \quad (i, j = 1, \ldots, n), \tag{8}$$

$$\frac{1}{nM} \sum_{i,j} |a_{ij} - b_{ij}| = \delta. \tag{9}$$

Then to every root μ_i of $\psi(\lambda)$ belongs to a certain root λ_i of $\varphi(\lambda)$ such that we have

$$|\mu_i - \lambda_i| \leq (n + 2)\, M \delta^{1/n}. \tag{10}$$

Furthermore, for a suitable ordering of λ_i and μ_i we have

$$|\mu_i - \lambda_i| \leq 2\,(n + 1)^2\, M \delta^{1/n}. \tag{11}$$

We need the concept of eigenvalue variation.

Definition 1. *Let $A, B \in \mathbb{C}^{n \times n}$. Assume that $\sigma(A) = \{\lambda_1, \ldots, \lambda_n\}$ and $\sigma(B) = \{\mu_1, \ldots, \mu_n\}$. Let S_n be the set of all permutations of $\{1, 2, \ldots, n\}$. The eigenvalue variation of A and B is defined by*

$$v(A, B) = \min_{\pi \in S_n} \left\{ \max_i \left| \mu_{\pi(i)} - \lambda_i \right| \right\}. \tag{12}$$

$v(A,B)$ is also called the (optimal) matching distance between the eigenvalues of A and B (see, e.g. [37] or [5]). The next result is a reformulation and improvement of Ostrowski's matrix perturbation theorem although the order of estimate is the same.

Theorem 5 (Bhatia, Elsner, Krause [4]). *Let $A, E \in \mathbb{C}^{n\times n}$. Then*

$$v(A, A+E) \le 4 \times 2^{-1/n} \left(\|A\| + \|A+E\|\right)^{1-1/n} \|E\|^{1/n}. \tag{13}$$

The above results suggest an $O\left(\varepsilon^{1/n}\right)$ size perturbation of the eigenvalues ($\varepsilon = \|E\|$). However, Bauer and Fike proved the following result in 1960.

Theorem 6 (Bauer, Fike, [2]). *If A is diagonalizable, i.e., $A = X\Lambda X^{-1}$ with $\Lambda = diag(\lambda_1(A), \ldots, \lambda_n(A))$, then to each $\lambda_i(A+E)$ there is a $\lambda_j(A)$ such that*

$$|\lambda_i(A+E) - \lambda_j(A)| \le \|X\| \left\|X^{-1}\right\| \|E\|$$

using any norm for which $\|\Lambda\| = \max_i |\lambda_i(A)|$.

Hence for diagonalizable matrices the perturbation order of eigenvalues is $O(\varepsilon)$ ($\varepsilon = \|E\|$), which is much better than $O\left(\varepsilon^{1/n}\right)$. For normal matrices this bound is even better since X can be unitary matrix with a norm 1.

The Bauer-Fike theorem indicates a significant difference between the polynomials and matrices. While Theorems 2 and 3 are sharp and in generally cannot be improved, the Bauer-Fike theorems guarantees that the eigenvalue perturbations of diagonalizable matrices are of order $O(\varepsilon)$ independently of the multiplicities of eigenvalues.

For non-normal matrices, Henrici [21] was the first to extend the Bauer-Fike result. His result was improved by Chu [8].

Let $J_k(\lambda) \in \mathbb{C}^{k\times k}$ be an upper Jordan block. For any $A \in \mathbb{C}^{n\times n}$, there exists a nonsingular matrix X such that

$$X^{-1}AX = \operatorname{diag}\left(J_{n_1}(\lambda_1), J_{n_2}(\lambda_2), \ldots, J_{n_k}(\lambda_k)\right) \tag{14}$$

and $\sum_{j=1}^{k} n_j = n$. The eigenvalues λ_i, $i = 1, \ldots, k$ are not necessarily distinct.

Denote by $g_m(c)$ the unique nonnegative real zero of equation

$$\phi_m(x) = \sum_{\ell=1}^{m} x^\ell = c \quad (c \ge 0). \tag{15}$$

Function $g_m(c)$ is strictly monotone increasing and

$$\min\left\{c/m,\ \sqrt[m]{c/m}\right\} \le g_m(c) \le \sqrt[m]{c} \tag{16}$$

(for proof, see Henrici [21]).

Theorem 7 (Chu [8]). *If $A \in \mathbb{C}^{n\times n}$ has the Jordan canonical form (14), then for any $\mu \in \sigma(A+E)$ there exists $\lambda_j \in \sigma(A)$ such that*

$$|\mu - \lambda_j| \le 1/g_{n_j}(1/\theta) \le \max\left\{n_j\theta, (n_j\theta)^{1/n_j}\right\} \tag{17}$$

holds with $\theta = \left\|X^{-1}EX\right\|_2$.

The result indicates an $O\left(\varepsilon^{1/n_i}\right)$ perturbation of the eigenvalue λ_i having multiplicity n_i in the Jordan form (14) like in the polynomial case. One can replace n_j by $m = \max_i n_i$, the maximum size of Jordan blocks, which might be less than the algebraic multiplicity of the eigenvalue λ_j. For $k \geq 2$, this estimate corresponds to those of Theorems 2 and 3 and is asymptotically better than those of Ostrowski-Elsner type. The result can be rephrased as

$$v\left(A, A+E\right) \leq \left(2n-1\right)/g_m\left(1/\theta\right) \leq \left(2n-1\right)\max\left\{m\theta, \left(m\theta\right)^{1/m}\right\}, \tag{18}$$

where $m = \max_i n_i$ and $\theta = \left\|X^{-1}EX\right\|_2$. The result also follows from a Hoffman-Wielandt type theorem of Song [35] (see also [14]).

Note that perturbation bounds of Theorems 2, 3 and 7 are sharp and cannot be improved generally.

The use of Theorem 7 and the companion matrix of polynomials yield the following polynomial perturbation theorem of global character [14].

Assume that $p(z) = z^n + a_1 z^{n-1} + \cdots + a_{n-1}z + a_n$ has the distinct zeros $z_1, \ldots, z_k$ with multiplicity $n_1, \ldots, n_k$. Then the Jordan form of its companion matrix

$$C = C\left(p\right) = \begin{bmatrix} -a_1 & -a_2 & & & -a_n \\ 1 & 0 & & & 0 \\ & 1 & \ddots & & \\ & & \ddots & \ddots & \\ \mathbf{0} & & & 1 & 0 \end{bmatrix} \tag{19}$$

is given by

$$C = \Pi V J V^{-1} \Pi^T, \tag{20}$$

where $\Pi = [e_n, e_{n-1}, \ldots, e_2, e_1]$, $J = \text{diag}(J_{n_1}\left(z_1\right), \ldots, J_{n_k}\left(z_k\right))$ and

$$V = [V_1, \ldots, V_k] \quad (V_i \in \mathbb{C}^{n\times n_i}), \quad \left(V_i\right)_{pq} = \begin{cases} 0, & \text{if } p < q \\ \binom{p-1}{q-1} z_i^{p-q}, & \text{if } p \geq q \end{cases} \tag{21}$$

(see, e.g. [39], [40], [31] or [17]). The matrix V is called the confluent Vandermonde matrix. The companion matrix is diagonalizable by similarity if and only if all its zeros are distinct, i.e., $k = n$ and $n_i = 1$ $(i = 1, \ldots, n)$, when V is the common Vandermonde matrix. Kittaneh [26] proved that C is normal (unitary) if and only if $p\left(z\right) = z^n + a_n$ with $|a_n| = 1$

Theorem 8. *([14]). Assume that $p\left(z\right) = z^n + a_1 z^{n-1} + \cdots + a_{n-1}z + a_n$ has the distinct roots $z_1, \ldots, z_k$ with multiplicity $n_1, \ldots, n_k$. Let $\widetilde{p}\left(z\right) = z^n + \widetilde{a}_1 z^{n-1} + \cdots + \widetilde{a}_{n-1}z + \widetilde{a}_n$ be a perturbation of p with $\widetilde{a}_i = a_i + \varepsilon_i$, $|\varepsilon_i| \leq \varepsilon$, $i = 1, \ldots, n$. For any root $\widetilde{z}_i$ of $\widetilde{p}\left(z\right)$, there exists a root z_j of $p\left(z\right)$ such that*

$$|\widetilde{z}_i - z_j| \leq \max\left\{n_j\theta, \left(n_j\theta\right)^{1/n_j}\right\} \tag{22}$$

with $\theta = \left\|V^{-1}\Delta V\right\|_2$ *and* $\Delta = -e_n w^T$ *(*$w^T = [\varepsilon_n, \varepsilon_{n-1}, \ldots, \varepsilon_1]$*). There also exists a permutation* $\pi \in S_n$ *such that for* $i = 1, \ldots, n$,

$$\left|\widetilde{z}_{\pi(i)} - z_i\right| \leq (2n-1) \max\left\{m\theta, (m\theta)^{1/m}\right\}, \tag{23}$$

where $m = \max_i n_i$.

Since $\theta = O(\varepsilon)$, perturbation bounds (22) and (23) are of order $O\left(\varepsilon^{1/n_j}\right)$ and $O\left(\varepsilon^{1/m}\right)$, respectively.

The perturbation of invariant subspaces is a much more complicated matter than the perturbation of eigenvalues (see, e.g. Davis, Kahan [10] or [37], [5]). A subspace $\mathcal{M} \subset \mathbb{C}^n$ is an invariant subspace of A if $Ax \in \mathcal{M}$ for every $x \in \mathcal{M}$. Particularly, each eigenvector x spans a one dimensional invariant subspace $\mathcal{V} = \{\alpha x \mid \alpha \in \mathbb{C}\}$. For the theory of invariant subspaces we refer to Gohberg, Lancaster and Rodman [18].

For Hermitan matrices there are other type of eigenvalue perturbation estimates that are related to subspace perturbations (see, e.g. [5], [32]). An example of such estimates is the following.

Assume that $A \in C^{n\times n}$ is Hermitian with eigenvalues $\lambda_1 \geq \cdots \geq \lambda_n$. If X has orthonormal columns that span an invariant subspace S of A and $M = X^H AX$, then $AX - XM = 0$. Assume that the columns of X span an approximate invariant subspace $\widehat{S}$ of A. Then the residual matrix $R = AX - XM$ is expected to be small. Assume that the eigenvalues of M are $\mu_1 \geq \cdots \geq \mu_k$ and $n-k$ eigenvalues are well separated from the eigenvalues of M, that is a number $\delta > 0$ exists such that exactly $n-k$ eigenvalues of A lie outside the interval $[\mu_k - \delta, \mu_1 + \delta]$. Then the following result holds.

Theorem 9 (Stewart [36]). *If* $\rho = \|R\|/\delta < 1$*, then there is an index* j *such that* $\lambda_j, \ldots, \lambda_{j+k-1} \in (\mu_k - \delta, \mu_1 + \delta)$ *and*

$$|\mu_i - \lambda_{j+i-1}| \leq \frac{1}{1-\rho^2}\frac{\|R\|^2}{\delta} \quad (i = 1, \ldots, k). \tag{24}$$

For nonnormal matrices Kahan, Parlett and Jiang [24] pointed out that "*the norms of residuals of the approximate eigenvectors are not themselves sufficient information to bound an approximate eigenvalue*".

The perturbation of invariant subspaces is measured by the Jordan or canonical angles between two subspaces. For definition and computation of canonical angles, we refer to [12], [13] or [19]. The kth subspace angle between the subspaces $\mathcal{M}$ and $\mathcal{N}$ will be denoted by $\theta_k(\mathcal{M}, \mathcal{N})$, where $k = 1, \ldots, j$ and $j = \min\{\dim(\mathcal{M}), \dim(\mathcal{N})\}$.

For Hermitan or normal matrices there are several estimates for the canonical angles given in various forms including quantities such as residual and/or separation, which are difficult to compute in general (see, e.g. [10], [5], [32], [27]). In order to give some insight we recall a result of Ipsen [23] for general matrices, which is close to the results of the subsequent sections at least in character.

Let the perturbed matrix $A+E$ have an invariant subspace $\widehat{\mathcal{M}}$, whose dimension is not necessarily the same as that of $\mathcal{M}$. Let P and $\widehat{P}$ denote the orthogonal projectors onto $\mathcal{M}$ and $\widehat{\mathcal{M}}$, respectively. The absolute separation between A and $A+E$ is defined by

$$\text{absep=absep}_{\{A,A+E\}} = \min_{\|Z\|=1,\ PZ\widehat{P}=Z} \|PAZ - Z(A+E)P\|. \tag{25}$$

Theorem 10 (Ipsen [23]). *If absep>0 then*

$$\max_i \sin\theta_i\left(\mathcal{M}, \widehat{\mathcal{M}}\right) \leq \|E\| / \textit{absep}. \tag{26}$$

Next we give a result on the perturbation of the invariant subspaces of unreduced Hessenberg matrices that provides a bound for subspace angles without using any concept of separation.

4 Perturbation Results for Hessenberg Matrices

A matrix is called nonderogatory if exactly one Jordan block may belong to each eigenvalue. A matrix is nonderogatory if and only if it is similar to an unreduced upper Hessenberg matrix. The upper Hessenberg matrix $H \in \mathbb{C}^{n\times n}$ is said to be unreduced, if all $h_{i+1,i}$ elements are nonzero. If H is unreduced, then the last and first entries of the right and left eigenvectors, respectively are nonzero.

Define vectors $x, y \in \mathbb{C}^n$ such that $y^H e_1 = e_n^T x = 1$ and

$$(H-\lambda I)x = p(\lambda)e_1, \tag{27}$$

$$y^H(H-\lambda I) = p(\lambda)e_n^T \tag{28}$$

hold, where λ is real or complex scalar. Here $p(\lambda)$ is the characteristic polynomial of H, which can be easily evaluated at any λ in a numerically stable way from any of the above equations by the Hyman's method (see [40], [41], [22] or [15]).

The following properties hold (see [15]).

Lemma 1. *The components of x and y are polynomials in λ : x_{n-j} and y_{1+j} have degree j ($j = 0, 1, \ldots, n-1$). The polynomial $p(\lambda)$ is of order n.*

Lemma 2. *The k-th derivative of y, x and $p(\lambda)$ with respect to λ satisfy the relations*

$$(H-\lambda I)\,x^{(k)} = kx^{(k-1)} + p^{(k)}(\lambda)\,e_1, \quad k = 0, 1, \ldots \tag{29}$$

and

$$y^{(k)H}(H-\lambda I) = ky^{(k-1)H} + p^{(k)}(\lambda)\,e_n^T, \quad k = 0, 1, \ldots, \tag{30}$$

where $y^{(k)H}$ denotes the conjugate transpose of $y^{(k)}$ and differentiation is done componentwise.

Lemma 3.

$$p^{(k)}(\lambda) = -ky^H x^{(k-1)} = -ky^{(k-1)H} x,\ k > 0 \tag{31}$$

Define

$$X(r,\lambda) = \left[x(\lambda), x'(\lambda), \frac{1}{2!}x''(\lambda), \ldots, \frac{1}{(r-1)!}x^{(r-1)}(\lambda) \right]. \tag{32}$$

It was shown in [15], that if λ_i is an eigenvalue of H with multiplicity n_i, then the columns of matrix $X(n_i, \lambda_i)$ are the right generalized eigenvectors belonging to λ_i and they span the corresponding invariant subspace. Gohberg, Lancaster and Rodman [18] showed that such an invariant subspace of dimension n_i can define additionally $n_i - 1$ different invariant subspaces of smaller dimension. However, with respect to an eigenvalue, we shall think on the invariant subspace of maximal dimension in the following. Observe that for $s < r$,

$$X(r,\lambda) = \left[X(s,\lambda), \frac{1}{s!}x^{(s)}(\lambda), \ldots, \frac{1}{(r-1)!}x^{(r-1)}(\lambda) \right] \tag{33}$$

and $\mathcal{R}(X(j,\lambda)) \subset \mathcal{R}(X(\ell,\lambda))$ for $j < \ell$. We proved the following results in [16].

Theorem 11 ([16]). *Assume that both $H \in \mathbb{C}^{n\times n}$ and its perturbation $\widehat{H} = H+E$ are unreduced upper Hessenberg matrices for $\|E\|$ ($\|E\| \le \varepsilon$) small enough. Assume that λ_i is an eigenvalue of H with multiplicity n_i and μ_i is a nearby eigenvalue of $\widehat{H}$ with multiplicity m_i ($1 \le m_i \le n_i$). Let P be the orthogonal projection on $\mathcal{R}(X(n_i,\lambda_i))$, $X_1 = X(m_i,\lambda_i)$, $\widehat{X}_1 = \widehat{X}(m_i,\mu_i)$ and $\Delta X_1 = \widehat{X}_1 - X_1$. If θ_k denotes the kth subspace angle between the corresponding invariant subspaces $\mathcal{R}(X(n_i,\lambda_i))$ and $\mathcal{R}\left(\widehat{X}(m_i,\mu_i)\right)$, then for $k = 1,\ldots,m_i$,*

$$0 \le \sin\theta_k \le \left(2 \left\| \left(X_1^H X_1 \right)^{-1} \right\| \right)^{1/2} \|(I-P)\Delta X_1\|. \tag{34}$$

Corollary 1. *There exists a constant $C > 0$ such that*

$$0 \le \sin\theta_k \le \left(2 \left\| \left(X_1^H X_1 \right)^{-1} \right\| \right)^{1/2} \|\Delta X_1\| \le C\varepsilon^{1/n_i} \quad (k = 1,\ldots,m_i). \tag{35}$$

Corollary 2. *Under the conditions of Theorem 11*

$$\sin\theta_k = O\left((\mu_i - \lambda_i)^{n_i - m_i + 1} \right) = O\left(\varepsilon^{\frac{n_i - m_i + 1}{n_i}} \right) \tag{36}$$

for $k = 1,\ldots,m_i$.

The first corollary is a consequence of the perturbation theorems of Sections 2 and 3. It is somewhat crude in view of Corollary 2 but corresponds to the classic eigenvalue perturbation results. It proves that invariant subspace perturbation is continuous in a sense. It also indicates a positive distance from the set of derogatory matrices (for other approach, see Gohberg, Lancaster, Rodman [18], and Gracia, de Hoyos, Velasco [20]).

The second corollary is based upon a refined estimate of $(I-P)\,\Delta X_1$ and it is somewhat surprising. If an eigenvalue λ of multiplicity n_i splits up into n_i simple ones, then $\sin\theta_1 = O(\varepsilon)$ in contrast to the eigenvalue perturbation, which might be of $O\left(\varepsilon^{1/n_i}\right)$. Examples show the possibility of even better perturbation results [16].

The results of this section were extended to dense perturbations of Hessenberg matrices and general nonderogatory matrices as well [16].

The aim of this paper is to show the computational character and goodness of the above results. Details of computations and numerical testing will be presented in the next section.

5 The Computational Algorithm and Testing

We need to compute the matrix $X(r,\lambda)$ for a given H, λ and r, where

$$x(\lambda) = \begin{bmatrix} x_1 \\ \vdots \\ \vdots \\ \vdots \\ x_{n-1} \\ 1 \end{bmatrix}, \quad x^{(k)}(\lambda) = \begin{bmatrix} x_1^{(k)} \\ \vdots \\ x_{n-k}^{(k)} \\ 0 \\ \vdots \\ 0 \end{bmatrix}.$$

First we consider equation $(H-\lambda I)\,x = p(\lambda)\,e_1$. The nth row of the system is

$$h_{n,n-1}x_{n-1} + (h_{nn}-\lambda) = 0.$$

For $1 < i < n$, the ith row is given by

$$h_{i,i-1}x_{i-1} + (h_{ii}-\lambda)\,x_i + h_{i,i+1}x_{i+1} + \cdots + h_{i,n-1}x_{n-1} + h_{in} = 0.$$

We obtain the solution by the following backward substitution algorithm

$$x_{n-1} = (\lambda - h_{nn})\,/h_{n,n-1}, \tag{37}$$

$$x_{i-1} = -\left(h_{in} + (h_{ii}-\lambda)\,x_i + \sum_{j=i+1}^{n-1} h_{ij}x_j\right)/h_{i,i-1}, \quad i = n-1,\ldots,2. \tag{38}$$

This gives the vector x and also $p(\lambda) = e_1^T\,(H-\lambda)\,x(\lambda)$.

We calculate $x^{(k)}(\lambda)$ for $0 < k < n$ using relation

$$(H-\lambda I)\,x^{(k)} = kx^{(k-1)} + p^{(k)}(\lambda)\,e_1, \tag{39}$$

which having the form

$$(H-\lambda I)\begin{bmatrix} x_1^{(k)} \\ \vdots \\ x_{n-k}^{(k)} \\ 0 \\ \vdots \\ 0 \end{bmatrix} = k\begin{bmatrix} x_1^{(k-1)} \\ \vdots \\ x_{n-k}^{(k-1)} \\ x_{n-k+1}^{(k-1)} \\ \vdots \\ 0 \end{bmatrix} + p^{(k)}(\lambda)\, e_1 \tag{40}$$

reduces to a $(n-k+1)\times(n-k)$ problem. The last equation (row $n-k+1$) reads as

$$h_{n-k+1,n-k}x_{n-k}^{(k)} = kx_{n-k+1}^{(k-1)}. \tag{41}$$

Equation i $(1<i<n-k+1)$ has the form

$$h_{i,i-1}x_{i-1}^{(k)} + (h_{ii}-\lambda)\, x_i^{(k)} + \sum_{j=i+1}^{n-k} h_{ij}x_j^{(k)} = kx_i^{(k-1)}. \tag{42}$$

Hence the algorithm is the following

$$x_{n-k}^{(k)} = kx_{n-k+1}^{(k-1)}/h_{n-k+1,n-k}, \tag{43}$$

$$x_{i-1}^{(k)} = \left(kx_i^{(k-1)} - (h_{ii}-\lambda)\, x_i^{(k)} - \sum_{j=i+1}^{n-k} h_{ij}x_j^{(k)} \right) / h_{i,i-1}, \quad i = n-k,\ldots,2. \tag{44}$$

Thus we obtain $x^{(k)}$ and also $p^{(k)}(\lambda)$ from the relation $e_1^T(H-\lambda I)\, x^{(k)} = kx^{(k-1)} + p^{(k)}(\lambda)$ (substitution into the first row). Observe that for computing $X(r,\lambda)$ we do not need to compute $p(\lambda)$ or $p^{(k)}(\lambda)$. Since the computations are performed on the same matrix $H-\lambda I$ in a numerically stable way (see Wilkinson [40], [41] or Higham [22]), the whole computation of $X(r,\lambda)$ is numerically stable.

For the numerical testing we wrote a Matlab program to compute $X(r,\lambda)$ for a given unreduced upper Hessenberg matrix H and eigenvalue λ with known multiplicity r.

The other essential elements of computing an estimate are provided in Matlab. However, instead of the original subroutine `subspace.m` for computing the largest subspace angle, we used subroutines `subspace.m` and `subspacea.m` which are due to Andrew Knyazev and can be downloaded from the site MATLAB Central File Exchange.

We made two different types of numerical testing of our estimate.

1. H and $H+E$ are companion matrices with known zeros (H, $H+E$ and the zeros are known exactly).

2. H and $H+E$ are given unreduced Hessenberg matrices with known zeros and the approximate eigenvalue μ_i is computed by Matlab's `eig` routine. This routine is based on the QR-algorithm that is backward stable, which means that it computes the exact eigenvalues of a perturbed matrix $A+E$ with $\|E\| \approx \epsilon_{machine} \|A\|$ (see Golub, van Loan [19], Tisseur [38] or Kressner [27]). However, the algorithm does not recognize the multiple eigenvalues and there are some precision problems as well (see, e.g. [15]).

Next we show some characteristic results of the numerical testing.

Test problem No. 1: $H = C(p(z))$, $H+E = C(\widetilde{p}(z))$, where $p(z) = z^3 - 2z^2 + z$ and $\widetilde{p}(z) = z^3 - (2+\varepsilon) z^2 + (1+\varepsilon) z - \left(\varepsilon - \varepsilon^2\right)$. H has the single eigenvalue $\lambda = 0$ and the double eigenvalue $\lambda = 1$ ($n_2 = 2$). $H+E$ has the nearby simple eigenvalues $\lambda = \varepsilon$, $\lambda = 1+\sqrt{\varepsilon}$ ($m_2 = 1$) and $\lambda = 1-\sqrt{\varepsilon}$. Selecting $\lambda_1 = 1$, $n_1 = 2$, $\mu_1 = 1+\sqrt{\varepsilon}$, $m_1 = 1$ and making elementary calculations we have

$$\sin\theta_1 \left(\mathcal{R}(X(2,1)), \mathcal{R}\left(\widehat{X}\left(1, 1+\sqrt{\varepsilon}\right)\right)\right) = \\ = \frac{\varepsilon}{\left(42\varepsilon + 6\varepsilon^2 + 36\sqrt{\varepsilon} + 24\varepsilon^{\frac{3}{2}} + 18\right)^{1/2}} = O(\varepsilon),$$

which is exactly the bound of Corollary 2.

The following and the subsequent figures show the following quantities versus $\|E\|$:

- the exact $\max_i \sin(\theta_i)$ values computed with the routine `subspace.m` by Knyazev [red line],
- the ratio $\max_i \sin(\theta_i) / \|E\|^a$ ($a = (n_i - m_i + 1)/n_i$) to see if estimate (36) can be improved [green line],
- the estimates (35) [*est1* or cyan dashed line] and (34) [*est2* or black dotted line].

Logarithmic scales are used for both axes.

The results of test problem No. 1 are the following.

These results clearly correspond to the theory. Estimate (35) is indeed crude, but it is still acceptable.

Test problem No. 2: $H = C(p)$, $H+E = C(\widetilde{p})$, where $p(z) = z^5 - z^4$ and $\widetilde{p}(z) = (z+\sqrt{\varepsilon})^2 (z-\sqrt{\varepsilon})^2 (z-1)$, respectively. Selecting $\lambda_1 = 0$, $n_1 = 4$, $\mu_1 = \sqrt{\varepsilon}$, $m_1 = 2$ we obtain by a simple calculation that

$$\sin\theta_1 \left(\mathcal{R}(X(4,0)), \mathcal{R}\left(\widehat{X}\left(2, \sqrt{\varepsilon}\right)\right)\right) = 0$$

and

$$\sin\theta_2 \left(\mathcal{R}(X(4,0)), \mathcal{R}\left(\widehat{X}\left(2, \sqrt{\varepsilon}\right)\right)\right) = O\left(\varepsilon^{3/2}\right),$$

which is definitely better than $O\left(\varepsilon^{3/4}\right)$ shown by estimate (36). The computational results are shown on the next figure.

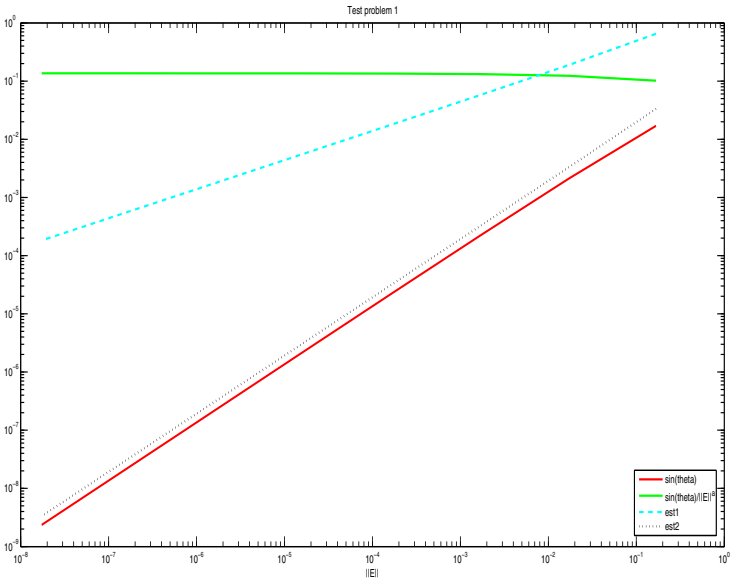

Fig. 1. Test problem 1

Estimate (34) is very sharp. The ratio $\max_i \sin(\theta_i) / \|E\|^a$ indicates that the perturbation order is much better than estimate (36).

Test problem No. 3: $H = C(p)$, $H + E = C(\widetilde{p})$, where

$$p(z) = (z-1)^3 (z+1)(z-2)$$

and

$$\widetilde{p}(z) = (z-1-\varepsilon)^2 (z-1+\varepsilon)(z+1-\varepsilon)(z-2+2\varepsilon).$$

Here $\lambda_1 = 1$, $n_1 = 3$, $m_1 = 1+\varepsilon$, $m_1 = 2$ and the computational results are shown on the next figure.

Here we see again that estimate (34) is very sharp. The $\max_i \sin(\theta_i) / \|E\|^a$ ratio indicates again that the perturbation order is much better than estimate (36). The precision problem shown for the range $\|E\| \lessapprox 10^{-6}$ is due to the fact, that the computed numbers are close to machine epsilon.

Test problem No. 4: $H = H_n^T(\alpha)$, $H + E = H_n^T(\alpha+\varepsilon)$, where $H_n(\alpha)$ is the Chow matrix [7], [11] defined by

$$H_n(\alpha) = [h_{ij}]_{i,j=1}^n, \quad h_{ij} = \begin{cases} \alpha^{i-j+1}, & i \geq j \\ 1, & i = j-1 \\ 0, & i < j-1 \end{cases} \tag{45}$$

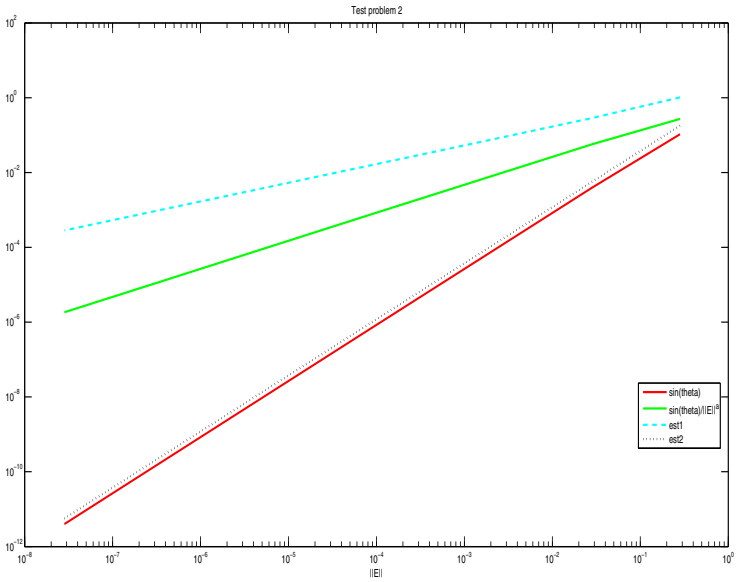

Fig. 2. Test problem 2

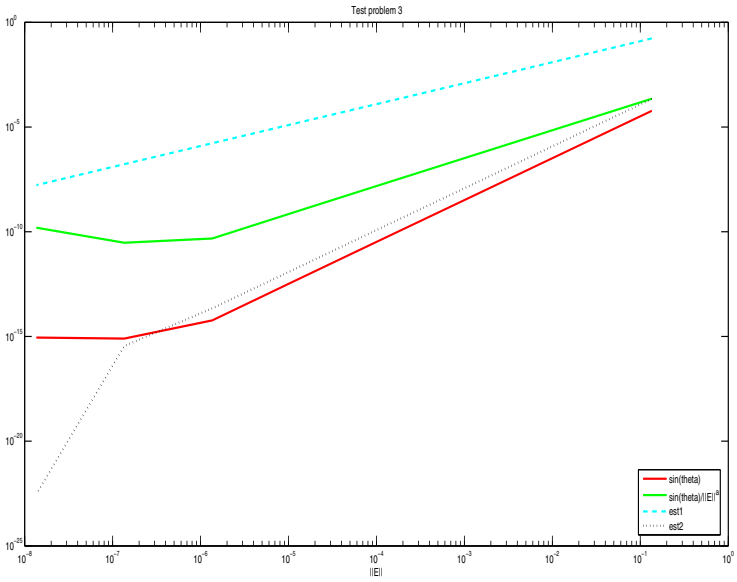

Fig. 3. Test problem 3

The Chow matrix can be found in Matlab gallery library. Chow [7] proved that H_n has $m = \lfloor n/2 \rfloor$ zero eigenvalues and $n - m$ eigenvalues of the form

$$4\alpha \cos^2 \frac{k\pi}{n+2} \quad (k = 1, \ldots, n-m),$$

where $\lfloor n/2 \rfloor$ stands for the lower integer part of $n/2$.

The computational results are shown in the next figure for the parameters $n = 8$, $H = H_n^T(1)$, $H + E = H_n^T(1+\varepsilon)$, $\lambda_1 = 0$, $n_i = 4$,. Observe that $H + E$ is also Chow matrix and it also has m zero eigenvalues. We present four cases (Version 1-Version 4):

1. μ_1 is the nearest to 0 eigenvalue of $H + E$ provided by Matlab's `eig` routine, $m_1 = 1$.
2. μ_1 is the nearest to 0 eigenvalue of $H + E$ provided by Matlab's `eig` routine, $m_1 = 4$.
3. μ_1 is the average of the eigenvalues (of `eig`) in the zero cluster near to 0, $m_1 = 0$.
4. $\mu_1 = 0$, $m_1 = 4$ (The exact values).

The use of average for clustered (and suspected multiple) eigenvalues was suggested by Saad [33] (Theorem 3.5). Numerical testing also indicates that the multiple eigenvalues when perturbed, show a symmetric pattern around the nonperturbed eigenvalue in the complex plane such that the mean of the errors is fairly zero [6].

Version 1 corresponds the 1-dimensional invariant subspace $\widehat{X}(1, \mu_1)$. The estimate seems to be sharp and it corresponds to theory even if μ_1 is only an approximate eigenvalue of $H + E$. Verson 2 simply shows that we can not take

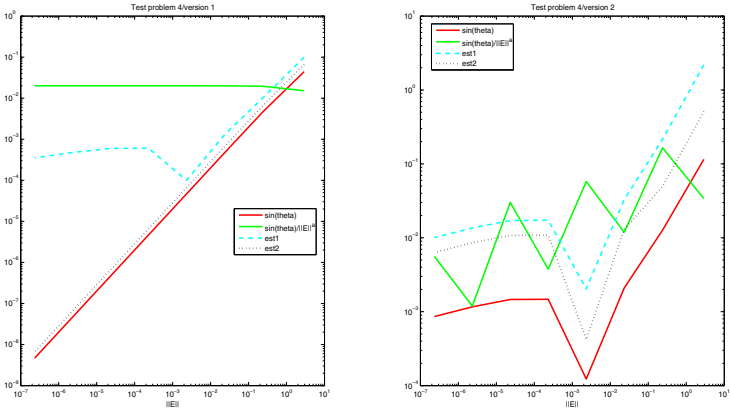

Fig. 4. Test problem 4/Versions 1-2

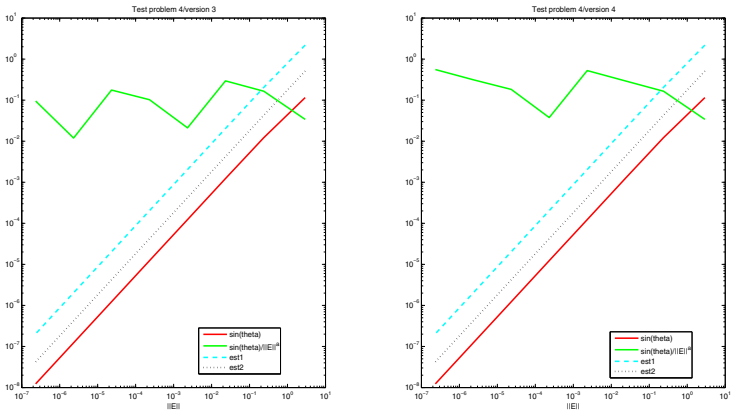

Fig. 5. Test problem 4/Versions 3-4

the approximate μ_1 as a multiple eigenvalue (for problems with Matlab's `eig` routine, see, e.g. [15]).

Figure 5 indicates that Version 3 gives a definitely much better result in agreement with Version 4 that uses exact values.

The presented numerical results show the high precision of estimate (34) and the limits of estimate (35). They also show that the obtained theoretical estimates can be further improved in many cases the reason of which is yet to be understood.

References

1. Baumgartel, H.: Analytic Perturbation Theory for Matrices and Operators. Birkhauser Verlag (1985)
2. Bauer, F.L., Fike, C.T.: Norms and exclusion theorems. Numerische Mathematik 2, 137–144 (1960)
3. Beauzamy, B.: How the roots of a polynomial vary with its coefficients: a local quantitative result. Canad. Math. Bull. 42, 3–12 (1999)
4. Bhatia, R., Elsner, L., Krause, G.: Bounds for the variation of the roots of a polynomial and the eigenvalues of a matrix. Linear Algebra and its Applications 142, 195–209 (1990)
5. Bhatia, R.: Matrix Analysis. Springer (1997)
6. Chatelin, F., Braconnier, T.: About the qualitative computation of Jordan forms. ZAMM 74, 105–113 (1994)
7. Chow, T.S.: A class of Hessenberg matrices with known eigenvalues and inverses. SIAM Review 11, 391–395 (1969)
8. Chu, E.K.: Generalization of the Bauer-Fike Theorem. Numerische Mathematik 49, 685–691 (1986)
9. Ćurgus, B., Mascioni, V.: Roots and polynomials as homeomorphic spaces. Expositiones Mathematicae 24, 81–95 (2006)

10. Davis, C., Kahan, W.M.: The rotation of eigenvectors by a perturbation III. SIAM J. Numer. Anal. 7, 1–46 (1970)
11. Fairweather, G.: On the eigenvalues and eigenvectors of a class of Hessenberg matrices. SIAM Review 13, 220–221 (1971)
12. Galántai, A.: Projectors and Projection Methods. Kluwer (2004)
13. Galántai, A., Hegedűs, C.J.: Jordan s principal angles in complex vector spaces. Numerical Linear Algebra with Applications 13, 589–598 (2006)
14. Galántai, A., Hegedűs, C.J.: Perturbation bounds for polynomials. Numerische Mathematik 109, 77–100 (2008)
15. Galántai, A., Hegedűs, C.J.: Hyman's method revisited. J. Comput. Appl. Math. 226, 246–258 (2009)
16. Galántai, A., Hegedűs, C.J.: Perturbations of invariant subspaces of unreduced Hessenberg matrices. Computers and Mathematics with Applications 65, 423–434 (2013)
17. Gilbert, R.C.: Companion matrices with integer entries and integer eigenvalues and eigenvectors. Amer. Math. Monthly 95, 947–950 (1988)
18. Gohberg, I., Lancaster, P., Rodman, L.: Invariant Subspaces of Matrices with Applications. SIAM (2006)
19. Golub, G.H., van Loan, C.F.: Matrix Computations. The John Hopkins Univ. Press (1996)
20. Gracia, J.M., de Hoyos, I., Velasco, F.E.: Safety neighborhoods for the invariants of the matrix similarity. Linear Multilinear A 46, 25–49 (1999)
21. Henrici, P.: Bounds for iterates, inverses, spectral variation and fields of values of non-normal matrices. Numerische Mathematik 4, 24–40 (1962)
22. Higham, N.J.: Accuracy and Stability of Numerical Algorithms. SIAM (1996)
23. Ipsen, I.C.F.: Absolute and relative perturbation bounds for invariant subspaces of matrices. Linear Algebra and its Applications 309, 45–56 (2000)
24. Kahan, W., Parlett, B.N., Jiang, E.: Residual bounds on approximate eigensystems of nonnormal matrices. SIAM Journal on Numerical Analysis 19, 470–484 (1982)
25. Kato, T.: Perturbation Theory for Linear Operators. Springer (1966)
26. Kittaneh, F.: Singular values of companion matrices and bounds on zeros of polynomials. SIAM J. Matrix Anal. Appl. 16, 333–340 (1995)
27. Kressner, D.: Numerical Methods for General and Structures Eigenvalue Problems. Springer (2005)
28. Ostrowski, A.: Recherches sur la méthode de Gräffe et les zeros des polynômes et des series de Laurent. Acta Math. 72, 99–257 (1940)
29. Ostrowski, A.: Über die Stetigkeit von charakteristischen Wurzeln in Abhängigkeit von den Matrizenelementen. Jahresber. Deut. Mat.-Ver. 60, 40–42 (1957)
30. Ostrowski, A.: Solution of Equations and Systems of Equations. Academic Press (1960)
31. Parlett, B.: Canonical decomposition of Hessenberg matrices. Mathematics of Computation 21, 223–227 (1967)
32. Parlett, B.: The Symmetric Eigenvalue Problem. SIAM (1998)
33. Saad, Y.: Numerical Methods for Large Eigenvalue Problems. Manchester University Press (1992)
34. Schönhage, A.: The fundamental theorem of algebra in terms of computational complexity. Technical report, Mathematisches Institut der Universität Tübingen (August 1982) (revised in July 2004)
35. Song, Y.: A note on the variation of the spectrum of an arbitrary matrix. Linear Algebra and its Applications 342, 41–46 (2002)

36. Stewart, G.W.: Two simple residual bounds for the eigenvalues of Hermitian matrices. Technical report, CS-TR 2364, University of Maryland (December 1989)
37. Stewart, G., Sun, J.: Matrix Perturbation Theory. Academic Press (1990)
38. Tisseur, F.: Backward stability of the QR algorithm. Technical report No. 239, UMR 5585 Lyon Saint-Etienne (October 1996)
39. Turnbull, H.W., Aitken, A.C.: An Introduction to the Theory of Canonical Matrices. Blackie & Son (1952)
40. Wilkinson, J.H.: The Algebraic Eigenvalue Problem. Oxford University Press (1965)
41. Wilkinson, J.H.: Rounding Errors in Algebraic Processes. Dover (1994)

Modeling Uncertainty and Nonlinearity by Probabilistic Metric Spaces

Endre Pap

Singidunum University, 11000 Belgrade, Serbia
Óbuda University, H-1034 Budapest, Hungary
pape@eunet.rs

Abstract. Many problems occurring in engineering, e.g., robotics and control, require mathematical models which cover uncertainties and nonlinearity. We present here one such model: the theory of probabilistic metric spaces. This theory is based on the idea that, since the value of the distance in measurement is always unprecise and uncertain, the value of the distance have to be a probability distribution function. The theory of fuzzy metric spaces, as another model for uncertainty, is closely related to the theory of probabilistic metric spaces. We consider nonlinear random equations using fixed point methods in probabilistic metric spaces. Probabilistic metric spaces, some constructions methods of triangle functions and some important classes of probabilistic metric spaces as those of Menger, Wald, transformation-generated, are recalled. Based on some additional properties of t-norms the corresponding generalizations of fixed point theorems in probabilistic metric spaces are obtained.

Keywords: Probabilistic metric space, Menger space, fuzzy metric spaces, triangular norm, triangle function, fixed point theory.

1 Introduction

The main idea behind the theory of probabilistic metric spaces is that the value of the distance in measurement is always unprecise and uncertain, so the value of the distance have to be a probability distribution function. Starting from K. Menger [19] and B. Schweizer and A. Sklar [28], who based the generalization of the property of triangle inequality of the metric triangle on the operation of the notion of the triangular norm T, a further development of probabilistic metric spaces was made by A. N. Šerstnev [33], introduced the notion of triangle function τ on distribution functions. There are many important applications, e.g., hysteresis of complex physical systems, see Section 3, more details in [5,29].

Many problems occurring in engineering, e.g., robotics and control, require mathematical models which cover uncertainties and nonlinearity. One of the basic abstract tools in mathematics for solving nonlinear equations is the well-known classical Banach fixed point theorem which has many generalizations and applications. Two basic notions of contraction mappings in probabilistic metric spaces were introduced by V. M. Sehgal [31] and H. Sherwood [34]. Starting

J. Fodor and R. Fullér (eds.), *Advances in Soft Computing, Intelligent Robotics and Control,* Topics in Intelligent Engineering and Informatics 8,
DOI: 10.1007/978-3-319-05945-7_17,

with first result by V. M. Sehgal and A. T. Bharucha-Reid [32] with a fixed point theorem in probabilistic metric spaces under the special t-norm $T_{\mathbf{M}} = \min$, there have appeared many papers on this topic, see [7]. Without some growth conditions on the mapping $\mathcal{F}: D \times D \to \Delta^+$ (the set of distribution functions) the problem of the existence of a unique fixed point of a probabilistic q-contraction $f: D \to D$ for complete Menger spaces $(D, \mathcal{F}, T)$ with a continuous t-norm T is completely solved. A necessary and sufficient condition that the set $\mathrm{Fix}(f)$ of all fixed points of the mapping f is non-empty, is that T is the t-norm of H-type [6]. R. M. Tardiff [36] imposed some growth conditions on the mapping $\mathcal{F}: D \times D \to \Delta^+$, which enabled the class of t-norms T to be enlarged for which the set $\mathrm{Fix}(f)$ is non-empty, where $f: D \to D$ and $(D, \mathcal{F}, T)$ is a Menger space. Namely, Tardiff's fixed point theorem holds if $T \geqslant T_{\mathbf{L}}$. Fixed point theorems in probabilistic metric spaces of other types can be found in [3,7,8,9,10,13,14].

Probabilistic metric spaces and some constructions of triangle functions (mostly related to triangular norms) are recalled in section 2. Important probabilistic metric spaces such as Menger, Wald, transformation-generated are briefly presented in section 3. Results on probabilistic q-contractions are presented in section 4. In section 5, using some results about infinitary operations from the theory of t-norms (geometrically convergent t-norms), under some stronger growth conditions on $\mathcal{F}$, we obtain some probabilistic versions of Banach contraction principles where T satisfies $T_{\mathbf{L}} > T$, or even is incomparable with $T_{\mathbf{L}}$.

2 Triangle Function

First, we shall give some definitions of basic notions. The family of all distribution functions $F: [0, \infty] \to [0, 1]$ which are left-continuous on $[0, \infty[$ we denote by Δ^+. $(\Delta^+, \leq)$ is a complete lattice. We have $\varepsilon_a \in \Delta^+$ for $a \in [0, \infty]$, where the *Dirac distribution function* $\varepsilon_a: [-\infty, \infty] \to [0, 1]$ is defined for $a \in [-\infty, \infty[$ by

$$\varepsilon_a(u) = \begin{cases} 0 \text{ if} u \in [-\infty, a], \\ 1 \text{ if} u \in]a, \infty], \end{cases}$$

and for $a = \infty$ by

$$\varepsilon_\infty(u) = \begin{cases} 0 \text{ if } u \in [-\infty, \infty[, \\ 1 \text{ if } u = \infty. \end{cases}$$

We recall that a triangular norm (t-norm for short), see [15,16], is a binary operation T on the unit interval $[0, 1]$ which is commutative, associative, monotone and has 1 as a neutral element. We shall use notions and notations related t-norms from [15]. Three basic continuous t-norms are: $T_{\mathbf{M}}(x, y) = \min(x, y)$, $T_{\mathbf{L}}(x, y) = \max(x + y - 1, 0)$, $T_{\mathbf{P}}(x, y) = x \cdot y$. A t-norm T is extended (by associativity) in a unique way to an n-ary operation for $(x_1, \ldots, x_n) \in [0, 1]^n$, $n \in \mathbb{N}$, by

$$\mathop{\mathsf{T}}_{i=1}^{0} x_i = 1, \qquad \mathop{\mathsf{T}}_{i=1}^{n} x_i = T\Big(\mathop{\mathsf{T}}_{i=1}^{n-1} x_i, x_n\Big) = T(x_1, \ldots, x_n).$$

Further, T is extended to a countable infinitary operation for any sequence $(x_n)_{n\in\mathbb{N}}$ from $[0,1]$ by

$$\mathop{\mathsf{T}}_{i=1}^{\infty} x_i = \lim_{n\to\infty} \mathop{\mathsf{T}}_{i=1}^{n} x_i,$$

where the limit on the right side exists since the sequence $\left(\mathop{\mathsf{T}}_{i=1}^{n} x_i\right)_{n\in\mathbb{N}}$ is non-increasing and bounded from below.

Now, we give the important generalization of the notion of triangular norm on the set Δ^+, see [7,29,33].

Definition 1. *A* triangle function τ *is a binary operation on* Δ^+ *that is commutative, associative, and non-decreasing in each place, and has* ε_0 *as identity.*

It is obvious that ε_∞ is the null element of τ. If τ_1 and τ_2 are triangle functions then τ_1 is weaker than τ_2 (or τ_2 is stronger than τ_1), $\tau_1 \le \tau_2$, if for all F, G in Δ^+ and all x in $\mathbb{R}^+$ $\tau_1(F,G)(x) \le \tau_2(F,G)(x)$. A triangle function is *continuous*, if it is continuous in the topology of the weak convergence on Δ^+.

Example 1. (i) Let T be a left-continuous t-norm. Then the function $\mathbf{T}\colon \Delta^+ \times \Delta^+ \to \Delta^+$ defined by $\mathbf{T}(F,G)(x) = T(F(x),G(x))$, $x \in [0,\infty]$ is a triangle function. Specially, $\mathbf{T_M}$ defined by $\mathbf{T_M}(F,G)(x) = T_\mathbf{M}(F(x),G(x))$ is the maximal triangle function.

(ii) The convolution $F * G$ of $F, G \in \Delta^+$ is defined on $[0,\infty]$ by $(F*G)(0) = 0$, $(F*G)(\infty) = 1$ and

$$(F*G)(x) = \int_{[0,x[} F(x-t)\,dG(t) \qquad x \in]0,\infty[\,.$$

The convolution is a commutative and associative binary operator on Δ^+ which is non-decreasing and has ε_0 as a neutral element and therefore it is a triangle function.

(iii) If T is a left-continuous t-norm, then τ_T, defined by

$$\tau_T(F,G)(x) = \sup\{T(F(u),G(v)) \mid u+v=x\}$$

is a triangle function (compare with the Zadeh extension principle [15] and the notion of the pseudo-convolution [23]).

(iv) Let L be a binary operator on $[0,\infty]$ such that L maps $[0,\infty]^2$ onto $[0,\infty]$, L is non-decreasing in both coordinates, L is continuous on $[0,\infty]^2$ (except possibly at the points $(0,\infty)$ and $(\infty,0)$). Then for a t-norm T, the function $\tau_{T,L}$ defined on $\Delta^+ \times \Delta^+$ and with values in Δ^+ given by

$$\tau_{T,L}(F,G)(x) = \sup\{T(F(u),G(v)) \mid L(u,v)=x\}$$

is a triangular function if T is left-continuous t-norm and L is commutative, associative, has 0 as identity and satisfies the condition if $u_1 < u_2$ and $v_1 < v_2$ then $L(u_1,v_1) < L(u_2,v_2)$.

(v) Let C be a copula, see [15,20], and let $L\colon [0,\infty]^2 \to [0,\infty]$ be a surjective and continuous function on $[0,\infty]^2 \setminus \{(0,\infty),(\infty,0)\}$ and for each $x \in [0,\infty[$ the set

$$L_x = \{(u,v) \in [0,\infty]^2 \mid L(u,v) < x\}$$

is bounded and $([0,\infty], L, \leq)$ is a partially ordered semigroup. The function $\sigma_{C,L}\colon \Delta^+ \times \Delta^+ \to \Delta^+$ is defined by

$$\sigma_{C,L}(F,G)(x) = \begin{cases} 0 & \text{if } x \in [-\infty, 0]\,, \\ \displaystyle\int_{L_x} dC(F(u),G(v)) & \text{if } x \in]0,\infty[\,, \\ 1 & \text{if } x = \infty, \end{cases}$$

where the integral is of Lebesgue-Stieltjes type. $\sigma_{C,L}$ is a triangle function if and only if $C = (\langle]a_\alpha, e_\alpha[\,, T_{\mathbf{P}}\rangle)_{\alpha\in A}$, see [29, Corollary 7.4.4].

Remark 1. (i) There is no characterization of the semigroup (Δ^+, τ) in a similar way as it was done for the semigroup $([0,1], T)$ (still an open problem stated in [29]) up to some special cases, see [26].

(ii) It is interesting to note that the semigroup (Δ^+, τ_T) is not cancellative, but the semigroup $(\mathcal{D}^+, \tau_{T_{\mathbf{M}}})$ is cancellative, i.e., $\tau_{T_{\mathbf{M}}}(F,G) = \tau_{T_{\mathbf{M}}}(F,R)$ implies $F = 0$ or $G = R$.

3 Probabilistic Metric Spaces

Starting from the idea of Menger [19] the first appropriate probabilistic generalization of metric spaces was given by by B. Schweizer and A. Sklar [27]. Extending an idea belonging to Wald, Šerstnev suggested the use of a triangle function in the definition of the probabilistic metric space, see [33].

Definition 2. *A probabilistic metric space is a triplet $(D, \mathcal{F}, \tau)$ where D is a nonempty set, $\mathcal{F}\colon D \times D \to \Delta^+$ is given by $(p,q) \mapsto F_{p,q}$, τ is a triangle function, such that the following conditions are satisfied for all p, q, r in D :*

(i) $F_{p,p} = \varepsilon_0$;
(ii) $F_{p,q} \neq \varepsilon_0$ *for* $p \neq q$;
(iii) $F_{p,q} = F_{q,p}$;
(iv) $F_{p,r} \geq \tau(F_{p,q}, F_{q,r})$.

Definition 3. *Let $(D, \mathcal{F}, \tau)$ be a probabilistic metric space and $\tau = \tau_T$, where*

$$\tau_T(F,G)(x) = \sup\{T(F(u),G(v)) \mid u + v = x\}$$

for a t-norm T. Then $(D, \mathcal{F}, \tau)$ is called a Menger space which will be denoted by $(D, \mathcal{F}, T)$.

Remark 2. (i) The preceding Definition 3 implies

$$F_{p,r}(x+y) \geqslant T\left(F_{p,q}(x), F_{q,r}(y)\right)$$

for all $p, q, r \in D$ and x, y real numbers. We can interpret this inequality in the way of the classical metric spaces that the third side in a triangle depends on the other two sides in the sense that if the knowledge of two sides increases then also the knowledge of third side increases or that knowing the upper bounds of two sides we have an upper bound for the third side.

(ii) As a very special case of a Menger space we obtain the classical metric space: if $(M, \mathcal{F}, \tau_T)$ is a Menger space, for some t-norm T, $d\colon M \times M \to [0, \infty[$ and

$$\mathcal{F}(p, q) = \varepsilon_{d(p,q)} \qquad \text{for every } p, q \in M,$$

then (M, d) is a metric space. Starting from a metric space (M, d), and taking $F_{p,q}$ defined by the last equality, then for any t-norm T the function $F_{p,q}$ is a probability distribution function such that conditions (i)–(iv) in Definition 2 are satisfied for τ_T.

(iii) Usually in many applications, e.g., fixed point theorems, it is supposed for Menger space $(D, \mathcal{F}, T)$ that t-norm T statisfies the following weak condition $\sup_{x<1} T(x, x) = 1$, which ensures the metrizability of the so called (ε, λ)-topology, see [7].

(iv) A very important class of probabilistic metric spaces is given in [4], which is useful for the applications of the fixed point theory in probabilistic metric spaces to random operator equations, see Theorem 7.

Further, we have the following special class of probabilistic metric spaces, see [7,29].

Definition 4. *A probabilistic metric space $(D, \mathcal{F}, \tau)$ for which τ is a convolution is called* Wald space.

Using the equality $\varepsilon_a * \varepsilon_b = \varepsilon_{a+b}$, it is easy to prove that for a function $d\colon M \times M \to [0, \infty[$ and $\mathcal{F}(p, q) = \varepsilon_{d(p,q)}$ the triplet $(M, \mathcal{F}, *)$ is a Wald space if and only if (M, d) is the classical metric space.

Theorem 1. *A probabilistic metric space $(D, \mathcal{F}, \tau)$ which is a Wald space is a Menger space $(D, \mathcal{F}, T_{\mathbf{P}})$.*

We shall present some other important probabilistic metric spaces. For more details see [7,29]. Let $\mathcal{D}^+ = \{F \mid F \in \Delta^+, \lim_{x\to\infty} F(x) = 1\}$. Starting from a metric space and a distribution function we can generate an important class of probabilistic metric spaces. Let (D, d) be a metric space, $G \in \mathcal{D}^+$, $G \neq \varepsilon_0$ and $\alpha > 0$. If for $p, q \in D$ we have $p = q$ let $F_{p,q} = \varepsilon_0$, and if $p \neq q$ let

$$F_{p,q}(x) = G\left(\frac{x}{d(p, q)^\alpha}\right) \qquad \text{for every } x \in [0, \infty[\,.$$

It was proved [29] that $(D, \mathcal{F}, T)$ is a Menger space for an arbitrary t-norm T, and it is called *α-simple space.* Simple spaces (for $\alpha = 1$) are very useful in modeling hysteresis in large-scale physical systems, see [5,29]. Namely, the macroscopic behavior of complex physical systems usually is described by two parameters.

One which describe the variation of external force (hysteresis coordinate v), and second characterizing the state of the system (configuration coordinate u). For example, in magnetic systems u represents the induced magnetization. A hysteresis cycle is a path in the (u,v)-plane from p to q such that $v(p)=v(q)$ and $u(p)\neq u(q)$. Making some physical assumptions, it turns out by [5], that the average energy loss per cycle related all hysteresis cycles between p and q whose length is less than x, is proportional to $\int_{[0,x[} t\,dF_{pq}(t)$, where for metric space (M,d) with finite measure m of *eliptic regions*

$$E(p,q;x)=\{r \mid d(p,r)+d(q,r)\leqslant x\} \quad (p,q\in D, x\geqslant 0)$$

for $d(p,q)<x<\infty$ the function F_{pq} for $\mu\in]0,\infty]$ is given by

$$F_{pq}(x)=\min\left(\frac{m(E(p,q;x))}{m(E(p,q;\mu\cdot d(p,q))},1\right)$$

for $p\neq q$ and $F_{pq}=\varepsilon_0$ for $p=q$.

An important class of probabilistic metric spaces is the *transformation generated spaces* defined as follows (t-norms and triangular functions are continuous). Let (D,d) be a metric space and $\psi\colon D\to D$. For any $p,q\in D$ and any $n\in\mathbb{N}$, let

$$F_{p,q}^{(n)}=\frac{1}{n}\sum_{m=0}^{n-1}\varepsilon_{d(\psi^m(p),\psi^m(q))},$$

where $\psi^m(p)$ is the value of the m-th iterate of the mapping ψ at p. If $\mathcal{F}^{(n)}$ is defined on $D\times D$ by $\mathcal{F}^{(n)}(p,q)=F_{p,q}^{(n)}$, then for every $(p,q)\in D\times D$

$$\mathcal{F}^{(n)}(p,p)=\varepsilon_0, \qquad \mathcal{F}^{(n)}(p,q)=\mathcal{F}^{(n)}(q,p),$$

i.e., $(D,\mathcal{F}^{(n)})$ is a probabilistic premetric space and $(D,\mathcal{F}^{(n)},\tau_{T_{\mathbf{L}}})$ is a probabilistic pseudo-metric space (in Definition 2 the condition (ii) is not necessarily satisfied). The following theorem of H. Sherwood holds, see [29].

Theorem 2. *Let (D,d) be a metric space and $\psi\colon D\to D$. For every $(p,q)\in D\times D$ let $\varphi_{p,q}$ be defined for $x\geqslant 0$ by*

$$\varphi_{p,q}(x)=\liminf_{n\to\infty}F_{p,q}^{(n)}(x)=\lim_{n\to\infty}(\inf\{F_{p,q}^{(m)}(x)\mid m\geqslant n\})$$

and $\mathcal{F}$ be defined on $D\times D$ by

$$F_{p,q}(x)=\varphi_{p,q}(x^-) \qquad x\in[0,\infty[\,.$$

Then $(D,\mathcal{F},\tau_{T_{\mathbf{L}}})$ is a probabilistic pseudo-metric space.

Remark 3. (i) The transformation generated spaces are important in the ergodic theory, see [29].

(ii) The preceding approach plays an important role in chaos theory, see [30], leading to a theory of distributional chaos. The example from [35], is connected with self-similar random fractal measures, which is a very interesting and important area of investigation, see [1,21].

(iii) Probabilistic metric spaces based on pseudo-additive (decomposable) measures ([22,23]) were investigated in [7,24].
(iv) New probabilistic metric spaces can be obtained making their direct products. To obtain that the τ-*product* of two probabilistic metric spaces is again probabilistic metric space we need some additional conditions.

4 Probabilistic q-Contraction

The following notion is well know for a metric space (M, d) and a function $f: M \to M$: if there exists a $q \in [0, 1[$ such that

$$d(fx, fy) \leqslant qd(x, y) \qquad \text{for every } x, y \in M,$$

then f is the so-called q-*contraction*. It is well known the Banach contraction principle that every q-contraction $f: M \to M$ on a complete metric space (M, d) has one and only one fixed point. V. M. Sehgal and A. T. Bharucha-Reid introduced in 1972 the notion of a probabilistic q-contraction ($q \in]0, 1[$) in a probabilistic metric space [32].

Definition 5. *Let $(D, \mathcal{F})$ be a probabilistic metric space. A mapping $f: D \to D$ is a* probabilistic q-contraction ($q \in]0, 1[$) *if*

$$F_{fp_1, fp_2}(x) \geqslant F_{p_1, p_2}\left(\frac{x}{q}\right) \tag{1}$$

for every $p_1, p_2 \in D$ and every $x \in \mathbb{R}$.

V. M. Sehgal and A. T. Bharucha-Reid [32] proved the following fixed point theorem in a special Menger space.

Theorem 3. *Let $(D, \mathcal{F}, T_{\mathbf{M}})$ be a complete Menger space and $f: D \to D$ a probabilistic q-contraction. Then there exists a unique fixed point x of the mapping f and $x = \lim_{n\to\infty} f^n p$ for every $p \in D$.*

After this first result many generalizations were made, see [7]. Some of them will be presented in the next section. We give now an important example.

Example 2. Let $(\Omega, \mathcal{A}, P)$ be a probability measure space, (M, d) a separable metric space, and $\mathcal{B}_M$ the family of Borel subsets of M. A mapping $f: \Omega \times M \to M$ is a *random operator* if for every $C \in \mathcal{B}_M$ and every $x \in M$

$$\{\omega \in \Omega \mid f(\omega, x) \in C\} \in \mathcal{A},$$

i.e., if the mapping $\omega \mapsto f(\omega, x)$ is measurable on Ω. A random operator $f: \Omega \times M \to M$ is *continuous* if for every $\omega \in \Omega$ the mapping $x \mapsto f(\omega, x)$ is continuous on M. If the random operator $f: \Omega \times M \to M$ is continuous then for every measurable mapping $X: \Omega \to M$ the mapping $\omega \mapsto f(\omega, X(\omega))$ is measurable on

Ω. Let D be the set of all equivalence classes of measurable mappings $X\colon \Omega \to M$ and let f be a continuous random operator. The mapping $\hat{f}\colon D \to D$, defined by

$$(\hat{f}\hat{X})(\omega) = f(\omega, X(\omega)) \quad \text{for every } \hat{X} \in D \qquad (\omega \in \Omega, X \in \hat{X})$$

is the so-called *Nemitskij operator* of f. If $f\colon \Omega \times M \to M$ is a random operator then a measurable mapping $X\colon \Omega \to M$ is a *random fixed point* of the mapping f if

$$X(\omega) = f(\omega, X(\omega)) \text{ a.e.} \tag{2}$$

Many authors investigated the problem of the existence of a random fixed point of a random operator (see references in [2]). If f is a continuous random operator then (2) holds if and only if $\hat{X} = \hat{f}\hat{X}$ for $X \in \hat{X}$. Hence in this case the problem of the existence of a random fixed point of a continuous random operator f reduces to the problem of the existence of a fixed point of the Nemitskij operator $\hat{f}$ of f.

Let for every $\hat{X}, \hat{Y} \in D$ and every $x > 0$

$$\begin{aligned} &P(\{\omega \in \Omega \mid d(f(\omega, X(\omega)), f(\omega, Y(\omega)) < qx\}) \\ &\geqslant P(\{\omega \in \Omega \mid d(X(\omega), Y(\omega)) < x\}), \end{aligned} \tag{3}$$

where $q \in]0,1[$. Since $(D, \mathcal{F}, T_{\mathbf{L}})$ is a Menger space, where

$$F_{\hat{X},\hat{Y}}(x) = P(\{\omega \in \Omega \mid d(X(\omega), Y(\omega)) < x\})$$

for every $\hat{X}, \hat{Y} \in D$ and $x \in \mathbb{R}$, then (3) implies that $F_{\hat{f}\hat{X},\hat{f}\hat{Y}}(qx) \geqslant F_{\hat{X},\hat{Y}}(x)$. Hence $\hat{f}$ is a probabilistic q-contraction if and only if (3) holds. For this class of probabilistic q-contractions the existence of the fixed point is ensured by Theorem 5.

To ensure the uniqueness of the fixed point we suppose further on that for the probabilistic metric space $(D, \mathcal{F}, \tau)$ always holds $\mathrm{Ran}(\mathcal{F}) \subset \mathcal{D}^+$. Namely, in the general case probabilistic q-contraction can have more fixed points (see [29], section 12.6).

5 Geometrically Convergent Triangular Norms and Fixed Point Theorems

A special class of t-norms (generally not continuous) was introduced in [6], characterizing for the continuous case the class of complete Menger spaces having a fixed point property, see Theorem 4.

Definition 6. *A t-norm T is of H-type if the family $(x \mapsto x_T^{(n)})_{n\in\mathbb{N}}$ is equicontinuous at the point $x = 1$, where $x_T^{(n)}$ is defined by $x_T^{(1)} = x, x_T^{(n)} = T\big(x_T^{(n-1)}, x\big)$, for $n \geqslant 2, x \in [0,1]$.*

Proposition 1. *If a continuous t-norm T is Archimedean then it cannot be a t-norm of H-type.*

The following characterization was proved in [24], see also [25].

Proposition 2. *A continuous t-norm T is of H-type if and only if*

$$T = (\langle]\alpha_k, \beta_k[, T_k\rangle)_{k\in K} \text{ and } \sup \beta_k < 1 \text{ or } \sup \alpha_k = 1.$$

For the relation with the abstract semigroup theory through Archimedean components see [18,17]. A t-norm T has the *fixed point property* if any probabilistic q-contraction $f: D \to D$, where $(D, \mathcal{F}, T)$ is a complete Menger space, has a fixed point. V. Radu [25] proved the following theorem.

Theorem 4. *Any continuous t-norm T with the fixed point property is of H-type.*

Thus, no continuous Archimedean t-norm has the fixed point property. Then it is clear that in order to obtain some kind of fixed point theorems for Menger spaces $(D, \mathcal{F}, T)$, where T is an Archimedean t-norm, one has to impose some additional conditions on the mapping $\mathcal{F}$. Important results in this direction are obtained in R. M. Tardiff's paper [36].

Theorem 5. *Let $(D, \mathcal{F}, T)$ be a complete Menger space and T a t-norm such that $T \geqslant T_{\mathbf{L}}$. If for every $x, y \in D$*

$$\int_1^\infty \ln(u)\, dF_{x,y}(u) < \infty.$$

holds, then any probabilistic q-contraction $f: D \to D$ has a unique fixed point x and $x = \lim_{n\to\infty} f^n p$ for every $p \in D$.

Using some results on geometrically convergent t-norms some further results [11] in this direction are obtained. In the fixed point theory it is of interest to investigate the classes of t-norms T and sequences $(x_n)_{n\in\mathbb{N}}$ from the interval $[0, 1]$, see [7,11], such that $\lim_{n\to\infty} x_n = 1$, and

$$\lim_{n\to\infty} \mathop{\mathsf{T}}_{i=n}^{\infty} x_i = \lim_{n\to\infty} \mathop{\mathsf{T}}_{i=1}^{\infty} x_{n+i} = 1. \tag{4}$$

In the classical case $T = T_{\mathbf{P}}$ we have for every sequence $(x_n)_{n\in\mathbb{N}}$ from the interval $[0, 1]$ with $\sum_{i=1}^{\infty}(1 - x_n) < \infty$ that

$$\lim_{n\to\infty} \mathop{\mathsf{T}}_{\mathbf{P}\ i=n}^{\infty} x_i = \lim_{n\to\infty} \prod_{i=n}^{\infty} x_i = 1.$$

The equivalence

$$\sum_{i=1}^{\infty}(1 - x_i) < \infty \quad \Longleftrightarrow \quad \lim_{n\to\infty} \mathop{\mathsf{T}}_{i=n}^{\infty} x_i = 1$$

holds also for $T \geqslant T_{\mathbf{L}}$. The condition $T \geqslant T_{\mathbf{L}}$ is satisfied by the families of t-norms (for notations see [15]): Schweizer-Sklar family of t-norms $(T_\lambda^{\mathbf{SS}})_{\lambda\in[-\infty,1]}$; Yager family of t-norms $(T_\lambda^{\mathbf{Y}})_{\lambda\in[1,\infty]}$; Sugeno-Weber family of t-norms $(T_\lambda^{\mathbf{SW}})_{\lambda\in[0,\infty]}$; Frank family of t-norms $(T_\lambda^{\mathbf{F}})_{\lambda\in[0,\infty]}$.

Proposition 3. *Let T be a t-norm. Sufficient conditions for (4) are given in the following two statements.*

(i) Let $(x_n)_{n\in\mathbb{N}}$ be a sequence of numbers from $[0,1]$ such that $\lim_{n\to\infty} x_n = 1$ and T be a t-norm of H-type. Then (4) holds.

(ii) Let T be a strict t-norm with additive generator t. For a sequence $(x_n)_{n\in\mathbb{N}}$ from the interval $]0,1[$ with $\lim_{n\to\infty} x_n = 1$ we have

$$\lim_{n\to\infty} \sum_{i=n}^{\infty} t(x_i) = 0$$

if and only if (4) is satisfied.

Example 3. Proposition 3 (ii) holds for the following families of t-norms.

(i) Let $(T_\lambda^{\mathbf{AA}})_{\lambda\in]0,\infty[}$ be the Aczél-Alsina family of t-norms given by

$$T_\lambda^{\mathbf{AA}}(x,y) = e^{-(|\log x|^\lambda + |\log y|^\lambda)^{1/\lambda}}.$$

(ii) For nilpotent t-norms $T_\lambda^{\mathbf{SW}}$, $\lambda \in]-1,0[$. It holds also for $\lambda \geqslant 0$ since in this case $T_\lambda^{\mathbf{SW}} \geqslant T_{\mathbf{L}}$.

Taking in the condition (4) a special sequence $(1-q^n)_{n\in\mathbb{N}}$ for $q \in]0,1[$, see [7,11], we obtain the following important notion.

Definition 7. *A t-norm T is* geometrically convergent *(*g-convergent*) if for some $q \in]0,1[$*

$$\lim_{n\to\infty} \overset{\infty}{\underset{i=n}{T}} (1-q^i) = 1. \tag{5}$$

Remark 4. (i) We have proved in [11] that (5) holds for every $q \in]0,1[$ if (5) holds for some q.

(ii) Since $\lim_{n\to\infty}(1-q^n) = 1$ and $\sum_{n=1}^{\infty}(1-(1-q^n))^s < \infty$ for every $s > 0$ we obtain that all t-norms from the class

$$\mathcal{T}_0 = \bigcup_{\lambda\in]0,\infty[} \{T_\lambda^{\mathbf{D}}\} \cup \bigcup_{\lambda\in]0,\infty[} \{T_\lambda^{\mathbf{AA}}\} \cup \bigcup_{\lambda\in]-1,\infty]} \{T_\lambda^{\mathbf{SW}}\} \cup \{T \mid T \text{ is of } H\text{-type}\}$$

are geometrically convergent.

The following proposition ensures that a t-norm T is geometrically convergent.

Proposition 4. *A strict t-norm T with additive generator t is geometrically convergent if we have one of the following cases:*

(i) There is a strict t-norm T_1 with additive generator t_1 such that there exists $b \in]0,1[$ and $t(x) \leqslant t_1(x)$ for every $x \in]b,1]$, and T_1 is geometrically convergent.

(ii) An additive generator t has a bounded derivative on an interval $]b,1[$ for some $b \in]0,1[$.

The following proposition enables to introduce a large class of geometrically convergent t-norms.

Proposition 5. *Let* $\psi:]0,1] \to [0,\infty[$ *and* T *be a t-norm such that for some* $\delta \in]0,1[$ *and every* $x \in [0,1]$ *and* $y \in [1-\delta, 1]$

$$|T(x,y) - T(x,1)| \leqslant \psi(y).$$

If for a sequence $(x_n)_{n\in\mathbb{N}}$ *from the interval* $[0,1]$ *with* $\lim\limits_{n\to\infty} x_n = 1$ *we have* $\sum\limits_{n=1}^{\infty} \psi(x_n) < \infty$, *then* $\lim\limits_{n\to\infty} \left(\mathop{\mathsf{T}}\limits_{i=n}^{\infty} x_i - x_n \right) = 0$.

Corollary 1. *Let* T *and* ψ *be as in Proposition 5. If for some* $q \in]0,1[$, $\sum_{n=1}^{\infty} \psi(1-q^n) < \infty$ *then* T *is geometrically convergent.*

Example 4. Let $\alpha > 0$, $p > 1$ and $h_{\alpha,p}:]0,1] \times [0,1] \to [0,\infty[$ is given by

$$h_{\alpha,p}(x,y) = \begin{cases} y - \frac{\alpha}{|\ln(1-x)|^p} & \text{if } (x,y) \in]0,1[\times [0,1], \\ y & \text{if } (x,y) \in \{1\} \times [0,1]. \end{cases}$$

Let T be a t-norm such that $T(x,y) \geqslant h_{\alpha,p}(x,y)$ for every $x \in [1-\delta, 1]$ and $y \in [0,1]$. We have

$$\sum_{n=1}^{\infty} \psi(1-q^n) = \sum_{n=1}^{\infty} \frac{\alpha}{|\ln(q^n)|^p} = \sum_{n=1}^{\infty} \frac{\alpha}{n^p |\ln(q)|^p} < \infty,$$

and therefore by Corollary 1 t-norm T is geometrically convergent, see [7].

Now, we have the following generalization of R. M. Tardiff's Theorem 5.

Theorem 6. *Let* $(D, \mathcal{F}, T)$ *be a complete Menger space such that* $\sup\limits_{a<1} T(a,a) = 1$ *and* $f : D \to D$ *a probabilistic* q*-contraction such that for some* $p \in D$ *and* $k > 0$

$$\sup_{x>0} x^k (1 - F_{p,fp}(x)) < \infty. \tag{6}$$

If t-norm T *is* r^k*-convergent for some* $r \in]q,1[$ *, then there exists a unique fixed point* z *of the mapping* f *and* $z = \lim\limits_{n\to\infty} f^n p$.

Remark 5. (i) The proof of Theorem 6 also holds if we assume instead of the condition (6) that for some $p \in D$ and $r \in]q,1[$

$$\lim_{n\to\infty} \mathop{\mathsf{T}}_{i=n}^{\infty} F_{p,fp}\left(\frac{1}{r^i}\right) = 1. \tag{7}$$

(ii) If $T = T_{\mathbf{L}}$, condition $\int \ln u \, dF_{p,fp}(u) < \infty$ is equivalent to (7).

Corollary 2. *Let* $(D, \mathcal{F}, T)$ *be a complete Menger space such that* $\sup\limits_{a<1} T(a,a) = 1$, $T \geqslant T_1$ *for some* $T_1 \in \mathcal{T}_0$, *and* $f : D \to D$ *a probabilistic* q*-contraction such that for some* $k > 0$ *and* $p \in D$ *(6) holds. Then there exists a unique fixed point* x *of the mapping* f *and* $x = \lim\limits_{n\to\infty} f^n p$.

If $(\Omega, \mathcal{A}, P)$ is a probability measure space, (M, d) a separable metric space and $f\colon \Omega \times M \to M$ a continuous random operator. Let D be the space of all classes $\hat{X}$ of measurable mappings $X\colon \Omega \to M$ ($X \in \hat{X}$, and $X, Y \in \hat{X}$ if and only if $X = Y$ a.e.). Then $\hat{f}\colon D \to D$, given by $(\hat{f}\hat{X})(\omega) = f(\omega, X(\omega))$ for $\omega \in \Omega$, is the Nemitskij operator for the mapping f, see Example 2. We have obtained in [12] the following fixed point theorem.

Theorem 7. *Let $(\Omega, \mathcal{A}, P)$ be a probability measure space, (M, d) a complete separable metric space and $f\colon \Omega \times M \to M$ a continuous random operator. If the following two conditions hold*

(i) for every $\hat{X}, \hat{Y} \in D$ and every $\varepsilon > 0$

$$P(\{\omega \in \Omega \mid d(f(\omega, X(\omega)), f(\omega, Y(\omega))) < q\varepsilon\})$$

$$\geqslant P(\{\omega \in \Omega \mid d(X(\omega), Y(\omega)) < \varepsilon\})$$

for some $q \in]0, 1[$,

(ii) there exists $\hat{X}_0 \in D$ such that

$$\sup\{u \cdot P(\{\omega \in \Omega \mid d(X_0(\omega), f(\omega, X_0(\omega))) \geqslant u\}) \mid u > 0\} < \infty,$$

then there exists a measurable $X\colon \Omega \to M$ such that $X(\omega) = f(\omega, X(\omega))$ a.e.

Acknowledgement. The author want to thank for the partial financial support of the Project MNTRS-174009, and the Vojvodina Academy of Sciences and Arts financed by the Provincial Secretariat for Science and Technological Development of Vojvodina.

References

1. Arbeiter, M: Random recursive constructions of self-similar fractal measures. The noncompact case. Prob. Theory Related Fields 88, 497–520 (1991)
2. Beg, I.: Approximation of random fixed points in normed spaces. Nonlinear Analysis 51, 1303–1372 (2002)
3. Chang, S.S.: On the theory of probabilistic metric spaces with applications. Acta Math. Sinica, New Series 1, 366–377 (1985)
4. Drossos, C. A.: Stochastic Menger spaces and convergence in probability. Rev. Roum. Math. Pures Appl. 22, 1069–1076 (1977)
5. Erber, T., Harmon, B. N., Latal, H. G.: The origin of hysteresis in simple magnetic systems. Advances in Chemical Physics 20, 71-134 (1971)
6. Hadžić, O.: Some theorems on the fixed point in probabilistic metric and random normed spaces. Boll. Unione Mat. Ital. 1-B, 381–391 (1982)
7. Hadžić, O., Pap, E.: Fixed Point Theory in Probabilistic Metric Spaces. Kluwer Academic Publishers, Dordrecht (2001)
8. O. Hadžić, O., Pap, E.: A fixed point theorem for multivalued mappings in probabilistic metric spaces and an application in fuzzy metric spaces. Fuzzy Sets and Systems 127, 333–344 (2002)

9. Hadžić, O., Pap, E.: Probabilistic multi-valued contractions and decomposable measures. Internat. J. Uncertain. Fuzziness Knowledge-Based Systems 10, 59–74 (2002)
10. Hadžić, O., Pap, E.: New classes of probabilistic contractions and applications to random operators. In Y. J. Cho, J. K. Kim and S. M. Kang, editors, Fixed Point Theory and Applications, Nova Science Publishers, Hauppauge, NY, 97–119 (2003)
11. Hadžić, O., Pap, E., Budinčević, M.: Countable extension of triangular norms and their applications to fixed point theory in probabilistic metric spaces. Kybernetika 38, 363–381 (2002)
12. Hadžić, O., Pap, E., Budinčević, M.: A generalization of Tardiff's fixed point theorem and applications to random equations. Fuzzy Sets and Systems 156, 124-135 (2005)
13. Hadžić, O., Pap, E., Radu, V.: Some generalized contraction mapping principles in probabilistic metric spaces. Acta Math. Hungarica 101, 111–128 (2003)
14. Hicks, T. L.: Fixed point theory in probabilistic metric spaces. Univ. u Novom Sadu, Zb. Rad. Prirod.-Mat. Fak. Ser. Mat. 13, 63–72 (1983)
15. Klement, E. P., Mesiar, R., Pap, E.: Triangular Norms. Kluwer Academic Publishers, Dordrecht (2000)
16. Klement, E. P., Mesiar, R., Pap, E.: Triangular norms: Basic notions and properties. (Eds. E.P. Klement, R. Mesiar) Logical, Algebraic, Analytic, and Probabilistic Aspects of Triangular Norms, Elsevier, 17-60, (2005)
17. Klement, E. P., Mesiar, R., Pap, E.: Semigroups and triangular norms. This volume, (Eds. E.P. Klement, R. Mesiar) Logical, Algebraic, Analytic, and Probabilistic Aspects of Triangular Norms, Elsevier, 63–93 (2005)
18. Klement, E. P., Mesiar, R., Pap E.: Archimedean components of triangular norms. J. Aust. Math. Soc. 78, 1-17 (2005)
19. Menger , K.: Statistical metric. Proc. Nat. Acad. USA 28, 535–537 (1942)
20. Nelsen, R. B.: An Introduction to Copulas. Springer, New York (1999)
21. Olsen, L.: Random geometrically graph directed self-similary multifractals. Longman, Harlow (1994)
22. Pap, E.: Null-Additive Set Functions. Kluwer Academic Publishers, Dordrecht and Ister Science, Bratislava (1995)
23. Pap, E.: Pseudo-additive measures and their applications. In E. Pap, editor, Handbook of Measure Theory, volume II, Elsevier, North-Holland, 1403–1465 (2002)
24. Pap, E., Hadžić, O., Mesiar, R.: A fixed point theorem in probabilistic metric spaces and applications in fuzzy set theory. J. Math. Anal. Appl. 202, 433–449 (1996)
25. Radu, V.: Lectures on probabilistic analysis. Surveys, Lectures Notes and Monographs Series on Probability, Statistics & Applied Mathematics 2, Universitatea de Vest din Timişoara (1994)
26. Riedel, T.: On sup-continuous triangle functions, J. Math. Anal. Appl. 184, 382–388 (1994)
27. Schweizer, B., Sklar, A.: Espaces métriques aléatoires. Comptes Rendus Acad. Sci. Paris 247, 2092–2094 (1958)
28. Schweizer, B., Sklar, A.: Statistical metric spaces. Pacific J. Math. 10, 313–334 (1960)
29. Schweizer, B., Sklar, A.: Probabilistic Metric Spaces. North-Holland, New York (1983)
30. Schweizer, B., Smítal, J.: Measures of chaos and a spectral decomposition of dynamical systems on the interval. Trans. Amer. Math. Soc. 344, 737–754 (1994)
31. Sehgal, V. M.: Some fixed point theorems in functional analysis and probability. Ph.D. Thesis, Wayne State University, Detroit (1966)

32. Sehgal, V. M., Bharucha-Reid, A. T.: Fixed points of contraction mappings on probabilistic metric spaces. Math. Syst. Theory 6, 97–102 (1972)
33. Sherstnev, A.N.: Random normed spaces: problems of completeness. Kazan. Gos. Univ. Učen. Zap. 122, 3–20 (1962)
34. Sherwood, H.: Complete probabilistic metric spaces and random variables. Ph.D. Thesis, University of Arizona (1965)
35. Soós, A.: Random fractals using contraction methods in probabilistic metric spaces. Ph.D. Thesis, University of Cluj-Napoca (2002)
36. Tardiff, R. M.: Contraction maps on probabilistic metric spaces. J. Math. Anal. Appl. 165, 517–523 (1992)

Scientific Research Information System as a Solution for Assessing the Efficiency of Applied Research

Vladimír Gašpar[1], Ladislav Madarász[1], and Rudolf Andoga[2]

[1] Dept. of Cybernetics and Artificial Intelligence, FEEaI, TU Košice
Letná 9, 042 00 Košice, Slovakia
{vladimir.gaspar,ladislav.madarasz}@tuke.sk
[2] Dept. of Avionics, Faculty of Aeronautics, TU Košice
Rampová 7, 041 21 Košice, Slovakia
rudolf.andoga@tuke.sk

Abstract. The aim of this paper is to discuss the possibilities of evaluating qualitative parameters (mostly physical and technical efficiency) in research of a certain complex system using an information system with intelligent elements. Our main objective is to create the possibility to test the quality of each research element or task. The research of a complex thermodynamic system, in our case a small turbojet engine MPM–20, requires assessing each element with respect to its nature. Nature of these elements may be physical (e.g. reaching limiting temperatures, fuel consumption), technical (e.g. quality of control algorithms, quality of diagnostics), financial (e.g. research funding quality), time related (e.g. latencies, dynamics) or informational (quality of research papers and research reports). A basis for quality assessment of each research element is provided by key performance indicators (KPIs), which are measureable and robust. Such an information system creates a new overview of the research process and progress, while serving as an integrating element of the whole research as well as an aid in the experimental identification of the particular complex system. Intelligent elements such as automatic generation of log reports and research schedules, parameter and measurement classification and clustering of atypical situations, which are discussed later in this article, add up to the simplification of research work and create an environment that is beneficial for improving the quality of research. In the future, we are planning to generalize the proposed concepts and modules to serve any kind of applied research.

1 Introduction

Every present research requires special care when it comes to efficient usage of available resources. Lack of information, quality of personnel, undercapitalization and time management belong to the greatest constraints of research and development. Each of these factors are involved in the research quality and outputs of the research. However, they may be overcome by certain approaches, which are specific for each constraint and are described in detail in [1] and [2].

J. Fodor and R. Fullér (eds.), *Advances in Soft Computing, Intelligent Robotics and Control,* Topics in Intelligent Engineering and Informatics 8,
DOI: 10.1007/978-3-319-05945-7_18,

General research information systems (RIS) provide basic information about the research resources. Depending on their level of deployment, different information come to use. If we consider a RIS at a country or university level (Current Research Information System – CRIS), information as contracts, projects, researchers, publications, study plans, patents and funding sources are stored. Moreover, only these information are supposed to be available for wide research environment. This means that assessment of the quality of research on a higher level may be achieved using CRIS systems [3].

However, it is difficult for a laboratory or department to evaluate the quality of its research that will reflect the amount of available data and achieved partial research goals (mostly of non-informational and non-financial character). Elementary research data of informational, financial and time-related character are present but in case of lower level of research (local level), also technical and physical data from measurements are accessible. They serve for local efficiency evaluation the best because of their influence on the operational efficiency, as well as other qualitative parameters (e.g. knowledge of researchers, publication quality, operational and tactical research plan success rate, measurement reports, etc.) that are present in the applied research. *Utilization of such amount of data on a country level is hardly possible and also not desirable.* This is why there is a need for a certain local information system below the CRIS level, which collects data from elementary research and provides basis for the local evaluation of the research quality. Such a system can be defined as a scientific research information system (SRIS) [4], which in addition, provides analytical functionalities, knowledge base and a cooperation space for groups and people involved in the tasks of a particular research. The proposal of basic concepts and pilot design of initial SRIS structure is described in our previous work [4]. This paper presents detailed elaboration of concepts, which are supposed to be present in the release candidate (RC). These concepts also provide space for using alternative intelligent algorithms that aid the data transformation process i.e. *from data to information to knowledge to actions to expertise* [5].

To be able to create an SRIS system, it is necessary to accommodate its functions onto the research type and its specific properties. Finally, the implementation and the deployment cover the rest of the research peculiarities, which have not been fully taken care of by the SRIS general concept.

In case of our research, the creation of a first working sample of an SRIS system is being done in the field of complex thermodynamic systems research. Particularly, the implementation and deployment will be done within the research of a small turbojet engine MPM–20 (further referred to as "the object") in the Laboratory of Intelligent Control systems of Jet Engines (abbr. LIRS LM)[1]. Modularization and design of this system is described in the following chapters of this paper.

[1] see `http://lirslm.fei.tuke.sk/wp_eng`

2 CRIS Versus SRIS

The main idea of a CRIS system is to integrate research data around a certain geographical area [4]. Although the size of stored data increases with the size of the area, the CRIS system only integrates the data of informational and financial character. In particular, the core components of CRIS system contain projects (source of finance and new information), publications and patents, people and human resources and research institutions. Each one of the components is presented as an entity and has certain attributes (describing properties) in the data model. Since it is hard to integrate data from different entities with different formats (different semantics), reported information have to contain certain required facts about the research. Also due to requirements for interchangeability and compatibility, the obtained data and metadata undergo formatting according to the CERIF (Common European Research Information Format) XML scheme. A better view on the components of the basic CERIF standard is depicted in Fig. 1.

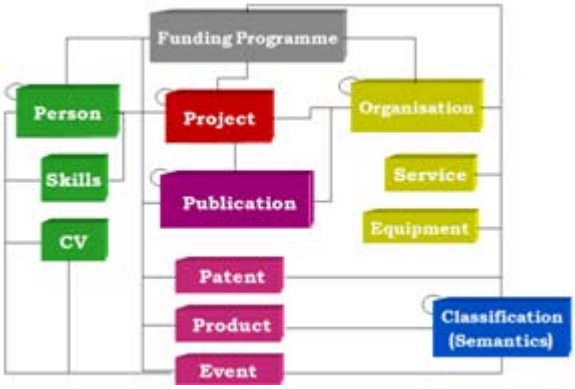

Fig. 1. Entities and relations in the CERIF

CRIS systems utilize the CERIF standard mostly because the main idea of CRIS systems is to evaluate the research efficiency (of informational and financial character) usually over a larger geographical area (country, group of countries), but on the other hand it is theoretically possible to evaluate the efficiency of an institution or a researcher (see Fig. 1) [6]. *Main drawback of this concept is the disregarding of technical, physical (functional) and time related efficiency, which cover the greatest part of total research efficiency in applied sciences.* In other words, CRIS systems do not deal with the utilization of the time and finance within other measurable results than products, publications, patents and events. In addition, the efficiency and research information is obtained as well as provided to institutions involved in the research processes, so that a continuous

growth of the research quality can be ensured by the "popularity factor" of the institution (see Fig. 2). This is why the CRIS system is an ideal solution for research efficiency evaluation in a greater (national or European) extent. Detailed information exchange possibilities are depicted in Fig. 2.

Fig. 2. Entities of the research and efficiency information dissemination process [6]

Observing Fig. 2, we may deduce that the reach of a CRIS system is wide. In case of a SRIS system the information should include less entities and institutions. *Unlike the CRIS systems, the basic idea of a SRIS system is to integrate da-ta from various data sources and different semantics within a certain research facility (constrained environment).* As it was previously mentioned at the local research level it is possible and desirable to receive and store technical, physical, informational, time and financially related data. These data may be used either to evaluate the research efficiency or for the cooperation purposes. Moreover, it is possible to utilize the differences between types of stored data to evaluate the final efficiency more precisely.

3 Requirements for a SRIS and Its Design

Requirements for a SRIS system mostly consist of requirements for a general information system (IS), which means that the IS has to cover processes occurring in the deployment company environment. Slightly different requirements are held in case of deployment at a research institution (SRIS deployment).The remaining requirements contain the identification of the research type and creation of a de-tailed description of research requirements. Research requirements vary according to the research type. For example, in case of a theoretical research a need for stor-ing research papers, reports, and non-technological information is

dominant. In case of an applied research, the dominant need is represented by storing techno-logical and physical data like measurements, simulations, testing, etc. It is neces-sary to list and map all outputs of the institution in a work-flow or a process. *Using this approach, the detailed needs for functionalities are discovered, user roles and data sources are identified, and optimization of existing processes is carried out.* Only after these processes are done, the analysis is complete and the creation and implementation of the SRIS may begin.

A lifecycle of an IS (even in general) contains steps that are not less important than the conceptual and development part. These steps ensure the sustainability of the IS in its lifespan. A lifecycle of an IS also holds for SRIS and is presented in Fig. 3.

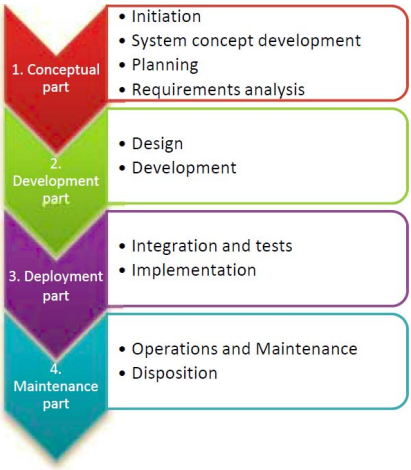

Fig. 3. Lifecycle of a SRIS

The conceptual part is similar for every SRIS system. However, the requirements analysis differs, depending on the particular needs of the research type and the research institution. Because there is no general SRIS to implement yet, the first two parts of the SRIS lifecycle have to be done for every new SRIS. The only possible unification of the conceptual and development parts of the SRIS creation may be carried out by general modules, which may be generalized for every type of applied research.

The greatest challenge is to scale the system properly. Every step of each part may be broken down into elementary steps that are essential in the final success of the SRIS deployment. For example *the requirements analysis in the end of the conceptual part* is an ex-ante analysis, which has to cover the requirements of the research institution but also has to predict possible extensions (gaps) of the system in the future. This means that the required output of the development part is to create interoperable classes that could be easily maintained and extended [10]. A modular approach is one of the solutions that ensures systems' scalability, as well as its simple understandability for new researchers that are supposed

to maintain the system. To reach the highest possible efficiency, the time and finance con-sumption of the maintenance staff should be minimal. Thus, the *requirements analysis* may be broken down into the following four steps:

1. Incorporate the requirements of the research institution.
2. Incorporate the scalability possibilities.
3. Incorporate the interoperability possibilities.
4. Incorporate easy maintenance best-practices.

Although the importance of every step is certain, it is necessary to reach only a certain system size and complexity. It means that the range of the system has to be limited according to the requirements, so that its size (by means of its functionalities and complexity) would not raise the difficulty of its usage. It is again possible to reach this scalability goal by creating separate modules and implement them to a certain level of functionality if needed. It is important to note that each sub-process of the research institution should be mapped into a single module. The connections between the modules (i.e. sub-processes) is then ensured by *inputs* (I), *outputs* (O), *constraints* (C) and *resources/mechanism* (M) relations (on the basis of IDEFØ conceptual modeling technique). Hands-on denotation of the relations and modules is depicted in Fig. 4.

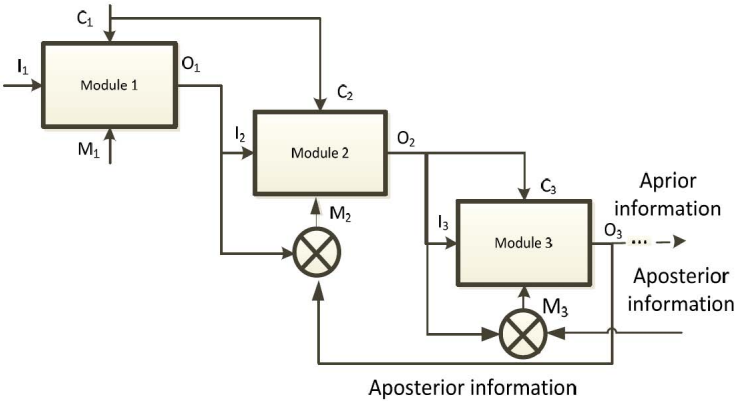

Fig. 4. A sample diagram of modules and their mutual relations [15]

As in case of a general IS, it is welcome if the system is tested by its future users. But this is only the logical testing, which has to be preceded by functionality, unit or stress testing. This minimizes sections with dead code and also highlights bottle necks of the system. In general the SRIS system is operated by only several researchers. However, the scalability of the system may allow the access of large amount of users with different roles, which use SRIS functions

with different pro-cessor time and memory consumptions. For example it is different if the user is downloading a journal paper from the SRIS library or carries out a correlation or hypotheses testing on a large sample of stored data.

4 Creating SRIS in the LIRS LM Laboratory

As it has been stated in the previous chapter, the main part of the SRIS creation is the specification of processes (workflow) that should be mapped into functional modules of the resulting SRIS system. Even if the SRIS system is created for a specific laboratory (e.g. the LIRS LM), its generalization is only the matter of extending the system with particular required functionalities and new modules. This is why we present the proposal and design background of the SRIS system in LIRS LM laboratory conditions with all its requirements, processes and peculiarities. We have to mention that some processes are not entirely internal. Knowledge sharing and efficiency reports may also be provided to external entities beyond the LIRS LM, for which mostly the reported information are typically important. They are usually represented by the chiefs of departments, deans, university research bureaus and the bureaucratic aperture.

In LIRS LM the following processes are dominant:

- Experiment planning, hypotheses design, design of proper evaluation methods
- Real-time measurements of the objects' parameters
- Storing the measured data
- Analyzing measured data
- Evidence of laboratory data in logbooks
  - Storing the objects' operation data, in the operation logbook
  - Storing changes, servicing and repairs in the service logbook
  - Storing failures, errors, error symptoms, stalls and breakdowns in the error logbook
- Knowledge storing and sharing
  - Sharing gained knowledge with other researchers
  - Sharing knowledge by teaching students

In addition, with the digitization of these processes, the efficiency, reliability and safety evaluation and prediction come to use.

4.1 Efficiency in Applied Research

We have to take various types of efficiency into account and evaluate each type separately to discover the composition of the resulting general research efficiency. As it has been previously stated, **basic types of efficiency** that occur in applied research include technical (physical), time related, informational and financial efficiency.

Technical (Physical) Efficiency. Technical efficiency is the efficiency of a system (object) influenced by its internal state parameters and environmental parameters with the highest degree of influence (environmental parameters highly correlated with internal state parameters). This type of efficiency may consist of a set of functions that describe the utilized work (effective output) in form of physical measures. *To discover the model of technical efficiency, we firstly need to know the functional relations or models of the independent variables and the dependent variable.* To optimize the technical efficiency, independent variables of these functions have to reach the values according to the requested (dependent) output. Achieving the state of optimal technical efficiency is a seriously difficult task, if we consider a nonlinear dynamic system. This is why the methods for system control (suboptimal) include best practices, probability and predictive models. *Thus, the maximization of the technical efficiency requires either a precise analytical model of the system (usable in noncomplex or deterministic systems) or a set of experimental models created by the system testing, i.e. detailed technological and physical system operation description.* For example, the technical efficiency of our research object is described by a set of the following nonlinear functional relations [8,9]:

$$\begin{aligned} M_T &= M_T\left(T_{3C}, G_T, \eta_T, \pi_{Tc}\right), \\ M_K &= M_K\left(G_K, RPM, \pi_{Kc}\right), \\ G_K &= G_K\left(p_{2C}, T_{3C}\right), \\ G_p &= G_p\left(p_{3C}, T_{3C}\right), \\ G_D &= G_D\left(p_{4C}, T_{4C}\right), \end{aligned} \tag{1}$$

where:

- M_T – critical turbine momentum,
- M_K – critical (load) compressor momentum,
- G_K – mass air flow of the compressor,
- G_p – mass gas flow of the turbine,
- G_D – mass gas flow of the exhaust nozzle,
- T_{3c} – gas temperature in front of the turbine,
- G_T – weight of the gas in front of the turbine,
- π_{Tc} – reduced gas compression on the turbine,
- RPM – rotations per minute of the compressor and the turbine,
- π_{Kc} – compression of the compressor,
- p_{2c} – reduced air pressure beyond the compressor,
- p_{3c} – reduced gas pressure in front of the turbine,
- T_{3c} – reduced gas temperature in front of the turbine,
- p_{4c} – reduced gas pressure behind the turbine,
- T_{4c} – reduced gas temperature behind the turbine.

Technical efficiency is highly related to the proper functioning of the object. Errors, failures, unexpected values, occurrence of danger and other atypical states in the system's operation, cause decrease in both the technical efficiency and the reliability. Then the methodological aim is the minimization of the loss

function ℓ of the measured parameter y for the time span t, which defines the loss of efficiency, i.e. the difference $\Delta y(t)$ between the achieved output value $y(t)$ and the model value $y(t)_M$ [9]. If A is a level of the highest achievable value of a qualitative parameter (e.g. efficiency, reliability, safety), then the mathematical hope $W(t, A)$ of achieving A is defined as (2).

The aim may also be defined as a probability of achieving less or equal loss of efficiency, which is a difference between actual loss function and demanded loss (2).

$$W(t, A) = \min\left[\ell(y, t)\right] = P\left\{\ell(y, t) \leq \ell(y, t)_d\right\} \tag{2}$$

Time Related Efficiency. Time related efficiency is the efficiency of the object, evaluated according to its dynamics. It may also be defined in form of a loss function, where we evaluate the difference between the measured time span of an event and the demanded (expected or estimated) time span of an event.

It is usually calculated for expected changes in the system's dynamics, e.g. time of the shift between engine's phases (electrical engine startup – ignition – bypass open – automatic combustion – normal regime – acceleration – deceleration – termination).

Moreover, the time relations may be also understood as a dynamics of a non-technological phenomenon, e.g. experimenting time span, servicing time span, paper writing time span, learning time span, plan preparation time span, etc. In this case, the demanded value is created either according to expert's prediction or a plan of an experiment, which hypotheses are based on the probability theory and the statistics.

Informational Efficiency. The informational efficiency is the efficiency of the informational content and exchange. It may occur either in a form of a difference between useful data and noise, filtered from the sensor values measurement, packet loss over the measure-ment network, etc. (technical phenomena) or in a form of information gain, which represents an impact of the information which has been created, measured or gained in any other way (non-technical phenomena – research papers, books, tacit knowledge).

Evaluation of the informational efficiency may be carried out as the evaluation of the information gain (in some literature "information function"). Its basis lies in the evaluation of the object's entropy, maximum and minimum boundaries of the output parameter values and the distribution density function of the output parameter [12,13].

Financial Efficiency. The financial efficiency is considered an overall efficiency of the capital spending, according to its output effect. Expenses can be understood as a direct consumption of the object (amount of liters of jet fuel at its mean price), which is a technical phenomenon. On the other hand, funding of conference registration fees, journal paper submission fees, etc., is considered a non-technical phenomenon.

In this case, the resulting efficiency parameter may consist of the informational and the financial efficiency of the paper, which is described as the overall efficiency of a research paper (for more information refer to the chapter 4.3.5).

4.2 Efficiency Assessment Using Key Performance Indicators

According to previous statements, the evaluation of efficiency in general may be done using the loss functions. However, as a substitution for unknown variables in the loss function that might be difficult to measure, we may use empirically created indexes called key performance indicators (KPIs). *A KPI is a performance indicator created according to "SMART" criteria, which holds for: "specific, measurable, attainable, realistic, time-related" [14].*

Using KPIs, even a combination of measured values may be used as the target variable for the assessment of efficiency. Moreover, it is easier to plan the KPI values and distinguish between successful or unsuccessful examples. Based on the source parameters, the KPIs differ in the units of measure and may take over one unit of measure or create a new one if combinations of more distinct units of measures are used.

In case of their deployment in the SRIS practice, they are usually defined as equalities or inequalities of:

- Single constrained parameters (two interval borders or one undefined),
- Constrained difference of two parameters (two interval borders or one undefined),
- Constrained ratio of two parameters.

Their evaluation is then carried out using the general efficiency formula (3) as the number of examples that successfully fulfill the constraint conditions divided by the number of all examples. The success rate is then considered the overall ef-ficiency evaluated for a single KPI.

$$E = \frac{Q}{S}, \tag{3}$$

wherewhere: E – resulting efficiency, Q – number of successful examples, S – all examples.

If we assume that every KPI, where n is number of KPIs of a single efficiency type ET has its importance v_{KPI}, then the efficiency for the specific efficiency type ET is evaluated as:

$$E_{ET} = \prod_{KPI=1}^{n} \frac{Q_{KPI}}{S_{KPI}} \cdot v_{KPI}. \tag{4}$$

If we assume that for every efficiency type ET, where m is number of efficiency types there is an importance v_{ET}, then the overall efficiency of an elementary research step (e.g. measurement or an operative plan) is evaluated as:

$$E_A = \prod_{ET=1}^{m} E_{ET} \cdot v_{KPI}. \tag{5}$$

With respect to formulas (4) and (5), if the importance is a number belonging to the interval $[0, 1]$, the E_A also belongs to this interval. We may continue to encapsulate this equation in the same manner as in the case of the transformation of (4) to (5) into higher levels of research steps (tactical plans, strategic plans). Then the overall efficiency of any qualitative parameter, including the efficiency, can be evaluated as a percentage of success, which has been achieved during the research step, i.e. **the research efficiency**.

The greatest asset of this method is the simple and fast evaluation of results and its simple algorithmization, which ensures a straightforward implementation and deployment in the computer program environment.

4.3 Components and Modules of the SRIS in LIRS LM

The core components of the SRIS system in LIRS LM cover the processes mentioned in the beginning of the chapter 4. Core components and modules include:

- Design of experiments,
- Laboratory logbook,
- Measurements handling,
- Data analysis,
- Library.

Since the efficiency evaluation is spread out in each module to different extent, it is not beneficial to create a separate module for the efficiency assessment. However, it is useful to compile functions (denoted as methods in the object oriented programming) into the form of a dynamic link library (DLL) collection and be used as an external framework in other SRIS systems with the same core structure.

Planning the Research and Its Life-Cycle. The research life cycle is the evolution of the research work since its proposal to its evaluation and projection (prediction) of new research possibilities. It may be done by any process modeling technique, which takes the time and efficiency or more selected qualitative parameters into account.

Research planning has to comply with the method of the evaluation of qualitative parameters. This ensures that the efficiency is indirectly planned before the research process and enables the researchers to compare the planned and the achieved values for each research work. In general, the research may be planned using:

Strategic plans – the highest level of research process activities. They consist of several tactical plans. A strategic plan describes the long term orientation of the research in 1 and more years.

Tactical plans – cover the middle level of research (phases) process activities. They consist of several operative plans. A tactical plan describes midterm re-search orientation (usually 3–12 months) with the same higher level goal described in the strategic plan.

Operative plans – elementary research plans, which contribute to the evaluation of qualitative parameters in case of individual measurements and short term research goals. Operative plans usually last from several hours to three months. They contain definitions of KPIs with their boundaries.

One of the crucial elements of the whole research life-cycle concept is its visualization. Simple and easily understandable visualization can be achieved using IDEFØ conceptual modeling technique and its modifications, which we described and proposed in our previous works in detail [15,16] (Fig. 5).

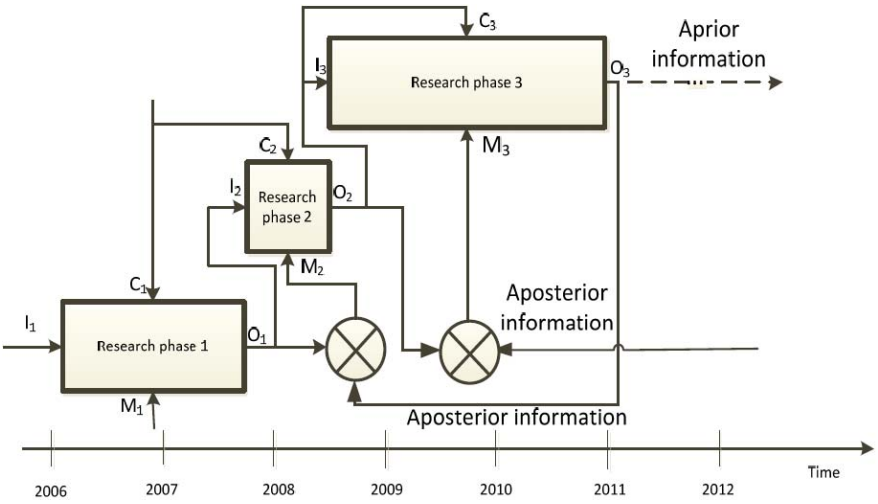

Fig. 5. Modified IDEFØ model used for research visualization and efficiency evaluation

A separate set of functions is being prepared in the form of "Research designer", which will be also integrated in the resulting SRIS system. Research plans also interact with each other as do the modules of a SRIS (see chapter 3). This is one of the reasons why the designing of the research is done by IDEFØ. *It also enables to carry out the design, driven by relations between research plans and new re-search possibilities that will emerge after the research plan is successfully real-ized in practice. The ability to assume and revise the impact of previous research activities and new research possibilities is the greatest asset of the research pro-cess visualization.*

Research History – Operation, Service and Error Logbook. Alongside with the research life-cycle visualization, the logbook completes the entire view on the research history. Depending on the events that occur in time, the logbook is logically divided into three categories but acts as one complex module (see Fig. 6).

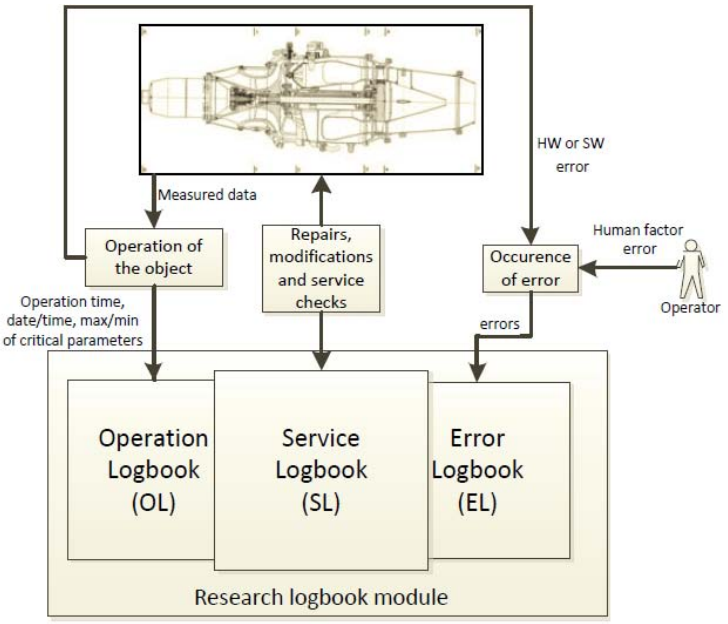

Fig. 6. Concept of the research logbook module

The logbook should be created as a submission form, in which some of data are filled automatically from the measured data and some are filled manually by the operator. The entries in the logbook may vary because of their nature. One entry may belong to all three logbooks if for example an error occurs (EL) during the operation (error is bound to the particular OL entry in which it occurred) and afterwards necessary measures to fix the error are carried out (fixing the error which occurred during operation by changing software or hardware configuration of the object is an entry in SL bound to respective entries in EL and OL).

This module can also contain a statistical overview, which shows the amount and seriousness of errors, operation hours, number of launches and service changes during a specific time span (e.g. for one operative/tactical/strategic plan). Entries in the logbook also contribute to the evaluation of overall efficiency. For example to technical efficiency (dependent on number of errors – covered by EL), time related efficiency (dependent on the number of launches and length of operation hours – covered by OL), financial efficiency (dependent on length of operation hours – OL, cost of servicing actions – SL, number of errors – EL).

In case of LIRS LM, the logbook contains following fields and lists:

ID of the engine – allows to distinguish an engine exchange or other engine type,

Date and time of the launch – brings the time parameter into logbook entries,

"Flight" hours – depend on the length of operation and the load,

Temperature peak – T3C peak value should not exceed 1200 °C for time longer than 3–5 seconds [18,19],
Maximal RPM – influence efficiency, reliability and safety [18,19],
List of errors – contains list of error codes along with their name, description and level of seriousness,
List of service actions and changes – contains list of changes and repairs in engines' aggregates, measuring aperture, control algorithms, electrical wiring and supply units,
Notes – enable describing the whole logbook entry.

If the logbook is filled with statistically relevant amount of data, following functions may be carries out:

- Trace the history of a specified aggregate,
- History of error occurrences,
- Graph of peak temperatures and maximum RPM in time with error events and service events,
- Highlighting of logbook entries where a service action could cause an error,
- Exporting PDFs of various operation/service/error reports.

Adding, Viewing and Replaying Measurements. When adding measurements, common problems emerge. First one is the form, in which the measured data is stored after the measurement. In LIRS LM, data are stored in separate LVM files and undergo the transformation and they are finally saved in XML format. The second problem is to pair the measured parameters in LVM file and SRIS database. Pairing may be done using either predefined rules for parameter classification or classification based on supervised learning (classification model). The second solution (slower) lets the operator choose the correct pairing manually. Measurement adding goes along with the new entry in the logbook, so it may be integrated into the adding form for the measurement. It has to be possible to open each measurement and view its values and properties either in a table or separately in a graph. In LIRS LM SRIS we utilized a free API called "HighStock" to provide the graphing functionality.

Moreover to view the whole operation process it is necessary to provide a platform for replaying measurements. In [20], we proposed and created a platform that allows the operator to replay a saved measurements in a desired speed. A simple measurement analysis, which marks each measured series during its replay as critical (red), abnormal (orange) and normal (green) and operation status (started, ignited, finished) has also been included for faster results evaluation. Classification of these values is briefly defined in article [18].

Analysis. There are various third-party platforms that allow operators to carry out different advanced analyzes (e.g. Matlab, R, SPSS, RapidMiner, MS Excel). However, integration of the most used methods for data analysis in the common platform of SRIS will save time and will enable to share the results and the reports with the rest of the research team (i.e. extends the explicit knowledge-base).

Intelligent algorithms. In general, algorithms of artificial intelligence (AI) are considered as intelligent algorithms. Their integration in the SRIS has various places. The place with the most potential of using intelligent algorithms proves to be the data analysis. This fact is mostly emphasized by methods for knowledge discovery, that include data cleansing (filtering and filling), integration, transformation, data mining. Classification, clustering, prediction and time series analyzes belong to the most common intelligent algorithms used in data mining [5]. For example they may be used in detection of measurements with atypical maximal temperatures (overheating) and RPMs or abnormal ignitions (ignitions with low maximal RPM – see Fig. 7).

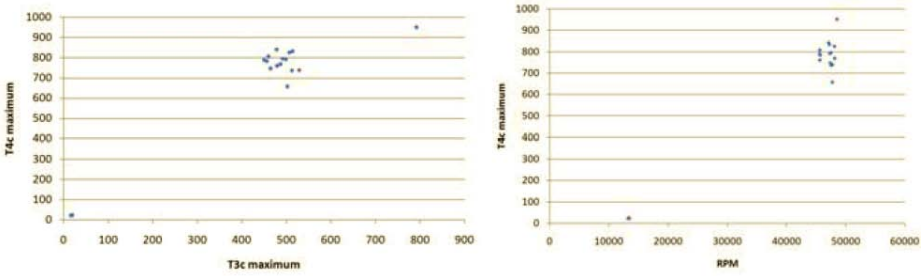

Fig. 7. Detection of atypical values (temperatures – left ; ignitions and RPM – right)

Numerical methods. In [17], we created a list of numerical methods with their possible usage in case of complex thermodynamic systems. To sum it up, methods with the most promising usage are:

First derivative – detects local extremes and possible oscillations,
Second derivative – inflexion points help to discover the change in dynamics,
Normalization – normalization according to the maximum allows to compare different parameters,
Definite integration – allows to evaluate differences of dynamics between measurements (e.g. comparing startup efficiency on the same time interval between two measurements),
Smoothing – smoothes the series, thus degrades elementary noise. Various smoothing (moving averages smoothing method, local regression filtering methods) and signal filtering (Savitzky–Golay filtering, Fast Fourier transform filtering – FFTF, etc.) functions may be of use.

Statistical methods. The most widely used statistical measures used in data analyzes are as well implemented in the SRIS core. Their usage although assumes that the measured data are clean and statistically significant.

Maximum, minimum, average, standard deviation and variance are basic measures incorporated in SRIS that allow to compare different measurements. However, they highly relay on the correctness of measured values. For example, if a

sensor fails or reads additive noise, the average and the maximum or the minimum will change, usually in a greater extent, thus they are not reliable in this case. Skewness and kurtosis, which are also implemented, allow more detailed statistical overview. Their values allows to discover measurements with sensor failures. In case of the experiment evaluation, the hypotheses testing is the most easily feasible solution.

Comparison of measurement sets. One of the most important functions in data analysis is visual, statistical or overall comparison of more measurements and parameters in one graph. However, it is also necessary to compare sets of measurements by means of e.g. two different operative plans. In this case, the operator may unveil the differences in the engine operation, which have been caused by concentration on a different research goal. This fact allows to track the origin of differences and thus propose a countermeasure or a solution.

Library. The library module provides the space for sharing both the documents and templates required for the bureaucracy tasks in the research, research papers of each researcher or student or final theses of students and researchers, which may be of use by other researchers either for educational or overview purposes.

This module creates possibility of sharing knowledge, which has been gained in the history of research in the particular institution. By means of knowledge discovery and the SECI model [11], the knowledge sharing represents the internalization of explicit knowledge and the externalization of tacit knowledge and allows the knowledge combination. Moreover, it allows to discover the research genesis up to its present state and thus provides an easily reachable knowledge base for either undergraduate students, junior researchers or even senior researchers. Explicit knowledge, represented in the library module is also one of the inputs of the informational efficiency evaluation. The evaluation of the efficiency is presented in chapter 4.1 in detail. However, as it has been previously mentioned, it is necessary to specify measurable KPIs that will cover the informational efficiency evaluation of the research. In case of the library module a different set of KPIs is created for each user role (see chapter 4.3.5.1). In general the informational efficiency of a single publication may be also calculated using the equation (6).

$$W_I = \frac{2rp\left(1 - \prod_{j=1}^{n}(1 - s_j)\right)}{1 + rp\left(1 - \prod_{j=1}^{n} 1 - s_j\right)}, \tag{6}$$

where

- W_I – efficiency of a single publication(scale 0–1),
- r – researcher index, according to his role (scale 0–1),
- p – publication quality index, according to the databases (scale 0–1),
- n – number of citing documents,
- s_j – citing document quality index (scale 0–1).

Financial efficiency of a publication may be calculated using the equation (7):

$$W_F = 1 - \frac{C_p}{C}, \tag{7}$$

where

W_F – financial efficiency of a publication (scale 0–1),
C_p – costs of a single publication,
C – disposable capital.

General functionalities. General functionalities of the library module differ according to the logged user. They consist of search, download and upload capability. Actions which are required for library management and maintenance in addition include adding, editing and removing of categories, subcategories, papers, documents and final theses.

For the purpose of efficiency evaluation, a personal publication and efficiency report may be created by each researcher for himself or in case of the teamleader, either a personal or a cumulative publication and efficiency report for the whole research group (see details in Tab. 1).

Table 1. User groups and allowed functions in the library module

User group	Functionality
Student	Search (view list of publications)
	Download (only selected documents)
	Add/Remove/Edit final thesis
Operator, Cooperative researcher	Search
	Download
	Add/Remove/Edit documents and categories
	Create personal report
	Confirm or reject proposals for own publications
Team leader	Search
	Download
	Add/Remove/Edit documents and categories
	Create personal or cumulative efficiency report
	Confirm or reject all proposals for publications
Public	Search (view list of publications)
Administrators	All functionalities

Intelligent functionalities of the library. Using application programming interfaces (APIs) of world renowned publication databases (e.g. SCOPUS, Google scholar) it is possible for the SRIS to gain knowledge about the published papers and their impact, thus propose possible new publications and citations of the whole research collective (registered users). Functionalities of SCOPUS and GOOGLE APIs (in case of Google only third party) help to keep the collection of the publication corpus actual. Other publications, which are not present in the

citation databases have to be added manually. Despite the need for manual addition of local papers, it is also possible to pair the library module with the official institutional library. For example, in case of LIRS LM it is the *publication evidence module of the university library*[2]. Detailed depiction of the semi-automatic publication collecting process may be observed in the Fig. 8.

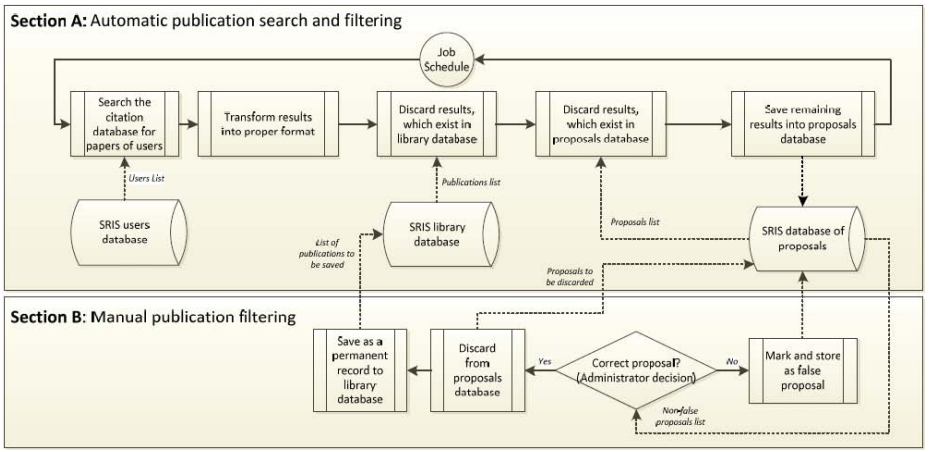

Fig. 8. Semi-automatic publication search and filtering

Basic User Groups and Roles. An SRIS system is a multi-user information system that integrates knowledge of researchers and allows other users to access specific permitted information. In addition to the permissions stated in the Tab. 1, the user groups, are described as follows:

Administrators – are superusers, which are granted all access roles with permissions to alter the user records.

Operators – are users that may access all modules, create, modify and delete records (measurements, enumerations in reference tables, experimental plans) except for user records.

Cooperating researchers – are allowed only to view measured results, stored analyzes and have full access to the library (for details in user groups and roles in the library module refer to chapter 4.3.5.1). They are only allowed to view the engine operation logbook.

Students – are allowed to view measured results, stored analyzes, download selected books and papers from the library.

Public – are restricted from any active operations. They are allowed only to view the research lifecycle as well as scheduled experiments and list of publications in the library. Research overview (remote monitoring see chapter 4.4)

[2] `https://epc.lib.tuke.sk/`

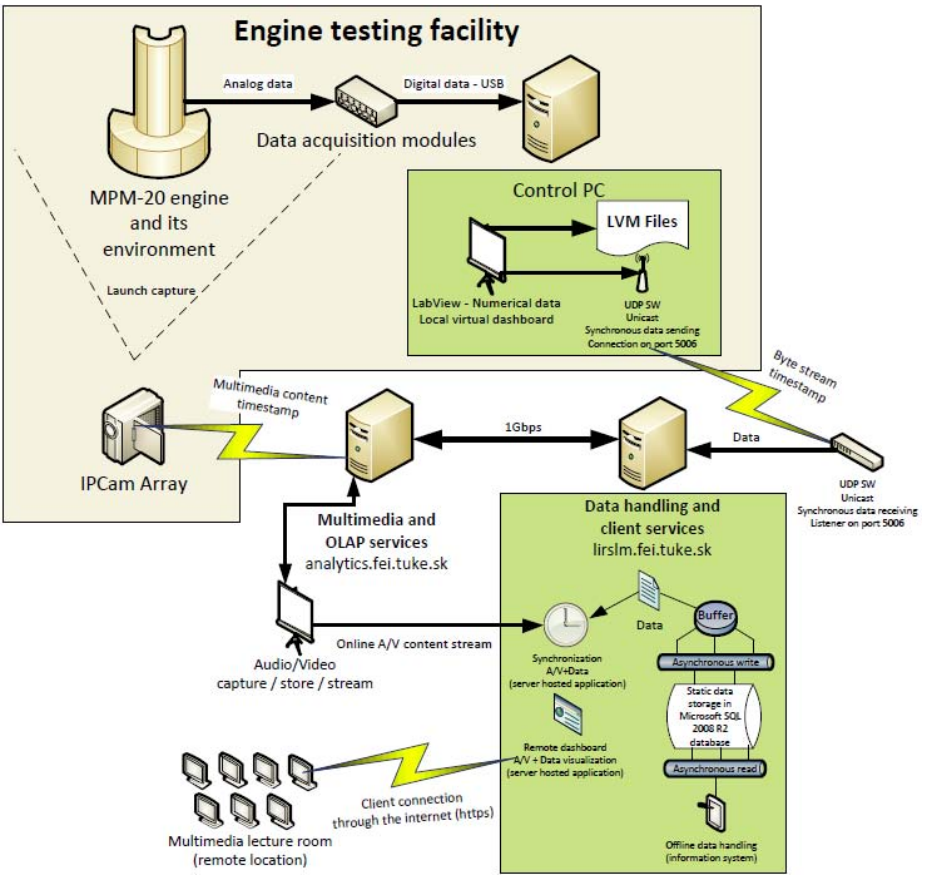

Fig. 9. Detailed conceptual description of the remote measurement overview module

is only provided to 2 simultaneous public users. However, one public user is reserved for Public live web stream. The remote monitoring operates in a constrained environment for the public users.

4.4 Remote Measurement Overview

SRIS system in LIRS LM also provides a module to view measurements from remote machines. It serves for both public and students, who may see the actual measurements and values that are being measured. The basic idea is to send measured values and audiovisual content, directly from the LabView environment in real time or with low latencies using UDP or TCP protocols to a central server application that forwards them to connected users. Detailed description of this module is presented in Fig. 9 and its concept may be obtained from [7].

5 Conclusions and Future Prospects

A SRIS system is a solution that is beneficial for research institutions that need to store, evaluate data and plan its research activities. Using large variety of basic and intelligent functions it creates a suitable framework to assess qualitative parameters that are produced by research activities. In addition, the evaluation of qualitative parameters including efficiency, reliability and safety helps to raise the quality of research. A knowledge base, which is built with the SRIS operation, allows new researchers to accommodate themselves in usually a new research environment. In this article, we denoted and described the core elements and modules of a SRIS system and distinguished the differences with a CRIS system. As a particular example of an implementation, we adapted the concepts in the environment of a real laboratory (LIRS LM). It participates in research of turbojet engines, which belong to the group of complex thermodynamic systems.

In the future, we are planning to complete the deployment of the SRIS system in the mentioned laboratory and unify the concepts and functions, so that the implementation will be easy and straightforward.

Acknowledgements. The work presented in this paper was supported by VEGA, Grant Agency of Ministry of Education and Academy of Science of Slovak Republic under Grant No. 1/0298/12 – "Digital control of complex systems with two degrees of freedom". The work presented in this paper was also supported by KEGA under Grant No. 018TUKE-4/2012 – "Progressive methods of education in the area of control and modeling of complex systems object oriented on aircraft turbo-compressor engines".

References

1. Overcoming barriers: access to research information content (A Research Information Network report), Research Information Network briefing, London, UK, 28 p. (December 4, 2009)
2. Bronwyn, H.H.: The Financing of Research and Development. UCB, Department of Economics, 27 p. (January 1, 2002)
3. Asserson, A., Jeffery, K.G.: Current Research Information Systems (CRIS): Past, Present and Future. In: Forschungs Information IV, pp. 41–44 (January 2009)
4. Gašpar, V., Madaráász, L., Andoga, R., Glodová, I.: On Scientific Research Information System. In: Proceedings of CINTI 2013, November 19-21, pp. 75–78. Óbuda University, Budapest (2013) ISBN 978-1-4799-0195-1
5. Paralič, J.: Objavovanie znalostí v databázach (Knowledge discovery in databases), 80 p. Elfa, Košice (2003) ISBN 80-89066-60-7
6. Dvořák, J.: CERIF 1.5 Tutorial. euroCRIS Membership Meeting, Porto, Portugal (November 13, 2013)
7. Madarász, L., Gašpar, V., Rudas, I., Andoga, R., Gašpar, L.: Proposal of dissemination and broadcasting of laboratory data within small time latencies. Acta Mechanica Slovaca 17(3), 9 p. (2013) ISSN 1335-2393
8. Lazar, T., Madarász, L. (eds.): Inovatívne výstupy z transformovaného experimentálneho pracoviska s malým prúdovým motorom (Innovative outputs from the transformed experimental laboratory with a small turbojet engine), pp. 276–291. Elfa, s.r.o, Košice (2011) ISBN 978-80-8086-170-4

9. Lazar, T., Madarász, L., Gašpar, V.: Procesná analýza odhadu efektívnosti identifikácie MPM s inteligentným riadením (Estimation process analysis of identification efficiency of small turbojet engine with intelligent control), 160 p. Elfa, s.r.o, Košice (2013) ISBN 978-80-8086-200-8
10. Bruckner, T., et al.: Tvorba informačních systémů (Prinipy, metodiky, architektury), 360 p. Grada Publishing, Praha (2012) ISBN 978-80-247-4153-6
11. Brožová, H., Houška, M., et al.: Modelování znalostí, 211 p. Professional Publishing, Praha (2011) ISBN 978-80-7431-069-0
12. Daňo, I., Ostertagová, E.: Numerické metódy, pravdepodobnosť a matematická štatistika v počítačovom prostredí MATLABu, Košice, 88 p. (2009) ISBN 978-80-8088-111-2
13. Vorobev, V., Konstantinov, V.D.: Nadežnosť a efektivnosť aviacionogo odorudovanija, Moskva, Transport, 133 p. (1995)
14. Doran, G.T.: There's a S.M.A.R.T. way to write management's goals and objectives. Management Review 70(11) (AMA FORUM), 35–36 (1981)
15. Gašpar, V.: Modification of IDEFØ box model for the purpose of experimental identification effectiveness evaluation. In: Proceedings of the SCYR 2013, FEI, TU Košice, Herľany, Slovak Republic. 3 p. (May 14, 2013) ISBN 978-80-553-1422-8
16. Gašpar, V., Madarász, L., Andoga, R., Glodová, I.: On Scientific Research Information System. In: Proceedings of CINTI 2013, November 19-21, pp. 75–78. Óbuda University, Budapest (2013) ISBN 978-1-4799-0195-1
17. Vantová, Z., Madarász, L., Gašpar, V.: Numerical Methods in Analysis of Thermodynamic Data. In: Proceedings of 5th IEEE International Symposium on Logistics and Industrial Informatics (LINDI 2013), Wildau, Germany, September 5-7, pp. 85–91 (2013) ISBN 978-1-4799-1258-2
18. Gašpar, V., Madarász, L., Andoga, R., Főző, L., Judičák, J.: Operational constraints definition of a turbojet engine MPM 20. In: Proceedings of SAMI 2013, Herľany, Slovak Republic, pp. 215–219 (2013) ISBN 978-1-4673-5927-6
19. Madarász, L., Andoga, R., Főző, L., Judičák, J., Gašpar, V.: Expansion of working envelope of a small turbojet engine MPM-20. In: Proceedings of CINTI 2012: 13th IEEE International Symposium on Computational Intelligence and Informatics, Budapest, Hungary, November 20–22, pp. 293–298. Óbuda University, Budapest (2012) ISBN 978-1-4673-5204-8
20. Gašpar, V., Madarász, L.: Purpose driven design of a KDD enabled application for experimental data analysis. In: Proceedings of IEEE 9th International Conference on Computational Cybernetics (ICCC), Tihany, Hungary, pp. 257–261 (2013) ISBN 978-1-4799-0060-2

Comparison and Visualization of the DNA of Six Primates

José A. Tenreiro Machado

Institute of Engineering, Polytechnic of Porto,
Dept. of Electrical Engineering,
Rua Dr. Antonio Bernardino de Almeida, 431,
4200-072, Porto, Portugal
jtm@isep.ipp.pt
http://ave.dee.isep.ipp.pt/~jtm/

Abstract. This study addresses the comparison of the deoxyribonucleic acid (DNA) of six primates in the perspective of fractals and signal processing. The species consist of Bonobo, Chimpanzee, Gorilla, Human, Orangutan, and Rhesus macaque. These primates are very close in the life evolution and, therefore, pose a problem for designing assertive algorithms to detect their phylogenetic tree. The paper associates logical and mathematical concepts inspired in signal processing and dynamical systems for the analysis of the DNA data of the chromosomes. The results are compared by means of computer visualization tools.

Keywords: DNA, Signal processing, Dynamics, Fractal, Visualization.

1 Introduction

Phylogenetics studies the evolutionary relations between groups of organisms. The progresses with genome sequencing and genome databases led to the emergence of considerable data presently available for computational processing. The informational structure embedded into the deoxyribonucleic acid (DNA) can be exploited for constructing more precise phylogenetic relationships. Understanding the DNA and extracting information is a challenging problem that motivates worldwide research [45,39]. The paper proposes an algorithm for converting the DNA string into a numerical signal. Once established this quantifying procedure, the concepts of state space, signal, fractal and computer visualization tools are adopted [48,21,9,10,52,26].

Are addressed six primates, namely the Bonobo, Chimpanzee, Gorilla, Human, Orangutan and Rhesus macaque [1,2,3,4,5,7], constituting species that are very close in evolutionary terms. Therefore, the corresponding set of chromosomes (chr) poses a formidable challenge for distinguishing details and extracting assertive phylogenetic information.

Having these ideas in mind, this paper is organized as follows. Section 2 presents the main genetic details of the primates under studied and proposes

J. Fodor and R. Fullér (eds.), *Advances in Soft Computing, Intelligent Robotics and Control,* Topics in Intelligent Engineering and Informatics 8,
DOI: 10.1007/978-3-319-05945-7_19,

the scheme for translating DNA information into a signal. Sections 3 and 4 develop the DNA sequence processing and phylogenetic analysis based on fractal and dynamical analysis, respectively. Finally, section 5 outlines the main conclusions.

2 Fundamental Concepts

This section presents the main concepts applied in the sequel. Sub-section 2.1 describes the DNA structure and presents the main primate details. Sub-section 2.2 describes the proposed algorithm for converting the DNA string into a numerical signal and the adopted mathematical tools.

2.1 DNA Structure and Primate Details

DNA consists of a double helix with a sequence of four nitrogenous bases {Thymine, Cytosine, Adenine, Guanine} represented by the symbols $\{T, C, A, G\}$. The chr data files includes a fifth symbol N which is considered to have no practical meaning for the DNA decoding. Usually the percentage of N is relatively smaller than the rest of the symbols. Each base present in one side connects only with another type of base on the second side of the double helix and forms the base pairing AT and CG. This information is being collected and is available for scientific research [47,38,58,41,22,11]. DNA embeds an intricate information, seemingly with distinct scales and redundancies [32,27,59,51,13]. Therefore, mathematical tools adopted in the study of dynamical systems may lead to an assertive analysis and quantitative results [34,35,36,18].

In the sequel we consider 6 primates {Bonobo, Chimpanzee, Gorilla, Human, Orangutan, Rhesus macaque} denoted as {Bo, Ch, Go, Hu, Or, Rh} making a total of 143 chrs (Table 1). Figure 1 depicts the main phylogenetic traces of the species under consideration.

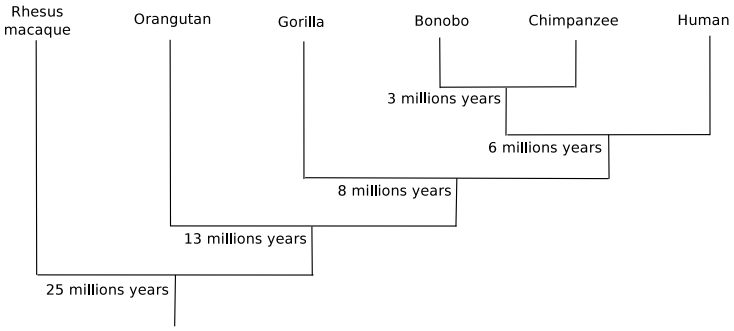

Fig. 1. Phylogenetic tree of the six primates

Table 1. Scientific classification of the six primates

Name	Order	Family	Genus	Chrs
Bonobo	Primates	Hominidae	Pan	24
Chimpanzee	Primates	Hominidae	Pan	25
Gorilla	Primates	Hominidae	Gorilla	24
Human	Primates	Hominidae	Homo	24
Orangutan	Primates	Hominidae	Pongo	24
Rhesus	Primates	Cercopithecidae	Macaca	22

2.2 Proposed Algorithm

The first phase of the proposed algorithm consists of translating the string of symbols into a string of numbers. The conversion of the DNA 4(+1)-symbol into a numerical signal is accomplished with a 2(+1)-dimensional space representation. First the AC and TG pairs are represented in the Cartesian coordinates x and y, respectively. The position along the DNA length L is represented by means of the z Cartesian axis. Second, each successive symbol in the DNA is converted to a one-step increment being $+1$ (-1) for the first (second) base in each bonding pair. For the symbol N no action is taken. By other words, our algorithm maps the genome sequence onto the points $P_k = (x_k, y_k, z_k)$ of a 3-dimensional random walk used the following 2 rules:

1. The walk starts at $P_0 = (0, 0, 0)$;
2. The nucleotides of a genome are read in succession, the coordinates of the next point $P_{k+1} = (x_{k+1}, y_{k+1}, z_{k+1})$ are obtained from present point $P_k = (x_k, y_k, z_k)$ as:

$$x_{k+1} = \begin{cases} x_k + 1, & \text{if the next nucleotide is A} \\ x_k + 1, & \text{if the next nucleotide is T} \\ x_k, & \text{otherwise} \end{cases}$$

$$y_{k+1} = \begin{cases} y_k + 1, & \text{if the next nucleotide is C} \\ y_k + 1, & \text{if the next nucleotide is G} \\ y_k, & \text{otherwise} \end{cases}$$

$$z_{k+1} = z_k + 1$$

This algorithm preserves the base pairing logic and does not introduce any preconception biasing the DNA information. The 3- and 2- (i.e., the projection over the horizontal plane) dimensional representations are going to be considered. These spaces will be denoted as the locus $\{AT, CG, L\}$ and $\{AT, CG\}$, respectively. For example, Figure 2 shows the trajectory $\{AT, CG\}$ and the corresponding locus $\{AT, CG, L\}$ for the chr 1 of the Bonobo and a quantifying cube of $500 \times 500 \times 500$.

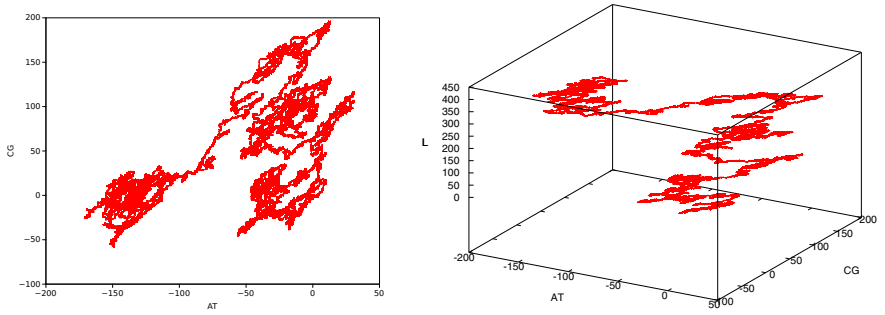

Fig. 2. Trajectory is locus $\{AT, CG\}$ and $\{AT, CG, L\}$ of the chr 1 of the Bonobo

According with Chargaff's second rule the number of symbols $\{T, C, A, G\}$ is approximately identical, not only for each of the two DNA strands, but also for long sequences [12,37,40]. Nevertheless, in the present case we are capturing the *order* of the symbols along the sequence and, therefore, considerable deviations from the 45 degree line in the x, y projection plane may occur. Computation of the complexity for DNA representations is interesting and we can mention the Z-curve [57]. Furthermore, it is worth nothing the so-called C-value paradox which states that organism complexity does not correlate with genome size [24,25,23].

3 Fractal Analysis of the DNA

The second phase consists of extracting information from the 3-dimensional trajectories. Since the plots reveal close resemblances with fractals it is adopted the box-counting method for their measurement [14,31,44]. For an object S lying in a n-dimensional space, let $N_\varepsilon(S)$ be the minimum number of n-dimensional cubes of side-length $\varepsilon > 0$ needed to cover S. If there is a number b so that $N_\varepsilon(S) \sim \frac{1}{\varepsilon^b}$ as $\varepsilon \to 0$ we say that the box-counting dimension of S is b. This leads to the expression:

$$N_\varepsilon(S) = a\frac{1}{\varepsilon^b}, \tag{1}$$

where a and b are the parameters that captures the size and the dimension of the object S. In our case S consists of the 3-dimensional DNA representation in the locus $\{AT, CG, L\}$.

The six primates involve to a total of 143 chrs to be analysed. Each chr is converted into a representation in the locus $\{AT, CG, L\}$. In a first step the chr information is read and the maximum and minimum limits along the (x, y, z) axes is determined. This information allows the calculation of a common scale factor so that the 3-dimensional trajectories have dimensions that reflect the information content and the chr length L. Once calculated the maximum/minimum limits and the global scale factor, each chr is read again and the corresponding trajectory in the locus $\{AT, CG, L\}$ is plotted. Finally, the resulting fractal trajectory is measured by means of (1) and the parameters (a, b) extracted.

Figure 3 shows the locus (a, b) for the 143 chrs. The parameter a reflects the length L of the chr. Therefore, we observe a tendency for smaller/larger values of the point labels in the right/left of the locus of (a, b). The parameter b is related with the information content, being lower/higher as the DNA "signal" has a fractal structure that resembles more a common line/surface. There is also a separation in the perspective of the six primates. It is visible Rm at the bottom and Go at the left, clearly apart from the rest. The group {Bo, Ch, Ho, Or} is very close and becomes more difficult to distinguish. There are differences from chr to chr but, in general, it is difficult to establish some order between them.

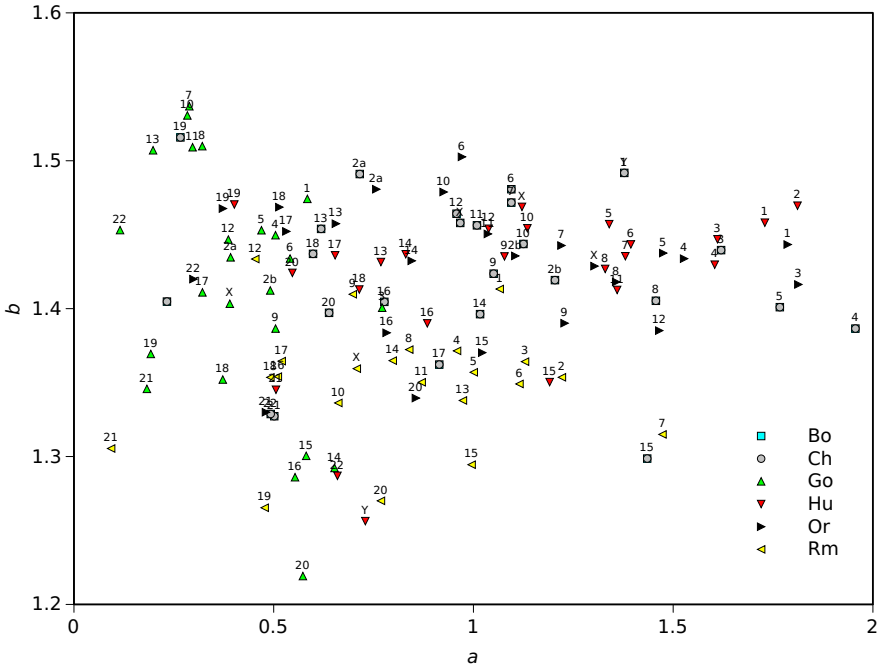

Fig. 3. Locus (a, b) of the 143 chromosomes

In the numerical representation $\{AT, CG, L\}$ the L coordinate may not provide additional scale information of the DNA sequence. By other words, the $\{AT, CG\}$ coordinates are those of the 2-dimensional DNA walk model of DNA sequences [33]. Fractal methods have been used to construct the phylogenetic trees [56,54,55]. It has been discussed that the fractal methods cannot give better phylogenetic trees than simple statistical models if the number of species becomes large [42,43,53]. Therefore, the adoption of the fractal dimension for characterizing the objects constructed in the $\{AT, CG, L\}$ locus seems to limit the visualization and that a more suitable method should be tried.

4 Dynamical Analysis of the DNA

In this section it is adopted a method inspired in dynamical systems analysis. The main idea comes from the fact that the z information can be considered as an "indexing" of the signal in the $\{AT, CG\}$ 2-dimensional space. Then, the signals can be compared among themselves and the results depicted by means of a suitable computer visualization tool.

The signals $\{x_i(z), y_i(z)\}$, $z = 0, \cdots, L_i$, and $\{x_j(z), y_j(z)\}$, $z = 0, \cdots, L_j$, of the i-th and j-th chrs, are compared by means of the 2-dimensional correlation measure [17,20]:

$$r_{ij} = \left| \frac{\sum_{z=0}^{min(L_i, L_j)} \left[x_i(z) x_j(z) + y_i(z) y_j(z) \right]}{\sqrt{\sum_{z=0}^{L_i} \left[x_i^2(z) + y_i^2(z) \right] \sum_{z=0}^{L_j} \left[x_j^2(z) + y_j^2(z) \right]}} \right| \tag{2}$$

where $min(L_i, L_j)$ denotes the minimum of the lengths, L_i and L_j, of the two signals. Since the chrs have distinct sizes, in (2) it is considered that the shortest signal has value zero after exceeding its length.

The index r_{ij} runs over the set of chrs performing an item-to-item comparison and producing a symmetrical matrix $R = [r_{ij}]$ that can be analysed using present day visualization tools. For comparing the chrs of the 6 primates it is produced a matrix R, 143×143 dimensional. For the visualization it is adopted the package PHYLIP with the Fitch-Margoliash algorithm and the "drawgram" and "drawtree" plotting methods [50,8], that are presented in Figures 4 and 5, respectively.

Besides the 2-dimensional visualization program adopted previously, it is also tested the Multidimensional scaling (MDS) by means of the algorithm 'ggvis" in the package GGobi [6,16,30]. MDS is a statistical technique for visualization information that explores similarities/distances in the data [49,46,28,29,19,15]. It arranges items in a space with a given number of dimensions, so as to reproduce the observed similarities between the group of objects. Figure 6 shows the 3-dimensional MDS plot for the 6 species based on index (2).

We observe again that the Ch and Bo are the species closer to the Hu, while the Go and Rm are considerably different. Since the set {Bo, Ch, Hu} are the closest set we decided to test the proposed methodology with the three species. Figures 6 and 7 show the plots for the 73 chrs of the set {Bo, Ch, Hu} using index (2) and visualizing by means of a 2-dimensional tree and a 3-dimensional MDS plot.

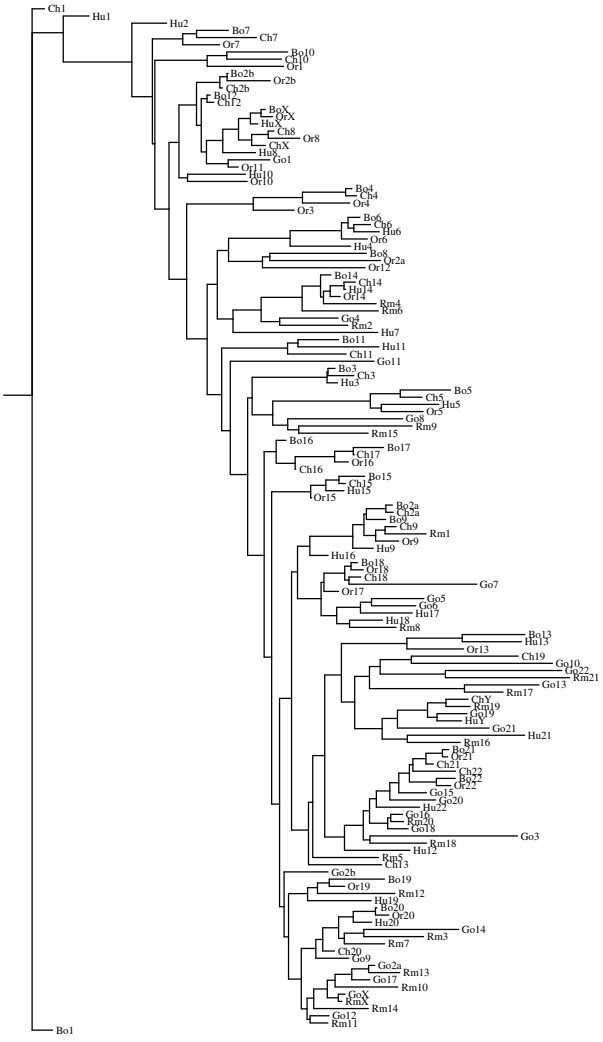

Fig. 4. Comparison of the chrs of the 6 primates using (2) and visualizing by means of a dendogram

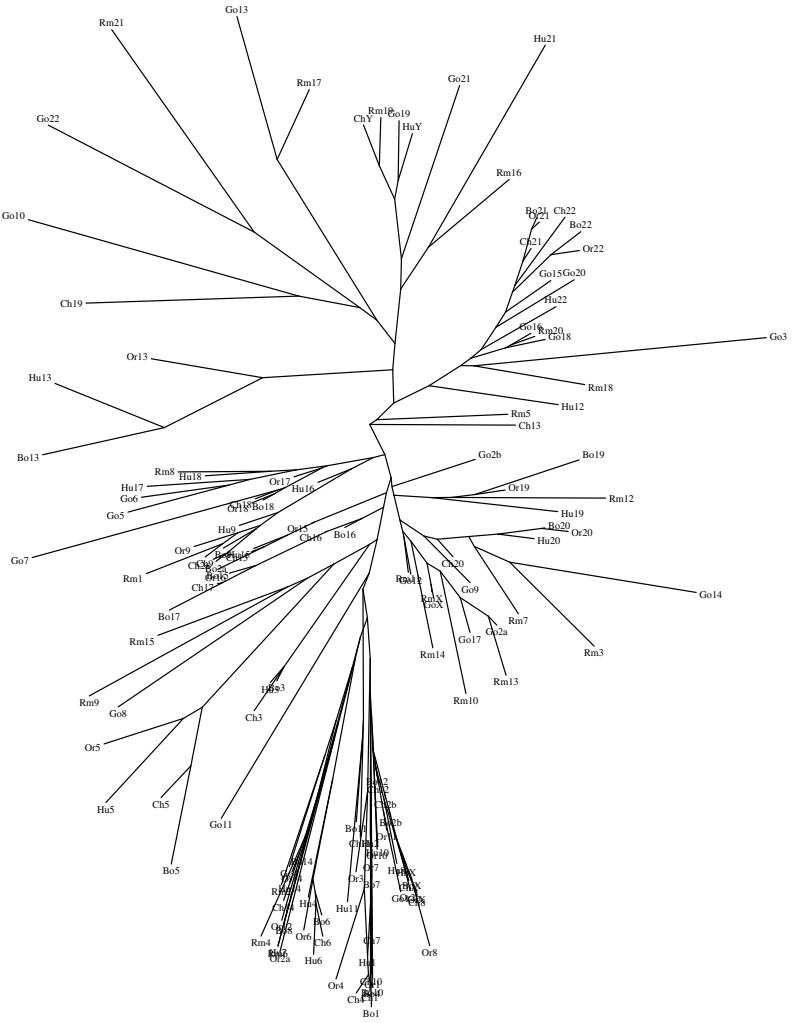

Fig. 5. Comparison of the chrs of the 6 primates using (2) and visualizing by means of a 2-dimensional tree

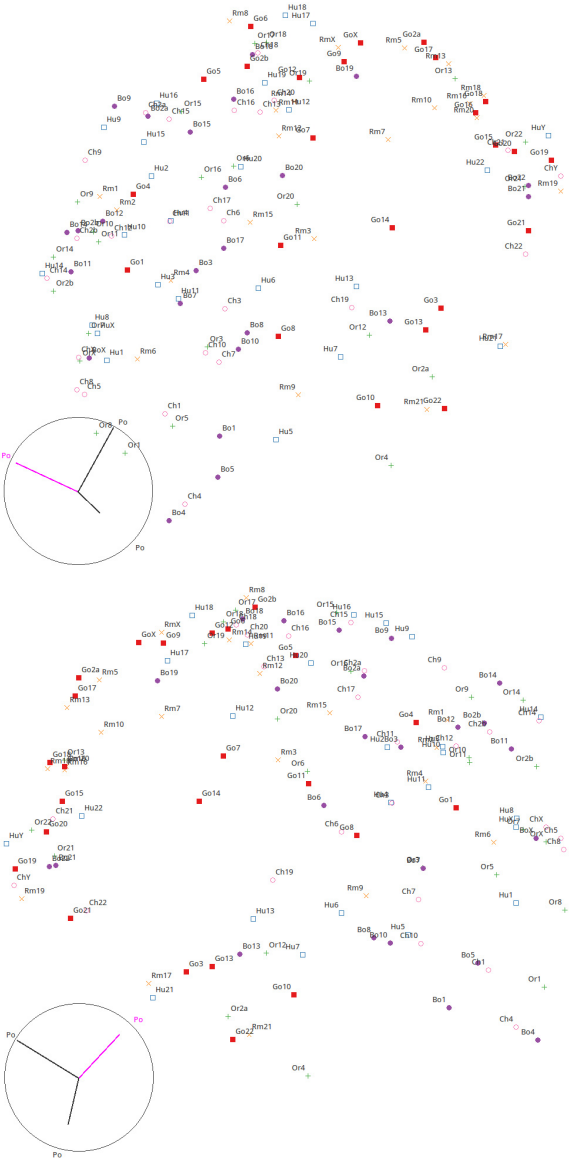

Fig. 6. Comparison of the chrs of the 6 primates using (2) and visualizing by means of a 3-dimensional MDS plot

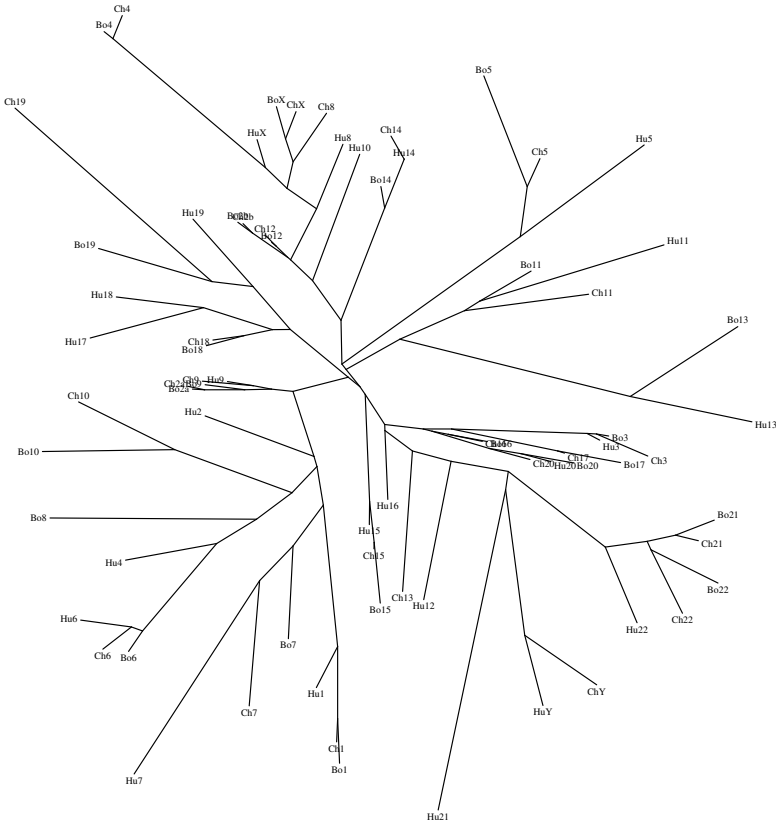

Fig. 7. Comparison of the chrs of the set {Bo, Ch, Hu} using (2) and visualizing by means of a 2-dimensional tree

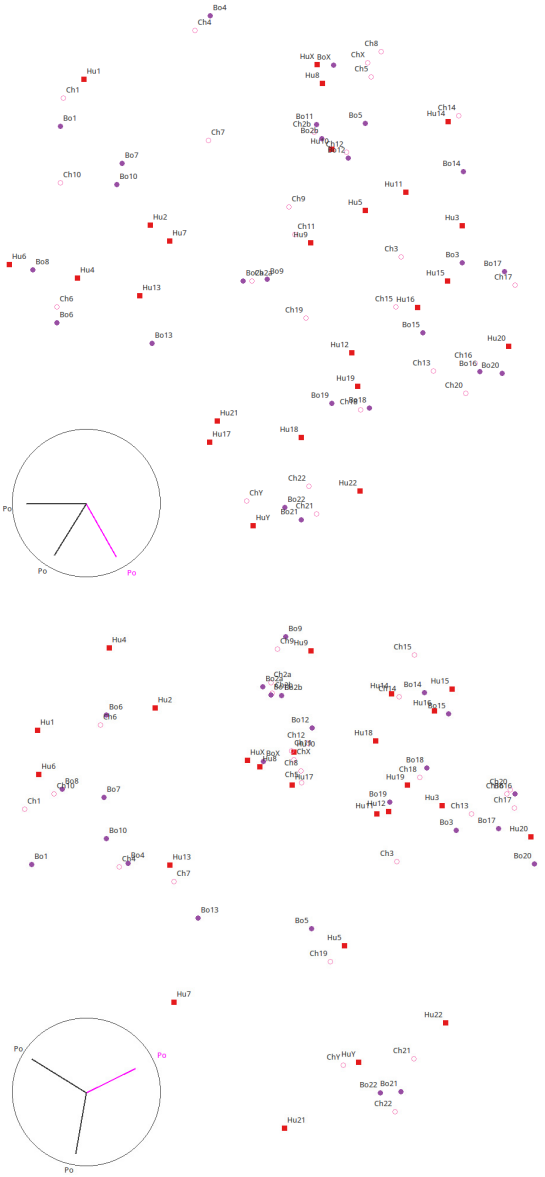

Fig. 8. Comparison of the chrs of the set {Bo, Ch, Hu} using (2) and visualizing by means of a 3-dimensional MDS plot

As expected, due to the smaller number of chrs we get a better visualization of the relationships between the distinct objects. The MDS visualization technique is slightly superior to the tree since it takes advantage of the 3-dimensional representation. However, it requires some additional time for the user to interact with the program by rotating, shifting and scaling the plot.

In conclusion, the dynamical analysis is superior to the fractal approach and leads to results in accordance with phylogenetics. In both cases the information is supplied by means of the mapping scheme in section 2, demonstrating the reliability of the methodology in analysing chr information even in the case of strong similarities.

5 Conclusions

In this paper was analysed the DNA of the Bonobo, Chimpanzee, Gorilla, Human, Orangutan and Rhesus macaque. These primates are very close and pose considerable difficulties for distinguishing them in the evolutionary tree. It was proposed an algorithm for converting the DNA information into a numerical "signal". The resulting object revealed a fractal structure but its description by geometrical dimension leads to limited results. It was also developed an approach inspired in signal processing by defining the cosine correlation measure. The comparison of the chrs was then performed and the results visualized taking advantage of modern computer tools.

References

1. Bonobo Max Planck institute for evolutionary anthropology, `http://www.eva.mpg.de/bonobo-genome/data.html`
2. Chimpanzee genome sequencing and analysis consortium
3. Ensembl, `http://www.ensembl.org/info/data/ftp/index.html`
4. Genome reference consortium, `http://www.ncbi.nlm.nih.gov/projects/genome/assembly/grc/`
5. Genome sequencing center at WUSTL
6. GGobi, `http://www.ggobi.org/`
7. Macaque genome sequencing consortium, `http://www.hgsc.bcm.tmc.edu/projects/rmacaque/`
8. Phylip, `http://evolution.genetics.washington.edu/phylip.html`
9. Afreixo, V., Ferreira, P., Santos, D.: Fourier analysis of symbolic data: A brief review. Digital Signal Processing 14(6), 523–530 (2004)
10. Afreixo, V., Ferreira, P., Santos, D.: Spectrum and symbol distribution of nucleotide sequences. Physical Review E 70(3), 03190.1–03190.4 (2004)
11. Dunn, C.W., et al.: Broad phylogenomic sampling improves resolution of the animal tree of life. Nature 452(10), 745–750 (2008)
12. Albrecht-Buehler, G.: Asymptotically increasing compliance of genomes with Chargaff's second parity rules through inversions and inverted transpositions. Proceedings of the National Academy of Sciences 103(47), 17828–17833 (2006)

13. Arniker, S., Kwan, H.: Graphical representation of DNA sequences. In: 2009 IEEE International Conference on Electro/Information Technology, Windsor, Ontario, Canada (2009)
14. Berry, M.: Diffractals. Journal of Physics A: Mathematical and General 12(6), 781–797 (1979)
15. Borg, I., Groenen, P.: Modern Multidimensional Scaling-Theory and Applications. Springer, New York (2005)
16. Buja, A., Swayne, D.F., Littman, M.L., Dean, N., Hofmann, H.: Interactive data visualization with multidimensional scaling (2004)
17. Cha, S.: Taxonomy of nominal type histogram distance measures. In: Proceedings of the American Conference on Applied Mathematics, Harvard, Massachusetts, USA, pp. 325–330 (2008)
18. Costa, A., Machado, J.T., Quelhas, M.: Histogram-based DNA analysis for the visualization of chromosome, genome and species information. Bioinformatics 27(9), 1207–1214 (2011)
19. Cox, T., Cox, M.: Multidimensional Scaling. Chapman & Hall/CRC, Boca Raton (2001)
20. Deza, M., Deza, E.: Encyclopedia of Distances. Springer, Heidelberg (2009)
21. Dodin, G., Vandergheynst, P., Levoir, P., Cordier, C., Marcourt, L.: Fourier and wavelet transform analysis, a tool for visualizing regular patterns in DNA sequences. Journal of Theoretical Biology 206(3), 323–326 (2000)
22. Ebersberger, I., Galgoczy, P., Taudien, S., Taenzer, S., Platzer, M., von Haeseler, A.: Mapping human genetic ancestry. Molecular Biology and Evolution 24(10), 2266–2276 (2007)
23. Elgar, G., Vavour, T.: Tuning in to the signals: noncoding sequence conservation in vertebrate genomes. Trends in Genetics 24(7), 344–352 (2008)
24. Gregory, T.R.: Coincidence, coevolution, or causation? DNA content, cell size, and the C-value enigma. Biological Reviews of the Cambridge Philosophical Society 76(1), 65–101 (2001)
25. Gregory, T.R.: The C-value enigma in plants and animals: A review of parallels and an appeal for partnership. Annals of Botany 95(1), 133–146 (2005)
26. Emanuele II, V.A., Tran, T.T., Zhou, G.T.: A Fourier product method for detecting approximate TANDEM repeats in DNA. In: 2005 IEEE/SP 13th Workshop on Statistical Signal Processing, Bordeaux, France (2005)
27. Jeng, C.-C., Yang, I.-C., Hsieh, K.-L., Lin, C.-N.: Clustering analysis for bacillus genus using Fourier transform and self-organizing map. In: King, I., Wang, J., Chan, L.-W., Wang, D. (eds.) ICONIP 2006. LNCS, vol. 4234, pp. 48–57. Springer, Heidelberg (2006)
28. Kruskal, J.: Multidimensional scaling by optimizing goodness of fit to a nonmetric hypothesis. Psychometrika 29(1), 1–27 (1964)
29. Kruskal, J., Wish, M.: Multidimensional Scaling. Sage Publications, Newbury Park (1978)
30. Lang, D.T., Swayne, D.F.: The GGobi XML input format (2006)
31. Lapidus, M., Fleckinger-Pellé, J.: Tambour fractal: vers une résolution de la conjecture de Weyl-Berry pour les valeurs propres du laplacien. Comptes Rendus de l'Académie des Sciences Paris Sér. I Math. 306, 171–175 (1988)
32. Leitao, H., Pessôa, L., Stolfi, J.: Mutual information content of homologous DNA sequences. Genetics and Molecular Research 4(3), 553–562 (2005)
33. Luo, L., Lee, W., Jia, L., Ji, F., Tsai, L.: Statistical correlation of nucleotides in a DNA sequence. Physical Review E 58(1), 861–871 (1998)

34. Machado, J.T., Costa, A., Quelhas, M.: Entropy analysis of DNA code dynamics in human chromosomes. Computers and Mathematics with Applications 62(3), 1612–1617 (2011)
35. Machado, J.T., Costa, A., Quelhas, M.: Shannon, Rényi and Tsallis entropy analysis of DNA using phase plane. Nonlinear Analysis Series B: Real World Applications 12(6), 3135–3144 (2011)
36. Machado, J.T., Costa, A., Quelhas, M.: Wavelet analysis of human DNA. Genomics 98(3), 155–163 (2011)
37. Mitchell, D., Bridge, R.: A test of Chargaff's second rule. Biochemical and Biophysical Research Communications 340(1), 90–94 (2006)
38. Murphy, W., Pringle, T., Crider, T., Springer, M., Miller, W.: Using genomic data to unravel the root of the placental mammal phylogeny. Genome Research 17(4), 413–421 (2007)
39. Pearson, H.: Genetics: what is a gene? Nature 441(7092), 398–401 (2006)
40. Powdel, B., Satapathy, S.S., Kumar, A., Jha, P.K., Buragohain, A.K., Borah, M., Ray, S.K.: A study in entire chromosomes of violations of the intra-strand parity of complementary nucleotides (Chargaff's second parity rule). DNA Research 16(6), 325–343 (2009)
41. Prasad, A., Allard, M.: Confirming the phylogeny of mammals by use of large comparative sequence data sets. Molecular Biology and Evolution 25(9), 1795–1808 (2008)
42. Qi, J., Luo, H., Hao, B.: Cvtree: a phylogenetic tree reconstruction tool based on whole genomes. Nucleic Acids Research 32(suppl. 2), W45–W47 (2004)
43. Qi, J., Wang, B., Hao, B.I.: Whole proteome prokaryote phylogeny without sequence alignment: A K-string composition approach. Journal of Molecular Evolution 58(1), 1–11 (2004)
44. Schroeder, M.: Fractals, Chaos, Power Laws: Minutes from an Infinite Paradise. W. H. Freeman, New York (1991)
45. Seitz, H.: Analytics of protein-DNA interactions. Advances in Biochemical Engineering Biotechnology. Springer, Heidelberg (2007)
46. Shepard, R.N.: The analysis of proximities: Multidimensional scaling with an unknown distance function. Psychometrika 27(I and II), 219–246 (1962)
47. Sims, G., Jun, S.R., Wu, G., Kim, S.H.: Alignment-free genome comparison with feature frequency profiles (FFP) and optimal resolutions. Proc. of the National Academy of Sciences of the United States of America 106(8), 2677–2682 (2009)
48. Tiwari, S., Ramachandran, S., Bhattacharya, A., Bhattacharya, S., Ramaswamy, R.: Prediction of probable genes by Fourier analysis of genomic sequences. Computer Applications in the Biosciences: CABIOS 13(3), 263–270 (1997)
49. Torgerson, W.: Theory and Methods of Scaling. Wiley, New York (1958)
50. Tuimala, J.: A primer to phylogenetic analysis using the PHYLIP package. CSC - Scientific Computing Ltd. (2006)
51. Yin, C., Yau, S.: Numerical representation of DNA sequences based on genetic code context and its applications in periodicity analysis of genomes. In: IEEE Symposium on Computational Intelligence in Bioinformatics and Computational Biology. Sun Valley, Idaho (2008)
52. Yin, C., Yau, S.T.: A Fourier characteristic of coding sequences: Origins and a non-Fourier approximation. Journal of Computational Biology 12(9), 1153–1165 (2005)
53. Yu, Z., Zhou, L., Anh, V., Chu, K., Long, S., Deng, J.: Phylogeny of prokaryotes and chloroplasts revealed by a simple composition approach on all protein se-

quences from complete genomes without sequence alignment. Journal of Molecular Evolution 60(4), 538–545 (2004)
54. Yu, Z.G., Anh, V., Lau, K.S.: Multifractal and correlation analyses of protein sequences from complete genomes. Physical Review E 68(2) (2003)
55. Yu, Z.G., Anh, V., Lau, K.S.: Chaos game representation of protein sequences based on the detailed HP model and their multifractal and correlational analysis. Journal of Theoretical Biology 226(3), 341–348 (2004)
56. Yu, Z.G., Anh, V., Lau, K.S., Chu, K.H.: The genomic tree of living organisms based on a fractal model. Physics Letters A 317(1), 293–302 (1998)
57. Zhang, C.T., Zhang, R., Ou, H.Y.: The Z curve database: a graphic representation of genome sequences. Bioinformatics 19(5), 593–599 (2003)
58. Zhao, H., Bourque, G.: Recovering genome rearrangements in the mammalian phylogeny. Genome Research 19(5), 934–942 (2009)
59. Zhou, Y., Zhou, L.Q., Yu, Z.G., Anh, V.: Distinguish coding and noncoding sequences in a complete genome using Fourier transform. In: IEEE Third International Conference on Natural Computation, Haikou, China (2007)

Reconstruction of Inner Structures Based on Radon Transform and HOSVD

András Rövid[1], László Szeidl[1], and Péter Várlaki[2]

[1] Óbuda University, John von Neumann Faculty of Infomatics,
1034 Budapest, Bécsi út 96/B, Hungary
rovid.andras@nik.uni-obuda.hu, szeidl@uni-obuda.hu
[2] Széchenyi István University, System Theory Laboratory
Egyetem tér 1., 9026 Győr, Hungary
varlaki@sze.hu

Abstract. In the paper the authors proposed a HOSVD based approach to enhance the reconstruction of inner structures based on projections from different angles which is strongly related to the well known Radon transform. It is shown that in case of less number of projections the HOSVD based approximation applied in the projection space can significantly enhance the output obtained by the inverse Radon transform.

Keywords: HOSVD, Radon transform, Approximation, Structure reconstruction.

1 Introduction

The approximation methods of mathematics are widely used in theory and practice for several problems. In this paper the reconstruction of inner structures based on projections obtained from different angles stays in the focus. The main aim was to enhance the resolution of the reconstructed function obtained by the well known inverse Radon transformation. The Radon transform is a widely used approach for various problems such as reconstruction of a 2-D object from its continuous projections [4] (the well known computer tomography), for tunnel seismic prediction [5], for multiple suppression of seismic data [6], for detection of curves in noisy digital images [2], exploiting the directional properties of Radon transform in order to extract new global features from fingerprint images [3], etc.

In order to reconstruct inner structures accurately many slices (projections) have to collected, which in case of human body measurement by the recently well known and efficient computer tomography (CT) means an increased exposure of medical XRay doses. Therefore methods able to maintain the obtained CT image quality on a similar level by reducing the number of projections is highly welcome. In recent years, the CT technology has advanced resulting in substantially wider beam width which ensures the acquisition of larger areas with fewer numbers of rotations and shorter scan time [1]. The method proposed in this paper is based on higher order singular value decomposition (HOSVD - the

J. Fodor and R. Fullér (eds.), *Advances in Soft Computing, Intelligent Robotics and Control,* Topics in Intelligent Engineering and Informatics 8,
DOI: 10.1007/978-3-319-05945-7_20,

generalized SVD) and on the inverse Radon transform (RT). [10][9]). As the HOSVD approximator works in whatever number of dimensions the method can be also extended to reconstruct a 3D body from the already reconstructed 2D slices, however in this paper we are going to show the efficiency of the approximation for one slices only. Many image processing tasks can be performed more efficiently in frequency or time-frequency domain than in the spatial one, e.g. compression standards "JPG", "JPG2000" (are based on such components), feature extraction, noise filtering, etc. While in these domains we are operating with trigonometrical components or in the latter case with wavelets and scaling functions, in case of HOSVD the components we are operating on are represented by specific orthonormal eigenfunctions (see in the upcoming sections) having specific properties which we are going to utilize to improve the reconstruction.

The main idea is to perform the HOSVD based approximation in the projection domain followed by the inverse RT. In our preceding research we showed how efficiently by HOSVD the behavior of linear parameter varying systems (LPV) can be approximated by blending a reduced set of so called local nodes (local linear time invariant models forming a convex hull, which are identified for certain parameter values) together by maintaining the accuracy of the system response at similar level. One of the most prominent property of the HOSVD is its complexity reduction support thus its approximation properties are outstanding compared to other known techniques [14]. Furthermore it has been shown in [11] that various filters can be achieved by manipulating the HOSVD-based components.

The paper is organized as follows: Section 2 gives a short overview of the Radon transformation, Section III describes how to express a multidimensional function using polylinear functions on HOSVD basis, and how to reconstruct these polylinear functions, in Section IV. the proposed enhancement of the inverse Radon transformation is described and finally future work and conclusions are reported.

2 Radon Transform Overview

Radon Transformation is generally used to construct optical image from the projection data in medical imaging [7]. The Radon transform of a two variable function along a line given by its parametric representation $r = x\cos(\varphi) + y\sin(\varphi)$ is defined as follows:

$$Rf(r,\varphi) = \int_{-\infty}^{\infty}\int_{-\infty}^{\infty} f(x,y)\delta(r - x\cos(\varphi) - y\sin(\varphi))\,\mathrm{d}x\,\mathrm{d}y,$$

where δ is the Dirac delta function [8]. For the continuous RT, backprojection is the adjoint operator to the transform,

$$R^*p(x,y) = \int_{-\infty}^{\infty}\int_{0}^{\pi} p(r,\varphi)\delta(r - x\cos(\varphi) - y\sin(\varphi))\,\mathrm{d}\varphi\,\mathrm{d}r.$$

Although the adjoint operator is not the same as the inverse, we will see that its discrete analog is a useful building block [9].

In case of the intensity function of an image the Radon transform is related with the sum of intensity values along given angles.

3 HOSVD Based Numerical Reconstruction of n-Variable Functions

The approximation methods of mathematics are widely used in theory and practice for several problems. If we consider an n-variable smooth function

$$f(\mathbf{x}),\ \mathbf{x} = (x_1, \ldots, x_N)^T,\ x_n \in [a_n, b_n]\,,\ 1 \le n \le N,$$

then we can approximate the function $f(\mathbf{x})$ with a series

$$f(\mathbf{x}) = \sum_{k_1=1}^{I_1} \cdots \sum_{k_N=1}^{I_N} \alpha_{k_1,\ldots,k_n} p_{1,k_1}(x_1) \cdot \cdots \cdot p_{N,k_N}(x_N). \tag{1}$$

where the system of orthonormal functions $p_{n,k_n}(x_n)$ can be chosen in classical way by orthonormal polynomials or trigonometric functions in separate variables and the numbers of functions I_n playing role in (1) are large enough. With the help of Higher Order Singular Value Decomposition (HOSVD) a new approximation method was developed in [12] in which a specially determined system of orthonormal functions can be used depending on function $f(\mathbf{x})$, instead of some other systems of orthonormal polynomials or trigonometric functions.

Assume that the function $f(\mathbf{x})$ can be given with some functions $\widetilde{v}_{n,i}(x_n)$, $x_n \in [a_n, b_n]$ in the form

$$f(\mathbf{x}) = \sum_{k_1=1}^{I_1} \cdots \sum_{k_N=1}^{I_N} \alpha_{k_1,\ldots,k_n} \widetilde{v}_{1,k_1}(x_1) \cdot \cdots \cdot \widetilde{v}_{N,k_N}(x_N). \tag{2}$$

Denote by $\mathcal{A} \in \mathbb{R}^{I_1 \times \cdots \times I_N}$ the N -dimensional tensor determined by the elements $\alpha_{i_1,\ldots,i_N}$, $1 \le i_n \le I_n$, $1 \le n \le N$ and let us use the following notations (see [10]).

- $\mathcal{A} \boxtimes_n \mathbf{U}$: the n-mode tensor-matrix product,
- $\mathcal{A} \boxtimes_{n=1}^{N} \mathbf{U}_n$: the multiple product as $\mathcal{A} \boxtimes_1 \mathbf{U}_1 \boxtimes_2 \mathbf{U}_2 \cdots \boxtimes_N \mathbf{U}_N$.

The n-mode tensor-matrix product is defined as follows:

Let $\mathbf{U}$ be a $K_n \times M_n$-matrix, then $\mathcal{A} \boxtimes_n \mathbf{U}$ is a $M_1 \times \cdots \times M_{n-1} \times K_n \times M_{n+1} \times \cdots \times M_N$-tensor for which the relation

$$(\mathcal{A} \boxtimes_n \mathbf{U})_{m_1,\ldots,m_{n-1},k_n,m_{n+1},\ldots,m_N} \stackrel{def}{=}$$

$$\sum_{1 \le m_n \le M_n} a_{m_1,\ldots,m_n,\ldots,m_N} U_{k_n,m_n}$$

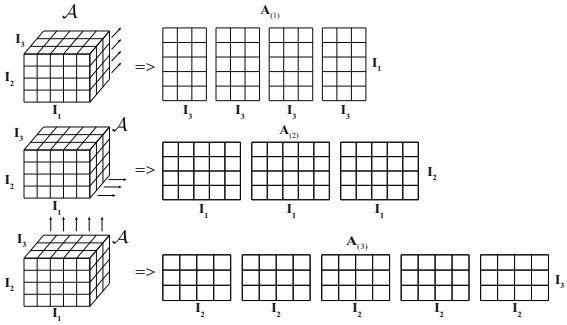

Fig. 1. The three possible ways of expansions of a 3-dimensional array into matrices

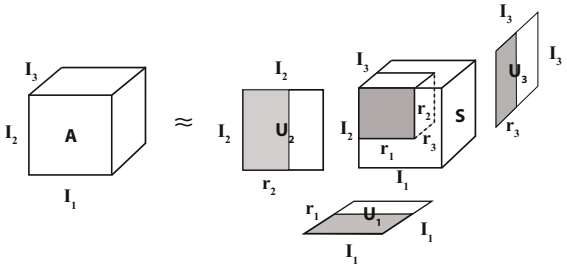

Fig. 2. Illustration of the higher order singular value decomposition for a 3-dimensional array. Here **S** is the core tensor, the $\mathbf{U}_l$-s are the l-mode singular matrices.

holds. Detailed discussion of tensor notations and operations is given in [10]. We also note that we use the sign $\boxtimes_n$ instead the sign $\times_n$ given in [10]. Using this definition the function (2) can be rewritten as a tensor product form

$$f(\mathbf{x}) = \mathcal{A} \boxtimes_{n=1}^{N} \widetilde{v}_n(x_n), \tag{3}$$

where $\widetilde{v}_n(x_n) = (\widetilde{v}_{n,1}(x_n), \ldots, \widetilde{v}_{n,I_n}(x_n))^T,\ 1 \leq n \leq N$. Based on HOSVD it was proved in [13] that under mild conditions the (3) can be represented in the form

$$f(\mathbf{x}) = \mathcal{D} \boxtimes_{n=1}^{N} v_n(x_n), \tag{4}$$

where

– $\mathcal{D} \in \mathbb{R}^{r_1 \times \cdots \times r_N}$ is a special (so called core) tensor with the properties:
  1. $r_n = \mathrm{rank}_n(\mathcal{A})$ is the n-mode rank of the tensor $\mathcal{A}$, i.e. rank of the linear space spanned by the n-mode vectors of $\mathcal{A}$:

$$\{(a_{i_1,\ldots,i_{n-1},1,i_{n+1},\ldots,i_N}, \ldots, a_{i_1,\ldots,i_{n-1},I_n,i_{n+1},\ldots,i_N})^T : \\ 1 \leq i_j \leq I_n,\ 1 \leq j \leq N\},$$

2. all-orthogonality of tensor $\mathcal{D}$: two subtensors $\mathcal{D}_{i_n=\alpha}$ and $\mathcal{D}_{i_n=\beta}$ (the n-th indices $i_n = \alpha$ and $i_n = \beta$ of the elements of the tensor $\mathcal{D}$ keeping fix) orthogonal for all possible values of n, α and β: $\langle \mathcal{D}_{i_n=\alpha}, \mathcal{D}_{i_n=\beta} \rangle = 0$ when $\alpha \neq \beta$. Here the scalar product $\langle \mathcal{D}_{i_n=\alpha}, \mathcal{D}_{i_n=\beta} \rangle$ denotes the sum of products of the appropriate elements of subtensors $\mathcal{D}_{i_n=\alpha}$ and $\mathcal{D}_{i_n=\beta}$,
3. ordering: $\|\mathcal{D}_{i_n=1}\| \geq \|\mathcal{D}_{i_n=2}\| \geq \cdots \geq \|\mathcal{D}_{i_n=r_n}\| > 0$ for all possible values of n ($\|\mathcal{D}_{i_n=\alpha}\| = \langle \mathcal{D}_{i_n=\alpha}, \mathcal{D}_{i_n=\alpha} \rangle$ denotes the Kronecker-norm of the tensor $\mathcal{D}_{i_n=\alpha}$).

– Components $v_{n,i}(x_n)$ of the vector valued functions

$$v_n(x_n) = (v_{n,1}(x_n), \ldots, v_{n,r_n}(x_n))^T,\ 1 \leq n \leq N,$$

are orthonormal in L_2-sense on the interval $[a_n, b_n]$, i.e.

$$\forall n : \int_{a_n}^{b_n} v_{n,i_n}(x_n) v_{n,j_n}(x_n)\,\mathrm{d}x = \delta_{i_n,j_n},$$
$$1 \leq i_n, j_n \leq r_n,$$

where $\delta_{i,j}$ is a Kronecker-function ($\delta_{i,j} = 1$, if $i = j$ and $\delta_{i,j} = 0$, if $i \neq j$)
The form (4) was called in [13] HOSVD canonical form of the function (2).

Let us decompose the intervals $[a_n, b_n]$, $n = 1..N$ into M_n number of disjunct subintervals $\triangle_{n,m_n}$, $1 \leq m_n \leq M_n$ as follows:

$$\xi_{n,0} = a_n < \xi_{n,1} < \ldots < \xi_{n,M_n} = b_n,$$
$$\triangle_{n,m_n} = [\xi_{n,m_n}, \xi_{n,m_n-1}).$$

Assume that the functions $v_{n,k_n}(x_n),\ x_n \in [a_n, b_n]\,,\ 1 \leq n \leq N$ in the equation (2) are piece-wise continuously differentiable and assume also that we can observe the values of the function $f(\mathbf{x})$ in the points

$$y_{i_1,\ldots,i_N} = (x_{1,i_1}, \ldots, x_{N,i_N}),\ 1 \leq i_n \leq M_n. \tag{5}$$

where

$$x_{n,m_n} \in \triangle_{n,m_n}, \quad 1 \leq m_n \leq M_n,\ 1 \leq n \leq N$$

Based on the HOSVD a new method was developed in [13] for numerical reconstruction of the canonical form of the function $f(\mathbf{x})$ using the values $f(y_{i_1,\ldots,i_N})$, $1 \leq i_n \leq M_n,\ 1 \leq i_n \leq N$. We discretize function $f(\mathbf{x})$ for all grid points as:

$$b_{m_1,..,m_N} = f(y_{m_1,..,m_N}).$$

Then we construct N dimensional tensor $\mathcal{B} = (b_{m_1,\ldots,m_N})$ from the values $b_{m_1,..,m_N}$. Obviously, the size of this tensor is $M_1 \times \cdots \times M_N$. Further, we discretize vector valued functions $\mathbf{v}_n(x_n)$ over the discretization points x_{n,m_n} and construct matrices $\mathbf{V}_n$ from the discretized values as:

$$\mathbf{V}_n = \begin{pmatrix} v_{n,1}(x_{n,1}) & v_{n,2}(x_{n,1}) & \cdots & v_{n,r_n}(x_{n,1}) \\ v_{n,1}(x_{n,2}) & v_{n,2}(x_{n,2}) & \cdots & v_{n,r_n}(x_{n,2}) \\ \vdots & & \ddots & \vdots \\ v_{n,1}(x_{n,M_n}) & v_{n,2}(x_{n,M_n}) & \cdots & v_{n,r_n}(x_{n,M_n}) \end{pmatrix} \tag{6}$$

Then tensor $\mathcal{B}$ can simply be given by (4) and (6) as

$$\mathcal{B} = \mathcal{D} \boxtimes_{n=1}^{N} \mathbf{V}_n. \tag{7}$$

Consider the HOSVD decomposition of the discretization tensor

$$\mathcal{B} = \mathcal{D}^d \boxtimes_{n=1}^{N} \mathbf{U}^{(n)} \tag{8}$$

where $\mathcal{D}^d$ is the so-called core tensor, and $\mathbf{U}^{(n)} = \left(U_1^{(n)}\ U_2^{(n)}\ \dots\ U_{M_n}^{(n)}\right)$ is an $M_n \times M_n$-size orthogonal matrix ($1 \le n \le N$).

Let us introduce the notation: $\widetilde{r_n}^d = \text{rank}_n\, \mathcal{B},\ 1 \le n \le N$ and consider the $\widetilde{r_1}^d \times \cdots \times \widetilde{r_N}^d$-size reduced version $\widetilde{\mathcal{D}}^d = (\mathcal{D}^d_{m_1,\dots,m_N}, 1 \le m_n \le r_n, 1 \le n \le N)$ of the $M_1 \times \cdots \times M_N$-size tensor $\mathcal{D}^d$. The following theorems were proved in [13]. Denote

$$\Delta = \max_{1 \le n \le N} \max_{1 \le i_n \le M_n} (\xi_{n,m_n} - \xi_{n,m_n-1}) \quad \text{and}$$

$$\rho = \prod_{n=1}^{N} \rho_n,\ \rho_n = (b_n - a_n)/M_n.$$

Theorem 1. *If Δ is sufficiently small, then $\widetilde{r_n}^d = r_n,\ 1 \le n \le N$ and the convergence $\sqrt{\rho}\widetilde{\mathcal{D}}^d \to D,\ \Delta \longrightarrow 0$ is true.*

Theorem 2. *If $\Delta \longrightarrow 0$ then*

$$\int_{a_n}^{b_n} (v_{n,i}(x) - u_{n,i}(x))^2\, \mathrm{d}x \to 0, \quad 1 \le i \le r_n, 1 \le n \le N$$

4 The Proposed Reconstruction

Let us assume that we have CT measurements (projections) encoded by image function $I_R(r, \varphi)$. Considering the decomposition described in the previous section we can express the function I_R with the help of specific orthonormal components obtained by SVD as follows:

$$I_R(r, \varphi) = \sum_{k_1=1}^{I_1} \sum_{k_2=1}^{I_2} \alpha_{k_1,k_2} \widetilde{v}_{1,k_1}(r) \cdot \widetilde{v}_{2,k_2}(\varphi). \tag{9}$$

To improve the efficiency of the inverse Radon transformation the function I_R is approximated through the numerically reconstructed uni-variate functions $\widetilde{v}_{1,k_1}(r)$ and $\widetilde{v}_{2,k_2}(\varphi)$. As illustrated in Fig. 2 the ith column of matrix U_1 corresponds to the function $\widetilde{v}_{1,j_1}(r)$ and the jth column of matrix U_2 corresponds to the function $\widetilde{v}_{2,j_2}(\varphi)$. The elements for instance in the jth column of matrix U_2 stand for function values $\widetilde{v}_{2,j}(\varphi_k)$ over equidistant nodes. The approximation is performed on these elements followed by multiplying the such approximated U_i matrices by the core tensor. The obtained I_R discrete function is then used to estimate the inverse Radon transform (see Fig. 3).

Here we are considering only the two variable case of the HOSVD thus the well known SVD. As we already mentioned in the introduction, if the aim is the 3D reconstruction of the inner structure of the target then we will have an additional dimension.

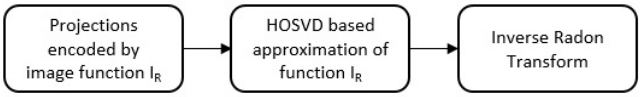

Fig. 3. The main steps of the proposed approach

5 Examples

The below examples represent the reconstruction of the structure depicted in Fig. 4(a). The example structure as well as the Radon transform and its inverse were generated with MATLAB Radon Toolbox. As the input of the reconstruction, projections (radon transforms) corresponding to the interval 0 to 180 degrees with 2 degrees step size were utilized. Such a Radon transformed image was approximated resulting approximate projections in the interval 0-180 degrees with step size 0.2 degrees (see Fig. 4(b)). The result of the inverse radon transform applied on the projections with step size 2 degrees can be followed in Fig. 5(a). Fig. 5(b) corresponds to the inverse radon transform applied on the approximated projections with step size 0.2 degrees. It can be recognized that the reconstructed structure based on the approximated projections is of higher quality, the edges are sharper than in the case of Fig. 5(a).

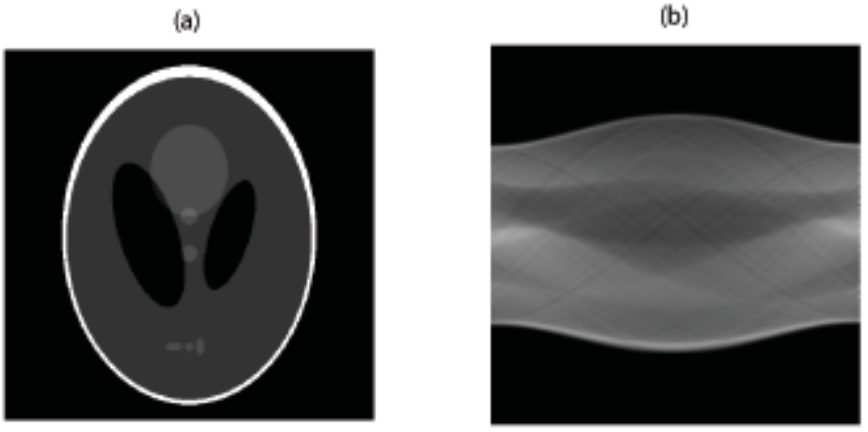

Fig. 4. The original structure (a), Radon transform followed by HOSVD based approximation (b)

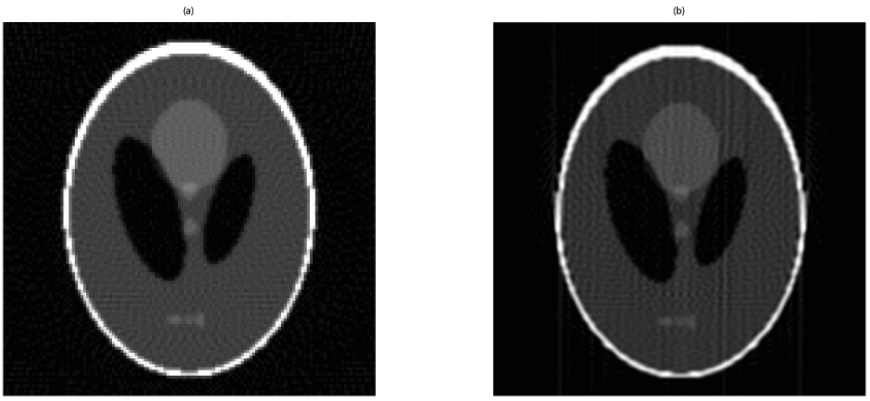

Fig. 5. The reconstructed structure by inverse Radon transform: (a) projections from 0-180 degrees. Step size: 2 degrees, (b) projections from 0-180 degrees. Step size: 0.2 degrees achieved by HOSVD

6 Future Work and Conclusions

In this paper an enhancement to the inverse Radon tranform have been proposed based on approximating the image encoding the measured projections by HOSVD. The performed experiments show that such kind of approximation in the "projection" domain can yield better accuracy. As future work we are going to perform additional experiments to enhance the 3D reconstruction of inner structures. Furthermore the HOSVD might be a useful tool for performing various kind of filtering.

Acknowledgements. This work was supported by the Hungarian National Found OTKA No. K 106392 and OTKA No. K 105529.

References

1. Kim, S., Song, H., Samei, E., Yin, F.-F., Yoshizumi, T.T.: Computed tomography dose index and dose length product for cone-beam CT: Monte Carlo simulations of a commercial system. Journal of Applied Clinical Medical Physics 12(2), 84–95 (2011)
2. Toft, P.A.: Using the generalized Radon transform for detection of curves in noisy images. In: 1996 IEEE International Conference on Acoustics, Speech, and Signal Processing, ICASSP 1996. Conference Proceedings, May 7-10, vol. 4, pp. 2219–2222 (1996)
3. Haddad, Z., Beghdadi, A., Serir, A., Mokraoui, A.: Fingerprint Identification using Radon Transform. In: First Workshops on Image Processing Theory, Tools and Applications, IPTA 2008, November 23-26, pp. 1–7 (2008)

4. Averbuch, A., Sedelnikov, I., Shkolnisky, Y.: CT Reconstruction From Parallel and Fan-Beam Projections by a 2-D Discrete Radon Transform. IEEE Transactions on Image Processing 21(2), 733–741 (2012)
5. Wang, Z., Liu, Z.: The research of Radon transform applied in the tunnel seismic prediction. In: 2011 International Conference on Consumer Electronics, Communications and Networks (CECNet), April 16-18, pp. 5429–5432 (2011)
6. Tong, S., Wang, R., Liu, H., Zhang, J., Bu, C.: High Resolution Radon Transform and its Applications in Multiple Suppression of Seismic Data in Deep-Sea. In: 2nd International Congress on Image and Signal Processing, CISP 2009, October 17-19, pp. 1–4 (2009)
7. Hossain, M.A., Ahsan-Ul-Ambia, Aktaruzzaman, M., Khan, M.A.: Implementation of Radon Transformation for Electrical Impedance Tomography (EIT). In CoRR, abs/1211.1252 (2012)
8. Hoilund, C.: The Radon Transform, Aalborg University, VGIS, 07gr721, p. 20 (2007)
9. William, H.: Discrete Radon transform has an exact, fast inverse and generalizes to operations other than sums along lines 103(51), 19249–19254 (2006)
10. De Lathauwer, L., De Moor, B., Vandewalle, J.: A multilinear singular value decomposition. SIAM Journal on Matrix Analysis and Applications 21(4), 1253–1278 (2000)
11. Rövid, A., Rudas, I.J., Sergyán, S., Szeidl, L.: HOSVD Based Image Processing Techniques. In: Proc. of the 10th WSEAS International Conference on Artificial Intelligence, Knowledge Engineering and Data Bases, Cambridge, UK, February 20-22, pp. 297–302 (2011) ISBN: 978-960-474-273-8
12. Szeidl, L., Várlaki, P.: HOSVD Based Canonical Form for Polytopic Models of Dynamic Systems. Journal of Advanced Computational Intelligence and Intelligent Informatics 13(1), 52–60 (2009)
13. Szeidl, L., Baranyi, P., Petres, Z., Várlaki, P.: Numerical Reconstruction of the HOSVD Based Canonical Form of Polytopic Dynamic Models. In: 3rd International Symposium on Computational Intelligence and Intelligent Informatics, Agadir, Morocco, pp. 111–116 (2007)
14. Harmati, I., Rövid, A., Várlaki, P.: Approximation of Force and Energy in Vehicle Crash Using LPV Type Description. WSEAS Transactions on Systems 9(7), 734–743 (2010)

Author Index